A Multidecadal Climate Signal Propagating Across the Northern Hemisphere through Indices of a Synchronized Network.

by

Marcia Glaze Wyatt

B.S. University of Southern California 1975

M.S. Mississippi State University 2004

A thesis submitted to the
Faculty of the Graduate School of the
University of Colorado in partial fulfillment
of the requirements for the degree of
Doctor of Philosophy in Geology
Department of Geology
2012

This thesis entitled:

A Multidecadal Climate Signal Propagating Across the Northern Hemisphere through Indices of a Synchronized Network.

Written by Marcia Glaze Wyatt

Has been approved for the Department of Geology

_____

Prof. Peter Molnar

_____

Prof. Roger Pielke, Sr.

_____

Prof. Anastasios Tsonis

Date_____

The final copy of this thesis has been examined by the signatories, and we find that both the content and the form meet acceptable presentation standards of scholarly work in the above mentioned discipline.

Wyatt, Marcia Glaze (Ph,D., Geology)

A Multidecadal Climate Signal Propagating Across the Northern Hemisphere through Indices of a Synchronized Network.

Thesis directed by Prof. Peter Molnar

Proxy and instrumental records reflect a quasi-cyclic 50-to-80-year climate signal across the Northern Hemisphere. Three studies, the collection of which is presented in this thesis, document evidence, or lack thereof, of this proposed climate signal.

In the first study[1], chapter two, an eight-member collection of geographically and dynamically diverse twentieth-century climate indices was analyzed with multivariate statistical techniques to assess collective behavior of the network. Emergent from the results was a picture of a climate signal propagating through a sequence of synchronized atmospheric and lagged oceanic circulations across the Northern Hemisphere. Tempo of the signal's multidecadal variability appears related to that of the low-frequency oscillatory pattern of sea-surface-temperature distribution across the North Atlantic basin, the Atlantic Multidecadal Oscillation (AMO).

The third chapter features the second study, the goals of which were two-fold: to gain insights into mechanism of the propagating signal identified in the first study and to probe the signal's history. Data sets included twentieth-century data and proxy data spanning the interval 1700 to 2000. Findings suggest i) the observed 20th century signal-propagation has existed in somewhat similar fashion for the 300-year length of this study; ii) Eurasian-Arctic Shelf sea-ice plays a strong role in the propagation of the hemispheric climate signal; and iii) dynamics fundamental to generation of the multidecadal component of the Northern Hemisphere's surface

[1] In-press paper (Climate Dynamics 2011) w/ co-authors Sergey Kravtsov and Anastasios Tsonis

temperature are encoded onto the records of key proxy indices, the combined signatures of which trace the hemispheric circumnavigation of the secularly varying, sequentially propagating climate signal.

In the final study in this collection, detailed in chapter four, a network of simulated climate indices, reconstructed from a data set generated by models of the third Coupled Intercomparison Project (CMIP3), were analyzed. Of sixty analyses performed on these networks, none succeeded in reproducing a propagating multidecadal quasi-oscillatory signal. This result, standing in stark contrast to those of the first two studies, may imply that physical mechanisms relevant to signal propagation may be missing from this suite of general circulation models.

Dedication

To my husband, David. Friend, cheerleader, and my rock.

Acknowledgements

I would like to thank my thesis advisors, Peter Molnar and Roger Pielke, Sr. for making possible my somewhat unconventional experience in academia. A few years ago, an idea took hold of my curiosity. It was not an idea familiar to my advisors. My choice was to change thesis topics or leave academia.

Being somewhat chronologically removed from the typical student situation, I failed to recognize the gravity of this choice. I continued study of this idea, inadvertently impervious to the potential consequences of that action. I can only blame it on this idea. It refused to relinquish its hold on my attention.

A study by Anastasios Tsonis, Kyle Swanson, and Sergey Kravtsov of the University of Wisconsin, Milwaukee, caught my eye. The premise of that article shared similarities with the subject I was pursuing. I contacted Dr. Tsonis. Thereafter, everything changed. He, Sergey Kravtsov, Peter Molnar, and Roger Pielke, Sr., made possible this dissertation. I cannot thank them enough for making this continued study happen. I thank Sergey Kravtsov, in particular. Without his day-to-day guidance and instruction on statistics and general scientific methods, this research would have gone nowhere. He did all of this without any compensation accrued to him.

I also extend my thanks to Tom Marchitto for his input over the years. Balaji Rajagopalan has offered guidance on occasion, for which I am grateful.

Thanks also to Judy Curry of the Georgia Institute of Technology. Her willingness to read a rather unwieldy piece of work, her expressed encouragement, and her readiness to join my committee gave me just the confidence I needed to carry out my most non-mainstream investigation of this collection of studies.

I am in a unique position. Most my age have their higher degrees or gave up long ago seeking one. Not enough in my prime to tackle this challenge for purposes of a career, I was able to take on more risks in my studies than the typical student is apt to do. What greater gift could there be than to research motivated only by passion! All of you have afforded me this dream that I once thought was out-of-reach.

TABLE of CONTENTS:

LIST of TABLES:

Chapter Two:

Chapter Three:

Chapter Four:

LIST of FIGURES:

Chapter Two:

Chapter Three:

Chapter Four:

Chapter One

Introduction

A quasi-cyclic 50-to-80-year climate signal emerges from instrumental and proxy data from across the Northern Hemisphere. Such secular variability has long held intrigue, while eluding definitive identification. Artifacts of statistical analysis; quality and character of data; and non-linearity of the climate system play significant roles in the latter. Incumbent upon any hypothesis regarding quasi-cyclic climate variability is the identification of said signal in a variety of data sets, and explainable in terms of a physical mechanism.

The research presented here attempts to meet both goals. Through rigorous statistical analysis applied to three sets of data – instrumental, proxy, and model-generated data sets, each set containing numerous individual climate and climate-related indices – the first criterion is sought.

Emergent from results of the trio of analyses is a hypothesis of a climate signal propagating hemispherically via a sequence of atmospheric and lagged oceanic teleconnections. While observation of multidecadally paced signals in a variety of climate indices across the Northern Hemisphere initially motivated this present inquiry, it was the subsequent recognition of a low-frequency alignment of synchronized[1], phase-shifted regional indices that indicated a hemispherically propagating signal, a signal termed here, the 'stadium wave'[2]. It is the

[1] Synchronization refers to the matching of rhythms of self-sustained (quasi)oscillators; not to be confused with "synchronous", which refers to "same timing", which typically involves non-self-sustained oscillators. Due to inherent natural oscillatory behavior of each synchronized system, a phase shift (lead-lag relationship), sometimes imperceptible, depending on frequencies involved, always exists between the systems.

[2] The term "stadium wave", chosen by the authors to describe a hemispherically propagating climate signal, derives from the well-known "audience wave", where groups of spectators briefly stand while raising their arms. They subsequently sit while spectators in successive sections repeat the pattern, transmitting the celebratory signal across an entire stadium – an apt visualization of the authors' "stadium wave" of the described climate-signal teleconnection pattern across the Northern Hemisphere.

hemispheric signal-propagation that distinguishes this study from one focused exclusively on low-frequency, quasi-cyclic behavior in a climate index.

Mechanisms explaining links among participating regional atmospheric and oceanic circulations are as varied as the connections themselves. But what overarching mechanism drives the climate engine, converting chaotic weather interactions into what appears to be, through the lens of long-term behavior, relatively stability? Research presented here suggests the following: A basin-scale meridional temperature gradient, particularly one in the North Atlantic, exaggerated (damped) by warm (cool) tropics and increased (decreased) ice-cover in the polar region, sets into motion a sequence of negative feedbacks involving hemispherically communicated atmospheric responses to varying degrees of meridional contrast, linked intimately to ocean-influenced sea-ice-inventories in the Arctic. This envisioned scenario guides the quest to meet criterion two.

Instrumental data strongly support a secularly varying hemispheric propagation of a signal throughout the twentieth century. Proxy data suggest a similar sequential communication. Model-generate data do not. Determining what these similar and dissimilar results divulge about climate, or about the tools used to examine climate, is the challenge of this presented collection of studies.

Chapter Two:

Atlantic Multidecadal Oscillation and Northern Hemisphere's climate variability[1]

Abstract Proxy and instrumental records reflect a quasi-cyclic 50-to-80-year climate signal across the Northern Hemisphere, with particular presence in the North Atlantic. Modeling studies rationalize this variability in terms of intrinsic dynamics of the Atlantic Meridional Overturning Circulation influencing distribution of sea-surface-temperature anomalies in the Atlantic Ocean; hence the name Atlantic Multidecadal Oscillation (AMO). By analyzing a lagged covariance structure of a network of climate indices, this study details the AMO-signal propagation throughout the Northern Hemisphere via a sequence of atmospheric and lagged oceanic teleconnections, which the authors term the "stadium wave". Initial changes in the North Atlantic temperature anomaly associated with AMO culminate in an oppositely signed hemispheric signal about 30 years later. Furthermore, shorter-term, interannual-to-interdecadal climate variability alters character according to polarity of the stadium-wave-induced prevailing hemispheric climate regime. Ongoing research suggests mutual interaction between shorter-term variability and the stadium wave, with indication of ensuing modifications of multidecadal variability within the Atlantic sector.

Results presented here support the hypothesis that AMO plays a significant role in hemispheric and, by inference, global climate variability, with implications for climate-change attribution and prediction.

Keywords Climate indices · Teleconnections · AMO · NAO · ENSO · PDO

[1] Published manuscript: see references (Marcia Glaze Wyatt, Sergey Kravtsov, and Anastasios A. Tsonis)

2.1 Introduction

A pressing challenge for climate science in the era of global warming is to better distinguish between climate signals that are anthropogenically forced and those that are naturally occurring at decadal and longer timescales. Identifying the latter is essential for assessing relative contributions of each component to overall climate variability.

Multi-century proxy records reflect the signature of such a low-frequency climate signal, paced at a typical timescale of 50 to 80 years, with pronounced presence in the North Atlantic (Stocker and Mysak 1992; Mann et al. 1995; Black et al. 1999, Shabalova and Weber 1999; Delworth and Mann 2000; Gray et al. 2004). A similar signature has been detected in the instrumental record (Folland et al. 1986; Kushnir 1994; Schlesinger and Ramankutty 1994; Mann and Park 1994, 1996; Enfield and Mestas-Nuñez 1999; Delworth and Mann 2000; Zhen-Shan and Xian 2007). Modeling studies, with divergent results dependent upon model design (Delworth et al. 2007; Msadek et al. 2010a, 2010b), qualitatively support this pattern and tempo of variability in terms of the Atlantic Meridional Overturning Circulation's (AMOC) influencing redistribution of sea-surface-temperature (SST) anomalies in the Atlantic Ocean (Delworth and Mann 2000; Dong and Sutton 2002; Latif et al. 2004; Knight et al. 2005). Observed multidecadal SST variability in the North Atlantic Ocean, believed consequent of variability in the AMOC, has been termed the Atlantic Multidecadal Oscillation (AMO: Kerr 2000; Enfield et al. 2001).

AMO significantly impacts climate in North America and Europe (Enfield et al. 2001, Sutton and Hodson 2005, Knight et al. 2006; Pohlmann et al. 2006). In fact, its influence may have a global character; a suite of studies have addressed bits and pieces of requisite interactions (Dong and Sutton 2002, 2007; Dima and Lohmann 2007; Grosfeld et al. 2008; Sutton and

Hodson 2003, 2005, 2007; Sutton et al. 2003; Timmermann et al. 2007; Zhang and Delworth 2005, 2007; Zhang et al. 2007; Polyakov et al. 2009).

Atlantic-related multidecadal variability reflected in geographically diverse proxy and instrumental records, combined with an abundance of numerical studies that link the hemispheric climate signal to AMO-related North Atlantic variability, guide our hypothesis and motivate our present investigation. We endeavor to put these previous results into perspective through use of a statistical methodology that characterizes Northern Hemispheric multidecadal climate variability and provides rigorous statistical bounds on the associated uncertainties. Emergent is a picture of a climate signal propagating from the North Atlantic throughout the Northern Hemisphere via a sequence of atmospheric and lagged oceanic teleconnections. We term this signal the "stadium wave". The stadium wave is examined here both in terms of its role in generating a multidecadally varying hemispheric climate signature and in its relationship with interannual-to-interdecadal climate variability.

Our philosophical approach, data sets, and analysis methods are described in section 2.2. Section 2.3 contains the results of our analyses. Section 2.4 summarizes our work and discusses potential mechanisms underlying the stadium wave.

2.2 Approach, data sets and methods

2.2.1 Approach

Our strategy was to evaluate collective behavior within a network of climate indices. Considering index networks rather than raw 3-D climatic fields is a relatively novel approach that has its own advantages — such as potentially increased dynamical interpretability, along with apparent increase of signal-to-noise ratio, and enhanced statistical significance — at the

expense of detailed phenomenological completeness. In particular, the climate indices may represent distinct subsets of dynamical processes — tentatively, "climate oscillators" — that might, however, exhibit various degrees of coupling (Tsonis et al. 2007). As these indices also pertain to different geographical regions, we directly address the question of the global multidecadal teleconnections. Using fairly standard multivariate statistical tools, we aim to characterize dominant mode of climate co-variability in the Northern Hemisphere and provide rigorous estimates of its statistical significance, namely: What are the chances that the low-frequency alignment of various regional climatic time series, alluded to in an impressive suite of previous climate studies (see section 2.1), is, in fact, random? Our methodology allows us to give a quantitative answer to this question. Furthermore, objective filtering of the multidecadal signal provides a clearer picture of higher-frequency climate variability and its possible multi-scale interactions within the climate system.

2.2.2 Data sets

Insights gained from extensive literature review regarding proxy records, instrumental data, and climate-model studies; completeness of data sets throughout the 20th century; and preliminary examination of linearly detrended 13-year smoothed index-anomaly time series (not shown), collectively prompted our choice to use two subsets of climate indices to address our hypotheses. A main set of eight indices focused on the role played by the stadium-wave teleconnection sequence in the evolution of the multidecadal hemispheric climate signal. Seven complementary indices were then used to generate a larger fifteen-member network (**Table 2.1**)[2]; the goals here were to (i) check the robustness of our results to the choice of index subset;

[2] The time series of the indices used is later shown in Fig. 2.7, in terms of their decomposition into multidecadal signal and remaining higher-frequency variability.

(ii) to paint a more complete picture of multidecadal variability; and (iii) to investigate more fully the role of higher-frequency behavior in relation to multidecadal stadium-wave propagation.

The original subset of eight indices contained the Northern Hemisphere area-averaged surface temperature (NHT), the Atlantic Multidecadal Oscillation (AMO), Atmospheric-Mass Transfer anomaly (AT), the North Atlantic Oscillation (NAO), El Niño/Southern Oscillation (NINO3.4), the North Pacific Oscillation (NPO), the Pacific Decadal Oscillation (PDO), and the Aleutian Low Pressure (ALPI) indices. The complementary set of seven indices used to generate our expanded network included: the North Pacific Gyre Oscillation (NPGO), ocean-heat-content anomalies of the upper 700 and 300 meters in the North Pacific Ocean (OHC700 and OHC300), the Pacific North American (PNA) pattern, the Western Pacific (WP) pattern, the Pacific Meridional Mode (PMM), and the Atlantic Meridional Mode (AMM) indices. In order to maintain consistency with previous studies to which we compare our results, some of the analyses below will also include another ENSO index, the NINO3 index based on the Kaplan et al. (1998) sea-surface temperature data set. All of these indices have been used extensively in previous studies and highlight distinctive subsets of climatic processes; see Table 2.1 for references and brief description of each index.

Table 2.1: Observed climate-index network.

Index Acronym	Reference/Data source	Description/General Information
ALPI	Beamish et al. (1997) http://www.pac.dfo-mpo.gc.ca/sci/sa-mfpd/downloads/indices/alpi.txt	**Aleutian Low Pressure Index** Relative intensity of SLP in N.Pacific (~50°N) in winter (DJFM). Calculated as mean area (km^2) w/ SLP<100.5kPa. Expressed as anomaly relative to the 1950–1997 mean.
AMO	Kerr (2000);Enfield et al. (2001); Sutton and Hodson (2003) http://www.esrl.noaa.gov/psd/data/timeseries/AMO/	**Atlantic Multidecadal Oscillation Index** North Atlantic SSTA averaged across 0–60°N, 75–7.5°W; 1871–2003 Monopolar SSTA pattern N. Atlantic
AMM	Chiang and Vimont (2004) http://www.cdc.noaa.gov/Timeseries/Monthly/AMM/ www.aos.wisc.edu/~dvimont/Research/MModes/Data/AMM.txt	**Atlantic Meridional Mode Index** SST projected onto 10-m wind field 21°S to 32°N; 74°W to 15°E;; SST gradient across Intertropical Convergence Zone (ITCZ) in Atlantic. (proxy for position of Atlantic ITCZ) (Observations available from 1949)
AT	Vangenheim (1940); Girs (1971) http://alexeylyubushin.narod.ru/ lyubushin@yandex.ru	**Atmospheric-Mass Transfer Anomaly Index** Dominance of air transfer direction 30°–80°N; 45–75°E; Proxy for atmospheric-heat transfer; reflects longitudinal/latitudinal shifts in position of atmospheric centers-of-action, w/ implications for hemispheric communication of climate signal.
NAO	Hurrell (1995) http://www.cgd.ucar.edu/cas/jhurrell/indices.data.html#npanom	**North Atlantic Oscillation Index** Normalized SLP difference Azores and Iceland ~ 1st PC (Principal Component) of SLP in the North Atlantic; re-distribution of atmospheric mass b/n subpolar and subtropical latitudes, reflecting jet-stream variations.
NHT	Jones & Moberg (2003); Rayner et al., (2006) ftp://ftp.cru.uea.ac.uk/data http://www.cru.uea.ac.uk/cru/data/temperature/hadcrut3nh.txt	**Northern Hemisphere Temperature** Average surface land and sea-surface temperatures of Northern Hemisphere 1850–2003 NHT characterizes overall climate variability, with strongest changes occurring at high northern latitudes.
NINO3.4	Calculated from the HadSST1 http://www.cdc.noaa.gov/gcos_wgsp/Timeseries/Data/nino34.long.data	**El Nino/Southern Oscillation Region 3.4** Average SSTA 5°N–5°S; 170°W –120°W Proxy for ENSO behavior
NPGO	Di Lorenzo et al. (2008) http://www.o3d.org/npgo/data/NPGO.txt http://eros.eas.gatech.edu/npgo/	**North Pacific Gyre Oscillation Index** 2-nd PC of SSH in NE Pacific. Measures changes in North Pacific gyre circulation (observations available since 1950)

NPO	Rogers (1981); Walker and Bliss (1982); Wang et al. (2007) wanglin@mail.iap.ac.cn cw@post.iap.ac.cn	**North Pacific Oscillation** Meridional dipole in SLP over North Pacific; pressure variations b/n Hawaii and Alaska/Alberta, reflective of meridional re-distribution of atmospheric mass. We used that of Wang et al. 2007: 2nd EOF SLPA 100ºE - 120ºW, 0º-90ºN.
OHCA300 **OHCA700**	Willis et al. (2004) jwillis@pacific.jpl.nasa.gov http://www.nodc.noaa.gov/OC5/DATA_ANALYSIS/basin_data.html	**Ocean-Heat-Content Anomaly Indices** Measured in North Pacific for 0 to 300m & 0 to 700m upper layers May serve as proxies for ocean-dynamic-induced SST variations (since these are presumably not confined to the oceanic mixed layer, while those caused by atmosphere-ocean heat flux are). (Observations available since 1955)
PDO	Mantua et al. (1997); Minobe (1997, 1999) ftp://ftp.atmos.washington.edu/mantua/pnw_impacts/INDICES/PDO.latest	**Pacific Decadal Oscillation Index** Leading PC of SSTA north of 20°N in North Pacific, with century-scale globally averaged SSTA removed; Strongly related to intensity and location of Aleutian Low
PMM	Chiang and Vimont (2004) http://www.cdc.noaa.gov/Timeseries/Monthly/PMM www.aos.wisc.edu/~dvimont/Research/MModes/Data/PMM.txt	**Pacific Meridional Mode Index** Anomalous meridional SST gradient across the Intertropical Convergence Zone (ITCZ) in the Pacific; proxy for Pacific ITCZ position; MCA of SST and 10-m winds 32ºN to 21ºS, 175ºE to 95ºW. (observations available since 1949)
PNA	Wallace and Gutzler (1981); Bell and Halpert (1995); Overland et al. (1999) http://www.jisao.washington.edu/data/pna/ http://www.cpc.ncep.noaa.gov/products/precip/CWlink/pna/norm.pna.monthly.b5001.current.ascii	**Pacific North American Pattern Index** Time series related to combination of standardized 500-hPa geopotential height values (Z) in four centers (Wallace and Gutzler 1981); upper tropospheric pattern associated with PDO; associated with intensity variations and longitudinal shifts of the Aleutian Low and with strength and eastward extent of the East Asian jet. PNA = 0.25 * [Z(20N,160W) - Z(45N,165W) + Z(55N,115W) - Z(30N,85W)]. (Observations available since 1951)
WP	Wallace and Gutzler (1981) http://www.beringclimate.noaa.gov/data/	**West Pacific Pattern Index** Difference in the normalized 500-hPa height anomalies between two points (60°N, 155°E and 30°N, 155°E); upper tropospheric pattern associated with NPO. Involves latitudinal shifts of AL, with resulting influence on oceanic-gyre frontal boundary and western-boundary dynamics – a potential "hotspot" of oceanic-atmospheric coupling (Sugimoto and Hanawa 2009; obs. since 1950)

We focused on boreal winter — the period when seasonally sequestered SST anomalies re-emerge (Alexander and Deser 1995), thereby enhancing conditions for potential oceanic–atmospheric coupling. Allied with this goal, the majority of our indices represent the months DJFM. Exceptions include AMO, AT, and OHC, which are annual; this due to logistics of data acquisition, with expectation of minimal impact on results.

Gapless time series of all eight primary indices over the 20th century period (1900–1999) are available[3]. Records are less extensive for the complementary set of seven indices — available for only the second half of the 20th century. To in-fill missing values, we used a covariance-based iterative procedure (Schneider 2001; Beckers and Rixen 2003; Kondrashov and Ghil 2008) described in section 2.2.3.2. This procedure assumes co-variability-statistics between continuous and gapped indices remain uniform throughout the century. Therefore, some detected relationships among reconstructed indices in the first half of the 20th century may partially reflect statistical co-dependencies of late 20th century indices. We guard against interpreting such relationships in dynamical ways (see section 2.3.2). Prior to analysis, all raw indices were linearly detrended and normalized to unit variance.

2.2.3 Methodology

2.2.3.1 Spatiotemporal filtering and climate-signal identification

Compact description of dominant variability implicit in the multi-valued index time series described in section 2.2.3 was accomplished by disentangling the lagged covariance structure of this data set via Multichannel Singular Spectrum Analysis (M-SSA: Broomhead and King 1986; Elsner and Tsonis 1996; Ghil et al. 2002). M-SSA is a generalization of the more widely used Empirical Orthogonal Function (EOF; Preisendorfer 1988) analysis. M-SSA excels

[3] This was one of the reasons to consider these as our primary subset.

over EOF analysis in its ability to detect lagged relationships characteristic of propagating signals and has been used extensively to examine various climatic time series (Vautard and Ghil 1989; Ghil and Vautard 1991; Vautard et al. 1992; Moron et al. 1998; Ghil et al. 2002 and references therein).

M-SSA is, in fact, EOF analysis applied to an extended time series, generated from the original time series, augmented by *M* lagged (shifted) copies thereof. In M-SSA terminology, each of the multivalued index time series (e.g., AMO, NAO, etc.) is referred to as a channel. Because each multivalued index time series represents a spatial region, eigenfunctions of this extended lagged covariance matrix provide spatiotemporal filters, which define modes that optimally describe lagged co-variability of the original multivariate data set — analogous to EOFs optimally describing zero-lag co-variability.

M-SSA modes are represented in the original index space by their reconstructed components (RC). Each RC is effectively the narrow-band filtered version of an original multivariate time series, whose filters are related to coefficients (EOF weights) of M-SSA decomposition of the time series under consideration. In contrast to principal components (PCs) of EOF analysis, RCs are not mutually orthogonal, but their sum across all M-SSA modes is identical to the original time series. We identify leading M-SSA modes with our climate signal and use the sum of their RCs to visualize variability associated with this climate signal.

2.2.3.2 Treatment of missing data

As mentioned in section 2.2.2, records are complete for the eight indices in the original subset, yet are limited for the seven indices comprised in our complementary set — these are available only since about 1950. M-SSA can be used to infill incomplete data sets; hence, we

applied this technique to our extended set of 15 climate indices. The imputation procedure was developed in Beckers and Rixen (2003) and Kondrashov and Ghil (2008); it is a simpler version of the method proposed by Schneider (2001). At the initial stage, missing values of each index were replaced by this index's time mean, which was computed over available data points. Anomalies associated with this stage's "climatology" were formed, followed by application of M-SSA to the resulting anomaly field. Time series in channels with missing data were then reconstructed (data at points with actual data were not changed). Only the first N M-SSA RCs were retained, where N was chosen to correspond to the number of modes that account for a certain fraction (we use 90%) of the full data set's variability. Remaining modes were regarded as noise and did not participate in the reconstruction. At the next iteration, the climatology based on a newly computed index time series was subtracted from the corresponding indices. The procedure was repeated until convergence, i.e., until in-filled data values stop changing within 10% of their standard error. Results of the data infilling were insensitive to the M-SSA window used, for window sizes M=10, 20, 30, and 40.

We stress our caution in interpretation of statistical relationships found between in-filled indices in the first part of the 20th century. These relationships will be considered real only if their counterparts exist in the late 20th century.

2.2.3.3 Assessing statistical significance of stadium-wave-related cross-correlations

We tested statistical significance of M-SSA identified multidecadal modes (section 2.3.1) and that of cross-correlations between interannual-to-interdecadal climate indices (section 2.3.2) using two different stochastic models. The first model is a red-noise model fitted independently to each index considered. It has the form

$$x^{n+1} = ax^n + \sigma w, \qquad (1)$$

where x^n is the simulated value of a given index at time n; x^{n+1} is its value at time $n+1$; w is a random number drawn from the standard normal distribution with zero mean and unit variance, while parameters a and σ are computed by linear regression. Model (1) produces surrogate time series characterized by the same lag-1 autocorrelation as the original (one-dimensional) data. However, by construction, true cross-correlations between surrogate time series of different indices are zero at any lag. Nonzero cross-correlations between these time series are artifacts of sampling due to finite length of the time series considered. Observed correlation between any pair of actual time series is considered to be statistically significant only if it lies outside of the envelope of correlation values predicted by multiple surrogate simulations of this pair generated by model (1).

The second model is a multivariate, two-level extension of model (1) [Penland 1989, 1996; Penland and Ghil 1993; Kravtsov et al. 2005]. Construction of this second model was based on 15-index *anomalies with respect to the multidecadal signal* in order to concentrate on interannual-to-interdecadal, rather than multidecadal, variability. The model produces random realizations of the 15-valued climate-index anomalies with lag 0, 1, and 2-yr covariance structure (including cross-correlations between the indices), which is statistically indistinguishable from the observed covariance structure. We used this model to test if cross-correlations between members of our climate network, *computed over various sub-periods of the full time series* (see sections 2.2.3.4 and 2.3.2.2), exceeded sampling thresholds quantified by this model's surrogate realizations. In other words, we looked into non-stationary relationships between pairs of indices characterized by stronger-than-normal cross-index synchronization, depending on time segment analyzed. Our detailed methodology for this part of analysis is summarized in section 2.2.3.4.

2.2.3.4 Testing for abnormal short-term synchronizations within the climate network

Definition of synchronization measure: Network connectivity. We first computed absolute values of cross-correlations between pairs of observed indices among all 15 members of our climate network over a 7-yr-wide sliding window[4]. This window size was chosen as a compromise between maximizing the number of degrees of freedom in computing cross-correlations, while minimizing the time segment allotted in order to capture the characteristically brief duration of synchronization episodes (Tsonis et al. 2007; Swanson and Tsonis 2009). This procedure resulted in 100-yr time series for each of the 105 cross-correlations among all possible pairs of the 15 indices; for each of the 100 years, we stored these cross-correlation values in the lower triangular part of the 15×15 cross-correlation matrix, with all other elements of this matrix being set to zero. We then defined the *connectivity* of our climate index network for a given year as the leading singular value of the Singular Value Decomposition (SVD; Press et al. 1994) of the above cross-correlation matrix, normalized by the square root of the total number of nonzero cross-correlations in this matrix (which equaled to 105 for the case of the full 15-index set). The connectivity defined in this way described a major fraction (typically larger than 80%; not shown) of the total squared cross-correlation within the network of climate indices, while providing a more robust measure of synchronization than the raw sum of squared correlations (cf. Swanson and Tsonis 2009). The maxima of connectivity time series defined local episodes of the climate network synchronization.

Identification of synchronizing subsets. Not all members of the climate network contribute equally to various synchronization episodes. To identify index subsets that maximize synchronization measure during such episodes, we employed the following re-sampling

[4] The M-SSA-defined multidecadal signal subtracted from indices prior to computing cross-correlations.

technique. We randomly drew a subset of K different indices (K varied from 6 to 10) from the full set of 15 indices and computed 100-yr long connectivity time series based on this subset. We repeated this procedure 10,000 times, producing 10,000 100-yr long connectivity time series. We then identified indices and years for which the connectivity value, based on at least one subset including this index, exceeded 95^{th} and 99^{th} percentiles of all connectivities that were based on the entire combined set of (100 yr) $\times$(10,000 samples) surrogate connectivity values.

Statistical significance of synchronizations. To estimate statistical significance of synchronizations, we produced 1000 random realizations of the 15-valued climate-index time series using the second stochastic model described in section 2.2.3.3. While these surrogates mimic actual observed indices in the overall (climatological) covariance structure, they, by construction, are mathematically unaware of the magnitude and/or phasing of the multidecadal signal that was subtracted from the original data.

Connectivity time series for surrogate indices were then computed for each of the 1000 realizations in the same way as for the original data. The 95^{th} percentile of surrogate connectivity for each year defines the 5% *a priori* confidence levels. These levels should be used if one tests for some pre-defined years in the climate record being characterized by statistically significant synchronizations.

If no such a priori reasons exist, one has to use *a posteriori* confidence levels, which can be defined as follows. For each synthetic realization, we determine the maximum value of connectivity *over the entire 100-yr period*; repetition of this procedure for all stochastic realizations results in 1000 values of maximum surrogate connectivities. The 95^{th} percentile of these maximum surrogate connectivities gives the 5% *a posteriori* confidence level for rejection

of the null hypothesis stating that connectivity for each year is statistically the same as its true stationary value based on the correlation matrix computed over the entire 100-yr period.

2.3 Results

2.3.1 Multidecadal "stadium wave"

Individual and cumulative variances of M-SSA modes for the main set of eight climate indices are shown in **Figs. 2.1**a, b. The leading pair of modes is well separated from the others according to the North et al. (1982) criterion. For the latter estimation, we have computed the number of effective temporal degrees of freedom N^* in our data set using the Bretherton et al. (1999) formula $N^* = N(1-r^2)/(1+r^2)$, where N=100 is the length of the time series, and $r \approx 0.65$ is the maximum lag-1 autocorrelation among our set of eight indices. We will hereafter identify this statistically significant leading M-SSA pair with our climate "signal." This dominant M-SSA pair *is unlikely to be due to random sampling of uncorrelated red-noise processes*, since it accounts for a substantially larger variance [exceeding the 97th percentile – upper dashed line in panel (a)] of the corresponding surrogate spectra generated by model (1).

Normalized RCs corresponding to joint M-SSA modes 1 and 2 are shown in **Fig. 2.2**; note that the reconstructions of *negative* NHT and AMO indices are displayed. Visual inspection of these RCs indicates they are dominated by a multidecadal climate signal with the time scale of about 50–80 yr. Maximum-entropy spectral analysis (Press et al. 1994) of each of these RCs centers on the period of the broadband variability identified at about 64 yr, indicative of long time scales associated with ocean dynamics.

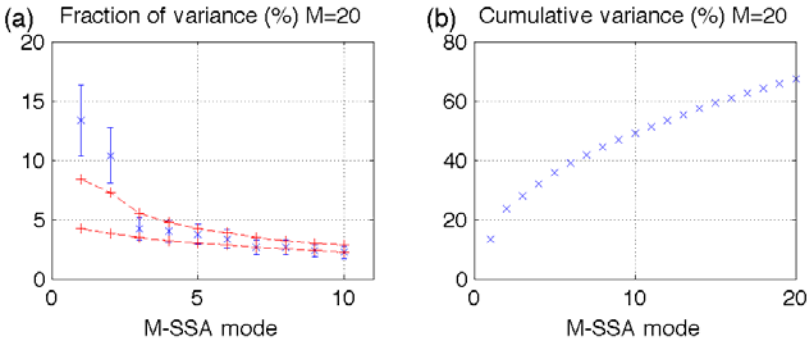

Fig. 2.1: M-SSA spectrum of the network of eight climate indices (see text): (a) Individual variances (%); (b) cumulative variance (% of the total). The M-SSA embedding dimension (window size) *M*=20. The error bars in (a) are based on North et al. (1982) criterion, with the number of degrees of freedom set to 40, based on the decorrelation time scale of ~2.5 yr. The +-symbols and dashed lines in panel (a) represent the 95% spread of M-SSA eigenvalues base on 100 simulations of the eight-valued red-noise model (1), which assumes zero true correlations between the members of the 8-index set.

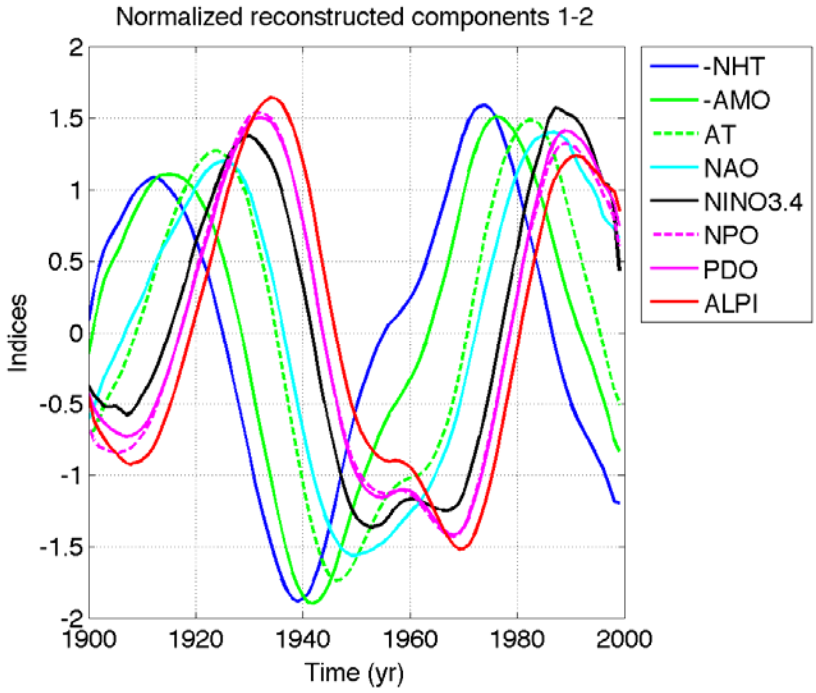

Fig. 2.2: Normalized reconstructed components (RCs) of the eight-index network. The RC time series shown have been normalized to have a unit variance. The indices are synchronized at, generally, non-zero lags, except for the indices NPO and PDO indices, whose rescaled RCs are virtually identical. Note that the reconstructions of *negative* NHT and AMO indices are displayed.

Our climate signal accounts for a substantial fraction of variance in several indices: NHT, AMO, PDO, and AT (see the values corresponding to zero low-pass filter time scale in **Fig. 2.3**a).

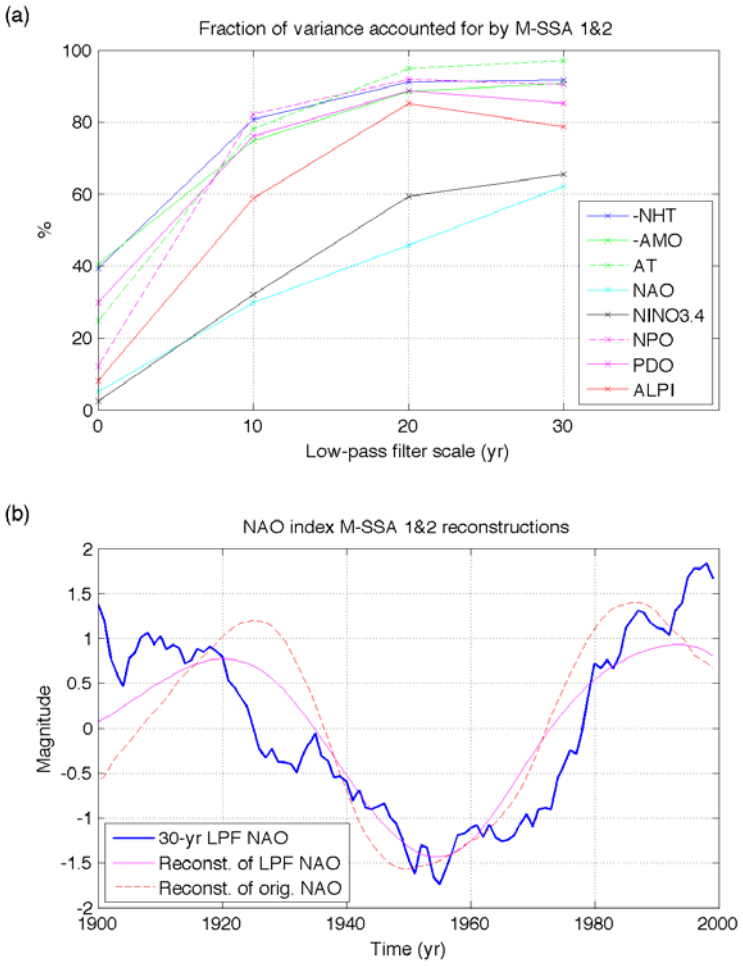

Fig. 2.3: (a) Fraction of each index variance (%) accounted for jointly by M-SSA modes 1 and 2, as a function of the low-pass filter time scale (yr). Boxcar low-pass filtering has been applied to each index prior to the M-SSA analysis; the value of 0 corresponds to no prior low-pass filtering (the normalized RCs for this case are shown in Fig. 2.2), the values 10, 20, and 30 indicate 10-yr, 20-yr, and 30-yr running-mean boxcar filtering. (b) Filtered NAO time series: heavy line — 30-yr running-mean boxcar filtered time series; light line — reconstruction based on M-SSA modes 1 and 2 of the 30-yr low-pass filtered 8-index set; dashed line — reconstruction based on M-SSA modes 1 and 2 of the raw 8-index set (the same as in Fig. 2.2). All time series have been normalized to have unit variance.

This latter manifestation (AT) demonstrates a clear atmospheric response to ocean-induced multidecadal climate variations. On the other hand, fractional weakness of the multidecadally varying climate signal exists in NAO, ALPI, NPO, and NINO3.4; these are dominated by shorter-term fluctuations. Despite dominance of higher frequency behavior in the NAO, ALPI, NPO, and NINO3.4 modes, M-SSA still identifies within these indices a statistically significant, coherent multidecadal signal.

To demonstrate robustness of these results, we repeated M-SSA analysis using the running-mean boxcar low-pass filtered indices. We used three filters, with sliding window sizes of 10, 20, and 30 years. Ends of the data series are processed using shorter-filter-size running means and one-sided (or asymmetric) filters. Fraction of variance accounted for by the leading M-SSA pair of low-pass filtered data generally increases with scale of low-pass filter, the fractional increase of variance being most dramatic for ALPI, NPO, NAO, and NINO3.4 (Fig. 2.3a). Normalized RCs of the leading M-SSA mode of low-pass filtered indices are close to their counterparts obtained via M-SSA analysis of raw indices. Fig. 2.3b shows this behavior in NAO. Note boxcar low-pass filtering is intrinsically characterized by a large phase error. This error is not entirely eliminated by M-SSA time–space covariance-based filtering, explaining shifts between the maxima and minima of filtered and raw RCs in Fig. 2.3b.

Figure 2.3b also illustrates well the distinction between M-SSA spatiotemporal filtering and time filtering, underscoring the former's advantage in analyzing climate data. Geophysical time series are typically characterized by presence of noise with substantial power in the low-frequency portion of the spectrum — the so-called red noise. Low-pass time filtering of a synthetic mixture of quasi-periodic time series with a strong red-noise component may erroneously reflect spurious low-frequency variability that has little to do with the shape of the

actual quasi-periodic signal used to construct this time series. On the other hand, if the quasi-periodic signal is characterized by a coherent spatial structure that is distinct from noise, and if multivariate time series representing geographically diverse indices possessing this signal are available, separation of signal from noise is more robust (see Ghil et al. 2002 for further details). Note M-SSA reconstruction of low-pass filtered NAO index in Fig. 2.3b (light solid line) does not follow exactly excursions of the original low-pass filtered NAO index (heavy solid line). Deviations from purely temporal filtering reflect corrections resulting from M-SSA, which relies on cross-index lagged correlations of the dominant multidecadal signal.

To confirm a truly multivariate nature of the leading M-SSA signal, we employed the following bootstrap procedure. We randomly generated multiple (~15,000) combinations of the eight primary indices and applied M-SSA to each randomly assembled set, resulting in multiple sets of eight-valued RC time series — in some cases with certain indices being repeated, and others being omitted. For each of the eight indices, this procedure resulted in 10,000 sets of RC time series corresponding to leading M-SSA pairs of random index sets. Any statistical characteristic based on RCs of the original index set can also be computed for surrogate sets. The latter estimates can be used to assess the expected spread of statistical quantities computed. For example, the bootstrap-based estimate of dominant timescale of the leading M-SSA signal produces the mean value of 63 yr, with the standard uncertainty of ±5 yr and 95% confidence interval close to twice the standard uncertainty. These estimates are thus consistent with results of the original eight-index analysis. *Robustness of bootstrap-based M-SSA reconstructions highlights lagged co-variability among the entire set of eight indices; the leading M-SSA signal is not "dominated" by the variability in a particular M-SSA channel (say, NHT or AMO).*

It is apparent from Fig. 2.2 that the climate-signal indices are correlated at nonzero lags, except for the normalized RCs 6 (NPO) and 7 (PDO), which turned out to be virtually identical. We objectively determined the lead–lag relationships between the RCs using the cross-correlation analysis (not shown), which unambiguously identifies, based on maximum cross-correlation, the order of RCs in the "stadium wave" propagation across the phase space of the reconstructed climate indices. The phase of each RC in the stadium-wave sequence was computed by least-square fitting two-predictor time series $\{\sin(2\pi t/64),\cos(2\pi t/64)\}$, with t changing from 0 to 100, to each of the RCs. The following phase shifts between the "adjacent" RC pairs resulted:

–NHT →(4 yr)→ –AMO →(7 yr)→ AT →(2 yr) → NAO →(5 yr)→ NINO3.4 (3 yr)→ NPO/PDO →(3 yr)→ ALPI →(8 yr)→ NHT →(4yr)→ AMO → (7 yr)→ –AT →(2 yr)→ –NAO →(5 yr)→ –NINO3.4→ (3 yr)→ –NPO/PDO→ (3 yr)→ –ALPI→ (8 yr)→ –NHT.

This "stadium wave" is summarized as a Hoffmuller diagram in **Fig. 2.4**. The complete cycle of the stadium wave has naturally a period of 64 yr, and a bootstrap-based standard uncertainty of ±5 yr. The bootstrap-based estimates of the above lags and their uncertainties are listed in **Table 2.2**. Note that the fractional uncertainties vary considerably from one transition leg to another, due mainly to differences in mean duration of various transitions in the presence of fairly uniform absolute uncertainty. This describes the case for all but the –NHT→–AMO and –AMO → +AT transitions, which involve indices strongly dominated by low-frequency anomalies. Uncertainty of lag-time between these indices is smaller than that associated with index pairs involving noisier raw indices.

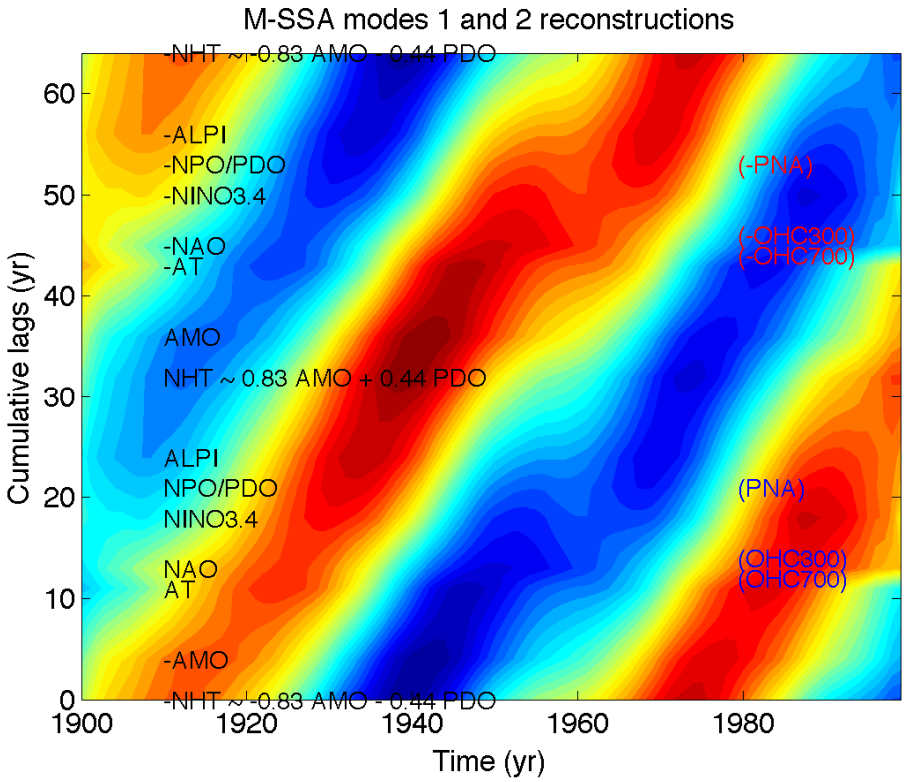

Fig. 2.4: Hoffmuller diagram of the "stadium-wave" propagation in the phase space of normalized RCs (for M-SSA modes 1 and 2 combined) of the extended set of 15 multidecadal indices (eight of the indices were described above, while the other seven indices are NPGO, OHC700, OHC300, PNA, WP, PMM, and AMM: see **Figs. 2.5, 2.6** and text). For the additional indices, only the ones with substantial fraction of variance within leading pair of RCs (see Fig. 2.5) are shown. The horizontal cross-section in locations marked by index names shown on the left for the original eight indices, and on the right for the additional indices would represent time series of the corresponding index as plotted in Figs. 2.2 and 2.5. The indices are sorted from bottom to top of the figure in the order determined by cross-correlation analysis, while the vertical "distance" between each index equals the lead time of maximum cross-correlation between adjacent indices. Negative indices are also included to show one complete cycle (with the estimated period of 64 yr) of the stadium-wave propagation.

Table 2.2: The stadium-wave lags and their uncertainties (yr) estimated using a bootstrap procedure (see text). The time scale *T* of the observed stadium-wave cycle is given by twice-the-sum of the first-row values, while its standard uncertainty — by the square root of twice-the-sum of the second row's squared values. These calculations result in the estimate of *T*=63±5 yr, consistent with the 64-yr scale obtained in the 8-index (and 15-index) M-SSA analyses.

	–NHT → –AMO	AMO → AT	AT → NAO	NAO → NINO3.4	NINO3.4 → NPO/PDO	NPO/PDO → ALPI	ALPI → NHT
Mean	4.3	6.8	2.4	4.8	2.4	2.9	8.2
STD	0.5	0.4	1.3	1.6	1.1	1.3	1.2
½ 95%	0.5	0.5	2.5	3.0	2.0	2.5	2.0

M-SSA results for the extended data set support those of the original stadium-wave analysis. Leading M-SSA modes 1 and 2 describe the multidecadal stadium wave, with no modification of phase relationships between the original eight indices (Fig. 2.4 and **Fig. 2.5)**. While all 15 indices reflect the dominant multidecadal signature, a stronger high-frequency component characterizes most of the seven complementary indices, rendering their fractional variance of the stadium-wave signal weak. Only those with strong fractional variance — PNA and OHC300/700 — are displayed in the Hoffmuller diagram in Fig. 2.4. OHC700 exhibits the strongest fractional variance among the trio from the complementary indices, with a strong multidecadal component nearly in phase with that of the AT index. OHC300, on the other hand, exhibits a much lower fractional variance and its phasing is close to the NAO and NINO3.4 multidecadal signals. These observations invite speculation that ocean-heat-content variability at various depths within the subsurface North Pacific is governed by different dynamical processes related to indices within the stadium-wave network (see also discussion in section 2.4.2).

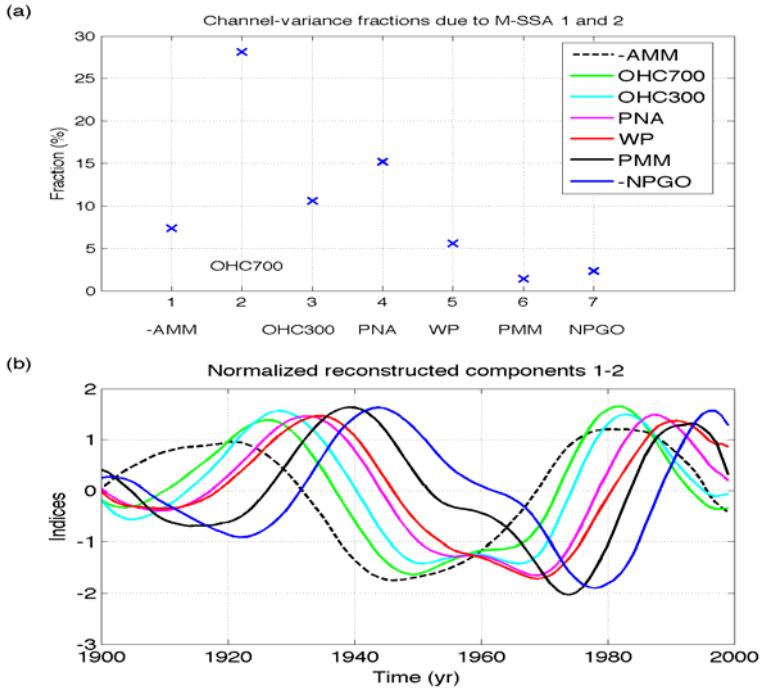

Fig. 2.5: The M-SSA results based on the analysis of the full 15-index data set. The quantities shown describe the statistics of the seven climatic indices considered in addition to the original 8-index set (see Figs. 2.2 and 2.3). (a) Fraction of raw-index variance accounted for jointly by M-SSA modes 1 and 2 (Fig. 2.3a shows this quantity for the original eight indices). (b) The same as in Fig. 2.2, but for the additional seven climate indices [see panel (a) and figure legend for abbreviated index names].

2.3.2 Interannual-to-interdecadal variability

2.3.2.1 Variability unrelated to the stadium wave

To extract a residual signal from our 15 indices, we subtract the multidecadal signal (**Fig. 2.6**, blue lines) associated with the stadium wave. This forms a network of climate indices (Fig.2.6, red lines) that emphasizes higher-frequency, interannual-to-interdecadal climate variability.

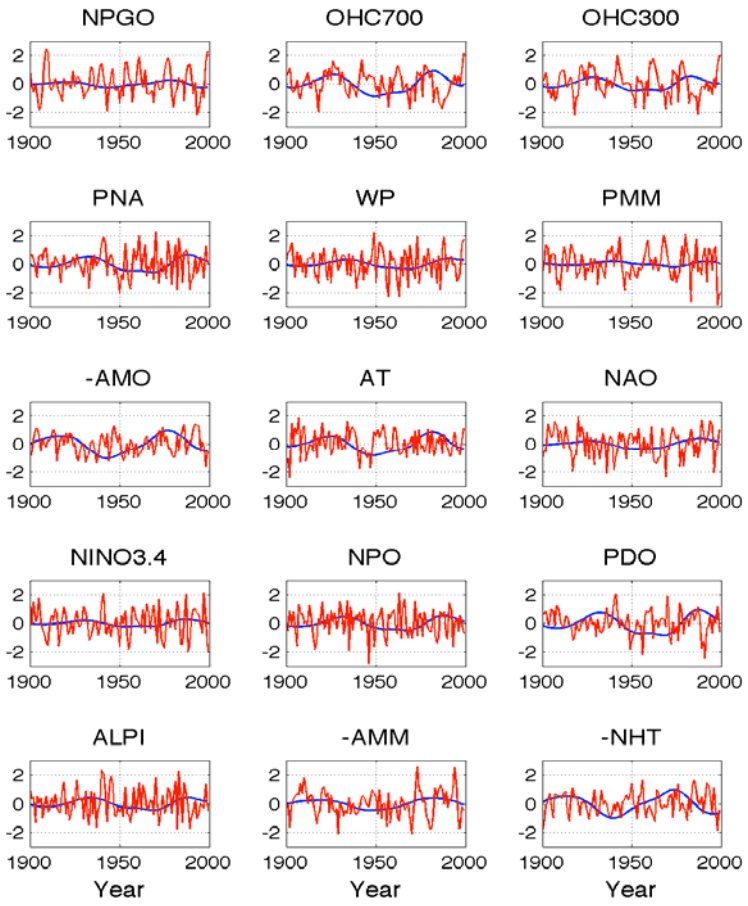

Fig. 2.6: The network of 15 climate indices: (i) M-SSA modes 1 and 2 RCs (blue); and (ii) anomaly with respect to the corresponding RC (red). The blue and red lines give the raw climate index (detrended and normalized to have a unit variance). The abbreviated index names are given in panel captions.

To study possible connections within this network, we first identify statistically significant (lagged) cross-correlations between index anomalies so computed (see **Table 2.3**). *A posteriori* significance levels were determined for each index pair using surrogate indices simulated by the red-noise model (1); see section 2.2.3.3. We computed maximum lagged correlations (using the entire 100-yr time series and over a range of all possible lags) for 100 sets of surrogate index time series, followed by sorting these correlations in ascending order, taking the 99th sorted values as the 1% significance level.

Table 2.3: Maximum lagged correlations (with corresponding lags) between climate indices computed over the full 100-yr 20th century record, as well as over its second half (1950–1999); the latter correlation values are shown in parentheses. Only the correlations that are statistically significant at 5% *a posteriori* level for *both* of these periods — relative to the null hypothesis of zero correlation at any lag — are shown. Correlations equal or exceeding 0.5 (upon rounding up) are in bold font. The negative lags correspond to the column-member of an index pair leading its corresponding row member[*]. For example, the maximum lagged correlation between NINO3.4 and PNA is equal to 0.47 (0.54 during the second half of the 20th century), with NINO3.4 leading by 1 yr.

	NPGO	OHC 7	PNA	WP	AMO	NAO	NINO 3.4	PDO
OHC3		**0.9 (0.9), 0**						
PMM	**–0.54 (–0.52), 0**							
NINO3.4			0.47 **(0.54)**, –1	**0.52** (0.49), –1				
NPO				0.45 (0.46), –1			0.36 (0.48), 0	
PDO			**0.75 (0.76), 0**				0.41 **(0.52)**, 1	
ALPI			**0.77 (0.86), 0**					**0.55 (0.64), 0**
AMM					**0.54 (0.6), 1**	**–0.57 (–0.52), 0**		
NHT			0.42 (0.44), 0		**0.66 (0.74) 0**			

Analysis results of high-frequency variability of the residual signal point to a Pacific-centered subset of indices — PNA, PDO, ALPI, NINO3.4, WP, NPO — whose members exhibit behavior similar to one another (that is, they are correlated at zero or one-year lags). Guided by this observation, we applied M-SSA to this select group of indices as a way to verify suspected

[*] Note: "column-members" arranged in the leftmost column; "row-members" arranged in the top row.

relationships among them and to more graphically describe the cross-correlations between them. Relationships identified in cross-correlation analysis are corroborated by M-SSA results (**Figs. 2.7** and **2.8**). In particular, we find NINO 3.4 and NPO correlated at zero lag; although the low fractional variance of NPO suggests caution regarding its degree of uncertainty. The same is true for WP (see section 2.4.3). NINO3.4 and NPO lead others within this subset by one year, with the typical time scale of variability being on the order of three to four years. Based on time scale and spatial confinement, behavior of the Pacific-centered set has strong association with ENSO.

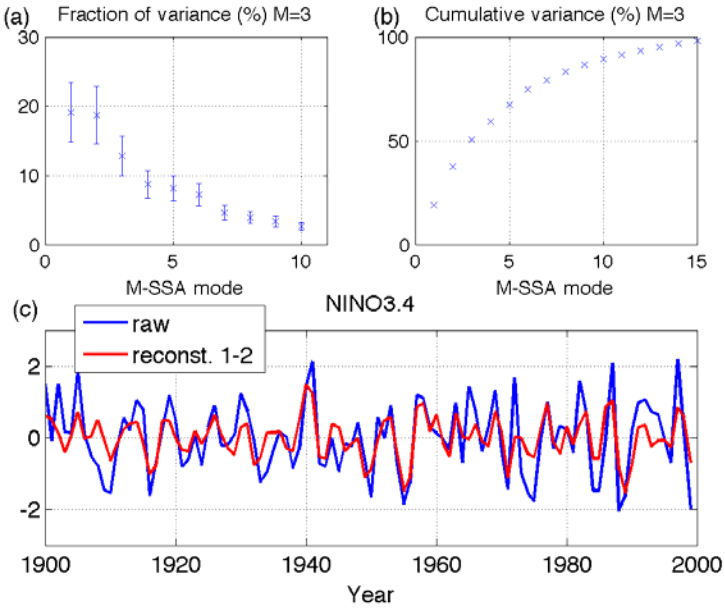

Fig. 2.7: M-SSA spectrum of the Pacific-centered multi-index set consisting of interdecadal anomalies (Fig. 2.6, red lines) of PNA, WP, NINO3.4, NPO, PDO, ALPI indices. The bottom panel shows raw time series of the NINO3.4 index and its RC based on M-SSA modes 1 and 2.

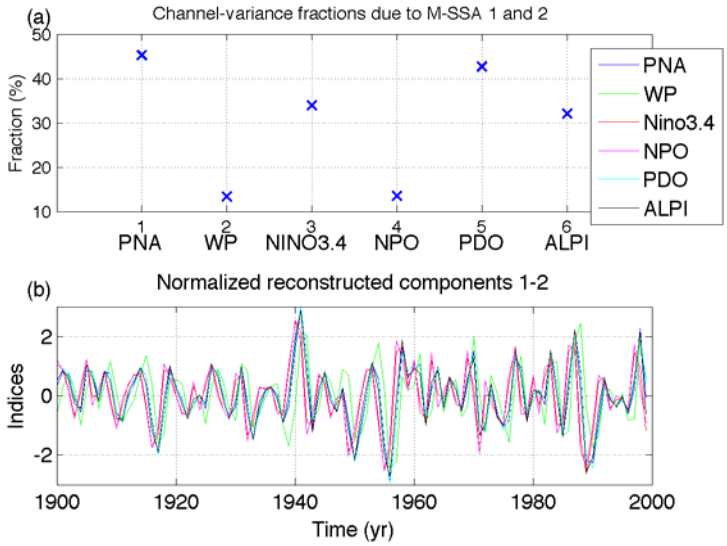

Fig. 2.8: The M-SSA results for the Pacific-centered index subset (see Fig. 2.7). See panel legend for abbreviated index names. Same conventions as in Fig. 2.5.

These results are not surprising or novel. However, they do demonstrate that the network approach we took is sound, as it corroborates previous findings by other researchers on ENSO teleconnections.

Another statistically significant cross-index relationship identified includes that between OHC700 and OHC300, which is, of course, not unexpected given the similar nature of the two indices. There is also the anti-correlation between the members of PMM/NPGO pair. Both of the latter indices are dominated by interdecadal anomalies (see Fig. 2.6). There is also a statistically significant positive simultaneous correlation between the interdecadal anomalies of AMO and NHT indices, demonstrating that the North Atlantic decadal-to-interdecadal SST anomalies directly explain a significant fraction of the NHT decadal-to-interdecadal variability. Finally, the cross-correlation analysis identifies substantial co-variability within the Atlantic-based index

trio: AMM, AMO, and NAO, thus suggesting interesting dynamical connections among various components of the coupled AMOC system.

2.3.2.2 Effects of the stadium wave on interannual-to-interdecadal climate anomalies

Next we wish to see if collective behavior of higher-frequency variability of the residual signal has a relationship with the stadium-wave multidecadal signal. This line of inquiry was motivated by work of Tsonis et al. (2007) and Swanson and Tsonis (2009). These authors identified five intervals within the 20th century during which certain climate indices abnormally synchronized — matching with strong statistical significance in both rhythm and phase of their interannual variability; the five intervals were centered at the years 1916, 1923, 1940, 1957, and 1976. Three of five synchronizations (1916, 1940, 1976) coincided with hemispheric climate-regime shifts, which were characterized by a switch between distinct atmospheric and oceanic circulation patterns, a reversal of NHT trend, and by an altered character of ENSO variability (intensity and dominant timescale of variability (Federov and Philander 2000; Dong et al. 2006; Kravtsov 2010, among others). As the authors had expected, based on synchronized chaos theory, these "successful" synchronizations (i.e., the ones preceding climate shifts) were accompanied by increased network coupling defined via the climate index network's phase-prediction measure. Two synchronizations *not* leading a climate-regime shift were *not* accompanied by increased network coupling. We observe here that the timing of the regime shifts has a multidecadal pace, consistent with the stadium wave; we are thus motivated to further explore synchronizations in our extended (compared to Tsonis et al.) climate network.

We first determine the years of abnormal synchronizations and synchronizing subsets within the main 15-index set using the methodology described in section 2.2.3.4. Results

presented in **Fig. 2.9** identify five time bands characterized by high connectivity values among the subsets of the full 15-index set; these bands are centered at years 1916, 1923, 1940, 1957 and 1976 — thus consistent with studies by Tsonis et al. Synchronizing subsets comprise the following indices (based on the 99th percentile of re-sampled sub-networks; see section 2.2.3.4): AMM, NAO, NPGO, PNA, WP, PDO for the 1916 subset; AMO, AMM, NAO, NPGO, PNA, ALPI for the 1923 subset; AMO, AT, NAO, PNA, PMM, ENSO, PDO, ALPI for the 1940 subset; PNA, ENSO, NPO, PDO, ALPI, NHT for the 1957 subset; and AMO, AT, NAO, OHC700, OHC300, PNA, WP, PDO ALPI, NHT for the 1976 subset.

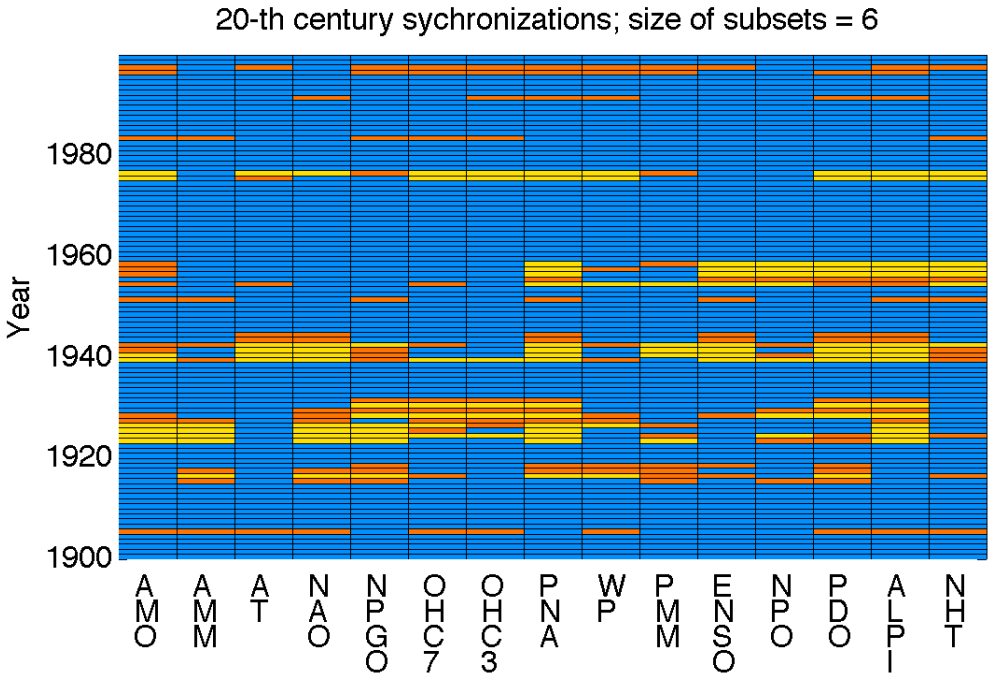

Fig. 2.9: Identification of index sub-networks. For a given year (on the vertical axis), bright yellow and orange cells indicate that there exists at least one six-index network that includes the index this cell represents (the indices are arranged along the horizontal axis), which is characterized by the network connectivity exceeding the 95th percentile of the connectivity for *all possible* 6-index networks and for *all years*; the yellow cells are characterized by the connectivity that exceeds the 99th percentile. See caption to Fig. 2.10 and text for the definition of network connectivity. The results for the subset sizes in the range from 4 to 8 (not shown) are analogous.

Connectivity time series computed for each subset exhibit statistically significant maxima during corresponding time bands (**Fig. 2.10**). While the statistical significance of connectivity maxima drops substantially if one accounts for degrees of freedom associated with possibility of drawing multiple index subsets of a given size from the full set of 15 indices, all of the connectivity maxima in Fig. 2.10 still exceed the 5% *a priori* levels in this case (not shown). The use of *a priori* levels may, in fact, be more appropriate for successful synchronization episodes, given the evidence for regime shifts and predictions of synchronized chaos theory that rationalize expected synchronizations preceding these shifts (Tsonis et al. 2007; Swanson and Tsonis 2009).

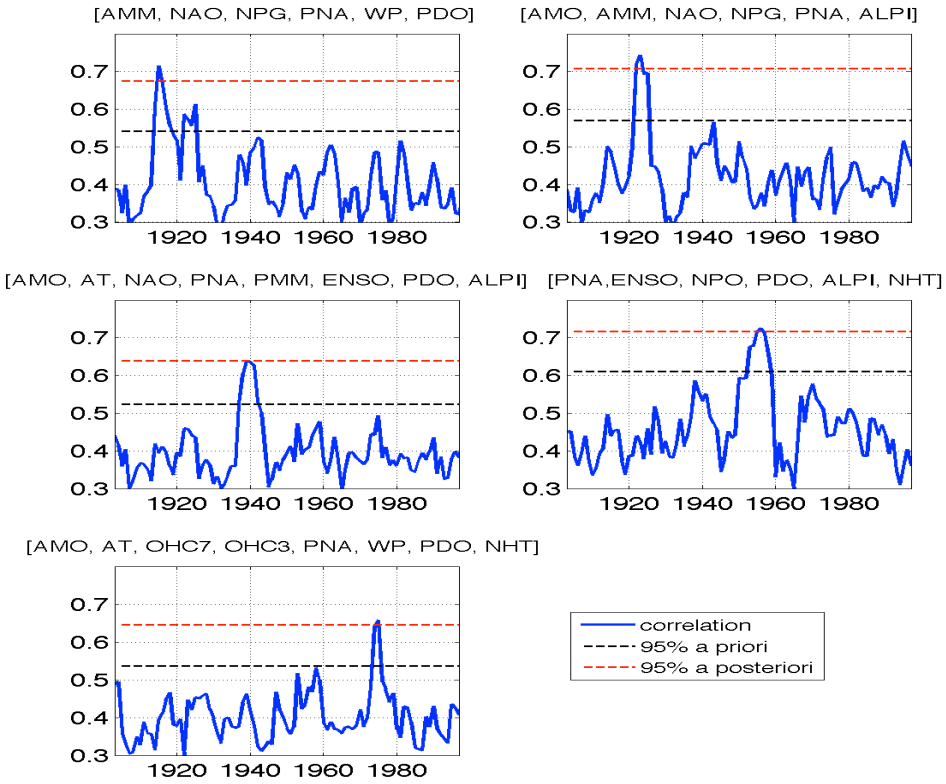

Fig. 2.10: The time series of index connectivity for the sub-networks identified in Fig. 2.9. The indices comprising each subset are listed in the caption of each panel. The measure of connectivity used here is the leading singular value of the lower triangular part of the index cross-correlation matrices computed over the 7-yr sliding window. The horizontal dashed lines indicate 5% a priori and a posteriori confidence levels based on the linear stochastic model that reproduces the *climatological* cross-correlations between the indices.

Our results here provide a more detailed picture of the 1916, 1940 and 1976 ("successful") synchronizations and expose differences between these three "successful" and two "unsuccessful" episodes (i.e., 1923 and 1957) in terms of index membership of corresponding synchronizing subsets. In particular, the 1957 episode is confined mostly within the Pacific; while the Atlantic reflects a greater influence during the 1923 synchronization. Successful synchronizations tend toward a more symmetrical contribution from both the Atlantic and Pacific sectors and PNA participates in all synchronizations. Note that timing between successful synchronizations, shifts between alternating periods of enhanced and diminished interannual variance of ENSO and NAO (**Fig. 2.11**), and the stadium-wave tempo share similar pace, thus suggesting possible stadium-wave influence on synchronizations within the climate network.

In summary, while our research on the interrelationships between the multidecadal signal and higher-frequency variability continues, the above results suggest that the major synchronization episodes and regime shifts of interannual-to-decadal climate variability all over the world are paced by the multidecadal climate variations originating in the North Atlantic (see section 2.4).

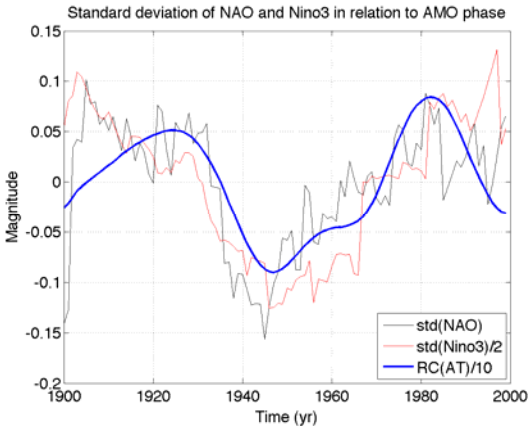

Fig. 2.11: Anomalies (with respect to the mean value of 1) of NAO (light black line) and Nino3 (light red line) standard deviations, along with the M-SSA mode's 1–2 RC of AT index (heavy blue line; this line is the same as that in the middle panel of Fig. 2.7, but multiplied here by a factor of 0.1). The Nino3 standard-deviation anomaly has been scaled by a factor of 0.5 for easier visual analysis. The standard deviations for each index shown were computed over the 31-yr-wide sliding window.

2.4 Summary and discussion

2.4.1 Summary

We considered the Northern Hemisphere's climate variability in a network of well-known indices describing climatic phenomena all over the Northern Hemisphere (NH). Our network approach — via data compression to a subspace of dynamically and geographically distinct indices — provides means to establish rigorous estimates of uncertainty associated with multidecadal variability observed in the instrumental climate records and to address the question of how likely these observed multidecadal teleconnections are to be due merely to random sampling of uncorrelated red-noise time series. Multi-channel Singular Spectrum Analysis (M-SSA) of this network (Figs. 2.1–2.5) identifies the dominant signal with a time scale of 50–80 yr, which propagates through the phase space of the indices considered as the "stadium wave" (Fig. 2.4, Table 2.2). In section 2.4.2 below, we interpret this stadium wave in terms of the sequence of atmospheric and multi-year-lagged oceanic teleconnections originating from the Atlantic Multidecadal Oscillation (AMO) — an extensively studied intrinsic oceanic mode associated with the variability of Meridional Overturning Circulation (MOC). The stadium-wave propagation is reflected in the NH area-averaged surface temperature signal, which explains, by inference, at least a large fraction of the multidecadal non-uniformity of the observed global surface temperature warming in the 20th century.

In section 2.3.2, we decomposed the climate indices into the stadium-wave multidecadal and shorter-term residual variability (Fig. 2.6). The dominant residual signal is the Pacific-centered suite of interannual ENSO teleconnections (Table 2.3 and Figs. 2.7 and 2.8). Results summarized in Table 2.3 also show that a major portion of the shorter-term (with respect to the stadium wave time scale), decadal-to-interdecadal variations of NH surface temperature (NHT)

is directly related to the corresponding variability of the North Atlantic sea-surface temperature (SST). In combination with the inferred AMO/NHT stadium-wave connections, these findings imply that the North Atlantic SSTs exert a strong influence on the hemispheric climate across the entire range of time scales considered.

One of the most intriguing findings that came out of our analysis is the apparent connection between the hemispheric climate regime induced by the stadium-wave dynamics and the character of interannual climate variability. In particular, the pacing of the stadium wave is consistent with the timing between the episodes of abnormal synchronization of Atlantic/Pacific teleconnections (Figs. 2.9–2.11). The termination of these synchronization episodes coincided with hemispheric climate-regime shifts characterized by the switch of the climate regime from the one characterized by the high ENSO variance (pre-1939), to the one with low ENSO variance (1939–1976), and back to the high ENSO variance regime (post-1976); see Fig. 2.11. The NAO interannual variance exhibits similar multidecadal variability, as shown in Fig. 2.11, suggesting Pacific–Atlantic feedback.

Thus, results presented in this note suggest that AMO teleconnections, as captured by our stadium-wave, have implications for decadal-scale climate-signal attribution and prediction — both significant to the developing field of climate research.

2.4.2 Discussion: Stadium-wave's hemispheric propagation

Statistical results developed above describe only co-variability within the climate-index network, not causality. We interpret these results based on a wide variety of observational and modeling studies, which rationalize the existence of the multidecadal climate signal — Atlantic Multidecadal Oscillation (AMO) — that originates dynamically in the North Atlantic Ocean and

propagates throughout the Northern Hemisphere via a suite of atmospheric and oceanic processes, or the stadium wave.

Inconsistent modeling results foil simple narrative, with dependency of the simulated low-frequency climate variability upon model configuration, initialization, and spatial resolution (Metzger and Hurlburt 2001; Yualeva et al. 2001; Kushnir et al. 2002; Kelly and Dong 2004; Minobe et al. 2008). Instrumental records, on the other hand, are short, and while they have been shown to reflect a multidecadal signature (Folland et al. 1986; Kushnir 1994; Schlesinger and Ramankutty 1994; Delworth and Mann 2000), their direct interpretation is difficult. These collective challenges are mollified somewhat by observations from proxy records (Mann et al. 1995, 1998; Black et al. 1999; Shabalova and Weber 1999; Gray et al. 2004), which do indicate the tendency of a diverse collection of paleo-climate indices to exhibit climate variability on a shared multidecadal cadence – a finding similar to ours.

Despite caveats of model studies, their results are instructive in context of our proposed stadium wave, describing potential mechanisms for climate-signal generation and its subsequent hemispheric propagation. Hypotheses for AMO origin often find common ground in the suspicion that AMOC plays a nontrivial role in generating and setting the pace of the AMO. Many models produce intrinsic interdecadal and multidecadal variability (Delworth et al. 1993; Delworth et al. 1997; Timmermann et al. 1998; Cubasch and Voss 2000; Delworth and Greatbatch 2000; Hilmer and Jung 2000; Eden and Jung 2001; Shindell et al. 2001; Bryden et al. 2005; Getzlaff et al. 2005; Delworth and Dixon 2006; Latif et al. 2004, 2006; Dima and Lohmann 2007; Vellinga and Wu 2004; Delworth et al. 2007; Msadek et al. 2010), although mechanisms behind the observed variations are still a matter of debate. Models with periodicities and boreal-winter atmospheric projections closest to observation seem to require a deep or

interactive ocean (Knight et al. 2005; Msadek et al. 2010b), underscoring the hypothesized AMO link to AMOC-related ocean dynamics.

The Atlantic SST Dipole — an index based on interhemispheric Atlantic SST anomalies — is thought to reflect AMOC-forced SST fluctuations related to the AMO (Black et al. 1999; Keenlyside et al. 2008). Motivated by this observation, we added the dipole to our MSSA mix of indices. What we found was the SST-dipole-index RC identical in phasing to that of the NHT RC. NHT leads AMO by about four years — and so does AMOC, according to the SST Dipole proxy. We also experimented with the addition of a paleo-proxy for the SST Dipole (*G.bulloides*; see Black et al. 1999) to our MSSA collection of indices and found, once again, the phasing identical to the NHT RC. Considering the collective evidence — the dipole phasing, paleo-proxy phasing, and model studies, we suggest the AMOC indeed plays a significant role in generating the AMO.

The AMOC generated multidecadal SST signal and its relationship with the overlying atmosphere: Bjerknes (1964) argued that long-term top-of-the-atmosphere radiative balance remains fairly constant and so is the total poleward heat transport accomplished by ocean and atmosphere. Therefore, when one vehicle of poleward heat transport weakens, the other strengthens to compensate, the phenomenon known as “Bjerknes Compensation.” Shaffrey and Sutton (2006) and Van der Swaluw et al. (2007) showed via modeling studies that Bjerknes compensation is operative in the northern North Atlantic Ocean, with maximum expression between 60ºN and 80ºN, on decadal and longer time scales. Note that the AMO SST index reflects the ocean surface signature of AMOC multidecadal variability and is thus not representative of the oceanic heat transport, which may exhibit decadal delays with respect to SST due to oceanic dynamical inertia (see, for example, Marshall et al. 2001a,b; Kravtsov et al.

2008, and references therein). Consistent with this notion, our results find that the –AMO index leads the AT index (related to atmospheric mass and heat transport) and NAO index (related to atmospheric mass) by 7 and 9 yr, respectively. This implies that oceanic/atmospheric heat transport has a minimum/maximum a few years after peak negative SST anomalies in the North Atlantic, with atmospheric transport causing NAO to peak shortly after. These timings are consistent with Msadek et al. (2010b).

Potential mechanisms transmitting the multidecadal SST signal to the overlying atmosphere: Mechanisms behind the North Atlantic SST anomalies' influence on the overlying atmosphere on decadal-to-multidecadal time scales, as suggested by the above energy-balance considerations, remain the subject of extensive research. For example, Kelly and Dong (2004) and Dong and Kelly (2004) found that strong basin-scale westerlies in both the North Atlantic and North Pacific co-occur with anomalously high ocean heat content and strong negative heat flux (out of the ocean) in the western-boundary currents and their extensions (see also Hansen and Bezdek 1996; Sutton and Allen 1997, McCartney 1997; Marshall et al. 2001a). These results argue that there exists a positive, reinforcing feedback on SST anomalies through oceanic modification of overlying atmospheric circulation (Palmer and Sun 1985; Latif and Barnett 1994, 1996; Kushnir and Held 1996; Rodwell et al. 1999; Latif et al. 2000; Mehta et al. 2000; Robertson et al. 2000; Czaja and Frankignoul 2002; Wu and Gordon 2002; Sutton and Hodson 2003; Wu and Rodwell 2004; Xie 2004; Xie and Carton 2004). Note, however, that details of this response are sensitive to the location of the heat source with respect to the mid-latitude storm track (Peng et al. 1997; Peng and Whittaker 1999; Peng and Robinson 2001; Czaja and Marshall 2001; Peng et al. 2002; Nakamura et al. 2004; Xie et al. 2004; Minobe et al. 2008), with

substantial inconsistencies among the models — see Kushnir et al. (2002) for a review and Msadek et al. 2010b.

Generation of the hemispheric response: Atlantic–Pacific teleconnections: A variety of models with prescribed AMO-related SSTs show consistent hemispheric response (Delworth et al. 1993; Kushnir 1994; Hakkinen 1999; Delworth and Mann 2000; Sutton and Hodson 2003; Sutton and Hodson 2005; Knight et al. 2006; Grosfeld et al. 2007; Sutton and Hodson 2007). Longitudinal and latitudinal migrations of atmospheric centers-of-action (COA) appear to govern circumpolar communication of regionally generated climate signals (Kirov and Georgieva 2002; Polonsky et al. 2004; Grosfeld et al. 2006; Dima and Lohmann 2007; Msadek et al. 2010b). Dominant direction of wind flow across the entire range of longitudes (AT) and inter-basin connectivity modify accordingly: Wang et al. (2007) find that COA migrations generate intervals when climate patterns over the North Pacific and over the Eurasian continent upstream are linked, as are regions downstream, via an enhanced PNA and an eastwardly extended jet stream. During these time segments of enhanced circum-hemispheric stationary wave patterns, ENSO influence on ALPI becomes secondary to mid-latitude dynamics (Wang et al. 2007). Latitudinal shifts in atmospheric COAs — strongly influenced by NPO/WP patterns (Sugimoto and Hanawa 2009; Frankignoul et al. 2011) — have also been shown to influence interdecadal-scale migrations of western-boundary-current extensions (oceanic-gyre frontal boundaries), with impact on western-boundary dynamics and air-sea interaction (Kwon et al. 2010; Frankignoul et al. 2011). These sets of processes, after accounting for interannual delays due to oceanic dynamical adjustment, rationalize the sequence of the hemispheric and Pacific centered indices in our stadium wave.

Other proposed mechanisms for conveying an Atlantic-born climate signal to the North Pacific include stability changes within the tropical thermocline (Dong and Sutton 2005; Dong et al. 2006; Zhang and Delworth 2005, 2007; Zhang et al. 2007; Timmermann et al. 2007) and latitudinal shifts of Intertropical Convergence Zones (ITCZ) (Vellinga and Wood 2002; Vellinga and Wu 2004; Vimont and Kossin 2007). Tropical Pacific multidecadal changes may further modify the North Pacific response to AMO via an atmospheric bridge (Lau and Nath 1994; Deser and Blackmon 1995; Zhang et al. 1996). All the while, the AMOC continues its quasi-oscillatory behavior; the related AMO teleconnection sequence evolves accordingly. Possibly the Pacific communicates back to the Atlantic via tropical connections; this hypothesis will be addressed in a future study.

2.4.3 Discussion: Interannual-to-interdecadal variability

Our results support the notion that higher-frequency variability, especially in the Pacific, is modified according to polarity of the multidecadal signal. A Pacific subset — PNA, PDO, ALPI, NINO3.4, WP, and NPO — thus becomes a focus for this multidecadally alternating interannual-to-interdecadal behavior (see Table 2.3 and Fig. 2.8). Perhaps striking is the comparatively low fractional variance displayed by the NPO and its upper-atmosphere counterpart — WP — both of which show significant correlation with NINO3.4. Potentially relevant to this conundrum is the observation of a non-stationary relationship between the NPO and ENSO (Wang et al. 2007), with ENSO-related signal in the ALPI strengthening and weakening at a multidecadal pacing and affecting the hemispheric interconnectedness of mid-latitude Pacific-centered indices, including NPO and WP.

Absent from our Pacific grouping are NPGO and PMM, which other studies have linked to ENSO by way of NPO. Our results suggest a strong negative relationship between higher-frequency behavior of NPGO and PMM, but not a significant relationship between NPGO and either NINO3.4 or NPO, in contrast to some other studies (Di Lorenzo et al. 2009; Alexander et al. 2010). This discrepancy may be due to differences underpinning methods and data used. For example, different authors used different versions of the NPO index (Di Lorenzo et al. 2008; Chhak et al. 2008; Ceballos et al. 2009; Di Lorenzo et al. 2009; and Di Lorenzo et al. 2010), with possibly large ensuing differences in the NPO–NPGO correlation. The same is true for various versions of ENSO related indices. Further potential explanations for our finding no significant correlations between NPO and PMM, as well as ENSO and PMM, include the seasonal dependence of these cross-correlations missed in our boreal-winter index analysis, and likely nonlinearity of the ENSO–PMM connection (Vimont et al. 2001, 2003 a, b; Chiang and Vimont 2004; Chang et al. 2007), which is not optimally described by linear correlation measures.

In conclusion, dynamics presented above — potential mechanisms underlying stadium-wave dynamics and related dynamics on interdecadal time scales — are topics of active and controversial research, reliant upon technological leaps in data retrieval and computer modeling to advance them toward consensus. We suggest momentum on these investigations is building and that our statistical analysis is consistent with these emerging hypotheses.

Acknowledgements We thank S. Minobe for a useful feedback on aspects of this study, and three anonymous reviewers for comments on an earlier version of the manuscript, which helped clarify the presentation. This research was supported by the Office of Science (BER), U. S.

Department of Energy (DOE) grant DE-FG02-07ER64428, NSF grant ATM-0852459 (SK), and NSF grant AGS-0902564.

References

Alexander MA, Deser C (1995) A mechanism for the recurrence of wintertime midlatitude SST anomalies. J Phys Oceanogr 25: 122-137.

Beamish RJ, Neville CM, Cass AJ (1997) Production of Fraser River sockeye salmon (*Oncorhynchus nerka*) in relation to decadal-scale changes in the climate and the ocean. Canadian Journ Fish and Aquat Sci 56: 516-526.

Bell GD, Halpert MS (1995) Atlas of intraseasonal and interannual variability, 1986-1993. NOAA Atlas No. 12. Climate Prediction Center, NOAA/NWS/NMC, Washington D. C. Request copy via e-mail from Gerald Bell at wd52gb@hp32.wwb.noaa.gov

Beckers J, Rixen M (2003) EOF calculations and data filling from incomplete oceanographic data sets. J Atmos Ocean Technol 20: 1839–1856. doi: 10.1175/1520-0426(2003)

Biasutti MA, Giannini A (2006) Robust Sahel drying in response to late 20th century forcings. Geophys Res Lett 33: L11706. doi:10.1029/2006GL026067

Bjerknes J (1964) Atlantic air-sea interaction. Advances in Geophysics 10. Academic Press: 1–82

Black D, Peterson LC, Overpeck JT, Kaplan A, Evans MN, Kashgarian M (1999) Eight Centuries of North Atlantic Ocean Atmosphere Variability. Science 286: 1709-1713. doi: 10.1126/science.286.5445.1709

Broomhead DS, King GP (1986) Extracting qualitative dynamics from experimental data. Physica D 20: 217–236

Bretherton, C.S, Widmann M, Dymnikov VP, Wallace JM, Blade I (1999) The effective number of spatial degrees of freedom of a time-varying field. J. Climate, 12: 1990–2009

Bryden H, Longworth HR, Cunningham SA (2005): Slowing of the Atlantic meridional overturning circulation at 25°N. Nature 438: 655-657. doi:10.1038/nature04385

Cassou C, Deser C, Terray L, Hurrell JW, Drevillion M (2004): Summer Sea Surface Temperature Conditions in the North Atlantic and Their Impact upon the Atmospheric Circulation in Early Winter. J Climate 17: 3349-3363. doi: 10.1175/1520-0042(2004)

Cayan DR (1992) Latent and Sensible Heat Flux Anomalies over the Northern Oceans, Driving the Sea Surface Temperature. J Phys Ocean 22: 859-881

Ceballos LI, Di Lorenzo E, Hoyos CD, Schneider N, Taguchi B (2009) North Pacific Gyre Oscillation synchronizes climate fluctuations in the eastern and western boundary systems. J Clim 22: 5163-5174.

Chang P, Zhang Li, Saravanan R, Vimont DJ, Chiang JCH, Link Ji, Seidel H, Tippett MK (2007) Pacific meridional mode and El Niño-Southern Oscillation. Geophys Res Lett 34. L16608. doi:10.1029/2007GL030302.

Chhak K, Di Lorenzo E (2007) Decadal variations in the California Current upwelling cells. Geophys Res Lett 314: L14604. doi10.1029/2007GL030203.

Chiang JCH, Vimont D (2004) Analogous Pacific and Atlantic Meridional Modes of Tropical Atmosphere-Ocean Variability. J. Climate 17: 4143-4158. doi: 10.1175/JCLI4953.1

Crowley TJ (2000) Causes of Climate Change Over the Past 1000 Years. Science 289: 270-277. doi: 10.1126/science.289.5477.270

Cubasch U, Voss R, Hergerl GC, Waszkewitz J, Crowley TJ (1997) Simulation of the influence of solar radiation variations on the global climate with an ocean-atmosphere general circulation model. Clim Dyn 13: 757-767

Cubasch U, Voss R (2000) The Influence of Total Solar Irradiance on Climate. Space Science Rev 94: 185-198. doi: 10.1023/A:1026719322987

Czaja A, Frankignoul C (2002) Observed Impact of Atlantic SST Anomalies on the North Atlantic Oscillation. J. Climate 15: 606-623

Czaja A, Marshall J (2001) Observations of Atmosphere-Ocean Coupling in the North Atlantic. OJR Met. Soc. 27: 1893-1916. doi:10.1002/qj.49712757603

Danabasoglu G (2008) On Multidecadal Variability of the Atlantic Multidecadal Overturning Circulation in the Community Climate System Model Version 3. J Climate 21: 5524-5544. DOI: 10.1175/2008JCLI2019.1

Delworth TL, Dixon KW (2006) Have anthropogenic aerosols delayed a greenhouse gas-induced weakening of the North Atlantic thermohaline circulation? Geophys Res Lett 33: L02606. doi:10.1029/2005GL024980

Delworth TL, Greatbatch RJ (2000) Multidecadal Thermohaline Circulation Variability Driven by Atmospheric Surface Flux Forcing. J Climate 13: 1481-1495

Delworth TL, Manabe S, Stouffer RJ (1993) Interdecadal Variations of the Thermohaline Circulation in a Coupled Ocean-Atmosphere Model. J Climate 6: 1993-2011

Delworth TL, Manabe S, Stouffer RJ (1997) Multidecadal climate variability in the Greenland Sea and surrounding regions: a coupled mode simulation. Geophys Res Lett 24 (3) 96GL03927: 257-260

Delworth TL, Mann ME (2000) Observed and simulated multidecadal variability in the Northern Hemisphere. Climate Dyn 16: 661–676. doi:10.1007/s003820000075

Delworth TL, Zhang R, Mann ME (2007) Decadal to centennial variability of the Atlantic from observations and models. In: Past and Future Changes of the Oceans Meridional Overturning Circulation: Mechanisms and Impacts, Schmittner A, Chiang JCH, Hemming SR, Eds., Geophysical Monograph Series 173, American Geophysical Union, pp. 131–148

Deser C, Blackmon ML (1995) On the Relationship between Tropical and North Pacific Sea Surface Temperature Variations. J. Climate 8: 1677-1680

Di Lorenzo E, Schneider N, Cobb KM, Franks PJS, Chhak K, Miller AJ, McWilliams JC, Bograd SJ, Arango H, Curchitser E, Powell TM (2008) North Pacific Gyre Oscillation links ocean climate and ecosystem change. Geophys Res Lett 35: L08607. doi:10.1029/2007GL032838

Di Lorenzo E, Fiechter J, Schneider N, Miller AJ, Franks PJS, Bograd SJ, Moore A, Thomas A, Crawford W, Pena A, Herman AJ (2009) Nutrient and salinity decadal variations in the central and eastern North Pacific. Geophys Res Lett 36: L14601. doi:10.1029/2009GL038261.

Di Lorenzo E, Cobb KM, Furtado JC, Schneider N, Anderson BT, Bracco A, Alexander MA, Vimont DJ (2010) Central Pacific El Niño and decadal climate change in the North Pacific Ocean. Nature Geosci 3 (11): 762-765. doi10.1038/NGEO984.

Dima M, Lohmann G (2007) A Hemispheric Mechanism for the Atlantic Multidecadal Oscillation. J Climate 20: 2706-2719. doi:10.1175/JCL14174.1

Dong BW, Sutton RT (2002) Adjustment of the coupled ocean-atmosphere system to a sudden change in the Thermohaline Circulation. Geophys Res Lett 29 (15): doi:10.1029/2002GL015229

Dong BW, Sutton RT (2005) Mechanism of interdecadal thermohaline circulation variability in a coupled ocean-atmosphere GCM. J. Climate 18: 1117–1135. doi: 10.1175/JCLI3328.1

Dong, BW, Sutton RT, Scaife AA (2006) Multidecadal modulation of El Niño Southern Oscillation (ENSO) variance by Atlantic Ocean sea surface temperatures. Geophys Res Lett 3: L08705. doi:10.1029/2006GL025766

Dong BW, Sutton RT (2007) Enhancement of ENSO Variability by a Weakened Atlantic Thermohaline Circulation in a Coupled GCM. J. Clim 20: 4920-4939. doi: 10.1175/JCLI4282.1

Dong BW, Sutton RT, Scaife AA (2006) Multidecadal modulation of El Nino Southern Oscillation (ENSO) variance by Atlantic Ocean sea surface temperatures. Geophys Res Lett 3**:** L08705. doi:10.1029/2006GL025766

Dong S, Kelly K (2004) Heat Budget in the Gulf Stream Region: The Importance of Heat Storage and Advection. J Phys Ocean 34: 1214-1231

Eden C, Jung T (2001) North Atlantic Interdecadal Variability: Oceanic Response to the North Atlantic Oscillation. J Clim 14: 676-691

Elsner JB, Tsonis AA (1996) Singular Spectrum Analysis: A New Tool in Time Series Analysis. Springer, 177 pp.

Enfield DB, Mestas-Nuñez AM (1999) Multiscale Variabilities in Global Sea Surface Temperatures and Their Relationships with Tropospheric Climate Patterns. J. Clim 12: 2719-2733

Enfield DB, Mestas-Nuñez AM, Trimble PJ (2001) The Atlantic Multidecadal oscillation and its relation to rainfall and river flows in the continental U. S. Geophys Res Lett 28: 277-280

Federov A, Philander SG (2000) Is El Niño Changing? Science 288**:** 1997-2002. doi: 10.1126/science.288.5473.1997

Folland CK, Palmer TN, Parker DE (1986) Sahel rainfall and worldwide sea temperature 1901-1985. Nature320: 602-607

Frankignoul C, Sennechael N, Kwon Y, Alexander M (2011) Influence of the Meridional Shifts of the Kuroshio and the Oyashio Extensions on the Atmospheric Circulation. J.Clim 24:762-777, doi 10.1175/2010 JCLI 3731.1

Georgieva K, Kirov B, Tonev P, Guineva V, Atanasov D (2007) Long-term variations in the correlation between NAO and solar activity: the importance of north-south solar activity asymmetry for atmospheric circulation. Adv in Space Res 40: 1152-1166. doi: 10.1016/j.asr.2007.02.091

Getzlaff J, Böning CW, Eden C, Biastock A (2005) Signal propagation related to the North Atlantic overturning. Geophys Res Lett 32: doi:10.1029/2004GL021002

Ghil M, Vautard R (1991) Interdecadal oscillations and the warming trend in global temperature time series. Nature 305: 324–327

Ghil M, Allen MR, Dettinger MD, Ide K, Kondrashov D, Mann ME, Robertson AW, Saunders A, Tian Y, Varadi F, Yiou P (2002) Advanced spectral methods for climatic time series. Rev Geophys **40**(1): 3.1–3.41. doi:10.1029/2000GR000092.

Girs AA (1971) Girs AA (1971) Multiyear oscillations of atmospheric circulation and long-term

meteorological forecasts. L. Gidrometeroizdat 480 p. (in Russian)

Girs AA (1974) Macrocirculation method for long-term meteorological prognosis. Hydrometizdat Publ, Leningrad, 480p. (in Russian)

Girs AA, Kondraovich KV (1978) Methods of Long Term Weather Forecasts. Gidrometeroizdat, Leningrad (in Russian).

Gray ST, Graumlich LJ, Betancourt JL, Pederson GT (2004) A tree-ring based reconstruction of the Atlantic Multidecadal Oscillation since 1567 A.D. Geophys Res Lett 31. L12205: doi:10.1029/2004GL019932

Grosfeld K, Lohmann G, Rimbu N, Fraedrich K, Lunkeit F (2007) Atmospheric multidecadal variations in the North Atlantic realm: proxy data, observations, and atmospheric circulation model studies. Clim of the Past 3: www.clim-past.net/3/39/2007 :39-50

Grosfeld K, Lohmann G, Rimbu N (2008) The impact of Atlantic and Pacific Ocean sea surface temperature anomalies on the North Atlantic multidecadal variability. Tellus A: doi: 10.1111/j.1600-0870.2008.00304.x

Hakkinen S (1999) A Simulation of Thermohaline Effects of a Great Salinity Anomaly. J Clim12: 1781-1795

Hansen DV, Bedzek HF (1996) On the nature of decadal anomalies in North Atlantic SST. JGR 101: 8749-8758

Hasegawa T, Yasuda T, Hanawa K (2007) Multidecadal Variability of the Upper Ocean Heat Content Anomaly Field in the North Pacific and its Relationship to the Aleutian Low ans the Kuroshio Transport. Papers in Meteorology and Geophysics 58: 155-166: doi: 10.2467/mripapers.58.155

Hasselmann K (1976) Stochastic climate models.Pt.1. Tellus 28:473-485

Hilmer M, Jung T (2000) Evidence for a recent change in the link between the North Atlantic Oscillations and Arctic sea ice export. Geophys Res Lett 27(7): 989-992. doi: 10.1029/1999GL010944

Hurrell JW (1995) Decadal Trends in the North Atlantic Oscillation: Regional Temperatures and Precipitation. Science 269: 676-679

Hurrell JW (2003) The North Atlantic Oscillation: Climatic significance and environmental effect. EOS 84(8): 73

Jones PD, Moberg A (2003) Hemispheric and large-scale surface air temperature variations: an extensive revision and an update to 2001. J Clim 16: 206-223. doi:10.1175/1520-0442(2003)

Jungclaus JH, Haak H, Latif M, Mikolajewicz U (2005) Arctic-North Atlantic Interactions and Multidecadal Variability of the Meridional Overturning Circulation. J Clim 18: 4013-4031. doi: 10.1175/JCLI3462.1

Kaplan A, Cane M, Kushnir Y, Clement A, Blumenthal M, Rajagopalan B (1998) Analyses of global sea surface temperature 1856–1991. J Geophys Res 103: 18, 567–18, 589.

Keenlyside N.S., Latif M, Jungclaus J, Kornblueh L, Roeckner E (2008) Advancing decadal-scale climate prediction in the North Atlantic sector. Nature 453: 84-88. doi:10.1038/nature06921.

Kelly K, Dong S (2004) The Relationship of Western Boundary Current Heat Transport and Storage to Midlatitude Ocean-Atmosphere Interaction. Ocean-Atmosphere Interaction and Climate Variability, Edited by Chunzai Wang, Shang-Ping Xie, and James A. Carton, AGU Monograph

Kelly K, Small RJ, Samelson RM, Qiu B, Joyce TM, Kwon Y-O, Cronin MF (2010) Western Boundary Currents and Frontal Air-Sea Interaction: Gulf Stream and Kuroshio Extension. J Climate 23: 5644-5667. DOI: 10.1175/2010JLCI3346.1

Kerr RA (2000) A North Atlantic climate pacemaker for the centuries. Science 288: 1984-1986. doi: 10.1126/science.288.5473.1984

Kirov B, Georgieva K (2002) Long-term variations and interrelations of ENSO, NAO, and solar activity. Physics and Chemistry of the Earth 27: 441-448

Klyashtorin LB Lyubushin AA (2007) Cyclic Climate Changes and Fish Productivity. Moscow, VNIRO Publishing, Editor for English version: Dr. Gary D. Sharp, Center for Climate/Ocean Resources Study, Salinas, CA. USA: 223pp

Knight JR, Allan RJ, Folland CK, Vellinga M, Mann ME (2005) A signature of persistent natural thermohaline circulation cycles in observed climate Geophy Res Lett 32: L20708. doi: 10.1029/2005GRL024233

Knight JR, Folland CK, Scaife AA (2006) Climate impacts of the Atlantic Multidecadal Oscillation. Geophys Res Lett 33: L17706. doi:10.1029/2006GL026242

Kondrashov D, Ghil M (2006) Spatio-temporal filling of missing points in geophysical data sets. Nonl Proc Geophys 13: 151–159

Kravtsov S (2010) An empirical model of decadal ENSO variability. J Climate, submitted

Kravtsov S, Dewar WK, Ghil M, McWilliams JC, Berloff P (2008) A mechanistic model of mid-latitude decadal climate variability. Physica D 237: 584–599. doi:10.1016/j.physd.2007.09.025

Kravtsov S, Kondrashov D, Ghil M (2005) Multi-level regression modeling of nonlinear

processes: Derivation and applications to climatic variability. J Climate 18: 4404–4424. doi: 10.1175/JCLI3544.1

Kug J-S, Jin F-F (2009) Left-hand rule for synoptic eddy feedback on low-frequency flow. Geophys Res Lett 36: L05709. doi: 10.1029/2008GL036435

Kushnir Y (1994) Interdecadal Variations in North Atlantic Sea Surface Temperature and Associated Atmospheric Conditions. J Climate 7(1): 141-157

Kushnir Y, Held I (1996) Equilibrium atmospheric response to North Atlantic SST anomalies. J Climate 9: 1208-1220

Kushnir Y, Robinson WA, Blade I, Hall NMJ, Peng S, Sutton R (2002) Atmospheric GCM response to extratropical SST anomalies: Synthesis and evaluation. J. Climate 15: 2233–2256

Kwon Y, Alexander MA, Bond NA, Frankignoul C, Nakamura H, Qiu B, Thompson L (2010) Role of the Gulf Stream and Kuroshio-Oyashio Systems in Large-Scale Atmosphere-Ocean Interaction: A Review. J Climate special collection: DOI: 10.1175/2010JCLI3343.1

Latif M, Barnett TP (1994) Causes of Decadal Climate Variability over the North Pacific and North America. Science 266: 634-637

Latif M, Barnett TP (1996) Decadal Climate Variability over the North Pacific and North America: Dynamics and Predictability. J Climate 9: 2407-2423

Latif M, Arpe K, Roeckner E (2000) Oceanic control of decadal North Atlantic sea level pressure variability in winter. Geophys Res Lett 27: 727-730. doi: 10.1029/1999GL002370

Latif M, Roeckner E. , Botzet M, Esch M, Haak H, Hagemann S, Jungclaus J, Legutke S, Marsland S, Mikolajewicz U, Mitchell J (2004) Reconstructing, Monitoring, and Predicting Decadal-Scale Changes in the North Atlantic Thermohaline Circulation with Sea Surface Temperature . J Climate 17: 1605-1614. doi: 10.1175/1520-0442(2004)

Latif M, Böning C, Willebrand J, Biastoch A, Dengg J, Keenlyside N, Schweckendiek U, Madec G (2006) Is the thermohaline circulation changing? J Climate 19 (18): 4631-4637. doi: 10.1175/JCLI3876.1

Lau N-C (1988) Variability of the observed midlatitude storm tracks in relation to low-frequency changes in the circulation pattern. J Atmos Sci 45: 2718-2743

Lau N-C, Nath MJ (1994) A modeling study of the relative roles of tropical and extratropical SST anomalies in the variability of the global atmosphere-ocean system. J Climate 7: 1184-1207

Mann ME, Park J (1994) Global-scale modes of surface temperature variability on interannual to century timescales. J Geophys Res 99: 25819–25833

Mann ME, Park J, Bradley RS (1995) Global interdecadal and century-scale oscillations during the past five centuries. Nature 378: 266-270

Mann ME, Park J (1996) Joint Spatiotemporal Modes of Surface Temperature and Sea Level Pressure Variability in the Northern Hemisphere during the Last Century. J. Climate 9: 2137-2162

Mann ME, Bradley RS, Hughes MK (1998) Global-scale temperature patterns and climate forcing over the past six centuries. Nature 392: 779-787

Mantua NJ, Hare SR, Zhang Y, Wallace JM, Francis RC (1997) A Pacific interdecadal climate oscillation with impacts on salmon production. Bull Amer Meteor Soc 78: 1069-1079

Marshall J, Johnson H, Goodman J (2001a) A study of the interaction of the North Atlantic Oscillation with ocean circulation. J Climate 14: 1399–1421

Marshall J, Kushnir Y, Battisti D, Chang P, Czaja A, Dickson R, Hurrell J, McCartney M, Saravanan R, Visbeck M (2001b) North Atlantic climate variability: phenomena, impacts and mechanisms. Internat J Climatology 21: 1863–1898. doi: 10.1002/joc.693

McCartney M (1997) Climate change: Is the ocean at the helm? Nature 388: 521-522

Meehl GA, Covey C, Delworth T, Latif M, McAveney B, Mitchell JFB, Stouffer RJ, Taylor KE (2007) The WCRP CMIP3 Multimodel Dataset: A new era in climate change research. Bull Amer Meteo Soc 88(9): 1383-1394. doi: 10.1175/BAMS-88-9-1383

Mehta VM, Suarez MJ, Manganello JV, Delworth TL (2000) Oceanic influence on the North Atlantic oscillation and associated Northern Hemisphere climate variations: 1959-1993. Geophys Res Lett 27(1): 121-124. doi: 10.1029/1999GL002381

Metzger EJ, Hurlburt HE (2001) The importance of high horizontal resolution and accurate coastline geometry in modeling South China Sea Inflow. Geophys Res Lett 28(6): 1059-1062. doi: 10.1029/2000GL012396

Miller AJ, Chai Fei, Chiba S, Moisan JR, Neilson DJ Decadal-Scale Climat and Ecosystem Interactions in the North Pacific Ocean (2004). J of Oceanog (60) 163:188.

Minobe S (1997) A 50-70-year climatic oscillation over the North Pacific and North America. Geophys Res Lett 24: 683-686

Minobe S (1999) Resonance in bidecadal and pentadecadal climate oscillations over the North Pacific: role in climatic regime shifts. Geophys Res Lett 26: 855-858

Minobe S, Kuwano-Yoshida A, Komori N, Xie S-P, Small RJ (2008) Influence of the Gulf Stream on the troposphere. Nature 452: 206-209. doi: 10.1038/nature06690

Moron V, Vautard R, Ghil M (1998) Trends, interdecadal and interannual oscillations in global sea-surface temperatures. Climate Dyn 14: 545–569.

Msadek R, Dixon KW, Delworth TL, Hurlin W (2010a) Assessing the predictability of the Atlantic meridional overturning circulation and associated fingerprints. Geophys Res Lett 37: L19608. doi: 10.1029/2010GL044517

Msadek R, Frankignoul C, Li LZX (2010b) Mechanisms of the atmospheric response to North Atlantic multidecadal variability: a model study. Climate Dyn online: DOI 10.1007/s00382-010-0958-0

Nakamura H, Sampe T, Tanimoto Y, Shimpo A (2004) Observed Associations Among Storm Tracks, Jet Streams, and Midlatitude Ocean Fronts. from AGU Monograph: The Earth's Climate: The Ocean-Atmosphere Interaction Geophysical Monograph 147: 329-346. doi: 10.1029/147GM18

North GR, Bell TL, Cahalan RF, Moeng FJ (1982) Sampling errors in the estimation of empirical orthogonal functions. Mon Wea Rev 110, 669–706

Overland JE, Adams JM, Bond NA (1999) Decadal Variability of the Aleutian Low and Its Relation to High-Latitude Circulation. J Climate12: 1542-1548

Palmer TN, Sun Z (1985) A modeling and observational study of the relationship between sea surface temperature in the northwest Atlantic and the atmospheric general circulation. QJR Meteorol Soc 111: 947-975

Pan L-L (2007) Synoptic eddy feedback and air-sea interaction in the North Atlantic region. Clim Dyn 29: 647-659. DOI: 10.1007/s00382-007-0256-7

Peng S, Robinson WA, Hoerling MP (1997) The modeled atmospheric response to midlatitude SST anomalies and its dependence on background circulation states. J Climate 10: 971-987

Peng S, Whitaker JS (1999) Mechanisms Determining the Atmospheric Response to Midlatitude SST Anomalies. J Climate 12: 1393-1408

Peng S, Robinson WA (2001) Relationships between atmospheric internal variability and the response to an extratropical SST anomaly. J Climate 14: 2943-2959. doi:10.1175/1520-0442(2001)

Peng S, Robinson WA, Li S (2002) North Atlantic SST forcing of the NAO and relationships with intrinsic hemispheric variability. Geophys Res Lett 29: 1276. doi: 10.1029/2001GL014043

Penland, C (1989) Random forcing and forecasting using principal oscillation pattern analysis. Mon Wea Rev 117: 2165–2185

Penland, C (1996) A stochastic model of Indo-Pacific sea-surface temperature anomalies. Physica D 98: 534–558

Penland C, Ghil M (1993) Forecasting Northern Hemisphere 700-mb geopotential height anomalies using empirical normal modes. Mon Wea Rev 121: 2355–2372

Pohlmann H, Sienz F, Latif M (2006) Influence of the Multidecadal Atlantic Meridional Overturning Circulation Variability on European Climate. J Climate (special section) 19: 6062-6067. doi: 10.1175/JCLI3941.1

Polonsky AB (1997) Variability in the NW Black Sea associated with the large-scale atmospheric processes. Meteor and Hydrol 3: 59-70 (in Russian)

Polonsky AB (2001) The role of the ocean in the recent climate changes. Marine Hydrophys. Journal 6: 32-58 (in Russian).

Polonsky AB, Basharin DV, Voskresenskaya EN, Worley SJ, Yurovsky AV (2004) Relationship between the North Atlantic Oscillation, Euro-Asian climate anomalies and Pacific variability. Marine Meteorology. Pacific Oceanography 2(1-2): 52-66

Polyakov IV, Alexeev VA, Bhatt US, Polyakova EI, Zhang X (2009) North Atlantic warming: patterns of long-term trend and multidecadal variability. Clim Dyn (Springerlink.com). DOI: 10.1007/s00382-008-0522-3

Preisendorfer RW (1988) Principal component analysis in Meteorology and Oceanography. Elsevier, Amsterdam, 425pp

Press, WH, Teukolsky SA, Vetterling WT, Flannery, BP (1994) Numerical Recipes. 2nd edition, Cambridge University Press, 994pp

Rayner NA, Brohan P, Parker DE, Folland CK, Kennedy J, Vanicek M, Ansell T, Tett SFB (2006) Improved analyses of changes and uncertainties in sea-surface temperature measured in situ since the mid-nineteenth century. J Climate 19: 446-469. doi: 10.1175/JCLI3637.1

Robertson AW, Mechoso CR, Kim Y-J (2000) The influence of Atlantic sea surface temperature anomalies on the North Atlantic Oscillation. J Climate 13: 122-138. doi: 10.1175/1520-0442(2000)

Rodwell MJ, Rowell DP, Folland CK (1999) Oceanic forcing of the wintertime North Atlantic Oscillation and European climate. Nature 398: 320-323

Roe G (2009) Feedbacks, Timescales, and Seeing Red. Annu Rev Earth Planet Sci 37: 5.1-5.23. doi: 10.1146/annurev.earth.061008.134734

Rogers JC (1981) The North Pacific Oscillation. Int J Climatol 1: 39-57

Rotstayn L.D, Lohman U (2002) Tropical rainfall trends and the indirect aerosols effect. J Climate 15: 2103-2116

Schlesinger ME, Ramankutty N (1994) An oscillation in the global climate system of period 65-70 years. Nature 367: 723-726

Schneider T (2001) Analysis of incomplete climate data: estimation of mean values and covariance matrices and imputation of missing values. J Climate 14: 853–871. doi: 10.1175/1520-0442(2001)

Schneider N, Miller AJ, Pierce DW (2002) Anatomy of North Pacific decadal variability. J Climate 15: 586–605. doi: 10.1175/1520-0442(2002)

Shabalova MV, Weber SL (1999) Patterns of temperature variability on multidecadal to centennial timescales. J Geophys Res 104: 31,023-31,041

Shaffrey L, Sutton R (2006) Bjerknes Compensation and the Decadal Variability of the Energy Transports in a Coupled Climate Model. J Clim19: 1167-1181. doi: 10.1175/JCLI3652.1

Shindell DT, Schmidt GA, Miller RL, Rind D (2001) Northern Hemisphere winter climate response to greenhouse gas, ozone, solar, and volcanic forcing. J. Geophys Res 106: 7193-7210. doi:10.1029/2000JD900547

Stocker TF, Mysak LA (1992) Climatic fluctuations on the century time scale: a review of high-resolution proxy data and possible mechanisms. Clim Change 20: 227-250

Stommel H (1961) Thermohaline convection with two stable regimes of flow. Tellus 13: 224–230

Stott PA, Tett SFB, Jones GS, Allen MR, Mitchell JFB, Jenkins GJ (2000) External Control of 20th Century Temperature by Natural and Anthropogenic Forcings. Science 290: 2133-2137. DOI: 10.1126/science.290.5499.2133

Sugimoto S, Hanawa K (2009) Decadal and Interdecadal Variations of the Aleutian Low Activity and Their Relation to Upper Oceanic Variations over the North Pacific. Journal of the Meteorological Society of Japan 87 (4): 601-614. DOI:10.2151/jmsj.87.601

Sutton RT, Allen MR (1997) Decadal predictability of North Atlantic sea surface temperature and climate. Nature 388: 563-567

Sutton RT, Hodson DLR (2003) Influence of the Ocean on North Atlantic Climate Variability 1871-1999. J Climate 16: 3296-3313. doi: 10.1175/1520-0442(2003)

Sutton RT, Hodson DLR, Mathieu P (2003) The Role of the Atlantic Ocean in Climate Forecasting, Proceedings of the ECMWF Workshop on the Role of the Upper Ocean in Medium and Extend Range Forecasting, ECMWF, Reading, UK

Sutton RT, Hodson DLR (2005) Atlantic Ocean forcing of North American and European summer climate. Science 309: 115-118. doi: 10.1126/science.1109496

Sutton RT, Hodson DLR (2007) Climate response to basin-scale warming and cooling of the North Atlantic Ocean. J Climate 20: 891-907. doi: 10.1175/JCLI4038.1

Swanson K, Tsonis AA (2009) Has the climate recently shifted? Geophys Res Lett 36. doi:10.1029/2008GL037022

Taylor KE, Stouffer RJ, Meehl GA (2008) A Summary of the CMIP5 Experiment Design.http://www.pcmdi.llnl.gov/ipcc/model_documentation/ipcc_model_documentation.php

Timlin MS, Alexander MA (2002) On the Reemergence of North Atlantic SST Anomalies. J Climate 15: 2707-2712. doi:10.1175/1520-0442(2002)

Timmermann A, Latif M, Voss R, Grotzner A (1998) Northern Hemispheric interdecadal variability: a coupled air-sea mode. J Climate 11: 1906-1931

Timmermann A, Okumura Y, An SI, Clement A, Dong B, Guilyardi E, Hu A, Jungclaus JH, Renold M, Stocker TF, Stouffer RJ, Sutton R, Xie SP, Yin J (2007) The influence of a weakening of Atlantic meridional overturning circulation on ENSO. J Climate 20: 4899–4919. doi:10.1175/JCLI4283.1

Tsonis AA, Swanson K, Kravtsov S (2007) A new dynamical mechanism for major climate shifts. Geophys Res Lett 34: L13705. doi:10.1029/2007GL030288

Van der Swaluw E, Drijfhout SS, Hazeleger W (2007) Bjerknes Compensation at High Northern Latitudes: The Ocean Forcing the Atmosphere. J Climate 20: 6023-6032. doi: 10.11752007JCLI1562.1

Vangenheim GYa (1940) The long-term temperature and ice break-up forecasting. Proc State Hydrological Institute Iss. 10: 207-236 (in Russian)

Vautard R, Ghil M (1989) Singular spectrum analysis in nonlinear dynamics, with applications to paleoclimatic time series. Physica D 35: 395–424

Vautard R, Yiou P, Ghil M (1992) Singular Spectrum Analysis: A toolkit for short, noisy and chaotic series. Physica D 58: 95 – 126

Vellinga M, Wood RA (2002) Global climatic impacts of a collapse of the Atlantic thermohaline circulation. Climatic Change 54: 251-267. doi: 10.1023/A:1016168827653.

Vellinga M, Wu P (2004) Low-latitude freshwater influence on centennial variability of the Atlantic thermohaline circulation. J Climate 17: 4498-4511. doi:10.1175/3219.1

Vimont DJ, Battisti DS, Hirst AC (2001) Footprinting: A seasonal connection between the Tropics and mid-latitudes. Geophys Res Lett 28: 3923:3926.

Vimont DJ, Battisti DS, Hirst AC (2003a) The seasonal Footprinting mechanism in the CSIRO general circulation models. J Climate 16: 2653-2667. doi:10.1175/1520-0442(2003)

Vimont DJ, Wallace JM, Battisti DS (2003b) The Seasonal Footprinting Mechanism in the Pacific: Implications for ENSO. J Clim 16: 2668-2675.

Vimont DJ, Kossin JP (2007) The Atlantic Meridional Mode and hurricane activity. Geophy Res Lett 34: L07709. doi:10.1029/2007/GL029683

Walker GT, Bliss EW (1932) World weather. Mem R Met Soc 4: 53-84

Wallace JM, Gutzler DS (1981) Teleconnections in the geopotential height field during the Northern Hemisphere winter. Mon Wea Rev 109: 784-812.

Wang L, Chen W, Huang R (2007) Changes in the Variability of North Pacific Oscillation around 1975/1976 and its relationship with East Asian winter climate. J Geophys Res 112: D11110. doi: 10.1029/2006JD008054

Willis JK, Roemmich D, Cornuelle B (2004) Interannual variability in upper ocean heat content, temperature, and thermosteric expansion on global scales. J Geophys Res 109: C12036. doi: 10.1029/2003C002260

Wu P, Gordon C (2002) Oceanic Influence on North Atlantic Climate Variability. J Climate 15: 1911-1925. doi: 10.1175/1520-0442(2002)

Wu LP, Rodwell M (2004) Gulf Stream forcing of the winter North Atlantic oscillation. Atm Sc Lett 5: 57-64. doi: 10.1016/j.atmoscilet.2003.12.002

Xie SP (2004) Satellite observations of cool ocean-atmosphere interaction. Bull Am Meteorol Soc 85: 195-208. doi: 10.1175/BAMS-85-2-195

Xie SP, Carton J (2004) Tropical Atlantic Variability: Patterns, Mechansims, and Impacts. Earth Climate: The Ocean-Atmosphere Interaction. C. Wang, S.P. Xie, and J. A. Carton (eds.), Geophys Monograph. AGU. Washington, D. C., pp 121-142. doi: 10.1029/147GM07

Yualeva EN, Schneider N, Pierce DW, Barnett TP (2001) Modeling of North Pacific climate variability forced by ocean heat flux anomalies. J Climate 14: 4027-4046. doi: 10.1175/1520-0442(2001)

Zhang YJ, Wallace M, Iwasaka N (1996) Is Climate Variability over the North Pacific a Linear Response to ENSO? J Climate 9: 1468-1478

Zhang R, Delworth TL (2005) Simulated tropical response to a substantial weakening of the Atlantic thermohaline circulation. J Climate 18: 1853-1860. doi: 10.1175/JCLI3460.1

Zhang R, Delworth TL (**2007**) Impact of Atlantic multidecadal oscillations on India/Sahel rainfall and Atlantic hurricanes. Geophys Res Lett 33: L17712. doi:10.1029/2006GL026267

Zhang R, Delworth TL, Held IM (2007) Can the Atlantic Ocean drive the observed multidecadal variability in Northern Hemisphere mean temperature? Geophys Res Lett 34: L02709. doi:10.1029/2006GL028683

Zhen-Shan L, Xian S (2007) Multi-scale analysis of global temperature changes and trend of a drop in temperature in the next 20 years. Meteor and Atmos Physics: 95: 115-121

Chapter Three:

Northern Hemisphere Multidecadal Climate Variability: dynamics and history of climate-signal hemispheric propagation: 1700 to 2000

Abstract: Instrumental and proxy records of diverse climate indices across the Northern Hemisphere share a multidecadal-scale tempo of variability. Previous analysis suggests the observed temporal commonality is rooted in synchronization of a hemispheric network of atmospheric and lagged oceanic circulations through which the climate signal propagates. Uncertainties regarding this dynamic's mechanisms and its historical longevity linger. To investigate these, proxy data are analyzed in context of a network of quasi-oscillatory climate indices. Findings suggest i) the observed 20th century signal-propagation has existed in somewhat similar fashion for the 300-year length of this study; ii) Eurasian-Arctic-Shelf sea-ice plays a strong role in the propagation of the hemispheric climate signal; and iii) dynamics fundamental to generation of the multidecadal component of the Northern Hemisphere's surface temperature (NHT) are encoded onto the records of key proxy indices, the combined signatures of which trace the hemispheric circumnavigation of the secularly varying, sequentially propagating climate signal.

Keywords: Climate · Network · Synchronize · Teleconnections · Arctic · solar · LOD

3.1 Introduction:

Distinguishing a naturally forced climate signal from an anthropogenically forced one is a challenge currently facing climate scientists. Identifying a natural component is critical to the success of assessing relative contributions of each.

Multidecadal quasi-periodicity of variability emerges from records of various indices. Examples include a low-frequency signal with a typical timescale of 50 to 80 years, with presence in the North Pacific (Minobe 1997, 1999) and the North Atlantic (Black et al. 1999; Shabalova and Weber 1999; Delworth and Mann 2000; Gray et al. 2004) regions. A similar signature has been found in the instrumental record (Folland et al. 1986; Kushnir 1994; Schlesinger and Ramankutty 1994; Mann and Park 1994, 1996; Delworth and Mann 2000; Zhen-Shan and Xian 2007). Signatures with similarly timed low-frequency rhythms are identified in basin-scale wind regimes (Vangenheim 1940; Girs 1971a,b; King et al. 1998), Arctic processes (Frolov et al. 2009 and references therein), and river-basin-flow patterns (Nowak et al. 2011). Numerous studies (Beamish and Boullion 1993; Beamish et al. 1997, 1999; Chavez et al. 2003; Klyashtorin 1998; Klyashtorin and Lyubushin 2007; Klyashtorin et al. 2009) cite a similar cadence etched into centuries-long historical records of various commercial-fish populations. Ogurtsov et al. (2002) and Patterson et al. (2004) have found spectral peaks at approximately 60 years characterizing cosmogenic nuclide accumulations. Furthermore, an analogous tempo has been noted in Earth's rotational-rate anomalies (Beamish et al. 1999; Sidorenkov et al. 2005; Sidorenkov 2005, 2009), and in geomagnetic-field variations (Courtillot et al. 2007, Roberts et al. 2007). Wyatt et al. (2011) analyzed 20th century records of a variety of atmospheric and oceanic teleconnections patterns and found a similar secular-scale signal propagating through them.

The apparent pervasiveness of this temporal signal motivates this investigation, which is intended to be a continuation of the original Wyatt et al. (2011) study. In that paper, we attempted to put into perspective this widely detected low-frequency signature documented in previous studies. In that original study, through application of multivariate statistical methods to 20th century time series of a collection of well-known climate indices, a picture emerged: secular-scale variability in a climate signal propagating across the Northern Hemisphere via a sequence of atmospheric and lagged oceanic teleconnections. For brevity of communication, we termed this propagating signal the "stadium wave" – a term alluding to the behavior often seen in a sports arena, where successive groups of spectators stand with arms raised and then sit, giving the visual impression of a wave passing through the crowd.

In this study, I broaden the data base used in that original study. To that original 20th century index set I have added a variety of 20th century index time series representing processes in the Arctic and the Tropics that appear to show coherent variability at this similar timescale. The goal here is to gain more detailed insight into the dynamics of the "stadium-wave" climate signal's propagation. I also wish to explore the signal's history. To that end, I have added 300-year-length time series of proxy reconstructions of climate indices used in the original study. To these extended data sets, I apply statistical methods used in our original study. Emergent from the analysis is a more detailed picture of the stadium-wave signal. Ocean/Arctic sea-ice coupling, particularly in the North Atlantic-West Eurasian sector, plays a strong role in generating a large-scale atmospheric response. In turn, assimilated impacts of protracted anomaly trends of this atmospheric response may, in turn, negatively feed back onto ocean processes. In addition, the analysis of proxy data reflects the possibility that stadium-wave propagation may have existed

prior to the 20th century, with modifications of amplitude and frequency, yet with apparent coherency in propagation sequence for the duration of the 300-year time interval considered.

3.2 Approach, Methods, and Data Sets:

3.2.1 Approach

In the original study by Wyatt et al. (2011), our strategy highlighted collective behavior – i.e. as a network. Viewing climate as a network allows the component parts of the climate system to be viewed as an interactive system rather than as a collection of independent regional patterns. That approach is continued here. The strategy frames multidecadally varying climate-related phenomena within the context of a signal propagating throughout a network of synchronized[1] chaotic quasi-oscillators, effectively compressing individual circulations into nodes of an interconnected network, with each node representing, or related to, a subset of processes.

In that first investigation into the stadium-wave signal, we used multivariate statistical analysis to characterize the dominant mode of a climate signal shared among co-varying climate indices in the Northern Hemisphere. Rigorous estimates of the shared signal's statistical significance highlighted the unlikelihood that observations could be explained by mere randomness. In this present study, the original approach is continued, supplemented by correlations between time series where appropriate, this latter addition guided by data-set availability and investigative goal. (Glossary of acronyms: **Table 3.1**.)

[1] Synchronization refers to the matching of rhythms of self-sustained (quasi)oscillators; whereas "synchronous" refers to "same timing".

Table 3.1: Glossary of acronyms and paper-specific terms.

Term	Description
ACI	Atmospheric Circulation Index. A measure of anomalous large-scale atmospheric zonal flow over the Atlantic Ocean and Eurasian continent. Cumulative-sum of AT
Atlantic ITCZ	The Atlantic sector's Intertropical Convergence Zone
ALPI	Aleutian Low-Pressure Index (high values reflect an intensified circulation, a lower sea-level-pressure)
AMO	Atlantic Multidecadal Oscillation (refer to Table 3.2)
AMOC	Atlantic Meridional Overturning Circulation
Arctic dT	Anomalies of Arctic surface temperature
AT	Atmospheric-Mass-Transfer anomalies. Positive anomalies indicate intensified basin-scale flow with a dominant zonal component; negative anomalies indicate weakened basin-scale flow with a dominant meridional component. Is the cumulative-sum-removed term of ACI.
Atlantic SSTA Dipole	Same as Dipole; reflects latitudinal migrations of Atlantic ITCZ. (See table 3.3 for details.)
Conventional proxy	Index reconstructions of teleconnections and single variables participating in stadium wave, e.g. NHT, AMO, PDO, NAO reconstructions. Conventional means are used: tree-rings, isotopic ratios in corals, ice cores.
csr	Cumulative-sum-removed or "difference" or time-derivative of a time series. Used in this study to examine potential forcings on an index.
cs or cum sum	Cumulative sum, time-integral, or anomaly trend of a time series; comparison of anomaly trends between/among indices can reveal processes that might share similar long-term behavior. When compared to non-transformed (single-index) time series, an anomaly trend might reveal a relationship to that index in the form of integral impacts.
DIFF	"difference" or csr or time-derivative of a time series;
Dipole	Atlantic SST Dipole, a proxy for the Atlantic sector's ITCZ (See Table 3.3).
Dynamic Proxies	Proxies that capture process more than typical raw-variable-based teleconnections. Used in this study to investigate potential mechanisms of stadium-wave-signal propagation. Ex: Japanese sardines, G.bulloides, ngLOD
EastIce	East Eurasian Arctic Shelf Sea ice: Laptev, East Siberian, and Chukchi Seas (~100ºEast eastward to ~ 150ºWest (north of Bering Strait)); pronounced interdecadal (~20y) variability, with multidecadal component (~60y). Correlated with positive polarity of NPGO.
EIE	East Ice Extent: same as East Ice
EsperNHT	An NHT proxy used in this study. The proxy reconstruction was done by Esper et al. (2004). See section 3.2.2.4 for details.

GB or G. bulloides	Globerina bulloides. Proxy for ITCZ migration in western Atlantic.
"Groupings"	Specific to this study; a heuristic tool to facilitate understanding of stadium-wave behavior. Indices are grouped into five different "clusters" according to temporal behavior. Groupings 1 to 5 are mirrored by oppositely signed Groupings -1 to -5. (Figures 3.6 - 3.10 and 3.14.) They are referenced in the text as "Grouping 1" or "Grouping -1", etc. If speaking generically about the group indices, a positive number is used (e.g. Grouping 1). If speaking specifically, either the positive or negative number is used, as appropriate. Groupings are contrasted with Process-Specific Groups.
Ice Total	West Eurasian Arctic Sea Ice + East Eurasian Arctic Sea Ice. Spans region from ~ 15ºW eastward to ~ 195º E (Sea-ice in shelf seas from east of Greenland to north of Bering Strait region.). Strongly correlated with AT (zonal winds).
ITCZ	Intertropical Convergence Zone; Related to sea-ice (Ice Total) in Eurasian Arctic Seas and to NHT. Migrates north with increased NHT and decreased Ice Total, and to south with decreased NHT and increased Ice Total.
"ITCZ"	Inferred ITCZ; reconstructed from detrended, normalized values of AMO-NPGO, based on inferred dynamics discussed in text.
JS	Japanese Sardine outbursts off coast of Japan, likely related to western-boundary dynamics
LOD	Length-of-day; refer to ngLOD. The latter is a proxy for Earth's rotational-rate-anomalies. LOD indicates a slowed rotation rate versus ngLOD, which indicates a faster rate.
MTG	Meridional Thermal Gradient; refers to the basin-scale temperature contrast between high and low latitudes, especially as related to sea-ice inventory in Eurasian Arctic. (Outten and Esau 2011)
M-SSA	Multi-channel Singular Spectrum Analysis. Refer to section 3.2.2.1.
NAO	North Atlantic Oscillation (unless otherwise designated, NAO refers to its boreal-winter index (DecJanFebMarch))
NAOw	Refers to boreal-winter index of NAO. Same as NAO (see above)
NAOan	Annual index of North Atlantic Oscillation
ngLOD	Negative length-of-day anomalies. A proxy for Earth's rotational-rate anomalies. Increased ngLOD indicates faster rotational velocity, a consequence of perturbations to Earth's moment of inertia (an object's resistance to changes to its rotation) and law of conservation of angular momentum.
NHT	Northern Hemisphere's mean surface temperature
NPGO	North Pacific Gyre Oscillation (Di Lorenzo et al. 2008). In this study, NPGO is actually an NPGO proxy (Nurhati et al. 2011), derived from Sr/Ca isotope ratios in North Central Pacific coral. See 3.2.2.6 for description.
NPO	North Pacific Oscillation (see Table 3.2)
NINO	Same as NINO3.4. Refers to a region known as NINO3.4 – a bounded

	region of SST anomalies used as an index reflecting behavior of the El Nino Southern Oscillation phenomenon.
PCI	Pacific Circulation Index. A measure of anomalous large-scale atmospheric zonal flow over the Pacific Ocean and North America.
PDO	Pacific Decadal Oscillation (See Table 3.2)
Process-Specific Groups	A heuristic tool to facilitate understanding of stadium-wave dynamics. Indices are grouped according to process or medium. For example, a process-specific group might be a network comprised solely of wind-related components, or of ice-related, etc.
RC	Reconstructed Component – a spatio-temporal filter based on an oscillatory pair of leading M-SSA-generated modes of climate variability. This filter, applied to an index's time series, allows visualization of the M-SSA-identified climate signal as it propagates through the index.
Solar	Refers to the solar constant (total solar irradiance index ((Lean (2000, 2004)). See Table 3.3)
SST or SSTA	Sea-surface-temperature or sea-surface-temperature anomalies.
TIE	Total Ice Extent. Same as Ice Total
West Ice	West Eurasian Arctic Shelf Sea Ice: includes Greenland, Barents, and Kara Seas: ~15ºWest eastward to ~ 100ºEast; a pronounced 60-year variability, strongly correlated to negative-polarity of AMO. Same as WIE.
WIE	Same as West Ice

3.2.2 Data and Methods

This study was divided into two steps. The first step was to evaluate the historical longevity of the stadium-wave signal. The second step, partially reliant on the first, was to explore mechanisms and dynamics of stadium-wave propagation. Insights gained from the latter led back to the original quest – assessment of historical longevity of the stadium-wave signal – this time based upon inferred contributing dynamics. Providing foundation for both steps was the original stadium-wave analysis, a description of which follows.

3.2.2.1 Data for Original Stadium Wave

Indices (see **Table 3.2** for references and general descriptions) of the original stadium-wave are used throughout this study. They include instrumental values of the Northern-

Hemisphere area-averaged surface temperature (NHT), the Atlantic Multidecadal Oscillation (AMO), Atmospheric-Mass Transfer anomalies (AT), the North Atlantic Oscillation (NAO), an index representative of the El Nino-Southern Oscillation (NINO3.4), the North Pacific Oscillation (NPO), the Pacific Decadal Oscillation (PDO), and the Aleutian Low Pressure Index (ALPI). The majority of these indices represent the months DJFM, when atmospheric variability is most intense and atmospheric modes (e.g. NAO) are most pronounced. Prior to analysis, all raw indices were linearly detrended (least squares method) and divided by the index's standard deviation to normalize it to a unit variance. This is done to eliminate large discrepancies in amplitude of variability between indices, facilitating inter-comparison of index behavior.

Table 3.2: Observed climate-index network: (adapted from Wyatt et al. 2011)

Index/Acronym	**Reference/Data source**	**Description/General Information**
Aleutian Low Pressure Index AL or ALPI	Beamish and Bouillon (1993) Beamish et al. (1999)	Relative intensity of SLP in N.Pacific (~50°N) in winter (DJFM). Calculated as mean area (km^2) w/ SLP<100.5kPa. Expressed as anomaly relative to the 1950–1997 mean.
Atlantic Multidecadal Oscillation Index AMO	Sutton and Hodson (2005) http://www.met.rdg.ac.uk/~dan/work.php	North Atlantic SSTA averaged across 0–60°N, 75–7.5°W; 1871–2003 Monopolar SSTA pattern N. Atlantic
Atmospheric-Mass Transfer Anomalies **AT**	Vangenheim (1940); Girs (1971) http://alexeylyubushin.narod.ru/ lyubushin@yandex.ru	Dominance of air transfer direction 30°–80°N; 45–75°E; Proxy for atmospheric-heat transfer; reflects longitudinal/latitudinal shifts in position of atmospheric centers-of-action, w/ implications for hemispheric communication of climate signal.
North Atlantic Oscillation Index **NAO**	Hurrell (1995) http://www.cgd.ucar.edu/cas/jhurrell/indices.data.html#npanom	Normalized SLP difference Azores and Iceland ~ 1st PC (Principal Component) of SLP in the North Atlantic; re-distribution of atmospheric mass b/n subpolar and subtropical latitudes, reflecting jet-stream variations.
Northern Hemisphere Temperature **NHT**	Jones & Moberg (2003); http://www.cru.uea.ac.uk/	Average surface land and sea-surface temperatures of Northern Hemisphere 1850–2003 NHT characterizes overall climate variability, with strongest changes occurring at high northern latitudes.

El Niño/ Southern Oscillation region 3.4 NINO3.4	Calculated from the HadSST1 http://www.cdc.noaa.gov/gcos_wgsp/Timeseries/Data/nino34.long.data	Average SSTA 5°N–5°S; 170°W –120°W Proxy for ENSO behavior
North Pacific Oscillation Index **NPO**	Wang et al. (2007) wanglin@mail.iap.ac.cn cw@post.iap.ac.cn	Meridional dipole in SLP over North Pacific; pressure variations b/n Hawaii and Alaska/Alberta, reflective of meridional re-distribution of atmospheric mass. We used that of Wang et al. 2007: 2nd EOF SLPA 100ºE - 120ºW, 0º-90ºN. Rogers (1981); Walker and Bliss (1982);
Pacific Decadal Oscillation Index **PDO**	Mantua et al. (1997); Minobe (1997, 1999) ftp://ftp.atmos.washington.edu/mantua/pnw_impacts/INDICES/PDO.latest	Leading PC of SSTA north of 20°N in North Pacific, with century-scale globally averaged SSTA removed; Strongly related to intensity and location of Aleutian Low

3.2.2.2 Methods for Original Stadium-Wave Analysis

Identifying the climate signal: Initial evaluation of a suspected hemispherically propagating signal was accomplished through use of Multiple-Channel Singular Spectrum Analysis (M-SSA: Broomhead and King 1986; Elsner and Tsonis 1996; Ghil et al. 2002). M-SSA is a spatio-temporal-filter technique and a generalization of Empirical Orthogonal Function (EOF) analysis. In fact, M-SSA is a generalization of EOF analysis applied to an extended time series. Both tools of analysis are intended to explore the underlying variance structure of a set of correlation coefficients. EOF analysis identifies zero-lagged relationships, while M-SSA excels in its ability to detect relationships at a non-zero lag, a feature characteristic of propagating signals (Ghil et al. 2002 and references therein). Questions to consider are: How much of an index's variability is related to each of the identified patterns? And for each pattern of variability, or mode, what is its temporal signature?

To address these questions, this M-SSA extended time series is generated from the original time series, augmented by *M* lagged, or shifted, copies thereof. Each of the index time series is referred to as a channel. Because in the stadium-wave studies, each index time series represents a spatial region, an eigenfunction - the function that best describes the variability of a given mode - of this extended lagged covariance matrix provide spatiotemporal filters. The filters are related to coefficients, or EOF weights, related to the eigenfunction that best captures the pattern of variability shared by the index set. It is through these filters that modes of climate variability are defined. These modes are patterns that best describe the lagged co-variability of the original data set.

The mode whose pattern explains the most variance (the common variations identified in the time series) in the extended time series is the leading mode – mode one. The variances explained by modes two, three, etc decrease progressively as the mode numbers increase. In the case of the stadium-wave, twenty modes were extracted. The mean values of the mode variances were plotted. This is the M-SSA spectrum. Modes one and two tend to capture most of the variance of the extended time series.

The mode of variability in each index's time series identified by the M-SSA filter is represented by a new time series. This new time series is termed 'reconstructed components' (RC). Reconstructed components are effectively the narrow-band filtered version of an original multivariate time series. The sum of reconstructed components of each M-SSA mode of an index is identical to the index's original time series.

For the stadium-wave, reconstructed components of the leading two modes were summed and normalized. Plotted, these normalized reconstructed components of the hybrid signature

allow visualization of the variability associated with this identified climate signal as it propagates through the index-network of indices.

Assessing Statistical Significance of the Identified Climate Signal: To assess the unlikelihood that the identified signal was merely a random consequence of noisy data, a red-noise model was fitted independently to the time series of each climate index in the original data set.

$$x^{n+1} = ax^n + \sigma w, \qquad (1)$$

where x^n is the simulated value of a given index at time n; x^{n+1} is its value at time $n+1$; w is a random number drawn from a normal distribution with zero mean and unit variance; parameters a and σ are computed by linear regression. Surrogate time series were generated, each characterized by a lag-one autocorrelation – consistent with treatment of the original time series in M-SSA. Modes of variability that explain the variance in the red-noise data set were identified. These red-noise modes are patterns found in random data. Thus, these patterns (or their correlations) are no more than coincidence. The range of such coincidental results was used to set an envelope - the envelope of uncertainty, or red-noise envelope. In order for "real data" values to be considered statistically significant, their time series must fall outside of this envelope of uncertainty to be considered likely to be non-random. Outside this envelope, there is a presumed 5% chance or less that this assumption of non-randomness is false. Such values are then considered to be significant at the $p < 5\%$ level, or significant at the 95% confidence level. The terminology is interchangeable.

Next, error bars were calculated for the "real data" modes that explained the variance of the data set. The error bars here represent the uncertainty of the mean of the variance. They represent the standard deviation of the red-noise surrogate data described in the previous

paragraph. One can consider the error bars on the "real data" modes to be the observed variance of each "real data" mode plus/minus the standard deviation of the variances generated by the red-noise data.

To calculate the error bars, the variance of the mode was multiplied by the square root of $2/N^*$, where N^*= the number of degrees of freedom. N^* was estimated using the Bretherton et al. (1999) formula $N^* = N(1-r^2)/(1+r^2)$, where N=100 is the length of each time series in the original stadium-wave index set, and $r \approx 0.65$ is the maximum lag-1 autocorrelation among the set of indices. Thus, the effective number of degrees of freedom, N^*, in the case of a 100-year time series, is equal to 40. And the estimated decorrelation time is $N/N^* = 100/40 = 2.5$. This term, decorrelation time, is used as a vague estimate of this dependence of one value on the next. And although there is no real physical meaning for the term, it is often considered to designate the minimum time required for two consecutive observations to be considered independent of one another.

The preceding operations are intended to assess statistical significance of the modes of variability. The plotted M-SSA spectrum summarizes these operations: a range of modes explaining the variance of the extended time series, each with error bars representing standard uncertainty of the mean variance, and a red-noise envelope, outside of which values are considered significant at the $p < 5\%$ level. See figure **3.1**a. This shows the M-SSA spectrum for the original stadium wave (Wyatt et al. 2011).

(a)

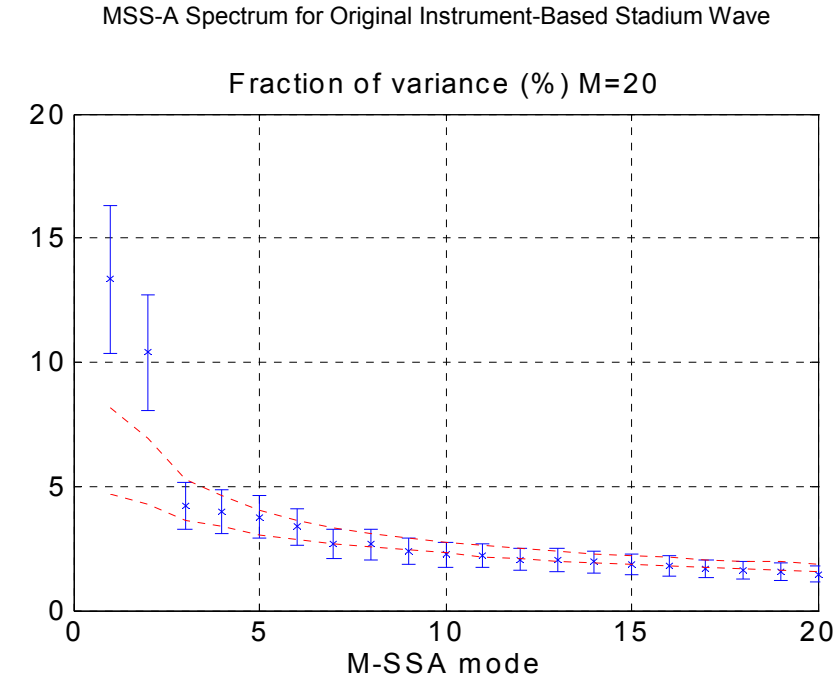

(b)

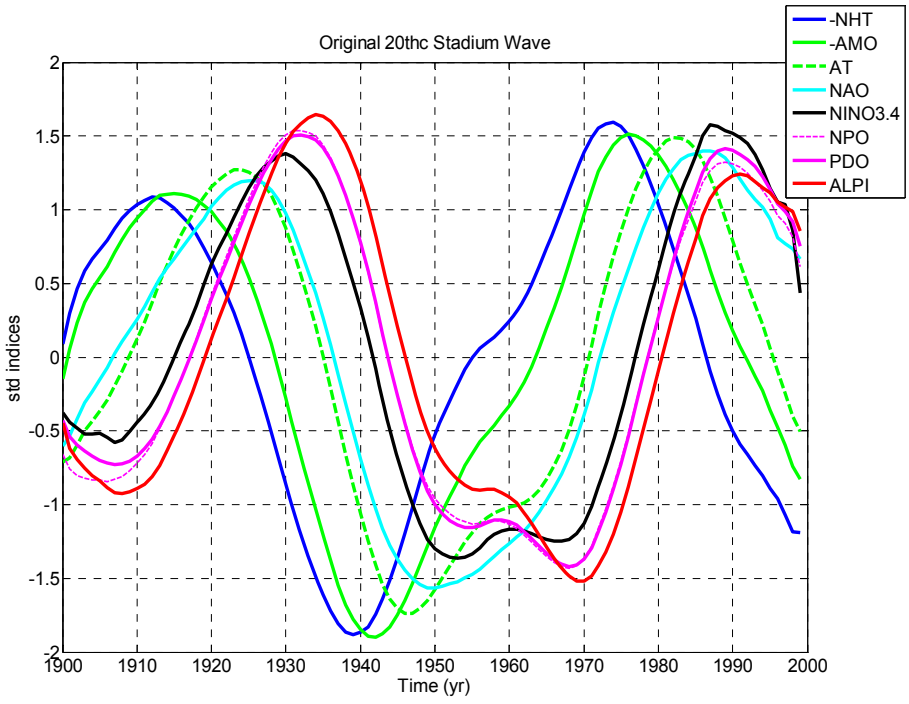

Fig. 3.1: (a) M-SSA spectrum for original stadium wave (b) Normalized reconstructed components (RCs) of M-SSA leading two modes of variability. Eight-index network of original "stadium wave", adapted from Wyatt et al. (2011). RC time series have been normalized to have unit variance. Note: RCs of NHT and AMO are negative.

Of the modes of variability whose mean variances were significant at the 95% confidence level, only the modes that were well separated from remaining modes, and whose error bars overlapped, were considered (according to the North et al. (1982) criterion). If two leading modes met the criteria described thus far, then the next step was addressed.

The leading modes must form an oscillatory pair. To establish that this was true for the identified leading modes, a so-called 'parity test' was necessary. Three requirements had to be met: 1.) For each of the two leading modes, corresponding error bars, representing the 95% confidence level (standard uncertainty) of the given mode's variance, must overlap. This overlap indicates the variance means of the two modes are not statistically different. 2.) Reconstructed components representing the individual leading modes in each of the indices must show similar timescales of variability for each of the two modes. 3.) And the phasing of the variability exhibited in the two sets of reconstructed components must be in-quadrature.

If the two leading modes met these criteria, their reconstructed components were combined and normalized. This new filter was the M-SSA identified climate signal.

To confirm the identified climate signal was not dominated by only one or two indices, Wyatt et al. (2011) analyzed an artificially re-configured index set. This artificially re-configured set contained eight members selected from the original collection of time series, but not necessarily eight different members of that collection. Using the bootstrap method, multiple (~10,000) random combinations were assembled from the original index set. A random collection selected from the original set might have represented all eight indices, but more likely would have represented only several, with some of the indices repeated and others deleted. To these re-configured index sets, M-SSA was applied in the same manner as previously described. If the hypothesized climate signal explained statistically significant variance in each

reconfigured index set, then results of the M-SSA and significance tests would be similar to those of analysis on the full set of eight original indices. And finally, if these criteria were met, it could then be assumed that the identified climate signal was not dominated by only one or two of the eight indices. The signal's nature would be truly multivariate.

I now apply these methods and criteria to the following steps of this study.

3.2.2.3 Data Set for Evaluation of Historical Longevity of the Stadium Wave

Reconstructed indices selected to evaluate stadium-wave historical behavior include: (i) reconstructions of the annual AMO based on tree rings from Eastern North America, Europe, Scandinavia, North Africa and the Middle East (Gray et al. 2004); (ii) a multi-proxy (tree-ring and ice-core) reconstruction of the winter NAO index (Cook et al. 2002); (iii) multi-proxy (tree-rings, ice cores, and Eurasian documentary and instrumental data) NAO reconstructions with monthly resolution (Luterbacher et al. 2002), from which I extracted the boreal winter (DJFM) averages; (iv) reconstructions using tree-ring chronologies from fourteen extratropical sites in the Northern Hemisphere for annual[2] NHT (Esper et al. 2002); (v) reconstructions of annual NHT from multi-proxy tree-ring, ice-core, coral, and historical documentation (Jones et al. 1998); (vi) an Asian tree-ring-based springtime reconstruction of PDO (D'Arrigio et al. 2006); (vii) a drought-flood index derived from historical documents of 28 regions spanning northeastern to southeastern China, which provide a proxy of summer monsoon-related rainfall for the reconstruction of PDO (Shen et al. 2006); and (viii) a tree-ring-based reconstruction of cool-season precipitation patterns in Southern and Baja California that provide a proxy for the PDO

[2] Tree-rings tend to capture warm-season temperatures; Esper et al. state that on low-frequency timescales (multi-decadal), annual and warm-season temperatures are virtually indistinguishable.

(Biondi et al. 2001). To simplify communication, I term these proxies "conventional proxies" throughout this paper.

3.2.2.4 Methods for Assessing Historical Longevity

Extending the stadium-wave sequence beyond the availability of observational data – most of which terminates between 1850 and 1900 – requires use of proxy data. As with all data sets, climate proxies have their limitations. First, climate proxies are inadequate to reconstruct all eight members of the original stadium wave. Furthermore, each index proxy comes with its own set of caveats. Examples of caveats shared by all proxy reconstructions to one degree or another include 1) noise-ridden data sets, 2) contamination of a climate signal from sources other than, but related to, the variable of interest, and 3) signal-quality deterioration in the record the further back in time the variable is measured. A combination of reconstructions, therefore, runs the risk of compounding uncertainties. For these reasons, a reduced member network was assembled.

The first step was to identify a statistically significant abbreviated network from the original index-set – i.e. a core group among previously tested observational indices. Permutations of abbreviated stadium-wave observational index collections were analyzed with the methods used in the original stadium-wave analysis described in section 3.2.2.2. The resulting culled instrumental-based index-set included NHT, AMO, NAO, and PDO. Adding the index for atmospheric-mass-transfer (AT), which represents basin-scale wind patterns, amplifies statistical robustness, a matter further explored in section 3.3.

Proxy reconstructions for NHT, AMO, NAO and PDO were chosen according to length of record and potential ability to capture low-frequency variability. M-SSA and statistical-

testing methods, as described in section 3.2.2.2, were applied to the 20th-century record of the proxy data.

Where it was necessary, I infilled data in gapped time series. This I did by using M-SSA imputation procedure, developed in Beckers and Rixen (2003) and Kondrashov and Ghil (2006)). These methods are described in Wyatt et al. (2011). Most proxy time series were continuous for the periods tested; where gaps existed, they typically spanned fewer than ten years.

Proxy reconstructions passing statistical testing for 20th century runs were used to evaluate the history of signal propagation for the periods: 1850-2000 and 1700-2000.

3.2.2.5 Data for Exploring Dynamics/Mechanisms of the Stadium-Wave Propagation

Data for 20th century analysis: In addition to the original instrumental-based index set and the aforementioned collection of 'conventional' proxies, five additional proxies, were included to explore mechanisms behind the stadium-wave hemispheric-signal propagation. To facilitate discussion, I termed the five additional proxies "dynamic proxies". The use of "dynamic" here is not intended to be descriptive of process; it merely designates the use of these indices in my investigation of stadium-wave dynamics.

I chose the proxies used in this step based on two things: literature research and how they appear to relate to the working hypothesis presented here. That working hypothesis is based on ocean-ice-atmospheric coupling, with associated latitudinal shifts of the Intertropical Convergence Zone and changes in hemispheric surface-temperature trend. My immediate goal is to show the connection between these "dynamic proxies" and sub-processes involved in stadium-wave propagation.

Data were drawn from the following: (i) an 825-year sub-decadally resolved record of *G. bulloides* (GB: Black et al. 1999) abundance (annual resolution extrapolated for the portion used in this study), as measured from marine sediment in the Cariaco Basin off the coast of Venezuela – a proxy associated with latitudinal migrations of the Atlantic mean Intertropical Convergence Zone (ITCZ); (ii) Sr/Ca isotope ratios in corals from Palmyra Island in the central Pacific tropics (160ºW, 6ºN), representing sea-surface-temperatures (SST) related to El Nino Modoki (Di Lorenzo et al. 2010) – a "flavor" of the El Nino-Southern Oscillation phenomenon associated with activity of the North Pacific Gyre Oscillation (NPGO: Nurhati et al. 2011); (iii) Japanese Sardines (JS) (Kawasaki 1994; Klyashtorin 1998), whose outbursts off the coast of Japan are spatially related to the western-boundary current (Kuroshio Current) and its associated extension; (iv) Earth's rotational-rate anomalies (Klyashtorin1998; Sidorenkov 2005, 2009), as reflected by low-frequency length-of-day variability, fluctuations of which are related to variations in Earth's moment-of-inertia; and (v) the record of reconstructed-irradiance anomalies of the solar "constant" by Lean (2000, 2004), used to represent solar variability.

I also added anomalies of Arctic surface temperature and Eurasian Arctic Shelf sea-ice (Frolov et al. 2009). August sea-ice-extent data for the Western Eurasian Seas (Greenland, Barents, and Kara Seas (~15ºW eastward to ~ 100ºE), the Eastern Eurasian Seas (Laptev, East-Siberian, and Chukchi Seas (~100ºE eastward to ~150ºW)), and mean annual Arctic surface temperature, were merged with original and 'dynamic proxy' indices.

Also appended to this collection was the Pacific Circulation Index (PCI: Beamish et al. 1997; King et al. 1998). PCI reflects protracted intervals of time during which anomalies of atmospheric-mass transfer over the North Pacific are either dominantly zonal (+ anomalies) or dominantly meridional (- anomalies). PCI is analogous to the Atmospheric Circulation Index

(ACI: Vangenheim 1940; Girs 1971a,b), which is the time-integral of Atmospheric-Mass-Transfer (AT) anomalies - an Atlantic-Eurasian-centered metric of dominant direction of air-mass flow.

Last of the additions to the original set was the Atlantic sea-surface-temperature-anomaly (SSTA) dipole ((Dipole): Keenlyside et al. 2008), considered a proxy for multidecadal migrations of the mean Atlantic Intertropical Convergence Zone (ITCZ), and by extension, the Atlantic Meridional Overturning Circulation (AMOC) (Latif et al. 2006). All newly added indices are detailed in **Table 3.3**.

Table 3.3: Index descriptions for indices appended to original stadium-wave network

Index/Acronym	Reference/Data source	Description/General Information
(GB) G.bulloides	Black et al. 1999 (and personal communication)	an 825-year sub-decadally resolved record of *G. bulloides* abundance (annually resolved for the portion used in this study), as measured from marine sediment in the Cariaco Basin off the coast of Venezuela – a proxy associated with latitudinal migrations of the Atlantic mean Intertropical Convergence Zone (ITCZ), and, by extrapolation, with the Atlantic Meridional Overturning Circulation (AMOC) and AMO
(JS) Japanese Sardine Outbursts	Klyashtorin and Lyubushin (2009) and direct and archive accounts; also Kawasaki 1994 and Klyashtorin 1998	Outbursts off coast of Japan, in western-boundary-current and extension, share similar tempo with stadium-wave behavior
(solar) Solar TSI reconstruction	Lean (2000; 2004)	Reconstructed-irradiance anomalies of the solar "constant"
(ngLOD) Earth's Rotational-Rate Anomalies	Sidorenkov (2005; 2009) and personal communication	low-frequency-variability of negative length-of-day (ngLOD) anomalies, revealing fluctuations related to perturbations in Earth's angular velocity, temporally coincident with observed multidecadal climate variability
(NPGO) NPGO proxy	Nurhati et al. (2011)	Sr/Ca isotope ratios in corals from Palmyra Island in the central Pacific tropics (160ºW, 6ºN), representing sea-surface-temperatures (SST) related to El Nino Modoki (Di Lorenzo et al. 2010) – a "flavor" of the El Nino-Southern Oscillation phenomenon associated with activity of the North Pacific Gyre Oscillation

(Arctic dT) Arctic surface temperature anomalies	Frolov et al. (2009)	Mean annual surface air temperature (SAT) in zone: 70 to 85ºN for 1900-2007
(Grnlnd) Greenland sea-ice extent	Frolov et al. (2009)	Mean monthly ice-index values for August.
(Barents) Barents sea-ice extent	Frolov et al. (2009)	Mean monthly ice-index values for August.
(Kara) Kara sea-ice extent	Frolov et al. (2009)	Mean monthly ice-index values for August.
(WIE) West Ice Extent = (Grnlnd+Barents+Kara)	Frolov et al. (2009)	Mean monthly ice-index values for August.
(Laptv) Laptev sea-ice extent	Frolov et al. (2009)	Mean monthly ice-index values for August.
(E.Sib) East Siberian sea-ice extent	Frolov et al. (2009)	
(Chuk) Chukchi sea-ice extent	Frolov et al. (2009)	Mean monthly ice-index values for August.
(EIE) East Ice Extent = (Laptv+ E.Sib+ Chuk)	Frolov et al. (2009)	Mean monthly ice-index values for August.
(TIE) Total Ice Extent = WIE + EIE	Frolov et al. (2009)	Mean monthly ice-index values for August.
(PCI) Pacific Circulation Index	Beamish et al. 1997; King et al. 1998	Reflects protracted intervals of time during which anomalies of atmospheric-mass transfer over the North Pacific are either dominantly zonal or dominantly meridional. PCI is analogous to the Atmospheric Circulation Index (**ACI**: time integral of AT (see table 1a for AT details))
(Dipole) Atlantic SST Dipole Index	Keenlyside et al. 2008	SST area averages (60–10W, 40–60N minus 50–0W, 40–60S); considered a reflection of ITCZ migration in Atlantic, and to be related to variability in the Atlantic Meridional Overturning Circulation (AMOC)

In M-SSA, the compaction of data – compressing raw variables into indices – allows for the enhancement of the signal-to-noise ratio. And because indices in the stadium-wave analyses are drawn from geographically diverse regions, a spatial component is added to the temporal filter. There is a risk, though, of adding too many indices. While additional observations in the

time domain are always desired, the same is not true for observations in the spatial structure. Too many variables representing one region fail to add information to the data set. There is a risk of overfitting. The number-of-degrees of freedom can be exceeded by the number of indices. Results will thereby be skewed.

I have kept this in mind with the additions of indices to the stadium-wave data set. Many of the newly added indices represent regions not represented in previous work. Thus, new information is gained regarding Arctic and tropical latitudes. Also, as will be seen in the methods section, I analyze subsets of this expanded data set in addition to analyzing the full set. This approach tests whether addition of indices in the fully expanded set impacted results. It did not.

Data for the 1700-to-2000 analysis: Availability of data sets for the full 300-year period was limited. Indices used in this step include: *G. bulloides*, Japanese Sardines, the solar constant, and Earth's rotational-rate anomalies (index details under Data for 20thc, section 3.2.2.5).

3.2.2.6 Methods for investigation of mechanisms and dynamics

20th century analysis: The first step in this part of the research was to determine if this newly expanded collection of indices, and subsets of such, shared a common dominant low-frequency climate signal. To this end, I used methods previously described (section 3.2.2.2). Through the methods detailed in section 3.2.2.2, I identified the apparent existence of a shared, statistically significant, multivariate, propagating, secularly varying climate signal in the expanded 20th century data set, as well as in numerous subsets of the expanded set. With this goal met, my next goal was to gain greater insight into low-frequency index relationships among indices of the expanded data set. To that end, in addition to performing M-SSA on the larger data set, I correlated pairs of raw time series of that expanded data set.

Correlations were computed between linearly detrended (least squares method), normalized raw time series, smoothed with a 13-year running-mean filter. Red-noise model (1) was fitted to the data and one thousand surrogate time series generated. Correlations between pairs of surrogate indices were computed, setting the 95% red-noise envelope for the standard range of random correlations. Correlations between original pairs of indices were then estimated. Only those original correlations, whose ranges of mean values fell outside the red-noise envelope, i.e. significant to at least the $p < 5\%$ level, were considered.

I also evaluated anomaly trends of indices. I did this because I think anomaly trends potentially convey insight into forcings and responses among indices whose behaviors are interconnected within a network. Wyatt et al. (2011) consider the stadium-wave signal to propagate through a network of interconnected indices; thus the anomaly trends I present here are intended to provide one more means of evaluating collective behavior within a network. I offer an example to edify this point. A plot of incremental measurements reflecting a sub-process may show a noisy collection of anomalies that are all positive over a range of a few decades, alternating with a multidecadal interval of negative anomalies. I'll call this time series 'itx". If an anomaly trend (cumulative sum) is generated from this time series and plotted, one would see the once-noisy collection of positive (negative) anomalies represented as a positively (negatively) sloping line, hitting its maximum (minimum) when the interval of positive (negative) polarity anomaly values of the original time series ceases. Continuing this example, consider another noisy time series. It may also exhibit multidecadal intervals of positive and negative anomalies, even though its time series may show little apparent resemblance to time series 'itx'. I'll call this time series 'atx'. If its anomaly trend closely correlates with the anomaly trend of 'itx', a relationship between the two processes may emerge. Moreover, if these time-integrated time

series correlate strongly with a *non*-transformed time series, a relationship between them might be more than coincidence, indicating assimilated impacts. Alekseev (1995) suggests that some characteristics of the ocean or ice cover "can result from the prolonged accumulation of stochastic forcing by the atmosphere." I incorporate that assumption with this approach. Causality, of course, cannot be determined from correlation alone. Yet a collection of correlated indices, whose interrelationships are ideally supported by model and observational studies, may give insight into the role played by assimilated impacts of a process. Thus, transformed time series are not "real" indices; they merely serve as tools.

To transform a raw time series into its anomaly trend, or time integral (Hurst 1951; Outcalt et al. 1997), I computed a "cumulative sum". Cumulative Sum (cs) of a time series of anomalies, X, is obtained via equation 2:

$$Xcs_{(t)} = X_{(t)} + Xcs_{(t-1)} \qquad (2)$$

First, I correlated pairs of cumulative-sum indices. In a subsequent iteration, I correlated cumulative-sum indices with non-transformed indices. The non-transformed indices are simply the raw time series that have been linearly detrended, normalized to unit variance, and filtered with a 13-year running mean prior to the calculation. In keeping with all previous tests, red-noise model (1) was applied to both sets of correlations to assess significance, in this case, significance of the correlations between time series, as described in section 3.2.2.2. Only those correlations significant to at least the $p < 5\%$ levels were considered to be of likely non-random occurrence and are retained.

Also of value to this investigation are index differences (Xdiff). Here I use the time-derivative of a time series. Again, I consider the resulting transformed time series not to be real indices, merely tools. I use them to gain insight into forcings on the time series. Again, I offer an example. A given index may have strong persistence, representing a process with a long memory. This is typical of ocean-related indices. If the time-derivative of such a series is calculated (the time-derivative here can be called 'cumulative-sum-removed'), correlation of this time-derivative time series with a non-transformed time series of a different index may show co-variance, thereby potentially providing insight into incremental forcings on the former by the latter. I interpret this co-variability as instructive in evaluating the network behavior of interacting indices. Differences - or approximations of time derivatives - were taken of select time series to evaluate changes per unit time, using the same methods as described above.

$$X\ diff_{(t)} = X_{(t)} - X_{(t-1)} \qquad (3)$$

Analysis for 1700-2000: Results of the 20th century investigation guided strategy for the extension of analysis to 1700. Time-series-transformation operations, computation of correlations of time series, M–SSA, and related statistical tests, all previously described (this section and in section 3.2.2.2) for the 20th-century analysis, were applied to the reduced-member data set.

3.3 Results

Results of the present study are best understood within the framework of the original study (**Figure 3.1**b). Stadium-wave signal-propagation is the foundation of the secular-scale

variability detected in 20th-century climate. The sequence below indicates the order of the signal's propagation through the network of eight climate indices originally evaluated. The years in parentheses indicate the mean phase shifts (lag times) between indices (Wyatt et al. 2011).

-NHT → (4y) → -AMO → (7y) → +AT → (2y) → +NAO → (5y)→ +NINO → (3y) → +NPO/+PDO → (3y) → +ALPI → (8y) → +NHT → (4y) → +AMO → (7y) → -AT → (2y) → -NAO → (5y)→ -NINO → (3y)→ -NPO/-PDO → (3y) → -ALPI → (8y) → -NHT .

The sequence depicted above suggests the propagation of an M-SSA-identified climate signal through a collection of atmospheric and oceanic teleconnections. The secular-scale duration of this hemispheric propagation was estimated to be ~ 64 years during the 20th century. Wyatt et al. (2011) note that while a periodicity for this variability cannot be identified with statistical significance for the one-hundred-year record analyzed, what is striking is that there appears to be a statistically significant succession of indices carrying this climate signal, where expression of the signal in one index is expected to follow in all other indices in successive lagged order.

3.3.1 Results for Stadium Wave of 'Conventional' Proxies: 1700-2000

The first step in evaluating the stadium-wave's historical longevity relied upon the conventional proxies described in section 3.2.2.4. **Figures 3.2a-c** show three proxy-based stadium-wave sequences for three time periods: 1900 to 2000, 1850 to 2000 and 1700 to 2000.

(a)

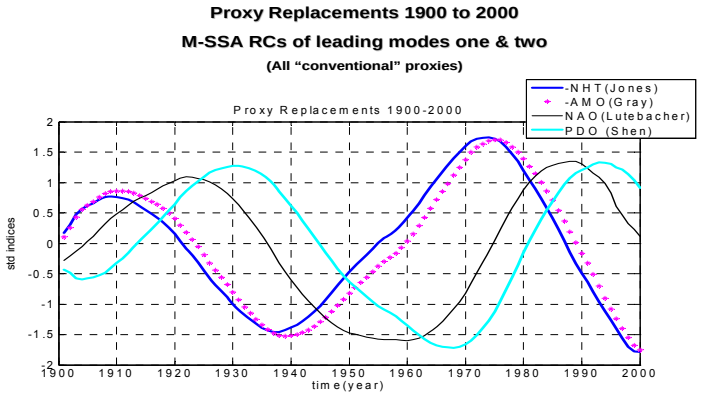

(b)

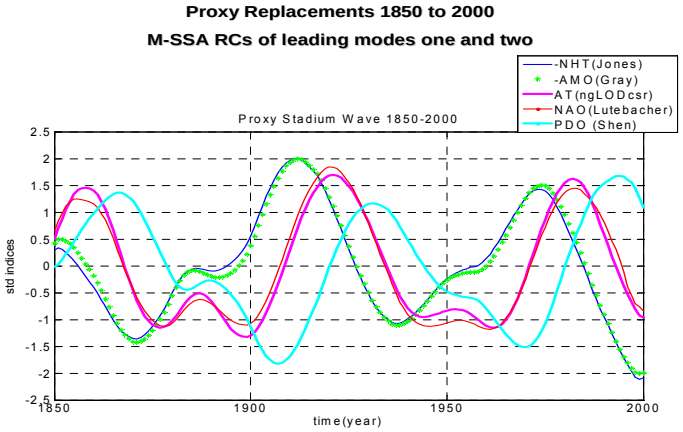

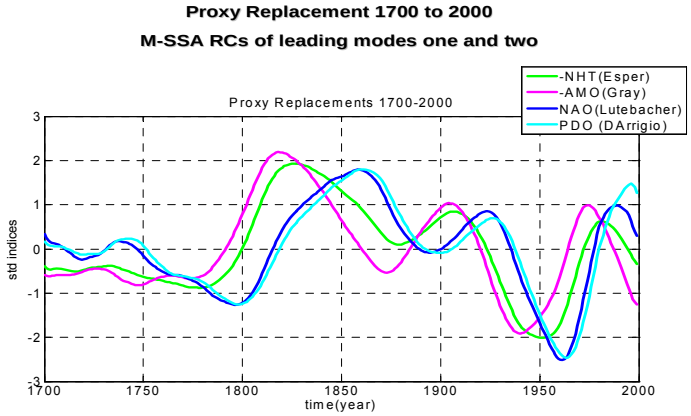

Fig. 3.2: Normalized reconstructed components (RCs) of M-SSA leading two modes of variability in "conventional" proxies represent an abridged set of stadium-wave indices for the 20th century (**a**), for the years 1850 to 2000 (**b**), 1700 to 2000 (**c**). (See text for proxy descriptions.) Each stadium wave is based on a slightly different set of indices.

The pattern of propagation through the proxy network in the 20th century is similar to analogous indices in the instrumental data set (Fig. 3.2**a**). Similar sequence order can be seen coursing through the proxy network for the interval 1850 to 2000 (Fig. 3.2**b**). The plot in Fig. 3.2**c** shows a strong stadium-wave pattern dating to 1800, before which time the sequence order remains constant; yet the amplitude of variability dramatically drops. Note that the Northern Hemisphere surface temperature index (NHT) has a slightly different temporal relationship with the Atlantic Multidecadal Oscillation in this plot. It lags the Atlantic Multidecadal Oscillation by a few years. This is likely due to idiosyncrasies related to the proxy selected. The proxy reconstruction used in this plot for NHT is a reconstruction done by Esper et al. (2002). A NHT reconstruction by Jones et al. (1998) was used in plots 3.2a and 3.2b. Availability of data prompted the substitution.

Statistical significance testing for each of these stadium-wave figures is summarized: For the 20th century, a statistically significant multidecadal climate signal was identified in the 'conventional proxy' network. The dominant M-SSA pair of leading modes (the climate signal) generated from the various proxy collections was unlikely to be due to random sampling of uncorrelated noise; for all proxy-reconstruction networks, the M-SSA identified multidecadal climate signal accounts for a fraction of variance exceeding 95th percentile of the corresponding surrogate spectra generated by the red-noise model (1). The M-SSA spectra for one such 20th century proxy-index network is shown in **Fig. 3.3**a. This figure shows the two leading modes identified by M-SSA are significant at the $p < 5\%$ level. Parity testing shows a multidecadal oscillatory pair for all proxy collections (not shown).

(a)

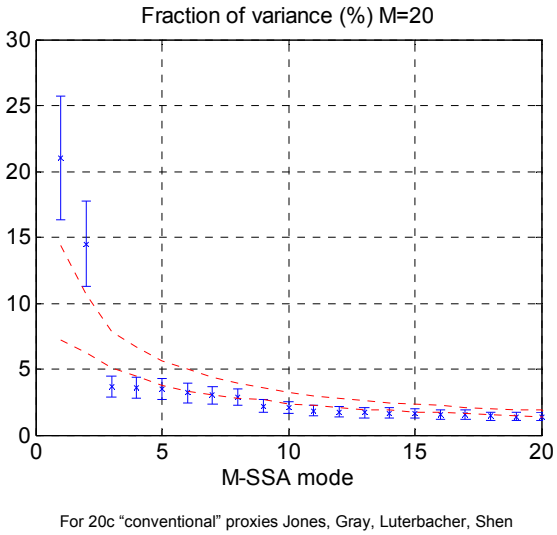

(b)

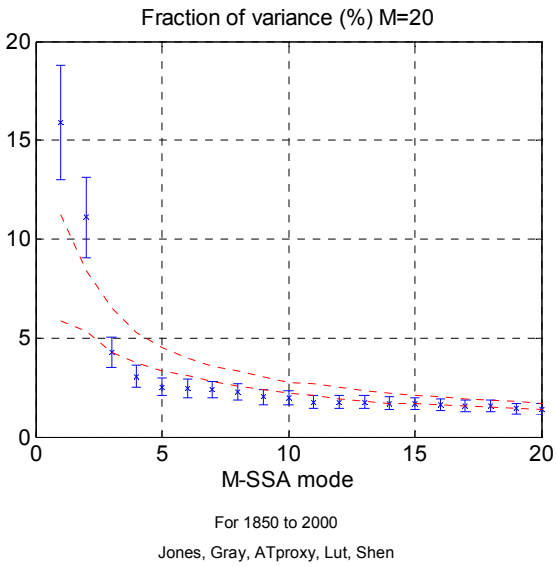

Fig. 3.3: M-SSA spectra of networks of conventional proxies (see text) representing individual variances (%) for the various modes of variability: (a) A four-member 20th-century network and (b) the same network for 1850 to 2000 with AT added.

Significance of $p < 5\%$ for the 1850 to 2000 interval was not found in the proxy-index network used for the 20th century. That network was based on proxy reconstructions of Northern Hemisphere Temperature (NHT), Atlantic Multidecadal Oscillation (AMO), North Atlantic

Oscillation (NAO), and the Pacific Decadal Oscillation (PDO). To see if a larger network would increase the significance, I added an index representing the large-scale zonal wind component in the Atlantic-Eurasian sector – the Atmospheric-Mass-Transfer index (AT). In the original Wyatt et al. (2011) study, this index was shown to have a relatively high channel-fractional variance, meaning the variability of this index could be, to a relatively large degree, explained by the pattern of the identified stadium-wave climate signal. In fact, this addition did increase the significance to $p < 5\%$ (Fig. 3.3b). The record of the atmospheric-mass transfer (AT) does not pre-date 1870. Its time-series must either be infilled or a proxy must be utilized. I did the latter. This is discussed further in section 3.3.2.

Prior to 1850, results showed no significant or near-significant results, despite the fact that a plot resembling the stadium-wave was produced for the interval 1800 to 2000. I am unable to determine in this current research whether this apparent deterioration of statistical significance with analysis further back in time is due to the signal being spurious prior to 1850 or due to the nature of proxy data prior to 1850. Proxy data are inherently noisy, and quality tends to deteriorate with increased time interval measured (Jones et al. 1998). Thus, conclusions regarding the stadium wave's statistically significant existence before 1850 are difficult to assert. That said; an apparent stadium-wave climate signal was identified in the conventional-proxy network for the interval 1900 to 2000 and in the network of conventional-proxies plus AT for the interval 1850 to 2000.

3.3.2 Results for Stadium Wave of 'Dynamical' Proxies – 20th century analysis:

20th century analysis: M-SSA and correlations of time series were done on the expanded data set and subsets of such. The goal here was to determine whether the stadium-wave signal

was expressed in indices other than those of the originally identified propagation sequence. If it was, the next goal was to determine if the new information could further my understanding of dynamics of stadium-wave propagation. Detailed results and strategies follow.

For the 20th century, all index-network collections for this time-frame yielded robust results. M-SSA results were statistically significant to at least the $p < 5\%$ level for each of the five dynamical proxies merged with the original stadium wave index set. Two leading M-SSA modes of variability of these index-collections were well separated from all others, their error-bars overlapped, indicating an oscillatory signal. Red-noise model (1) testing showed the identified leading modes were not likely a random consequence of noisy data. The same was done with Arctic data and the Dipole. An M-SSA spectrum reflecting these results is given in **Fig. 3.4**a. Cumulative variance of all modes is shown in Fig. 3.4b.

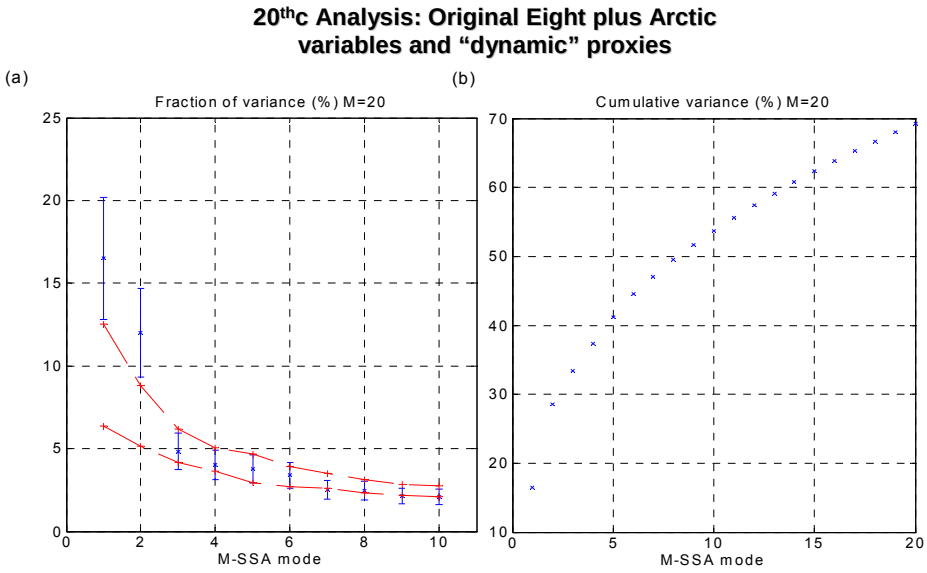

Fig. 3.4: M-SSA spectrum of the network of eight climate indices plus the addition of five "dynamic" proxies and addition of Arctic variables (see text): (a) Individual variances (%); (b) cumulative variance (% of the total). See section 3.2.2.2 for full description of method.

The bootstrap method was applied to a total of thirteen[3] original-plus 'dynamic-proxy' indices to generate a random 13-member collection of indices to which M-SSA and statistical-testing methods were applied. The same was done with Arctic data and the Dipole. This was done to ensure all included indices exhibited variability that could be explained by the stadium-wave climate signal (see section 3.2.2.2).

The original eight-member stadium wave, augmented by all "dynamic proxies" and Arctic parameters used in this study, is shown in **Fig. 3.5**. In order to facilitate visualization of this expanded network, and to explore clues for potential mechanisms, the expanded-index network is partitioned in various ways. First, the propagation sequence is broken into five groups. These groups are temporally clustered indices**.** I chose an arbitrary term to refer to these time-based groups. I call them *Groupings*. In the second iteration, indices of the propagation sequence are categorized according to process or medium. For example, in one subset, all indices related to sea-ice form a network: West Eurasian Arctic sea-ice, East Eurasian Arctic sea-ice, the Eurasian Arctic sea-ice total, etc. In another subset, all indices relate to atmospheric circulation. I refer to these subset collections as "*Process-Specific Groups*".

Together, both strategies – "groupings" and "process-specific groups" - unfold the stadium-wave dynamics.

Time Groups or "Groupings": Each Grouping is populated by indices whose peaks and valleys occur at similar times. Plots of these over the succeeding pages illustrate the reconstructed components (RCs) of these indices, reflecting each index's expression of that propagating climate signal. Correlations between raw time series (detrended, normalized, and smoothed with a 13-year filter) of index pairs are given in tables that accompany descriptions of index relationships. Most of the correlations are significant to the 1st percentile.

[3] -NHT, -AMO, AT, NAO, NINO3.4, NPO, PDO, ALPI, GB, solar, NPGO(proxy), JS, ngLOD

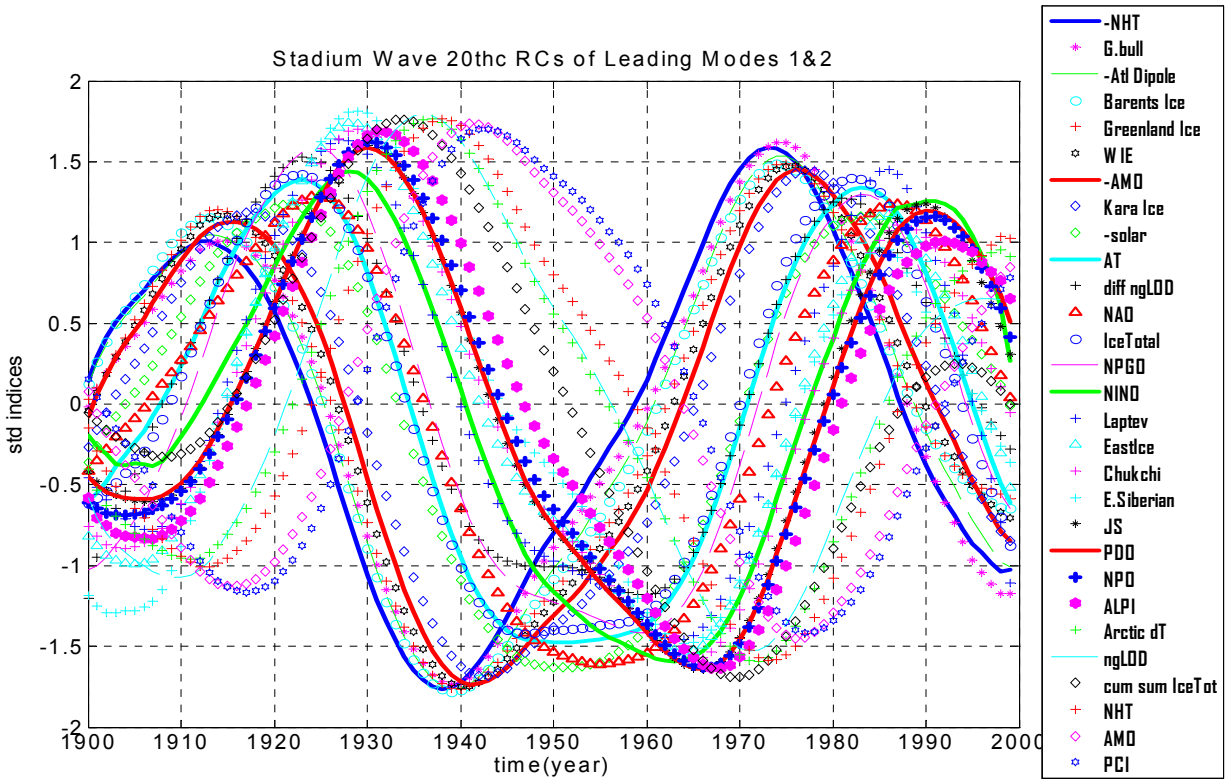

Fig. 3.5: Normalized reconstructed components (RCs) of a multiple-index network reflect signal propagation. Original stadium-wave members are mixed with five dynamic proxies (see text) and all components of the Arctic data set (see text). This dense network is broken into segments in subsequent figures in order to facilitate understanding. The RC time series shown have been normalized to have a unit variance. The indices are synchronized at, generally, non-zero lags. (Note that some indices are negative polarity (see legend and glossary (table 3.1)).)

Dynamic Sequence in Figure 3.5:

In general, in the 20thc, the signal propagation can be visualized as starting in a cool Atlantic with a southward-shifted Atlantic ITCZ, the ITCZ reaching its furthest southerly extent ~1915. A positive abundance of G.bulloides (GB) and a negative SSTA dipole indicate this. In addition, collective sea-ice-extent in the Western Eurasian Shelf Seas trends to its maximum, also ~1915. Solar (negative polarity on plot) trends toward its minimum just as basin-scale zonal winds (AT) in the Atlantic-Eurasian sector accelerate, reaching a maximum ~1923, the timing of maximum total Eurasian Arctic (west Eurasian +east Eurasian) ice. The North Atlantic Oscillation (NAO), the North Pacific Gyre Oscillation (NPGO), and NINO follow closely; all peak in succession in the 1920s. Sea-ice in the Eastern-Eurasian Arctic reaches a maximum, leading positive polarity (centered on ~1930) of the Pacific circulations (Pacific Decadal Oscillation (PDO), the North Pacific Oscillation (NPO), followed by intensification of the Aleutian-Low-Pressure index (ALPI)). By the mid-1930s, positive anomalies of the Eurasian-Arctic total sea-ice-extent give way to a trend of negative anomalies, as indicated by the cresting of the RC representing the cumulative-sum of Ice Total. The Arctic temperature reaches its

maximum warmth at this time (~1935), followed closely by the maximum of NHT (~1938). With a minimum in total sea-ice-extent in the Eurasian Arctic (in particular, in the Western Eurasian Arctic), the Atlantic ITCZ (dipole) is at its most northerly extent. The Atlantic, as indicated by the Atlantic Multidecadal Oscillation (AMO), is at its warmest (~1942) a few years after NHT has peaked. The positive anomalies of Pacific-centered circulations (i.e. PDO, NPO, and ALPI) become negative at about the same time AMO reaches its maximum positive polarity. This anomaly trend is indicated by the Pacific Circulation Index (PCI) RC. When AMO and PCI are at their maxima, the solar constant is at its maximum (the RC is negative). The related Atlantic-centered atmospheric circulations (AT, NAO) are at a minimum, in concert with the minimum in sea-ice total. This scenario, with peaks of RCs spanning from ~1915 to 1943, repeats, with peaks spanning from ~ 1970 to century's end (and slightly beyond).

I offer a rough overview of these time-related collections in hopes of facilitating communication of the tedious detail of index correlations. Five groups capture the propagation of the signal through time. Grouping-one begins with an Atlantic focus, with the main theme being Atlantic Ocean variability co-varying with the Eurasian Arctic sea-ice. Grouping-two's dominant theme is ice-atmosphere relationships, with a focus on ice and atmospheric response within the mid-Eurasian Arctic region, from the Kara Sea at ~ 60ºE to Chukchi Sea at ~ 150ºE. Grouping-three involves the North Pacific and Grouping-four highlights accumulated impacts of anomalies of sub-processes related to sea-ice extent and related atmospheric circulation, leading to Arctic T extremes. Grouping-five marks transition of regime polarities. Hemispheric temperature extremes, shifts of the Intertropical Convergence Zone, and an apparent Pacific feedback onto Atlantic processes co-occur. The cycle returns to Grouping-one.

Acronyms defined in the glossary in Table 3.1 and information detailed in section 3.2.2.5 will facilitate reading the many terms.

"Groupings"

Grouping-One – ocean and ice with an Atlantic focus (See **Figure 3.6** and **Table 3.4**.). Peaks of index RC plots occur near ~1915 and 1975. Troughs of the plots occur near ~ 1940 and ~ 2000. Correlations between pairs of 'Grouping-One' indices reveal the positive covariance among three key features: the negative polarity of the Atlantic Multidecadal Oscillation (AMO), positive Western Eurasian Arctic sea-ice (WIE), and southward-latitudinal displacement of the Atlantic Intertropical Convergence Zone (Atlantic ITCZ)[4]. Correlations values between these pairs hover around 0.90 at a $p < 1\%$ significance level.

Table 3.4: Grouping One: Correlations between pairs of raw time series of indices related to Grouping One, detrended, normalized, and smoothed with a 13-year filter prior to computation. Red-noise model (1) used to test for significance. Only values significant to at least 95% retained. Those values significant to the 99% level are shown in red; those significant to the 95% level in blue. See fig.3.6 for Grouping One stadium wave.

Index	-NHT	-AMO	WIE	Grnlnd Ice	Barents Ice	Kara Ice	ngDipole[5]	+GB
-NHT	1.0	0.83	0.77	0.70	0.76	0.63	0.87	0.84
-AMO	0.83	1.0	0.89	0.86	0.85	0.73	0.90	0.69
WIE	0.77	0.89	1.0	0.90	0.94	0.87	0.75	
Grnlnd Ice	0.70	0.86	0.90	1.0	0.86	0.65	0.79	0.60
Barents Ice	0.76	0.85	0.94	0.86	1.0	0.69	0.70	
Kara Ice	0.63	0.73	0.87	0.65	0.69	1.0		
ngDipole	0.87	0.90	0.75	0.79	0.70		1.0	
+GB	0.84	0.69		0.60				1.0

[4] A south-shifted Atlantic ITCZ is indicated by the peak of the *negative* Atlantic SSTA Dipole and by a positive abundance of G. bulloides. This coincides with ngAMO, ngNHT and posWIE.

[5] The positive polarity of the Dipole indicates a northward displacement of the Atlantic ITCZ (and corresponds to negative abundance of *G. bulloides*).

(a)

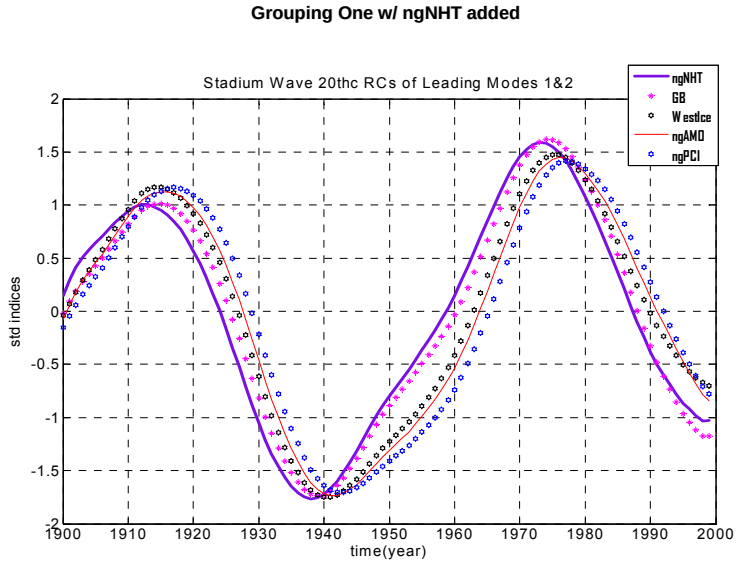

(b)

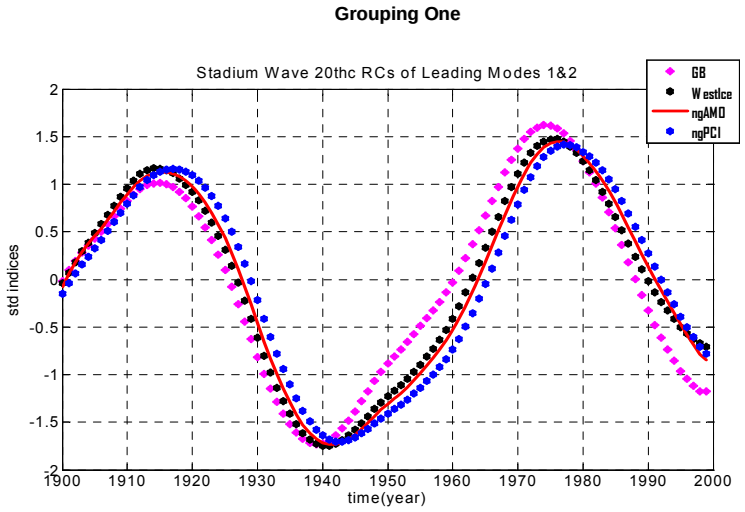

Fig. 3.6: Grouping One: (a) Peaks of index RC plots are centered on the 1910s and the 1970s. Maximum negative polarity of AMO coincides with maximum sea-ice inventories in the Western Eurasian Shelf Seas – the Greenland, Barents, and Kara Seas. Positive polarity of G.bulloides (GB) – proxy for the Atlantic Intertropical Convergence Zone (Atlantic ITCZ) - reveals a maximally south-shifted ITCZ. (b) The same plot with NHT (from preceding Grouping (-5) added for continuity). The extrema of this first grouping closely approximate previously identified hemispheric climate-regime shifts - 1918, 1944, and 1976 – after each of which, NHT trend reverses. (Refer to **Table 3.3** for 13-year-filtered raw-index correlations of indices participating in Grouping-One.)

Pacific-circulation-anomalies (reflected in PCI) co-vary with this grouping (R values ~ 0.90 at 1% significance level (discussed with Grouping-Five)). This may be due, in part, to a collective remote low-frequency influence on freshwater-export (Schmittner et al. 2000; Latif et al. 2000; Latif 2001) in the Atlantic, thereby providing a negative feedback to the Atlantic Meridional Overturning Circulation (AMOC), and by extension, the Atlantic Multidecadal Oscillation (AMO).

Peak and valley clusters of grouping-one align closely with timings of previously identified climate-regime shifts (1918, 1944, and 1976). The negative polarity of the Northern Hemisphere Temperature (NHT) slightly leads Grouping-One. It is added to the plot to provide context (figure 3.6b).

Grouping-Two – ice-atmosphere: Atlantic/Pacific (See **Figure 3.7** and **Table 3.5**a). While ocean-ice coupling dominates Grouping-One, Grouping-Two reflects the atmospheric co-variance with the changing ice inventory. This co-variance is consistent with a basin-scale wind response to the meridional temperature gradient (Outten and Esau 2011.).

Indices of Eurasian Arctic sea-ice (Ice Total[6]), AT, and NPGO dominate the character of this collection. The index RCs reach a maximum value ~1923 and another one ~ 1983 (fig 3.7a). R values are as follows: between Ice Total and AT = 0.76, between AT and NPGO = 0.69 (both at $p < 1\%$ significance level), and between NPGO and Ice Total = 0.54 at the $p < 5\%$ level.

How are AT and NPGO correlated to Ice Total?

[6] Ice Total = West Ice (includes Greenland, Barents, and Kara Seas) + East Ice (includes Laptev, East Siberian, Chukchi Seas)

Table 3.5: Grouping Two: Correlations between pairs of raw time series of indices related to Grouping Two, detrended, normalized, and smoothed with a 13-year filter prior to computation. Red-noise model (1) used to test for significance. Only values significant to at least 95% retained. Those values significant to the 99% level are shown in red; those significant to the 95% level in blue. In (a), total-ice-inventory relationships with circulations in Grouping Two are highlighted; while those in (b) focus on East Eurasian Ice extent. Single-index-pair correlations in (c) show co-variance of NAO with the dynamic proxies in this grouping. See figure 3.7 for Grouping Two stadium wave.

(a) Single Index Correlations associated with grouping two:

Single index	Ice Total	AT	NAO	NPGO
Ice Total	1.0	0.76		0.54
AT	0.76	1.0		0.69
NAO			1.0	
NPGO	0.54	0.69		1.0

(b) Single Index Correlations associated with grouping two:

Single index	NPGO	AT	East Ice	Chukchi	Laptev
NPGO	1.0	0.69	0.67	0.67	0.58
AT	0.69	1.0		0.57	
East Ice	0.67		1.0	0.91	
Chukchi	0.67	0.57	0.91	1.0	
Laptev	0.58				

(c) Single Index Correlations associated with grouping two:

Single index	NAO	Solar Constant	Diff ngLOD
NAO	1.0	-0.77	0.54
Solar Constant	-0.77	1.0	
Diff ngLOD	0.54		1.0

(a)

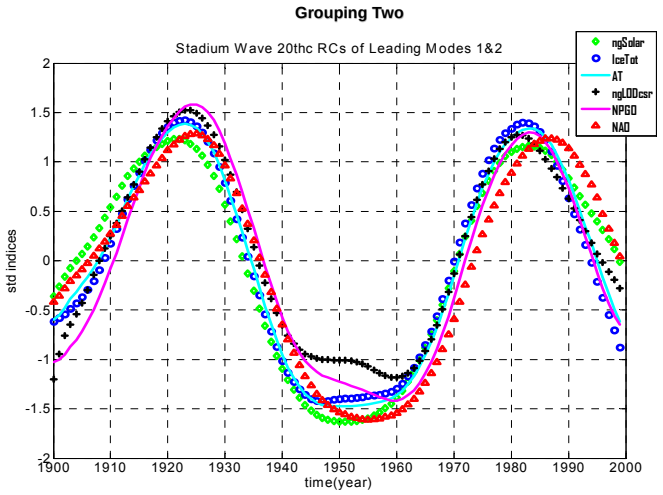

(b)

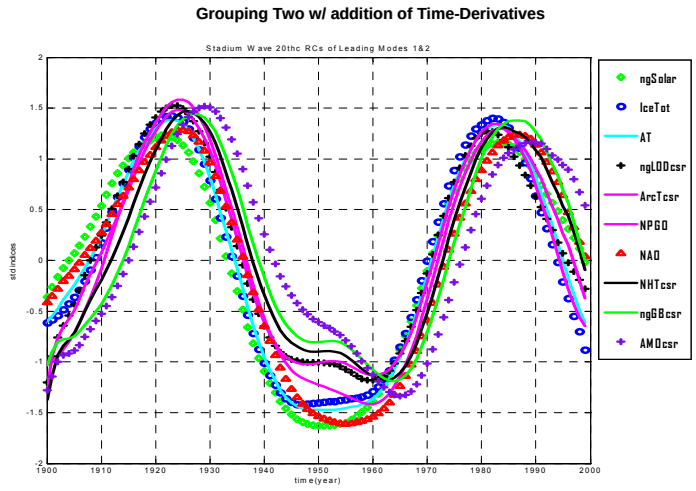

Fig. 3.7: Grouping Two. (a) Index-peaks of Grouping-two center on the mid-1920s and mid-1980s. Note the coincidence of atmospheric-mass transfer anomalies (AT) – dominant large-scale zonal winds - and sea-ice total (Ice Total), [Western (Greenland, Barents, and Kara) and Eastern (Chukchi, Laptev, and East Siberian) Eurasian Shelf seas]. NAO peaks in this grouping, as does NPGO. A weak signal of the solar constant (negative polarity) co-varies with this grouping. Also of interest is the covariance of this index set with the differential of Earth's rotational rate anomalies (ngLOD cumulative sum removed). (b) Shows the addition of several other time-derivatives, which reveals incremental forcing on Arctic dT, NHT, the dipole (via ngGB), and AMO. Implications are significant. It is within this cluster that ngSolar *appears* to be synchronized to the system. In the early century, IceTotal increases; zonal winds (AT) over the Atlantic and Eurasian continent intensify, carrying warmth from low latitudes to the mid-latitudes and east across Eurasia. In the Pacific, NPGO strengthens at similar timing. Incremental positive forcing is co-occurring on several indices: ngLOD, NHT, ngGB, and AMO. See **tables 3.5a through c** for associated correlation values for the 13-year-smoothed-raw time series.

AT finds the connection to Ice Total through the Kara Sea (R=0.7 at p < 1% level), the most easterly member of the West Eurasian Arctic sector. AT is also correlated with sea-ice in the East Ice collection, specifically the Chukchi Sea (R=0.57 at p < 5% level). NPGO is correlated with Laptev and Chukchi Seas (R=0.58 and 0.67, respectively; both significant at the p < 5% level). A snapshot of the geography shows from west to east: Greenland, Barents, Kara, Laptev, East Siberian, and Chukchi Seas. Chukchi Sea, just north of the Bering Strait, appears to be a nexus between the West and East circulations of AT and NPGO, respectively.

The North Atlantic Oscillation winter index (NAO) falls in this second grouping. Correlation between it and most other index members is insignificant. The only significant correlations (Table 3.5**c**) with winter-NAO are with the two 'dynamic proxies' that co-vary with this grouping: these include the differential of Earth's rotational rate (R between ngLODcsr and NAO = 0.54 at p < 5% level) and the negative polarity of the solar constant (R=0.77 at p < 1% level).

I added time-derivative indices of several indices to this grouping. Plots of these time derivatives reflect incremental changes in these indices. These indices were chosen based on the fact that the variability of each of these indices in their non-transformed version is substantially accounted for by the stadium-wave climate signal. (The indices reflect a high channel-fractional variance, a term discussed further later in this section.) Time-derivatives of the following indices fall into grouping-2: Northern Hemisphere Temperature, the Arctic T, the Atlantic Multidecadal Oscillation, the Earth's rotational-rate anomalies, and the negative polarity of G. bulloides (Figure 3.7b).

Grouping-Three – Pacific-centered circulations (**Fig 3.8** and **table 3.6**). Centered approximately on 1930 and 1990 are RC peaks of Grouping-Three – a cluster of indices associated with the North Pacific sector (Fig. 3.8). Correlations between pairs of these indices (table 3.6a) and between pairs of the associated anomaly trends (Table 3.6b) reflect the interconnectedness among these atmospheric and oceanic circulation patterns.

Pacific-based circulations exhibit a positive co-variance with East Ice. NPO correlates with East Ice (through Chukchi), and while that correlation is minor, less than 0.5 (table 3.6a), its correlation with Chukchi Sea ice is 0.65, both at the $p < 5\%$ level. Anomaly trends between Chukchi sea ice and NPO are correlated at 0.88 at the $p < 1\%$ level (table 3.6b).

As with the ice-wind positive relationship identified in the North Atlantic/Eurasian area (Grouping-Two), the same appears to be true in the North Pacific sector, as suggested by the Pacific Circulation Index (PCI) differential (PCIcsr (Figure 3.8b)). PCI is an index of time-integrated wind-direction anomalies (i.e. an anomaly trend) over the North Pacific. As with the time-derivatives introduced in Grouping-Two, the PCI differential captures incremental changes in wind structure, reflecting forcings on the non-transformed index. PCIcsr is strongly correlated with each of the trio of Pacific circulations: PDO, NPO, and ALPI (table 3.6a). All these correlations are between 0.95 and 0.96 at the $p < 1\%$ significance level.

Japanese Sardine outbursts are in this grouping. These outbursts occur only during the positive polarity of PDO (R=0.95), perhaps speaking to western-boundary-current ocean-heat-related dynamics that occur during positive wind-regime phases (Kelly and Dong 2004).

NINO falls in this grouping, co-varying with PDO (R=0.67) and NPO (R=0.63) (table 3.6a). Distinguishing NINO from other indices in this grouping is its negative correlation with solar ($R = -0.61$; $p < 1\%$). While NINO patterns of frequency and intensity vary on a

multidecadal timescale, in tempo with stadium-wave variability, its dominant character is interannual.

Table 3.6: Grouping-Three: Correlations between pairs of raw time series of indices, detrended, normalized, and smoothed with a 13-year filter prior to computation. Values significant to the 99% level shown in red; those significant to the 95% level in blue. (a) Correlations between single indices. In (b), anomaly trends of Grouping Three indices are highlighted. (Fig. 3.8)

(a) Single-index Correlations for Grouping Three (red=99%; blue=95%)

Indices	NINO	JS	PDO	NPO	ALPI	PCIcsr	Chukchi ice	East Ice
NINO[7]	1.0		0.67	0.63				
JS		1.0	0.84	0.72	0.72	0.81		
PDO	0.67	0.84	1.0	0.84	0.82	0.87		
NPO	0.63	0.72	0.84	1.0	0.71	0.82	0.65	0.49
ALPI		0.72	0.82	0.71	1.0	0.88		
PCIcsr		0.81	0.87	0.82	0.88	1.0		
Chuk Ice				0.65			1.0	0.91
East Ice				0.49			0.91	1.0

(b) Anomaly-Trend Correlations for Grouping Three (red=99%; blue=95%)

Cum sums	csNINO	csJS	csPDO	csNPO	csALPI	csPCIcsr	csChukchi ice
csNINO	1.0						
csJS		1.0	0.95				
csPDO		0.95	1.0	0.95	0.88	0.95	
csNPO[8]			0.95	1.0	0.90	0.96	0.88
csALPI			0.88	0.90	1.0	0.95	
csPCIcsr			0.95	0.96	0.95	1.0	
csChukchi ice				0.88			1.0

[7] Nino and solar constant negatively correlated (R=-0.61) at the 99% significance level (not included in table)

[8] Also not shown is the correlation of the anomaly trend of the annual NAO index (as opposed to the winter NAO index used in the stadium-wave study). NAO-annual's anomaly trend correlates with NPO's anomaly trend R=0.86 at the 95% significance level.

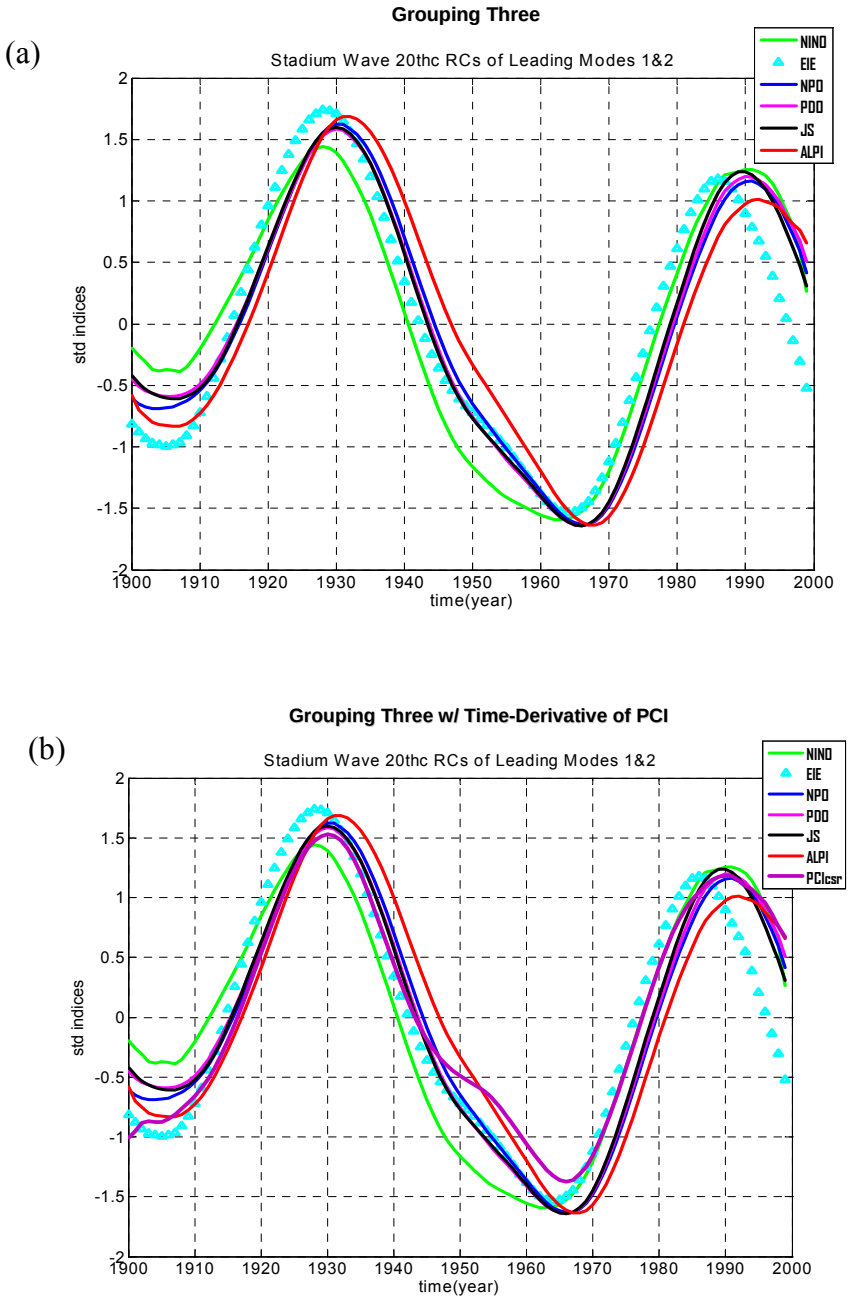

Fig. 3.8: Grouping Three**.** (a) In this set of indices, one can "see" the stadium-wave signal has reached the Pacific. Peaks of this grouping center on ~1930 and 1990. RCs indicate a rough coincidence of East Eurasian Sea Ice with NINO and PDO. One can see that Japanese Sardine (JS) outbursts follow PDO. (b) Addition to the graph of a time-derivative, the PCIcsr (differential of Pacific Circulation Index). PCIcsr is analogous to AT (see text). As with basin-scale winds (AT) over the Atlantic co-varying tightly with sea-ice extent, these winds appear to be similarly covariant with sea-ice in the Pacific's Arctic sector.

Grouping-Four (Arctic Extremes): Figure 3.9a gives a snapshot of index RCs that peak near the end of the propagating, quasi-oscillatory signal's first half-cycle. Anomaly trends (cumulative sums) of the Eurasian-Arctic Ice Total and of AT from Grouping-Four lead these extrema. These lead by a couple of years the maximum values of the Arctic temperature and Earth's rotational-rate anomalies, which peak around 1938 and again ~1995. Correlation between the anomaly trend of AT (csAT) and Arctic T is 0.92 at the 1% level (**Table 3.7**). Anomaly trends of negative solar (csSolar) and AT (csAT) correlate strongly (R=0.94 at the $p < 1\%$ level (also Table 3.7)). The plot of the cumulative sum of the negative solar index is plotted with other Grouping-Four indices in Fig. 3.9b.

Grouping-Five – the Transition ***(*****Figure 3.10** and Table 3.7*)* is more a transition than an actual grouping (included in table 3.7). Indices in this collection link the preceding half-cycle to the one to follow. In fact, this grouping is not characterized with a particular ice or wind regime; nor does there exist a specific proxy identifying its occurrence. The sole measurable index in this grouping is NHT, peaking around 1940 and possibly again at century's end. Members from Groupings 4 and 1 straddle this transitional collection. They are plotted (Fig. 3.10) to provide context.

At the end of the 20th century's first half-cycle, West Eurasian Arctic Ice has now melted to its fullest extent within this cresting of the transition. NHT maximum follows, as does the most northerly extent of the Atlantic ITCZ, represented by peaks in the positive Atlantic Dipole and negative *G. bulloides* abundance. Maximum warm phase of the AMO co-varies with this index collection, as does maximum PCI[9] – marking the end of positive anomalies of PDO, NPO, and ALPI. A negative feedback to the stadium-wave quasi-oscillation may thereby be indicated.

[9] Note PCI's strong correlation to Arctic dT; R=0.99 at the 99% significance level.

Table 3.7: Grouping-Four and Grouping-Five: Correlations between pairs of raw time series of indices related to Groupings Four and Five. Because Grouping-Five contains few indices and roughly co-occurs with Grouping-Four, it is merged with Four. The time series are detrended, normalized, and smoothed with a 13-year filter prior to computation. Red-noise model (1) was used to test for significance. Only values significant to at least 95% were retained. Those values significant to the 99% level are shown in red; those significant to the 95% level in blue. Both cumulative sum indices (anomaly trends) and single indices are included in this table; indices are thus labeled. *A few notables*: Anomaly trends of negative solar correlate strongly with anomaly trends of AT and NAO. Anomaly trend of +AT correlates strongly with Arctic dT; anomaly trend of +NINO correlates strongly with NHT. (Refer to fig.3.9).

Index	cs Sol	ACI (csAT)	ngLOD	Arctic dT	NHT	GB	DIPOLE	Bar ice	Grn Ice	WIE	AMO	Kara Ice	PCI	cs Nino
Cs SO-LAR	1	-0.94			-0.78									
csAT (ACI)	-0.94	1		0.92										
Ng LOD	-0.82		1	0.76	0.70		0.79	-.74	-.74		0.75			
ARC-TIC dT		0.92	0.76	1	0.91	-.77	0.84	-.79	-.71	-.76	0.75	-.57		
NHT	-.78		0.70	0.91	1	-.84	0.87	-.76	-.70	-.77	0.83		0.72	0.91
GB				-.77	-.84	1	-.87		0.60		-.69			
DI-POLE			0.79	0.84	0.87	-.87	1	-.70	-.79	-.75	0.90		0.77	
Barents Ice			-.74	-.79	-.76		-.70	1	0.86	0.94	-.85	0.69	-.80	
Green-land Ice			-.79	-.71	-.70	0.60	-.79	0.86	1	-.90	-.86	0.65	-.78	
WIE				-.76	-.77		0.75	-.94	-.90	1	-.89	0.87	-.90	
AMO			0.75	0.75	0.83	-.69	0.90	-.85	-.86	0.89	1	-.73	0.92	
Kara Ice				-.57	0.63			0.69	0.65	0.87	0.73	1	-.86	
PCI				0.99	0.72		0.77	-.80	-.78	-.90	0.92	-.87	1	
csNino					0.91									1
csNAO	-0.92													

(a)

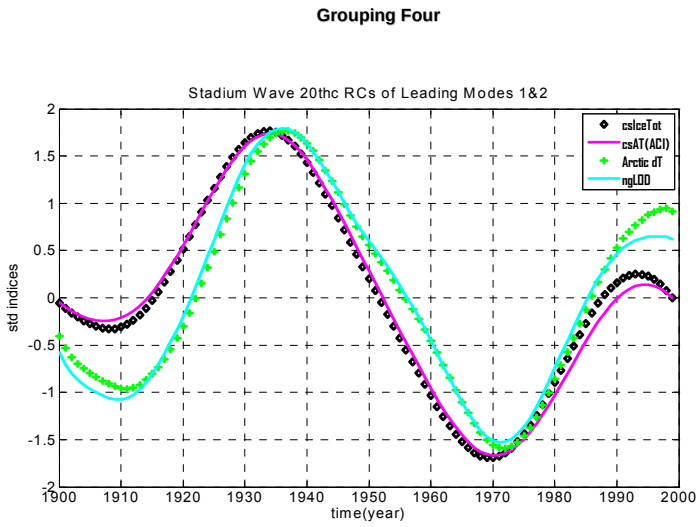

(b)

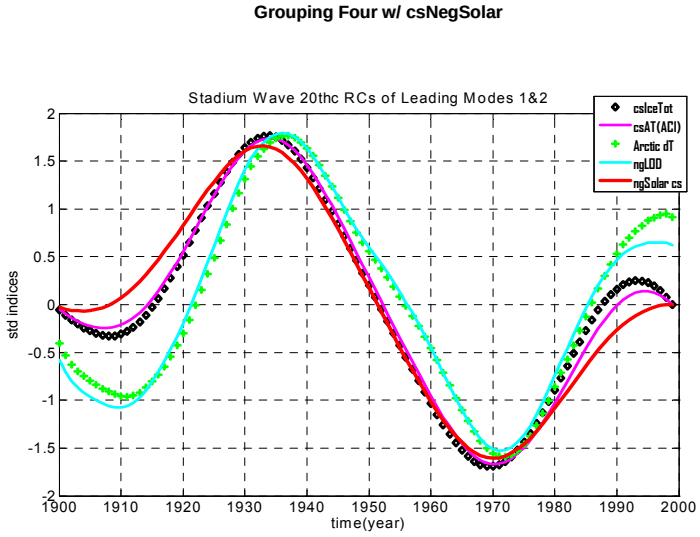

Fig. 3.9: Grouping-Four RCs reflect the integral impacts of key indices in Grouping-Two. Cumulative-sums (anomaly trends) of Ice Total and AT lead Arctic dT by a couple of years. Correlation of raw time series between csAT and Arctic dT is 0.92 at 99% significance level. See table 3.7. Note the coincidence of the anomaly trend of negative solar. Not to be confused with a forcing, but its coincidence with a group of indices, both as a single index and a transformed index, give potential to its use as a proxy for associated sub-processes.

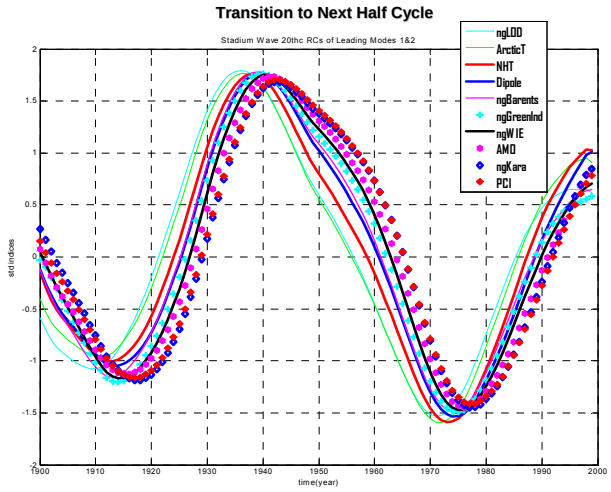

Fig. 3.10: Grouping-Five - Transition. Peaks of this grouping collectively signal a transition between the end of the first half-cycle and the beginning of the last half-cycle of the stadium-wave's secular variability or quasi-oscillation (identified previously as ~64 years in the 20th century (Wyatt et al. 2011)). NHT is the sole distinct "member" of this transition group. Members from adjacent groupings four and negative-one are combined with NHT to provide context for its evolution. Recall, this is the "real" NHT (or at least the stadium-wave signal inherent in the NHT time series). Apparent forcings on it occurring from processes in Grouping-Two are perhaps responsible for the perpetuation and reversal of trends.

A summary of Groupings one through five can be reduced to a collection of ice/wind indices; their relationships with one another and with NHT are shown in **Figure 3.11**.

"Process-Specific Groups"

Ocean-ice-atmospheric coupling lies at the heart of the temporally defined groupings detailed above. Indices of groupings 1-5 can be re-arranged according to process or medium, generating stadium waves from networks of indices whose behaviors have common roots (**Figs. 3.12**a-d). Resulting RC plots of the different index-networks are strikingly similar. Whether the stadium wave is generated from indices associated with wind, or with ice, or with teleconnection patterns, or with dynamic-proxy index networks, the peaks and troughs of the indices in each network fall

at similar times. (An RC's "timing" might vary slightly (~1-3y), according to indices with which they are analyzed, as the signal is shared among indices in a given network.)

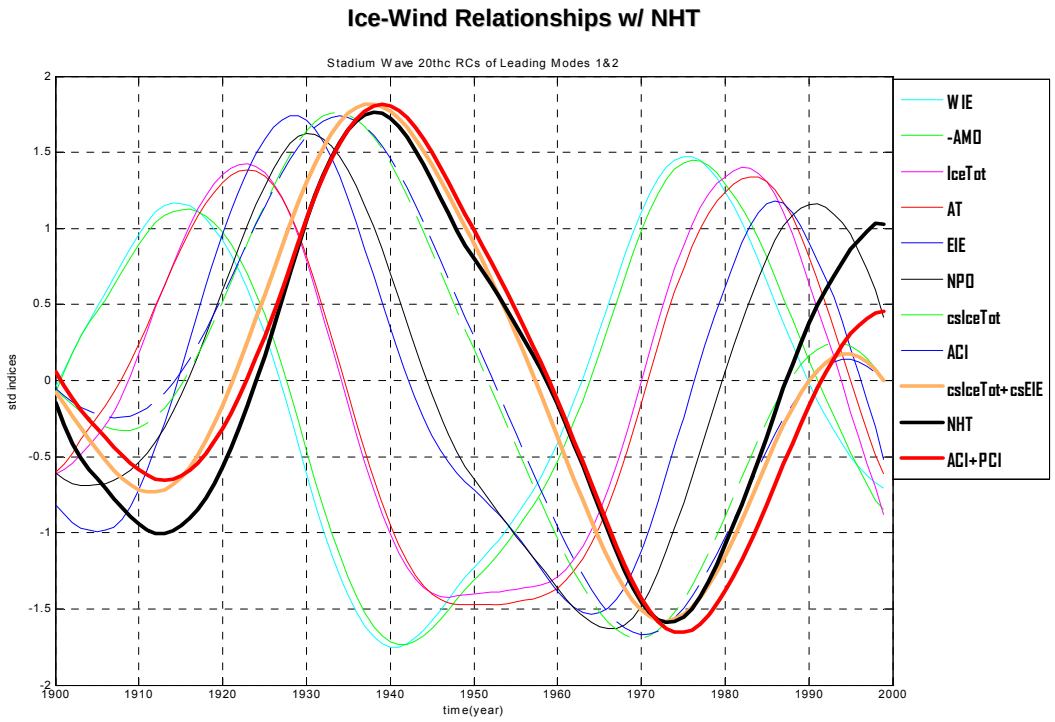

Fig. 3.11: Plotted here are select RCs from Groupings-One through Grouping-Five, representing the close correlation between ice and wind. While correlation is not to be confused with causation, studies suggest causation in this case. A strong basin-scale meridional-temperature gradient (MTG) is a function largely dictated by sea-ice-extent, particularly in the multidecadally varying sea-ice-inventories of the Western Eurasian Arctic Shelf Seas (Greenland, Barents, Kara). Large-scale mid-to-high-latitude atmospheric circulation responds to the MTG with enhanced zonality of wind direction and strengthened wind velocities, with consequent surface air temperature changes occurring far downwind over the Eurasian continent. Numerous changes occur in tandem with shifts in dominant wind regime, not the least of which is the latitudinal/longitudinal migration of atmospheric centers-of-action, with ensuing local and remote impacts on freshwater balance in the Atlantic, affecting conditions for sea-ice-growth/melt cycles. See text. Also see Wyatt et al. (2011) for discussion on teleconnections and references within.

(a)

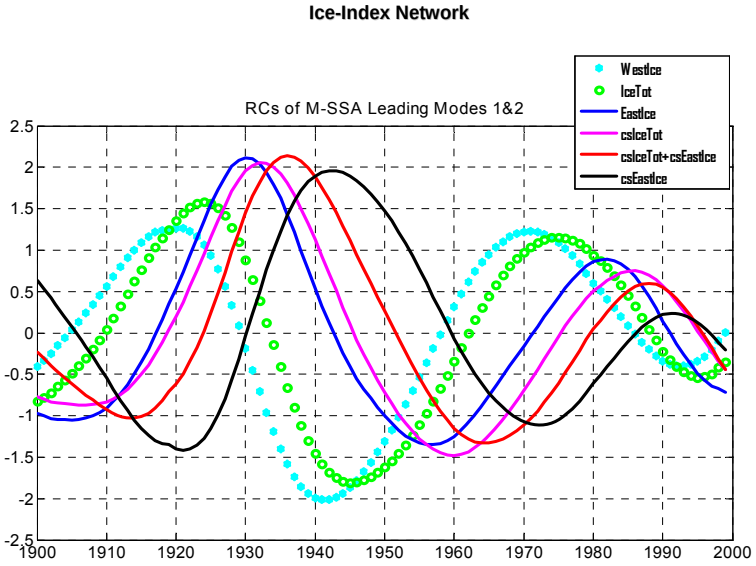
Ice-Index Network
RCs of M-SSA Leading Modes 1&2
WestIce
IceTot
EastIce
csIceTot
csIceTot+csEastIce
csEastIce
2.5
2
1.5
1
0.5
0
-0.5
-1
-1.5
-2
-2.5
1900
1910
1920
1930
1940
1950
1960
1970
1980
1990
2000

(b)

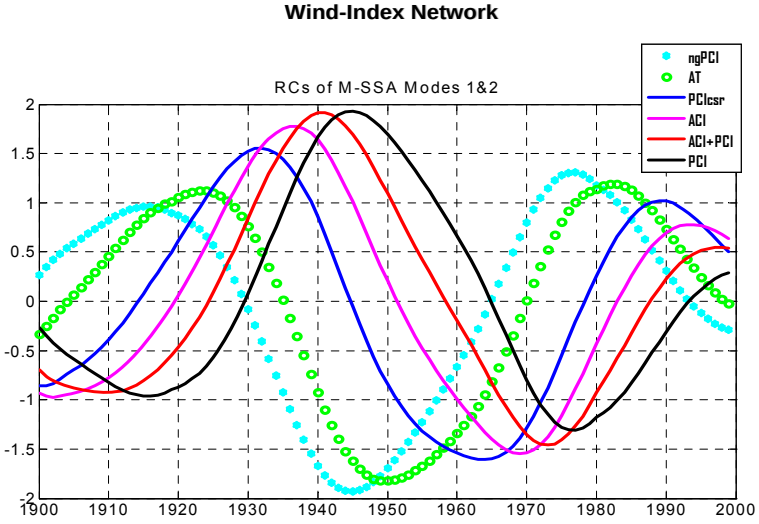
Wind-Index Network
RCs of M-SSA Modes 1&2
ngPCI
AT
PCIcsr
ACI
ACI+PCI
PCI
2
1.5
1
0.5
0
-0.5
-1
-1.5
-2
1900
1910
1920
1930
1940
1950
1960
1970
1980
1990
2000

(c)

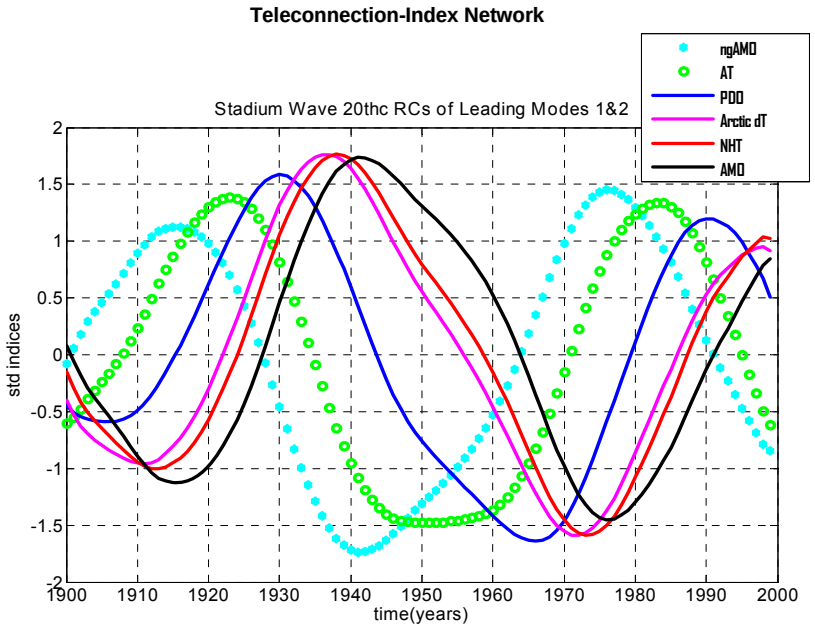

(d)

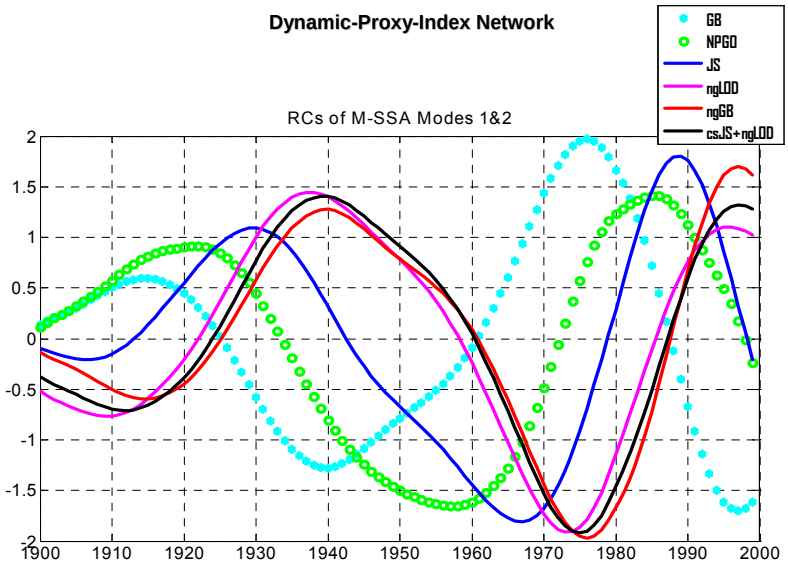

Fig. 3.12: M-SSA applied to four individual sets of indices yields normalized reconstructed components (RCs) that allow visualization of the stadium wave's hemispheric climate-signal propagation through the distinct six-index networks: (a) consists of members associated with Eurasian Arctic sea-ice, while (b) comprises atmospheric indices. (c) hosts several indices (teleconnections) from the original stadium wave, merged with Arctic dT; And (d) a network of dynamic proxies is shown.

Each index in a network has variability. The amount (or percentage) of that variability that can be accounted for by the stadium-wave climate signal is indicated by a measure called channel-fraction variances. The channel-fraction variances for the expanded 20th century index network are shown in **Figure 3.13**. Indices are aligned on the x-axis. The amount of variability accounted for in each index by the stadium-wave signal is designated "fraction (%)". It is plotted on the y-axis.

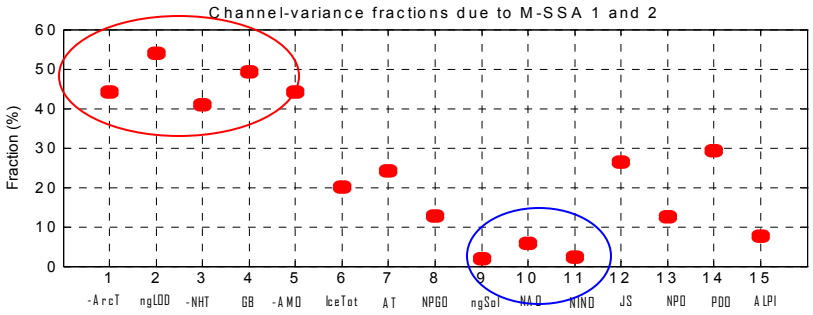

Fig. 3.13: Fraction of each expanded network member's raw-index variance that is accounted for jointly by M-SSA modes one and two is indicated on this chart. The climate signal is most noticeably expressed in Earth's rotational-rate anomaly index (ngLOD). The signal also is strongly pronounced in: *G. bulloides* (representing the Atlantic ITCZ), AMO, the Arctic dT, and NHT. (circled in red: indices from Groupings Four, Five, and One). On the other hand, variance in AT, IceTotal, Japanese Sardines, and PDO is accounted for to a similar degree by the M-SSA-identified climate signal. Little variance in ngSolar, NAO, or NINO (circled in blue) accounted for by the climate signal is seen. This may be to the more dominant presence of higher-frequency variability in these latter-mentioned indices. Cumulative-sum trends of these latter three indices reflect a greater apparent role in stadium-wave dynamics than their single indices suggest (not shown; see text).

The climate signal (the stadium wave) accounts for similar fractions of variance among indices within an individual grouping or closely timed groupings. Indices from Groupings One, Four, and Five (represented by Arctic T, ngLOD, NHT, GB, and AMO in Figure 3.13 (circled in red)) tend toward the highest fractional variances. Indices in Groupings Two and Three show similar channel-variance fractions to one another, with a mix of moderately high to very low.

These include indices such as Ice Total, AT, NPGO, NAO, and solar from Grouping-Two and NINO, NPO, PDO, and ALPI from Grouping-Three. Notable is the trio consisting of solar, NAO, and NINO (circled in blue). The stadium-wave-signal accounts for minimal variance in these three. This may be due to dominance of higher-frequency variability in all three.

Figure 3.14 provides an "at-a-glance" summary of Network-Groupings and Process-Specific Networks that doubles as a heuristic tool. This is a schematic presentation designed to help visualize both types of groups – the "Groupings" and the "Process-Specific Groups". Not every index is listed; yet most are.

To illustrate the "Groupings", I have divided an oval "pie" into 10 "slices". Beginning at the 12 o'clock position on the oval, follow clockwise. Five consecutive "slices" represent the positive polarities of the groupings in chronological order "Groupings One, Two, Three, Four, and Five". Five more "slices" represent the negative polarities of these five groupings. In each "slice", indices belonging to the "Grouping" are listed. These are the indices that co-occur simultaneously or nearly so. Dates during the 20th century when indices in a given grouping attained maximum values are given. They are found on the perimeter of the appropriate "slice". At the center of the oval, at the points of each "slice", there are numbers. These are the numbers of each "Grouping". Indices of these "pie slices" (Groupings) are illustrated in figures 3.6 through 3.10.

The "Process-Specific Groups" in Figure 3.14 are arranged in the differently colored "rows". There are four differently colored "rows". From the outermost row, the rows represent the following index networks: green row=dynamic proxies, blue row=atmospheric-circulation indices, yellow row=ice-related indices, and gray row=ocean/atmospheric circulations of

"original" stadium wave index network. Each one of these "rows" represents a network of indices through which the climate signal propagates over the course of the 20th century.

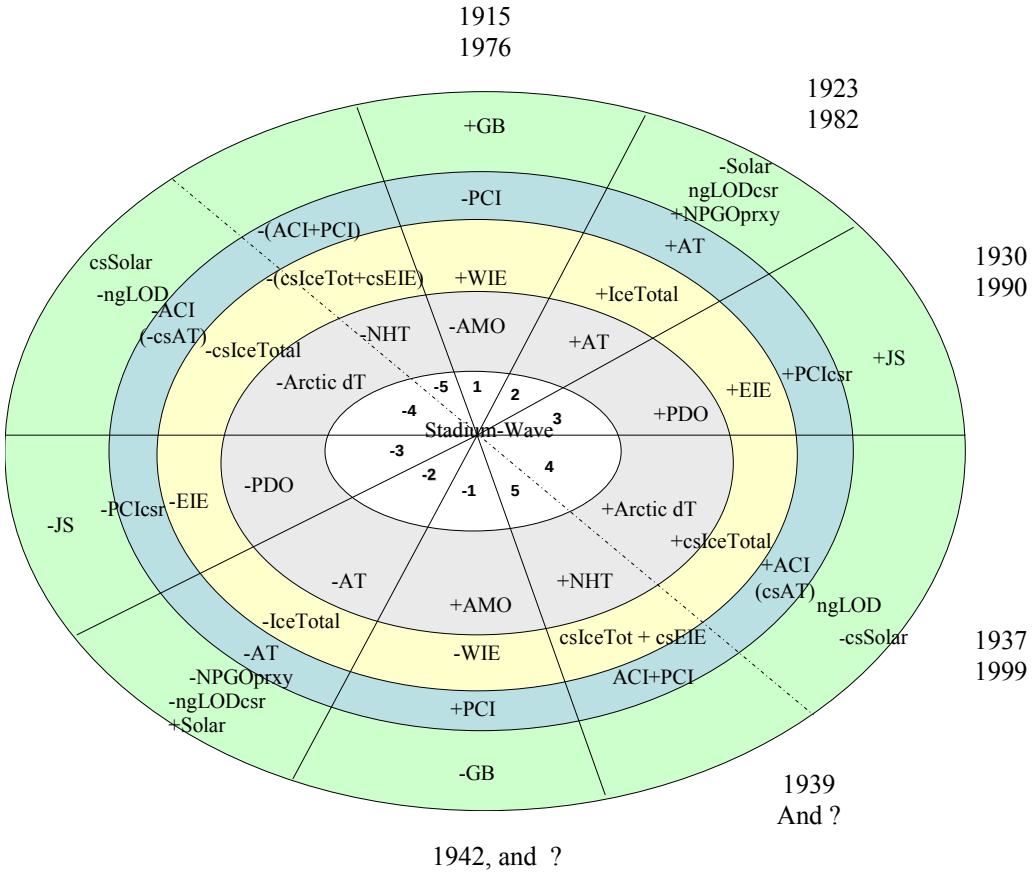

Fig. 3.14: A schematic presentation is offered to help visualize groupings one through five (with five being transitional; the lines delineating it are therefore less distinct (Figs. 3.6 through 3.10 depict stadium-wave renditions of these index collections)). Pie-shaped sections divide groupings of indices. Numbers along the outside of the "pie" sections are approximate years when the climate-signal of the associated "grouping" indices peaked (maximum value). At the center of the "pie" are numbers 1 through 5 (and -1 through -5 for opposite polarity indices). These numbers represent groupings of indices, as discussed in the text. Each Grouping (stadium-wave analogues figures 3.6 through 3.10) is analogous to a section of people participating in a "stadium-wave". The transmitted signal goes through each Grouping in sequential order. All indices within a pie co-occur. An added twist on this sequential progression is that the 'carriers' of the signal can be broken down into *type* of index (climate index, ice, wind, and proxy). Differently colored ovals host different network-sets of indices (seen in Figures 3.12a-d: process-specific indices). The purpose of this heuristic tool is to illustrate that stadium-wave propagation can be shown to occur through a variety of index sets. To "read", begin with the gray oval. In pie-section 1 of this oval is ngAMO. Proceeding clockwise, one traces the stadium-wave sequence in climate teleconnections of the original stadium wave: ex: -AMO, AT, PDO, Arctic T, and NHT. In the yellow oval, one traces the stadium-wave signal-propagation through ice-related indices. The blue-green oval hosts the stadium-wave progression in wind-related indices. And the light green outer oval follows the signal through the related dynamic proxies.

Begin at the 12 o'clock position on the gray strip. You can see that in 1915 and 1976, the negative polarity of AMO reached a maximum. The Atlantic was at its coolest. By 1923 and 1982, AT was at its maximum. Large-scale winds were strong with a pronounced zonal component. Then PDO crested in ~1930 and 1990. The Arctic T (aka Arctic dT indicating anomalies) reached a maximum shortly thereafter, followed by a peak in the Northern Hemisphere's temperature and then to a peak in the positive AMO.

The same approach can be used in the yellow row. This band represents ice-related indices with a sequence of West Ice Extent, Ice Total, East Ice Extent, the cumulative sum of Ice Total, and ultimately back to a negative value of West Ice Extent. The blue row hosts atmospheric-circulation indices, and the green one, dynamic proxies.

As this device is a tool, there are some indices that are included that are more mathematical constructs than actual indices. This can be seen in the case of combined indices.

I would suggest that the most useful application of this tool is combining the two types of groups in order to gain a more complete picture of the working hypothesis presented here. For example, at the 12 o'clock position, Grouping-One, a cold Atlantic co-varies with maximum ice in the Western Eurasian Arctic Seas. This coincides with the culmination of negative anomalies of Pacific circulations, which coincides with positive abundances of *G. bulloides* in the Cariaco Basin, indicating a maximum shift southward of the Intertropical Convergence Zone (ITCZ) in the western Atlantic. Times coinciding with this collection are times of previously identified climate-regime shifts, specifically in ~ 1915 and 1976, when a multidecadal cooling trend reversed to a multidecadal warming trend. The mirror image of this collection can be seen in the 6 o'clock position, Grouping-(negative)One. This collection peaked in ~ 1942. This was the timing of another documented climate-regime shift, this one a reversal from a multidecadal

warming trend to a multidecadal cooling trend. This Grouping may have peaked late in the first or early in the second decade of the 21st century. Such cannot be ascertained with confidence until more time has passed.

Characteristics of a climate-regime shift can now be described, and perhaps predicted, in terms of stadium-wave dynamics. In short, these regime-shifts during the twentieth century occurred at times when the ITCZ was to its farthest southerly (northerly) extent and ice extent in the western Eurasian Arctic was at its maximum (minimum).

Another useful application is seen in pie "slice" 4, with dates of peaks occurring at 1937 and 1999. It was around these times that the multidecadal component of Arctic surface air temperature reached its maximum. Arctic T co-varies strongly with the anomaly trend peak of AT (csAT, same as ACI) and the anomaly trend peak of Ice Total (cs Ice Total). Wind anomalies over the Atlantic Ocean and Eurasian continent – ACI – have reached the culmination of positive values. All of these co-occur with the cumulative sum of solar. No hint of a forcing role by solar emerges in this study. What I take from the relationship among indices is the opportunity for a proxy.

To explain my point; I see that the according to the index relationships for the twentieth century shown in Table 3.7, the cumulative sum of negative solar output is strongly correlated with the csAT ($R = 0.94$ at the $p < 1\%$ level). Also strongly correlated is the csAT with cs Ice Total ($R=0.86$ at $p < 5\%$ level (not shown)). The Arctic temperature correlates with csAT ($R=0.92$ at the $p < 1\%$ level). Data records for the indices AT, Ice Total, and Arctic T are short. They extend only to the mid-to-late 1800s. But the solar record is long. From this chart, it appears that I can use the solar proxy to estimate the Arctic temperature. And knowing the relationship between the Arctic T and NHT, the estimation becomes a mathematical exercise

rooted in the index relationships of stadium-wave dynamics. Of course, these dynamics have just been examined for the 20th century. A test will be required to see if my hunch has merit. That is described in the next section.

In closing out this section, **Figure 3.15** captures the expanded 20th-century stadium wave in a Hoffmuller diagram. It is simply another tool to facilitate visualization of this rather complicated set of dynamics. Viewed along the x-axis, the signal's propagation through each index can be seen. Alternatively, viewed along the y-axis, one can see the signal as it is expressed in each network index for a specific year. And finally, viewed along an imaginary diagonal trend, one can follow the peak or valley of the climate-signal as it courses through the collection of network members.

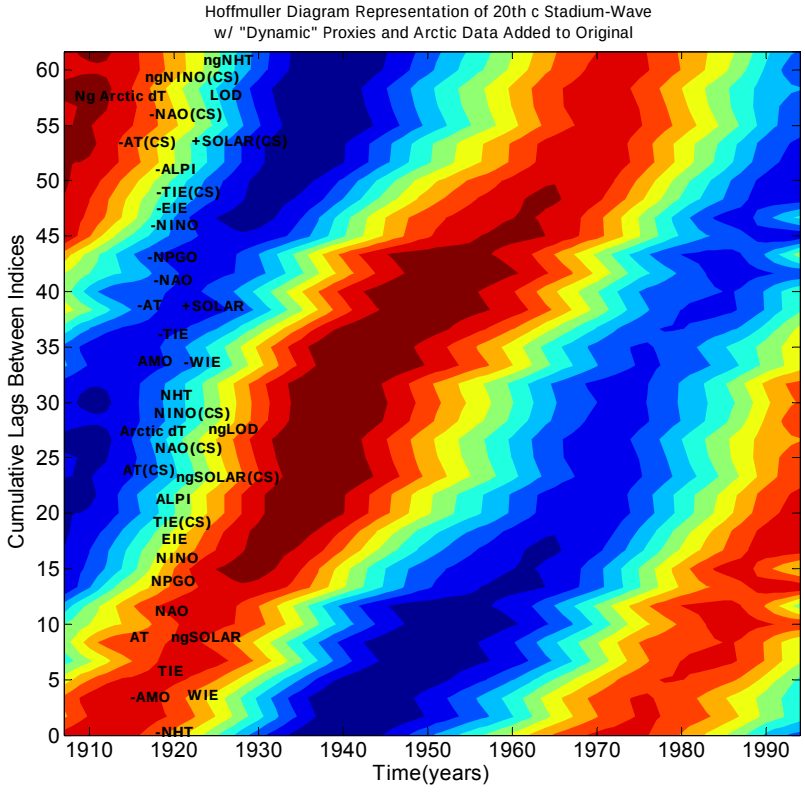

Fig. 3.15: A Hoffmuller diagram of RCs of 20thc indices (original, dynamic, and Arctic indices) shows the progression of the climate signal. Refer to text for tips on reading the plot.

To read the Hoffmuller in Figure 3.15, first follow a horizontal trace through one of the indices plotted vertically along the left side of the diagram. Following this index horizontally across the chart reveals its evolution over time. On the other hand, following a vertical trace through a given year marked along the x-axis allows visualization of the phase of each index during the year represented by the vertical line. Note that the indices that are plotted on the left of the chart are arranged vertically in sequence of their occurrence, with years of lag-time between them denoted along the y-axis. And last, if one follows a diagonal trace, say following a blue band of color or a red band of color, this track illustrates how a warm or cool signal propagates through the sequence of indices over time. Refer to Figure 3.5 for a stadium-wave view of the same.

Results for 1700-2000 Analysis: Within the 1700-to-2000 reduced-member[10] dynamic-proxy network, a familiar stadium-wave sequence emerges in the index RCs (**fig. 3.16**), suggestive of a hemispherically propagating signal with a multidecadal pacing of between 50 and 60 years. This quasi-oscillatory character extends back to ~1770. Prior to 1770, the stadium-wave pattern is similar to that in subsequent years, but with a subdued amplitude and modified tempo. M-SSA results showed leading modes one and two of the propagating climate signal to be widely separated from other modes of variability, with error bars overlapping and whose RCs are similar in periodicity and in-quadrature phasing – all traits of an oscillatory pair. But a caveat does exist. While all other results on this longer, reduced-member data set appear supportive of a strong signal, the oscillatory pair of leading modes does not fall fully outside the envelope of uncertainty **(Fig. 3.17**). Random occurrence of the signal in this index collection cannot be ruled out. Thus, a statistically significant stadium-wave climate signal cannot be verified with the tests

[10] NPGO proxy is unavailable for this time span; the reduced index set = *G. bulloides*, solar, JS, ngLOD.

used for the 20th-century stadium-wave, despite the otherwise convincing sequence illustrated in Figure 3.16.

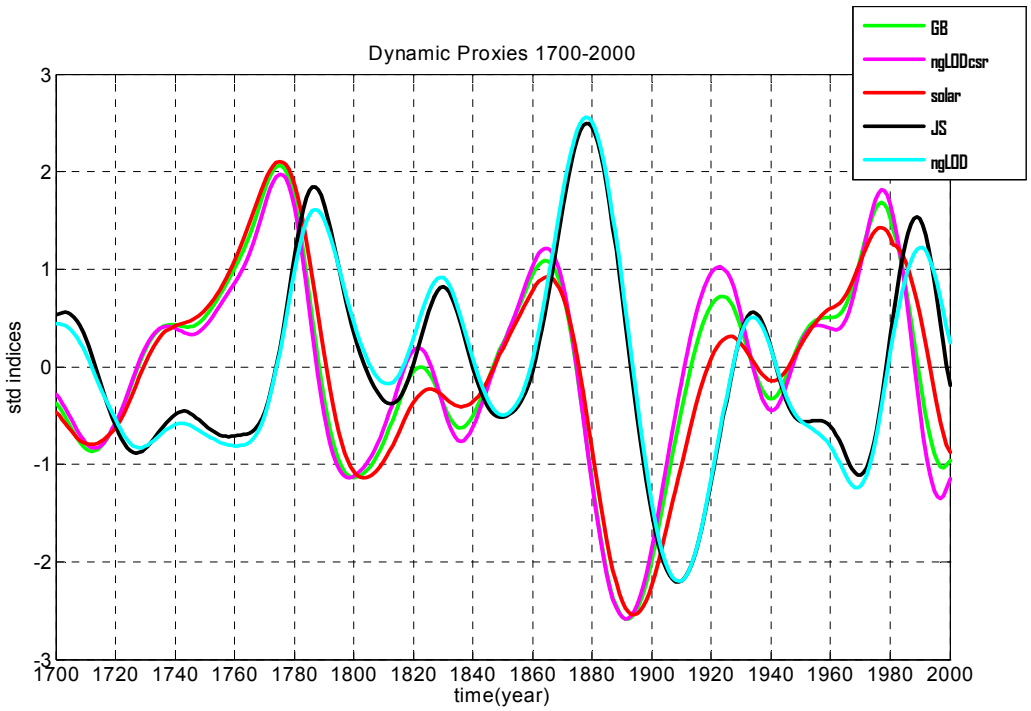

Fig. 3.16: RCs of MSS-A leading modes one and two reflect the climate signal in various dynamic proxy indices over a three-hundred-year interval (1700 to 2000). Isolating from this plot just the years 1900 to 2000, the behavior of these "dynamic proxy" indices appears consistent with that of analogous indices of the original stadium wave (and with the 20th-century dynamic-proxy "wave"). Networks of "conventional proxies" reflect similar cadence and timing of peaks as that shown here, but only to about 1800. Prior to 1800, little to no activity is seen in the conventional-proxy record (figures 3.2a-c). Signal propagation is indicated in this figure by the RC plots of dynamic proxies, albeit with a somewhat irregular nature over the 300-year period and with a significant damping of amplitude in the 1700-to-1780 interval.

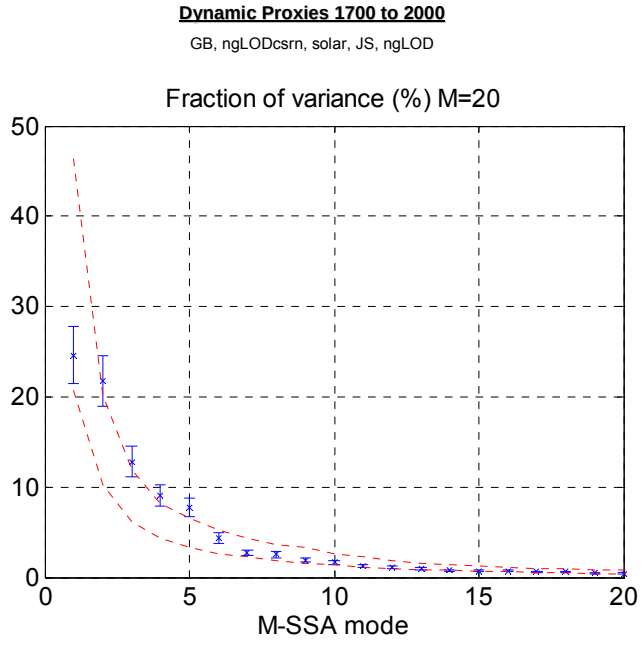

Fig. 3.17: The M-SSA spectrum of a network of five "dynamic proxy" indices is shown for the expanded time interval, 1700 to 2000. No NPGO proxy exists for this longer time series. As with results for the 20th century, this longer-term analysis generates two leading modes of variability, overlapping (oscillatory pair indicated), and well-separated from the rest. But, unlike results for the 20th century, we see here that the leading modes do not fall fully outside the envelope of randomness. This may be an inevitable consequence of a lengthy proxy record, where noise and quality degradation with length of series can diminish apparent statistical significance. We do know that the twentieth-century results for this same grouping do lie outside this envelope. Despite this difference in significance levels between the results for the 20th century and the 1700-to-2000 interval, it is assumed that this longer-time-series climate signal is analogous to the one identified for the 20th century, based on the context of this entire analysis. The RC plot of that signal propagating through the dynamic proxy indices reflects this signal (Fig. 3.16).

Significance testing used for the 20th-century analysis is not convincing in analysis for the 1700-to-2000 interval. This may be due to inherent caveats in using lengthy records of proxies; such time series tend to be inherently noisy, capturing numerous signals ancillary to the signal intended. This leads me to the following reasoning: 1) Because the stadium-wave propagation

sequence was supported by both statistics and apparent mechanisms of ocean-ice-atmospheric interactions in the 20th century; and 2) because dynamic proxies also scripted the stadium-wave sequence, with both statistical and mechanistic support in the 20th century; and 3) because there is an apparent stadium-wave progression throughout most of the 1700-to-2000 interval, I conclude that it is worth evaluating the stadium-wave signal propagation by an approach other than the significance test used for the 20th century.

To that end, I next use an alternate strategy to investigate the signal's past behavior. I base this strategy on associations previously discussed and shown in Figure 3.14. Because the solar index and the Earth's rotational-rate index have long, annually resolved records[11], I will use them for this next step. But first, a question must be addressed: *What relationships do anomalies of Earth's rotational-rate and solar have with climate?*

Touched on earlier was the relationship of ngLOD to climate. That topic is considered more in-depth here. Numerous researchers have noted multidecadal variability of ngLOD (Rudyaev et al. 1985) and the relationship of that multidecadal behavior with the multidecadal component of various climate indices (Beamish et al. 1999). Klyashtorin and Lyubushin (2007) observe co-variability between ngLOD, anomaly trends of large-scale wind patterns, and the Arctic temperature, all of which slightly lead the Northern Hemisphere temperature. Minobe (personal communication) finds a connection between ngLOD and PDO. And Mazzarella and Scafetta (2011) suggest a strong relationship of the annual index of the North Atlantic Oscillation and ngLOD.

[11] Records for ngLOD are annually resolved back to about 1800. Frequency of observations was less consistent prior to this time. Prior to the mid-20th century, measurements were based on measurements of the Moon and planetary objects with respect to Earth. Since 1955, observations are frequent and based on advanced technologies (atomic clock) – an important advance for the study of higher-frequency variability of this index (e.g. annual variation ~ 0.0003s). For our purposes here, the record is considered to be temporally well-resolved for low-frequency behavior (60-70-year variability of ~0.002 s) back to ~ 1800 and less so back to 1700 (Sidorenkov 2005).

Winds related to atmospheric-circulation regimes could influence Earth's angular momentum, but are insufficient, by themselves, to account for the magnitude of variability observed (Sidorenkov 2005a, 2009). Sub-processes associated with atmospheric-circulation regimes may hold the key. Sidorenkov (2009) hypothesizes that the ultimate controlling factor on low-frequency fluctuations in Earth's moment-of-inertia, and therefore in ngLOD, are the low-frequency fluctuations in distribution of water between the ocean and land ice. Atmospheric-circulation regimes are associated with specific patterns of precipitation, ice-growth and ice-melt patterns. These would modify the meridional distribution of planetary water. Sidorenkov cites ice sheets of Greenland and Antarctica as contributors to this latitudinal water re-distribution, with major emphasis on Antarctica. One might assume a strong co-variance between land ice and sea ice (Rennermalm et al. 2009).

How might ngLOD be deconstructed in terms of stadium-wave dynamics? Observing that, for whatever ultimate reason, Eurasian-Arctic sea-ice is linked to ngLOD, it could be inferred that ice-related sub-processes are encoded onto ngLOD's record. Established in this study is the strong correlation between West Eurasian sea-ice and the negative polarity of AMO and between East Eurasian sea-ice and NPGO, the two sea-ice series varying in quadrature (**Tables 3.8, 3.9**). An algorithm emerges: NPGO+AMO=ngLOD. **Figure 3.18** is a plot of this reconstruction. Curves of both the ngLOD index and the reconstructed ngLOD index closely co-vary ($R=0.95$ at the $p < 1\%$ significance level).

Can this inferred ngLOD de-coding inform about past NHT? Can NPGO and AMO, extractable from ngLOD (NPGO=ngLOD-AMO), be used to reconstruct NHT?

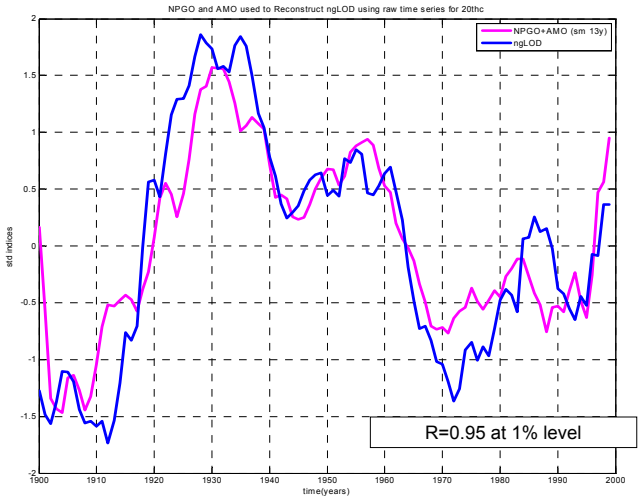

Fig. 3.18: Plotted above are the raw 20th-century time-series (detrended, normalized) of ngLOD [blue line] and of the combined indices, NPGO plus AMO [pink line] (normalized and smoothed with a 13-year filter). The selection of indices is based on stadium-wave dynamics as discussed in text. The resulting NPGO+AMO combination correlates strongly with ngLOD, similarly processed. (R=0.95 at the 99% significance level), suggesting that subsets of processes and behaviors related to each circulation interact in such a way as to affect Earth's angular velocity, with compensating fluctuations of Earth's length-of-day.

Table 3.8: Correlations between pairs of raw time series of indices related to the individual Eurasian Arctic Shelf Seas, to East Ice, to West Ice, and to Total Ice. The time series are detrended, normalized, and smoothed with a 13-year filter prior to computation. Red-noise model (1) was used to test for significance. Only values significant to at least 95% retained. Those values significant to the 99% level are shown in red; those significant to the 95% level in blue. *Notable*: Total Ice is strongly dominated by West Ice and Kara Sea Ice, in particular.

Indices	Greenland	Barents	Kara	WIE	Chukchi	Laptev	E.Siberian	EIE	Tot Ice
Greenland	1.0	0.86	0.65	0.90					0.65
Barents	0.86	1.0	0.69	0.94					0.66
Kara	0.65	0.69	1.0	0.87					0.94
WIE	0.90	0.94	0.87	1.0					0.83
Chukchi					1.0	0.69	0.72	0.91	
Laptev					0.69	1.0	0.68	0.85	
E.Siberian					0.72	0.68	1.0	0.91	
EIE					0.91	0.85	0.91	1.0	
Total Ice	0.65	0.66	0.94	0.83					1.0

Table 3.9: Shown below are correlations between pairs of raw time series of indices related to Eurasian Arctic Shelf Sea Ice and various climate-related indices. The time series are detrended, normalized, and smoothed with a 13-year filter prior to computation. Red-noise model (1) was used to test for significance. Only values significant to at least 95% retained. Those values significant to the 99% level are shown in red; those significant to the 95% level in blue. *Notables*: ngAMO, ngPCI (the anomaly trend of negative-polarity Pacific circulations), and ice inventory in the Western Eurasian Shelf Seas are strongly correlated. Also, Chukchi Shelf Sea (East Ice), north of the Bering Strait, correlates with both the Atlantic-Eurasian sector of atmospheric flow (AT) and the North Pacific sector's circulations (NPO atmospheric/NPGO oceanic).

index	ngAMO	ngPCI	AT	NPGO	NPO	Arctic dT	ngLOD	Dipole	NHT
Greenland	0.86	0.78				-0.71	-0.74	-0.79	-0.70
Barents	0.85	0.80				-0.79	-0.74	-0.70	-0.76
Kara	0.73	0.86	0.70					-0.58	-0.63
WIE	0.89	0.90				-0.76	-0.65	-0.75	-0.77
Chuckchi			0.57	0.67	0.65				
Laptev				0.58					
E.Siberian									
EIE									
Total Ice	0.74	0.85	0.76	0.54		-0.53		-0.62	-0.62

This analysis has shown the close relationships among 20th-century indices of negative Ice Total, the ITCZ, and NHT (minimum ice; north-shifted ITCZ, warm NHT). A closer look (e.g. fig. 3.14) shows NHT leads ITCZ (dipole and -GB), which leads negative IceTotal – all within less than a decade. Within a 300-year context, a rough correlation between the negative polarity of the Eurasian Arctic Ice Total (ngIceTotal) and the Northern Hemisphere temperature (NHT) could be argued. The ng(Ice Total) would also be a rough proxy for latitudinal shifts of

the ITCZ. Negative Ice Total = negative(WestIce + EastIce) . If this relationship is put into terms of related sub-processes, ngIceTotal can be expressed roughly as [-(-AMO + NPGO)][12].

This combination of anomalies (termed here: NHT_LOD) should relate to ITCZ position, and therefore roughly to the NHT. A 300-year NHT proxy (Esper et al 2002) is used to test the relationship. Plots of EsperNHT and NHT_LOD are shown in **Figure 3.19**; R=0.80 at the p < 1% significance level.

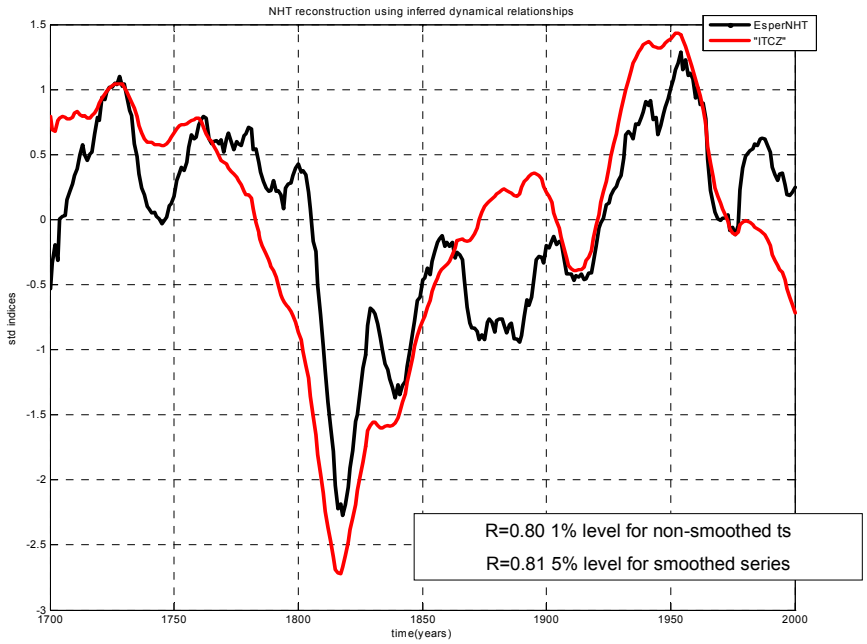

Figure 3.19: Raw time series for the period 1700 to 2000 are used. Prior to reconstruction, indices are detrended and normalized. Plotted with the 300-year Esper et al. (2002) NHT proxy reconstruction [black line] is a NHT-reconstruction ('NHT_LOD') [red line] based on inferred stadium-wave dynamics. Indices used to generate this reconstruction include an AMO proxy (Gray et al. 2004) and the inferred NPGO index. The latter was generated from the ngLOD index. (See text for details.) The combination for the NHT_LOD reconstruction = [AMO–NPGO], labeled "ITCZ" in legend. Correlation of NHT_LOD with the EsperNHT is 0.80 at the 99% level for the non-smoothed series (and 0.81 at the 95% level for series smoothed with a 13-year filter). Plotted are the smoothed series.

[12] Not to be confused: 'NHT_LOD' = AMO-NPGO; while ngLOD = AMO+NPGO

As strong as this relationship appears, this reasoning can take us only so far. As it turns out, EsperNHT and instrumental NHT show poor correspondence with one another during the 20th century, their correlation only 0.60 at the p < 5% level (**Fig. 3.20**a)[13]. This casts doubt on the EsperNHT proxy's use as an accurate means to test inferred stadium-wave dynamics. Figure 3.20b indicates a dominant Arctic T influence on instrumental NHT (R=0.91, p < 1% level); while the 20th-century Esper NHT (Fig. 3.20c) appears to exhibit additional influence from AMO (R=0.85, p < 1% level). While the Gray et al. (2004) proxy-AMO correlation with EsperNHT is strong in the 20thc, the same is not true for a 300-year comparison of the same, where correlation drops to 0.68 at p < 1% significance level (not shown).

In conclusion regarding this reconstruction, ng(-AMO+NPGO), using ngLOD to extract NPGO, reproduces the EsperNHT with a robustly significant 0.80 correlation. How the EsperNHT captures the Northern Hemisphere temperature signal, and how that compares to the instrumental NHT record, is less clear.

Next I use the solar index in my attempt to reconstruct a 300-year record of NHT. Solar variability is the second of two dynamic-proxies for which records are long and well resolved. Recent studies highlight the apparent synchronization of a low-frequency solar signal with the climate multidecadal signature (Loehle and Scafetta 2011; Scafetta 2011). Yet inconsistencies plague assignment of cause-and-effect, particularly observation that the solar constant plotted with temperature shows NHT *leading* solar by a few years. The stadium-wave sequence offers a possible explanation.

[13] EsperNHT captures warm season temperatures, which, according to Esper et al. (2002) are same as annual at low-frequency time scales. NHT used in this paper is the boreal winter index.

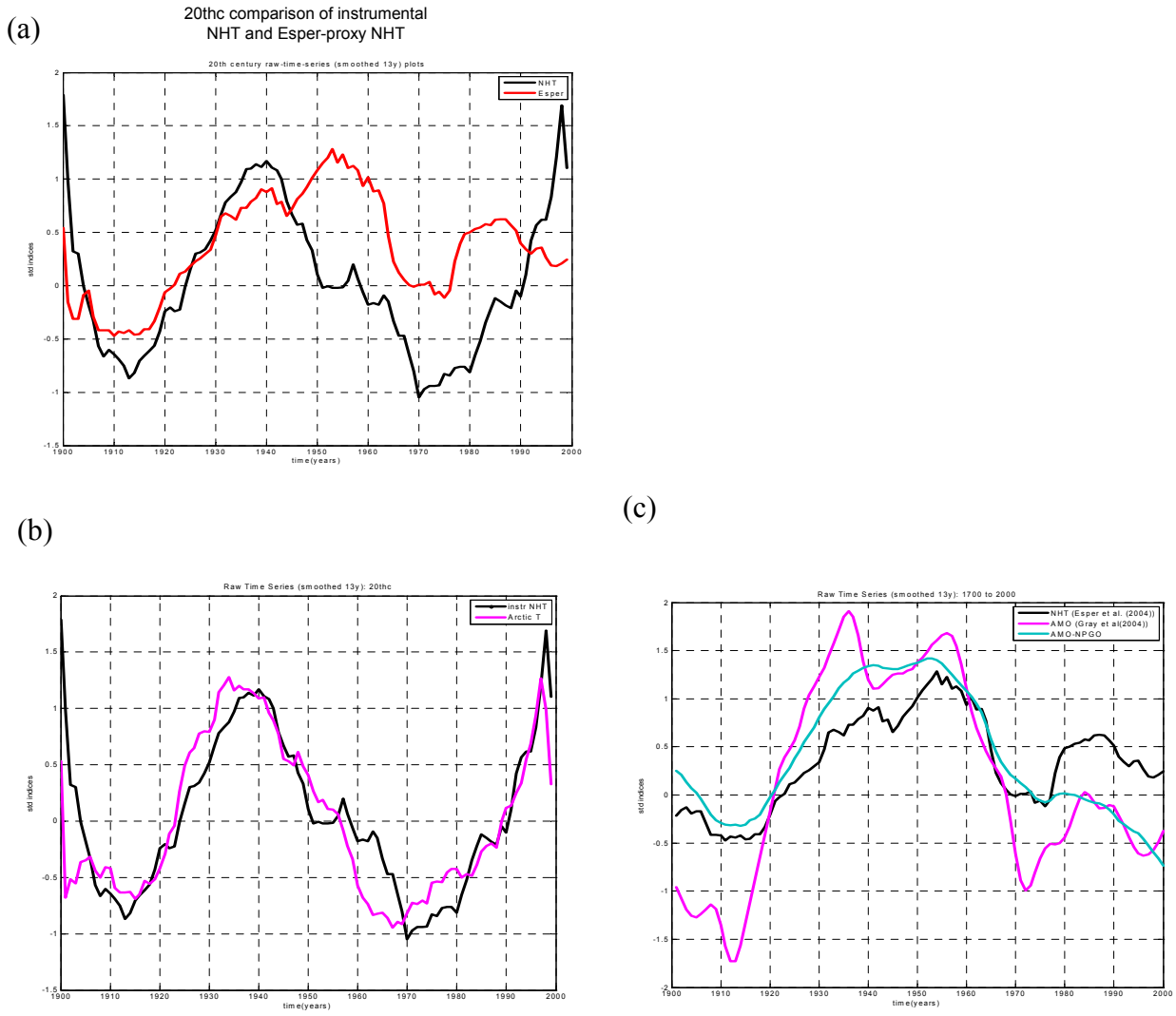

Fig. 3.20: 20thc comparison of plots of raw time series (detrended, normalized, smoothed 13y) is shown for (a) NHT instrumental and NHT Esper proxy (Esper et al. 2002). (b) Instrumental NHT and with instrumental Arctic dT (c) the Esper NHT proxy with both AMO (Gray et al. (2004) proxy) and the ngLOD-inferred "ITCZ". Conclusion: Instrumental and the Esper proxy for NHT are poorly correlated for the 20th century. The instrumental NHT, a boreal-winter index, reflects a dominant Arctic component; EsperNHT-proxy, an annual temperature record at low-frequency time scales, captures more of the lower latitude influence (AMO and ITCZ). Figure 3.14 shows in Grouping-Four that the Arctic dT reflects *anomaly* trends of the +AT and of +IceTotal (essentially –ITCZ). In contrast, Groupings negative One and negative Two show that AMO and –AT/-IceTotal, to which the EsperNHT are most closely correlated, are "real-time" anomalies that *follow* the winter-NHT index used in this paper.

Recall indices of Grouping-Two (Fig.3.7): Ice Total, AT, NPGO, winter-NAO, and negative solar. Correlations between pairs of single indices and between pairs of anomaly trends in this grouping show these members[14] to have the only significant links to solar variability, despite the fact that each of these indices accounts for a relatively low fractional variance of the climate signal, as indicated in Fig. 3.13. **Table 3.10** focuses on relationships of various indices with both the single-index of the solar constant and with its cumulative-sum (anomaly trend).

Table 3.10: Correlations between pairs of raw time series of indices – some single index, some cumulative sum – are repeated here to focus on the shared relationships among the negative solar constant, NINO, NAO, AT, and their cumulative sums (anomaly trends).. The time series are detrended, normalized, and smoothed with a 13-year filter prior to computation. Red-noise model (1) used to test for significance. Only values significant to at least 95% retained. Those values significant to the 99% level are shown in red; those significant to the 95% level in blue. *Notables*: Non-transformed indices of NAO and NINO correlate negatively with solar. Anomaly trends of NAO and AT correlate negatively with anomaly trend of solar. The anomaly trend of AT also correlates strongly positively to the Arctic dT. That of NINO correlates with NHT.

index	Solar	NAO	NINO	Arctic dT	NHT	csSolar	csAT	Cs NAO	Cs Nino	Cs ArcT
Solar	1.0	-0.77	-0.61							
NAO	-0.77	1.0								
NINO	-0.61		1.0							
Arctic dT				1.0	0.91		0.92			
NHT				0.91	1.0		0.84		0.91	
Cs Solar						1.0	-0.94	-0.92		
csAT				0.92		-0.94	1.0		0.78	
Cs NAO						-0.92		1.0		
Cs Nino					0.91				1.0	
Cs NHT										0.97

[14] Solar does correlate with NINO (grouping three); R=-0.61 at the 99% level. This correlation is less than solar's correlation with NAO, and NINO and solar anomaly trends do not significantly co-vary. So grouping two does stand out as the collection most "in synch" with solar (negatively correlated).

Why the solar cycle appears synchronized to the ocean-ice-atmosphere cycle - and in particular NAO, NINO, AT, and Ice Total - is left for other studies, but entrainment (or frequency locking) is one possibility. An external quasi-oscillator can connect with the intrinsic frequency of a self-sustaining oscillator, which the ocean-ice-atmospheric system appears to be. If the external source is weak and if the two systems have somewhat similar cadences (difference in cadence = frequency-detuning) and if the two systems are in some way linked (coupled), the external one can nudge the tempo of the intrinsic system (Pikovsky et al. 2001). Both frequency-detuning and coupling conditions between oscillators must be "just right" for synchronization to be maintained. Noting the coincidence of *negative* solar with positive ice inventory and enhanced circulations (AT, NAO, NINO) suggests that ice could be a factor that increases the sensitivity of the stadium-wave system to being entrained by this weak external forcing.

Can this information be used in NHT reconstruction? Plots of the solar constant with NHT reveal similarities; yet NHT slightly leads solar. Stadium-wave dynamics can justify this observation. Figure 3.14 shows the relationships.

It has previously been established that instrumental NHT strongly reflects influence from Arctic temperature (Grouping-Four), with the Arctic temperature leading NHT by a few years during the 20th century. It has also been argued that positive NHT (Grouping-Five), a north-shifted ITCZ (Grouping-negOne), and minimum ice total (Grouping-negTwo) follow one another in sequence over an interval of about a decade during the 20th century. For a 300-year interval, a decadal-scale time span is relatively short, and therefore, for purposes here, these aforementioned indices can be considered to roughly co-occur. Thus, given our limitations in attempting historical investigation of stadium-wave dynamics, if we have only the solar proxy to work with, how might this be used?

Minimum ice total shares a temporal relationship with positive solar (both indices in Grouping-negTwo). The Arctic temperature is associated with cumulative sums of a variety of indices, one of which is the cumulative sum of negative solar (both indices in Grouping-Four). Recall, this "cumulative-sum" is not a "real" index. This cumulative-sum value is only a tool. I am using this "tool" as a proxy for sub-processes that underlie the generation of NHT. To do this, I consider co-variability of indices established in the 20th century analysis.

Using these two solar components as representatives of co-occurring sub-processes, one leading NHT, one lagging NHT, I submit that the following algorithm can be justified: solar + ng-cum-sum-solar = NHT_solar. Plotted with the 300-year time series of EsperNHT (**Fig. 3.21**), a solid relationship is apparent, with R=0.77 at the $p < 5\%$ level, the aforementioned caveats with the proxy NHT guiding interpretation of results.

A final note on these variables: ngLOD and solar. There are similarities between them. Groupings 2 and 4 show this. Negative solar and ngLODcsr co-occur, as do the cumulative-sum-of-negative-solar and ngLOD. Associated ice and wind parameters are not to be ignored. While it is beyond the scope of this paper to explore these connections, it is worth mention that some authors suggest an external forcing. Wilson et al. (2008) and Sidorenkov (2009) suggest atmospheric circulation regimes are possibly synchronized to an external forcing that also modifies core-mantle dynamics, explaining their observed co-variance with ngLOD at an approximate 60-year periodicity. Scafetta (2010) finds an astronomical oscillation linked to planetary motion that he proposes is synchronized to climate circulations, again at an approximate 60-year periodicity. This is left to future study, but synchronized networks are pervasive throughout nature, whether externally nudged or not. Results here suggest

multidecadal climate variability poses no exception. **Table 3.11** summarizes correlations of EsperNHT and the reconstructed NHT_LOD and NHT_Solar.

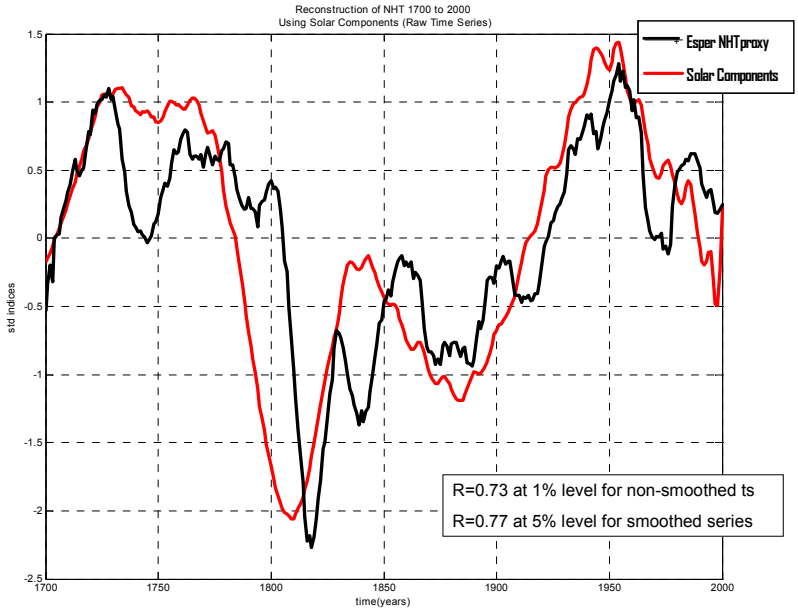

Fig. 3.21: Plotted here are raw 300-year time series (detrended, normalize,13-y smoothed) of the EsperNHT reconstruction [black line] (Esper et al. 2002) and a solar-based NHT reconstruction [red line] are plotted (see text). Using inferences made regarding solar's relationship to various sub-processes operating within the stadium-wave teleconnection sequence, the "solar components" were carefully chosen. The solar-based NHT reconstruction (NHT_solar) is not meant to be interpreted as solar's direct forcing on climate. Instead, each component of this solar combination [cumulative-sum of negative solar + solar] reflects processes involved in evolution of the NHT signature; Correlation between 13-year smoothed series of Esper NHT and Solar-NHT over a 300-year period is 0.77 at the 95% level. (For non-smoothed series, R=0.73 at the 99% level.)

3.4 Discussion

In this study, I expanded previous work by Wyatt et al. (2011) on a hypothesized low-frequency climate signal propagating throughout a network of indices across the Northern Hemisphere during the 20th century. Analogous low-frequency signal propagation was identified in this study for the 20th century. The signal was identified in a variety of index-networks, including those

networks representing geographical regions not investigated in the original study. High and low-latitude indices not previously considered include time series of Eurasian Arctic sea-ice, Arctic temperature, and proxies for latitudinal migrations of the Intertropical Convergence Zone.

These additions facilitated further development of a working hypothesis on how this signal propagates. Ocean-ice-atmospheric coupling is the fundamental piece to this working hypothesis. Sub-processes related to this coupling are critical to understanding the stadium-wave propagation.

Table 3.11: Correlations between pairs of indices (both non-smoothed and smoothed (13y)) representing NHT reconstructions are calculated for the years 1700 to 2000. Esper et al's NHT reconstruction (**Esper NHT**) is correlated with an index of solar components ('**NHT_solar'** = cs of ngsolar+solar), chosen based on the inferred dynamics associated with each component (see text). Likewise, an "ITCZ" index was calculated from inferred dynamics associated with each component ('**NHT_LOD'** = AMO+ngNPGO[15]). NPGO was inferred from the ngLOD index. See text for NPGO derivation and for explanation for selected components. Note: values in red are significant at the 99% level; those in blue are significant at the 95% level.

indices	Esper NHT	NHT_ solar	NHT_ LOD	Esper NHTsm	NHT_ solar smoothed	NHT_ LOD smoothed
Esper NHT	1.0	0.73	0.80			
NHT_Solar	0.73	1.0				
NHT_LOD	0.80		1.0			
Esper NHTsm				1.0	0.77	0.81
NHT_solar smoothed				0.77	1.0	
NHT_LOD smoothed				0.81		1.0

[15] 20th century correlation of raw time series of NPGO+AMO and ngLOD = R=0.95 at 99% significance level

The working hypothesis is pictorially captured in **Figure 3.22**. In simplest form, a cool Atlantic leads increased sea-ice-extent in the West Eurasian Arctic. The increased sea-ice leads increased winds, which lead increased temperatures downwind. Pacific circulations accelerate, ultimately leading a warm hemispheric surface temperature (NHT) and a warm Atlantic, marking the end of a half-cycle of the stadium-wave propagation. The reverse sequence ensues for the other half-cycle of propagation, with a warm Atlantic ultimately manifesting as cool hemispheric temperatures and cool Atlantic sea-surface temperatures.

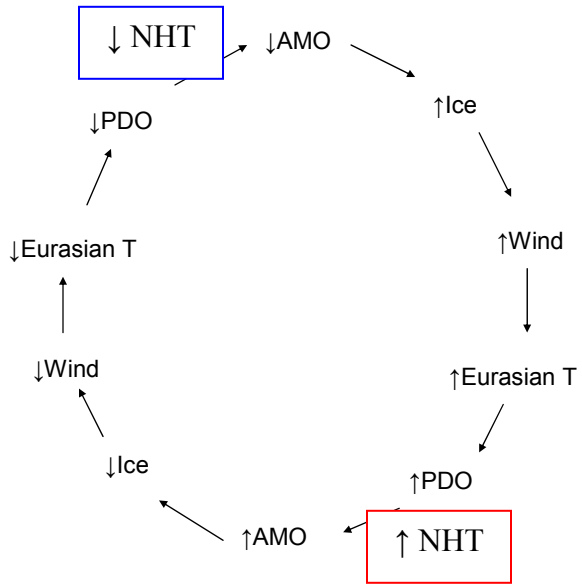

Fig. 3.22: A schematic depiction shows an abbreviated index-sequence that describes stadium-wave signal propagation as hypothesized by the author. Arctic dT is not shown (occur between PDO and AMO, just prior to NHT). Eurasian T is shown; temperatures there are directly linked to the sea-ice-induced zonal winds. Discussion of links between "nodes" of the climate network and studies supporting these links can be found in this paper and in the original Wyatt et al. 2011 paper (chapter 2 of this thesis).

In this working hypothesis's less simple form, there are nuances involved. Details perhaps, yet they play disproportionately large roles in the final outcome. They include: 1)

multidecadal patterns of internal saline Rossby modes and North Atlantic-Arctic salinity exchange (Frankcombe and Dijkstra 2011); 2) multidecadal fluctuations of heat and salt advection (Gudkovich and Kovalev 2002 a,b) and their role in sea-ice formation (Frolov et al. 2009 and references within)); 3) the interrelationship between sea-ice cover and Arctic temperature (Frolov et al. 2009); 4) the ice-induced basin-scale meridional temperature gradient (Outten and Esau 2011); 5) the atmospheric response to this ice-induced temperature gradient (Karklin et al. 2001; Outten and Esau 2011; Petoukhov and Semenov 2010); and 6) the many consequences of that atmospheric response, largely due to the regime-related geographical shifts of the atmospheric and oceanic centers-of-action (Frolov et al. 2009 and references within). These geographical shifts affect precipitation patterns, ocean-flow patterns, Arctic-ice-export patterns, and ratio of sea-ice-cover to open water (Gudkovich et al. 1972; Rigor et al. 2002), with ensuing modifications on ocean-to-atmosphere heat flux, and therefore on Arctic temperature (Frolov et al. 2009). Heat advection related to wind-patterns carry heat from the ocean to the continents, manifesting as increases in the Northern Hemisphere temperature (Wallace et al. 1995; Klimenko 2007). The half-cycle of this signal propagation across the hemisphere culminates with impacts of anomalies of Pacific circulations, which appear to feedback onto the Atlantic (Schmittner et al. 2000; Latif et al. 2001), initiating changes in the freshwater balance of the Atlantic. These salinity modifications lead changes in sea-ice-extent of the Eurasian Arctic Seas, in particular, those of the West Eurasian sector. An approximate 60-to-65 year cycle was identified for the 20th century in this study. This finding is supported by those of Karklin et al. (2001) and Polyakov et al. (2004), who identified an approximate 60-year variability of sea-ice-extent, atmospheric-circulation regimes, and Arctic temperature between 72ºN and 87ºN.

Drawing from this working hypothesis, I speculated on what proxies might be used to represent these sub-processes. Figure 3.14 captures these index relationships and provides, I propose, a tool that gives insight to potential proxies. Statistically significant correlations have been detailed throughout this paper to support these proposed index relationships.

Analysis limited to the twentieth century does not speak to stadium-wave behavior prior to 1900. To investigate the historical profile of the stadium wave, I used three approaches.

The first approach relied on what I termed "conventional proxies". These proxy reconstructions are those based on tree rings, isotope ratios in ice cores and corals, archival evidence, and the like. I used proxy reconstructions for the Northern Hemisphere temperature, the Atlantic Multidecadal Oscillation, the North Atlantic Oscillation, and the Pacific Decadal Oscillation. I included a proxy for the atmospheric-mass-transfer anomalies (AT) for select cases[16]. A statistically significant M-SSA-extracted stadium-wave signal was identified for the time interval 1850 to 2000. Prior to 1850, non-random occurrence of this identified signal could not be ruled out at the $p < 5\%$ level.

The second approach to this investigation into the signal's history relied upon a different set of proxies. These included Earth's rotational-rate anomalies, *G. bulloides* abundances in the Cariaco Basin, Japanese Sardine outbursts in the western-boundary region of the North Pacific, the coral-proxy record associated with variability in the North Pacific Gyre Oscillation, and the solar constant. Selection of these indices was based on literature review and previous research done with them in relation to the stadium-wave signal. A statistically significant M-SSA-extracted stadium-wave signal was identified in all indices in the 20th century. As with the results

[16] ngLODcsr, the time-derivative of ngLOD, co-occurs with AT. This relationship can be explained thusly: A strong basin-scale meridional temperature gradient, related to increased polar ice inventory (sea ice and presumed co-occurrence of land ice), triggers increased basin-scale winds (AT). Increased polar ice inventory exerts incremental forcing on Earth's increased rotational rate (ngLOD), i.e. ngLODcsr.

in the first approach, non-random occurrence of this signal further back in time could not be established at the $p < 5\%$ level.

The third approach was based on the working hypothesis described in this work. Two indices had annually, to near-annually resolved records dating to 1700, the full duration of time series used in this study. These included the solar constant and Earth's rotational-rate anomalies. Using associations as depicted in Figure 3.14, I developed algorithms that I thought should reflect climate variability if stadium-wave signal propagation was a fundamental piece of the low frequency climate footprint. I had only a proxy for the Northern Hemisphere temperature (Esper NHT: Esper et al. 2002) as the measure of this footprint. Thus, each index came with its own set of errors. Despite the data issues, I reconstructed two Northern Hemisphere Temperature (NHT) time series based on the stadium-wave-based algorithms. Plots of these are shown in figure 3.19 and figure 3.21.

I used Earth's rotational rate (ngLOD) in the first NHT reconstruction. This ultimately led to the construction of a time series reflecting latitudinal migrations of the Intertropical Convergence Zone (ITCZ). Northward (southward) shifts of the ITCZ were shown to coincide with increases (decreases) of Northern Hemisphere temperature in 20th century analyses. Correlation between non-smoothed time series of the first NHT reconstruction and Esper NHT was $R=0.80$ at the $p < 1\%$ level of significance and for the 13-year smoothed time series, correlation was $R=0.81$ at the $p < 5\%$ level.

For the second NHT reconstruction I invoked the temporal relationship of the solar constant with a variety of stadium-wave indices. It is possible that the temporal alignment is merely coincidence. But it may be entrainment. Entrainment of tempo by an external quasi-oscillatory system is common among synchronized networks (Pikovsky et al. 2001). I envision

entrainment as a possible low-frequency role for solar in the stadium wave: solar as a metronome, of sorts, perhaps working through a very slight influence on sea-surface-temperatures in the Tropics. This conjecture underlies the construction of the algorithm used. Correlation between non-smoothed time series of this second NHT reconstruction and Esper NHT was R=0.73 at the $p < 1\%$ significance level and for the 13-year-smoothed time series, correlation was R=0.77 at the $p < 5\%$ level.

3.5 Conclusion

Results from this study strengthen the case for the existence of a secularly varying climate signal that propagates hemispherically. Additional stadium-wave-related features emerged in the present study: i) the importance of Eurasian Arctic sea-ice, and the consequent atmospheric response, in driving signal propagation; ii) the possible negative feedback of accumulated effects of Pacific-centered circulations on activity in the Atlantic; iii) identified relationships between stadium-wave sub-processes and 'dynamic proxies', offering potential for understanding past climate in terms of the stadium-wave teleconnection sequence; iv) and evidence for stadium-wave propagation in all proxies for at least 150 years, and in dynamic proxies for possibly at least 300 years.

Acknowledgements: My thanks go to Sergey Kravtsov and John Peters for their guidance on statistical methods used in the present study, to Peter Molnar for his in-depth editing advice, to Balaji Rajagopalan for his helpful comments, and to Judy Curry for her suggestions and kind support.

References

Alekseev GV (1995) Interaction of atmosphere and ocean in the polar regions. Problems of the Arctic and the Antarctic 70: 193-200 [in Russian]

Alexander MA, Deser C (1995) A mechanism for the recurrence of wintertime midlatitude SST anomalies. J Phys Oceanogr 25: 122-137

Beamish RJ, Boullion DR (1993) Pacific salmon production trends in relation to climate. Canadian Jour Fish and Aquat Sci 50:1002-1016.

Beamish RJ, Neville CM, Cass AJ (1997) Production of Fraser River sockeye salmon (*Oncorhynchus nerka*) in relation to decadal-scale changes in the climate and the ocean. Canadian Jour Fish and Aquat Sci 54: 543-554

Beamish RJ, Noakes D, McFarlane GA, Klyashtorin L, Ivanov VV, Kurashov V (1999) The regime concept and natural trends in the production of Pacific salmon. Canadian Journal of Fisheries and Aquatic Sciences 56: 516-526

Beckers J, Rixen M (2003) EOF calculations and data filling from incomplete oceanographic data sets. J Atmos Ocean Technol 20: 1839–1856. doi: 10.1175/1520-0426(2003)

Biondi F, Gershunov A, Cayan DR (2001) North Pacific Decadal Climate Variability since 1661. J. Climate, 14: 5-10

Black D, Peterson LC, Overpeck JT, Kaplan A, Evans MN, Kashgarian M (1999) Eight Centuries of North Atlantic Ocean Atmosphere Variability. Science 286: 1709-1713. doi: 10.1126/science.286.5445.1709

Broomhead DS, King GP (1986) Extracting qualitative dynamics from experimental data. Physica D 20: 217–236

Bretherton, C.S, Widmann M, Dymnikov VP, Wallace JM, Blade I (1999) The effective number of spatial degrees of freedom of a time-varying field. J. Climate, 12: 1990–2009

Ceballos LI, Di Lorenzo E, Hoyos CD, Schneider N, Taguchi B (2009) North Pacific Gyre Oscillation synchronizes climate fluctuations in the eastern and western boundary systems. J Clim 22: 5163-5174.

Chang P, Zhang Li, Saravanan R, Vimont DJ, Chiang JCH, Link Ji, Seidel H, Tippett MK (2007) Pacific meridional mode and El Niño-Southern Oscillation. Geophys Res Lett 34. L16608. doi:10.1029/2007GL030302

Chavez PF, Ryan J, Lluch-Cota SE, Niquen MC (2003) From Anchovies to Sardines and Back: Multidecadal Change in the Pacific Ocean. Science 299: 217- 221

Chhak K, Di Lorenzo E (2007) Decadal variations in the California Current upwelling cells. Geophys Res Lett 314: L14604. doi10.1029/2007GL030203

Chiang JCH, Vimont D (2004) Analogous Pacific and Atlantic Meridional Modes of Tropical Atmosphere-Ocean Variability. J. Climate 17: 4143-4158. doi: 10.1175/JCLI4953.1

Cook ER, D'Arrigio RD, Mann ME (2002) A Well-Verified, Multiproxy Reconstruction of the Winter North Atlantic Oscillation Index since A.D. 1400. Jour of Clim 15: 1754-1764

Courtillot V, Gallet Y, Le Mouel JL, Fluteau F, Genevey A (2007) Are there connections between the Earth's magnetic field and climate? Earth and Planetary Science Letters 253: 328-339

D'Arrigio R, Wilson R (2006) On the Asian Expression of the PDO. International Jour of Climatology 26: 1607-1617

Delworth TL, Mann ME (2000) Observed and simulated multidecadal variability in the Northern Hemisphere. Climate Dyn 16: 661–676. doi:10.1007/s003820000075

Di Lorenzo E, Schneider N, Cobb KM, Franks PJS, Chhak K, Miller AJ, McWilliams JC, Bograd SJ, Arango H, Curchitser E, Powell TM (2008) North Pacific Gyre Oscillation links ocean climate and ecosystem change. Geophys Res Lett 35: L08607. doi:10.1029/2007GL032838

Di Lorenzo E, Fiechter J, Schneider N, Miller AJ, Franks PJS, Bograd SJ, Moore A, Thomas A, Crawford W, Pena A, Herman AJ (2009) Nutrient and salinity decadal variations in the central and eastern North Pacific. Geophys Res Lett 36: L14601. doi:10.1029/2009GL038261

Di Lorenzo E, Cobb KM, Furtado JC, Schneider N, Anderson BT, Bracco A, Alexander MA, Vimont DJ (2010) Central Pacific El Niño and decadal climate change in the North Pacific Ocean. Nature Geosci 3 (11): 762-765. doi10.1038/NGEO984

Dima M, Lohmann G (2007) A Hemispheric Mechanism for the Atlantic Multidecadal Oscillation. J Climate 20: 2706-2719. doi:10.1175/JCL14174.1

Elsner JB, Tsonis AA (1996) Singular Spectrum Analysis: A New Tool in Time Series Analysis. Springer, 177 pp.

Esper J, Cook ER, Schweingruber FH (2002) Low-Frequency Signals in Long Tree-Ring Chronologies for Reconstructing Past Temperature Variability. Science 295 (5563)

Folland CK, Palmer TN, Parker DE (1986) Sahel rainfall and worldwide sea temperature 1901-1985. Nature320: 602-607

Frankcombe LM and Dijkstra HA (2011) The role of Atlantic-Arctic exchange in North Atlantic multidecadal climate variability. Geophy Res Lett 38: L16603. doi:10.1029/2011GL048158.

Frolov IE, Gudkovich AM, Karklin BP, Kvalev EG, Smolyanitsky VM (2009) Climate Change in Eurasian Arctic Shelf Seas, Springer-Praxis Books, ISBN 978-3-540-85874-4, 165p.

Ghil M, Allen MR, Dettinger MD, Ide K, Kondrashov D, Mann ME, Robertson AW, Saunders A, Tian Y, Varadi F, Yiou P (2002) Advanced spectral methods for climatic time series. Rev Geophys 40(1): 3.1–3.41. doi:10.1029/2000GR000092.

Girs AA (1971a) Multiyear oscillations of atmospheric circulation and long-term meteorological forecasts. L. Gidrometeroizdat 480 p. (in Russian)

Girs AA (1971b) Long-term fluctuations of the atmospheric circulation and hydrometeorological forecasts. L., Hydrometeorological monographs, St. Petersburg, Russia. 280p

Gray ST, Graumlich LJ, Betancourt JL, Pederson GT (2004) A tree-ring based reconstruction of the Atlantic Multidecadal Oscillation since 1567 A.D. Geophys Res Lett 31. L12205: doi:10.1029/2004GL019932

Gudkovich ZM, Kirillov AA, Kovalev YeG, Smetannikova AV, and Spichkin VA (1972) Long-range Ice Forecasting Mehodology for the Arctic Seas. Leningrad: Gidrometeoizdat.: 348pp [in Russian]

Gudkovich ZM and Kovalev YeG (2002a) On some mechanisms of cyclic climate changes in the Arctic and the Antarctic. Oceanology 42(6): 1-7 [in Russian]

Gudkovich ZM and Kovalev YeG (2002b) Fluctuations of sea-ice extent of the Russian Arctic Seas in the 20th century and assessment of its possible changes in the 21st century. Paper presented at Hydrometeorological Support for Economic Activity in the Arctic and the Ice-covered Seas, St. Petersburg, March 27-29, pp 36-45.

Hurst HE (1951) Long-Term Storage Capacity of Reservoirs. Transactions of the American Society of Civil Engineers 116: 770-799

Jones PD, Briffa KR, Barnett TP, Tett SFB (1998) High-resolution Palaeoclimatic Records for the last Millennium: Interpretation, Integration and Comparison with General Circulation Model Control-run Temperatures. The Holocene 8: 455-471

Jones PD, Moberg A (2003) Hemispheric and large-scale surface air temperature variations: an extensive revision and an update to 2001. J Clim 16: 206-223. doi:10.1175/1520-0442(2003)

Karklin VP Yulin AV, Karelin ID, and Ivanov VV (2001) Climatic fluctuations of sea-ice extent of the Arctic Seas of the Siberian shelf. AARI Proc. 443: 5-11 [in Russian].

Kawasaki, T (1994) A decade of the regime shift of small pelagics – from the FAO expert Consultation (1983) to the PICES III(1994). Bull. Japanese Soc. Fish. Oceanogr 58: 321-333

Keenlyside NS, Latif M, Jungclaus J, Kornblueh L, Roeckner E (2008) Advancing decadal-scale climate prediction in the North Atlantic sector. Nature 453: 84-88. doi:10.1038/nature06921

Kelly K, Dong S (2004) The Relationship of Western Boundary Current Heat Transport and Storage to Midlatitude Ocean-Atmosphere Interaction. Ocean-Atmosphere Interaction and Climate Variability, Edited by Chunzai Wang, Shang-Ping Xie, and James A. Carton, AGU Monograph

King, JR, Ivanov VV, Kurashov V, Beamish RJ, McFarlane GA (1998) General Circulation of the atmosphere over the North Pacific and its relationship to the Aleutian Low. (NPAFC Doc. No. 318) 18p, Dept. of Fisheries and Oceans, Sciences Branch

Klimenko VV (2007) Climatic sensation: What awaits us in the near and distant future? "Polit. Ru" public lectures. Available at www.polit.ru/lectures/2007/02/15/klimenko.html

Klyashtorin LB (1998) Long-term climate change and main commercial fish production in the Atlantic and Pacific. Fisheries Research (37): 115-125

Klyashtorin LB, Lyubushin AA (2007) Cyclic Climate Changes and Fish Productivity. Moscow, VNIRO Publishing, Editor for English version: Dr. Gary D. Sharp, Center for Climate/Ocean Resources Study, Salinas, CA. USA: 223pp

Klyashtorin LB, Borisov V, Lyubushin AA (2009) Cyclic changes of climate and major commercial stocks of the Barents Sea. Marine Biology Research 5: 4-17

Kondrashov D, Ghil M (2006) Spatio-temporal filling of missing points in geophysical data sets. Nonl Proc Geophys 13: 151–159

Latif M, Roeckner E, Mikolajewicz U, Voss R (2000) Tropical Stabilization of the Thermohaline Circulation in a Greenhouse Warming Simulation. J of Clim 13: 1809-1813.

Latif M (2001) Tropical Pacific/Atlantic Ocean Interactions at Multi-Decadal Time Scales. Geophy Res Lett 28: 539-542.

Latif M, Boning C, Willebrand J, Biastoch A, Dengg J, Keenlyside N, Schweckendiek U (2006) Is the Thermohaline Circulation Changing? J of Clim 19: 4631-4637.

Lean J (2000) Evolution of the Sun's Spectral Irradiance Since the Maunder Minimum. Geophysicsl Res Lett 27 (16): 2425-2428

Lean J (2004) Solar Irradiance Reconstruction. IGBP PAGES/World Data Center fro Paleoclimatology. Data Contribution Series # 2004-035

Loehle C, Scafetta N (2011), Climate Change Attribution Using Empirical Decomposition of Climatic Data. The Open Atm Sc Jour 5: 74-86.

Luterbacker J, Xoplaki E, Dietrich D, Jones PD, Davies TD, Portis D, Gonzalez-Rouco JF, von Storch H, Gyalistras D, Casty C, Wanner H (2002) Extending North Atlantic Oscillation Reconstructions Back to 1500. Atmos Sci Lett. Doi:10.1006/asle.2001.0044

Mantua NJ, Hare SR, Zhang Y, Wallace JM, Francis RC (1997) A Pacific interdecadal climate oscillation with impacts on salmon production. Bull Amer Meteor Soc 78: 1069-1079

Mazzarella A, Scafetta N (2011) Evidences for a quasi 60-year North Atlantic Oscillation since 1700 and its meaning for global climate change. Theor Appl Climatol DOI 10 1007/s00704-011-0499-4

Minobe S (1997) A 50-70-year climatic oscillation over the North Pacific and North America. Geophys Res Lett 24: 683-686

Minobe S (1999) Resonance in bidecadal and pentadecadal climate oscillations over the North Pacific: role in climatic regime shifts. Geophys Res Lett 26: 855-858

Niebauer H (1998) Variability in Bering Sea ice cover as affected by a regime shift in the North Pacific in the period 1947-1996. J Geophys Res 103 (C12): 27717-27737.

Nowak K, Hoerling M, Rajagopalan B, Zagona E (2011) Colorado River Basin Hydro-Climatic Variability. (in press Journ Climate)

Nurhati IS, Cobb KM, Di Lorenzo E (2010) Decadal-scale SST and Salinity Variations in the Central Tropical Pacific: Signatures of Natural and Anthropogenic Climate Change. Jour of Clim 24 (13): 3294-3308. DOI: 10.1175/2011JCLI3852.1

Ogurtsov MG, Nagovitsyn YA, Kocharov GE, Jungner H (2002) Long-period cycles of the Sun's activity recorded in direct solar data and proxies. Solar Physics 211: 371-394

Outcalt SI, Hinkel KM, Meyer E, Brazel AJ (1997) Application of Hurst Rescaling to Geophysical Serial Data. Geographical Analysis 29 (1): 72-87

Outten SD, Esau I (2011) A link between Arctic sea ice and recent cooling trends over Eurasia. Climate Change. DOI 10.1007/s1058-011-0334-z

Patterson RT, Prokoph A, Chang A (2004) Late Holocene sedimentary response to solar and cosmic ray activity influenced climate variability in the NE Pacific. Sedimentary Geology 172: 6784

Petoukhov V, Semenov VA (2010) A link between reduced Barents-Kara sea ice and cold winter extremes over northern continents. J Geophy Res 115 (D21111). Doi:1029/2009JD013568.
Philander GS (1990), El Nino, La Nina, and the Southern Oscillation, Academic Press. ISBN 0 12 553235 0, 289p

Pikovsky A, Rosenblum M, Kurths J (2001; reprinted 2003), Synchronization: A universal concept in nonlinear sciences. Cambridge University Press. ISBN 0 521 59285 2, 370p

Polyakov IV, Alekseev GV, Timokhov LA, Bhatt JS, Colony RL, Simmons HL, Walsh D, Walsh JE, and Zakharov VF (2004) Variability of the intermediate Atlantic water of the Arctic Ocean over the last 100 years. J of Clim 16(12): 2067-2077.

Rigor, IG, Wallace JM, Colony RL (2002) Response of sea ice to the Arctic Oscillation, J of Clim 15: 2648-2663.

Roberts PH, Yu ZJ, Russell CT (2007) On the 60-year signal from the core. Geophysical and Astrophysical Fluid Dynamics 101: 11-35

Rudyaev FI, Trofimov VK, Kravchuk YA (1985) Rhythmic changes of the Earth's rotation speed during the period 1664 to 1976. Izvestiya VO 117(3):252-257 [in Russian]

Scafetta N (2011), A shared frequency set between the historical mid-latitude aurora records and the global surface temperature. Jour Atm and Solar-Terrestrial Physics (in press).

Schmittner A, Appenzeller C, Stocker TF (2000). Enhanced Atlantic freshwater export during El Nino. Geophy Res Lett 27(8):1163-1166.

Shabalova MV, Weber SL (1999) Patterns of temperature variability on multidecadal to centennial timescales. J Geophys Res 104: 31,023-31,041

Shen C, Wang WC, Gong W, Hao Z (2006) A Pacific Decadal Oscillation record since 1470 AD reconstructed from proxy data of summer rainfall over eastern China. Geophysical Res Lett 33: L03702. doi:10.1029/2005GL024804

Sidorenkov NS (2005a) Physics of the Earth's rotation instabilities. Astronomical and Astrophysical Transactions 24 (5): 425-439 DOI:10.1080/10556790600593506

Sidorenkov NS, Lutsenko OV, Bryazgin NN (2005b) Variation of the mass of the sheet of Antarctica and instability of the Earth's rotation. Russian Meteorology and Hydrology 8: 5-13

Sidorenkov NS (2009) The interaction between Earth's rotation and geophysical processes. WILEY-VCH Verlag GmbH and Co. KGaA, Weinheim 305pp

Sutton RT, Hodson DLR (2005) Atlantic Ocean forcing of North American and European summer climate. Science 309: 115-118. doi: 10.1126/science.1109496

Vangenheim GYa (1940) The long-term temperature and ice break-up forecasting. Proc State Hydrological Institute Iss. 10: 207-236 (in Russian)

Wallace JM, Zhang Y, and Renwick JA (1995) Dynamic contribution to hemispheric mean temperature trends. Science 270: 780-783.

Wang L, Chen W, Huang R (2007) Changes in the Variability of North Pacific Oscillation around 1975/1976 and its relationship with East Asian winter climate. J Geophys Res 112: D11110. doi: 10.1029/2006JD008054

Wilson IRG, Carter BD, White IA (2008) Does a Spin-Orbit Coupling Between the Sun and the Jovian Planets Govern the Solar Cycle? Publications of the Astronomical Society of Australia 25: 85-93

Wyatt MG, Kravtsov S, Tsonis AA (2011) Atlantic Multidecadal Oscillation and Northern Hemisphere's climate variability. Clim Dyn DOI: 10.1007/s00382-011-1071-8

Chapter Four:

A Secularly Varying Hemispheric Climate-Signal Propagation Previously Detected in Instrumental and Proxy Data Not Detected in CMIP3 Data Base [1]

Abstract: Previous study results suggest the existence of a multidecadal, quasi-oscillatory climate signal, propagating through a network of synchronized climate indices across the Northern Hemisphere. In this present model-data-based study, we seek to detect this same signal. Methods used in the two preceding studies on climate-signal propagation guide the strategy for this companion study. We analyze a network of simulated climate indices, reconstructed from a data set generated by models of the third Coupled Intercomparison Project (CMIP3). Of the sixty analyses performed on these networks, none succeeded in reproducing a propagating multidecadal oscillatory signal. In general, model data reflect high frequency modes with the occasional single mode exhibiting century-scale variability. In contrast, the leading two modes of variability found in our previous work were typified by multidecadal variability. These contrasts in results may imply that physical mechanisms relevant to signal propagation may be missing from this suite of general circulation models.

Keywords: Climate · Network · Synchronize · CMIP3 · stadium-wave

4.1 Introduction: Multidecadal fluctuations are pervasive in records of diverse indices – from climate-related parameters to similarly cadenced variations in cosmogenic nuclide accumulations, geomagnetic-field intensity, and Earth's rotational-rate anomalies. Recent work using instrumental data of the 20th century by Wyatt et al. (2011) suggests that a synchronized

[1] Significant contributions toward this work were given by John M. Peters and Sergey Kravtsov. Also helpful in the oversight of the project was Anastasios Tsonis.

network of indices, through which a low-frequency, quasi-oscillatory signal propagates, can offer explanation for the observed secularly varying behavior shared by a variety of regional climate indices. Wyatt (2012, *submitted manuscript*) subsequently found evidence for a 20th-century propagating signal in a large variety of proxy and geophysical indices, with apparent long-term persistence of this behavior, possibly as far back as to at least 1700, a result that supports the existence of a synchronized network of indices.

Model support for various regional links within this proposed signal propagation, which Wyatt et al (2011) termed 'the stadium wave[2]', is detailed in their 2011 paper. While model inquiries into regional processes and links between individual climate patterns appear to show great promise, it is not clear that hemispheric behavior involving a network of interlinked regional processes is similarly well modeled. In short, can success in modeling the dynamics of component parts of a hemispherically spanning system be expanded to a similar degree of success in simulating the entire hemispherically spanning system?

The present study explores 'stadium-wave' dynamics in indices reconstructed from model-generated data archived by the third version of the Coupled Model Intercomparison Project (CMIP3 (Meehl et al. 2007)). In one sense, by so doing, a hypothesis is being tested by a hypothesis. Yet, with previous instrumental and proxy-based studies conveying credibility to the hypothesized hemispherically propagating sequence, how the model-generated data perform may speak more to the model design than to the proposed climate signal.

Section 4.2 details the methods and data; section 4.3 the results; section 4.4 the discussion of results; and 4.5 the conclusion.

[2] Stadium-wave is a term alluding to the behavior often seen in a sports arena, where successive groups of spectators stand with arms raised and then sit, giving the visual impression of a wave passing through the crowd.

4.2 Methods and Data Sets

In accord with previous investigations into a multidecadally varying, hemispherically propagating climate signal, in this study, we applied multivariate statistical methods to a network of well-known ocean and atmospheric circulation indices that have been reconstructed from model-generated data. We downloaded these data from the third version of the Community Model Intercomparison Project (CMIP) site – a site comprising a vast collection of data sets generated by atmospheric-oceanic general circulation models used in Intergovernmental Panel on Climate Change (IPCC)-related research projects. Twenty-two models are represented by CMIP3. Dozens of experiments have been performed by each model, most with several runs each. And from these model-simulations, variables (e.g. sea-surface-temperatures, sea-level-pressure, surface-temperature, sea-surface-height, etc.) were generated. Our task was to take model-generated raw variables relevant to our study and reconstruct from them the climate indices used in previous studies on “stadium-wave” signal propagation.

4.2.1 Data Sets

Considered in this present study are the indices used in the original work on “stadium-wave” dynamics. These include the Northern Hemisphere averaged-surface temperature (NHT), the Atlantic Multidecadal Oscillation (AMO), the North Atlantic Oscillation (NAO), a sea-surface-temperature-anomaly-based index of the El Nino Southern Oscillation (NINO3.4), the Pacific Decadal Oscillation (PDO), the North Pacific Oscillation (NPO), and the Aleutian Low-Pressure Index (ALPI). An eighth index was used in the original instrumental-based study: atmospheric-mass-transfer anomalies (AT). Reconstruction of this index proved impractical with the CMIP model-generated data; thus it was omitted from this study. We cannot claim to know if

results of our work would have been the same with this index's inclusion, but we find rationale in its exclusion based on results of a previous study by Wyatt (2012; *submitted manuscript*).

In that previous study, Wyatt analyzed an expanded collection of instrumental and proxy data. The set consisted of the original stadium-wave indices plus about a dozen additional indices representing diverse geographical regions and geophysical processes. Wyatt analyzed the full set, as well as numerous subsets. A statistically significant stadium-wave signal was identified in each data set for the 20th century. Some of the subsets contained none of the original index members. Some contained exactly those indices used here. See **Table 4.1** for references and description details of indices.

Table 4.1: Indices used in study and descriptions for index-reconstructions.

Index	General Description for Index-Reconstruction:	Reference
NHT	Average surface land temperature and SST of the Northern Hemisphere	Jones & Moberg (2003); Rayner et al., (2006)
AMO	SSTA averaged over 0 to 60ºN, 75ºW to 7.5ºW	Kerr (2000);Enfield et al. (2001); Sutton and Hodson (2003)
NAO	Normalized pressure (SLP) difference between the Azores High-Pressure system (~33.2ºW, 32.2ºN) and the Icelandic Low-Pressure system (~33.15ºW, 59.6ºN). [~1st PC of SLP in North Atlantic]	Hurrell (1995)
NINO3.4	Average SSTA 5ºN to 5ºS, 170ºW to 120ºW	Trenberth (1997)
NPO	2nd EOF of SLPA from 100ºE to 120W, 0 to 90ºN	Wang et al. (2007)
PDO	Leading PC of SSTA north of 20ºN in North Pacific; globally averaged SSTA subtracted from SSTA in Pacific to remove global-warming signal.	Mantua et al. (1997)
ALPI	Relative intensity of SLP in North Pacific around 50ºN in winter (DJFM). The mean area in km^2 with SLP less than 100.5kPa. Expressed as anomaly relative to 1950 to 1997 mean.	Beamish et al. 1997

In the present study, we considered all 22 models participating in the CMIP data base. Matlab code was written for the extraction of data from the CMIP site and for the reconstruction of indices. The procedure was far from straight-forward, including encounters with idiosyncrasies with each data set in its download, to corrupted-data issues – both minor and significant. Upon completion of the project, 21 of the 22 available models were successfully processed, but the 22nd model contained corrupted data sets necessary to our analysis; thus it could not be used. We evaluated at least one 20th-century experiment for each of the 21 models analyzed. For several of the models, analysis of a second run of the 20th-century experiment was performed. In addition, for six of the models, we analyzed one run of a pre-industrial control experiment. Both annual and 5-year-smoothed samplings were used on all iterations. A total of 60 analyses were completed.

Twentieth-century models generally cover the historical period – 1850 to 2000. Such model runs incorporate observed radiative forcings (greenhouse gases (with CO2 increases of 1% per year), aerosols, volcanic eruptions, etc.) throughout the period, the exact levels and proportions of forcings differing among models (Reichler and Kim 2007). Control experiments, also termed “long controls”, generally cover 500-plus years. Incorporated in them are atmospheric forcings that were held constant, in particular, that of CO2, which is held at 280ppm. Data for most runs are available on daily, monthly, and annual bases. For this study, monthly data were downloaded.

Using an index-specific code (Table 4.1), we converted model-generated raw variables into index-members of the original stadium-wave sequence. Boreal winter months (DJFM) were extracted from the annual index reconstructions, and the boreal-winter-mean of each calculated.

Once a model-run's index set was complete, time series of each index were prepared for analysis. To duplicate our original study's methodology exactly, all time series for this collection of models were truncated. Only the years 1900 to 1999 were used. For pre-industrial runs, the time series lengths varied, from 150 years to 500 years. We worked with various lengths of time series from these control-run simulations.

4.2.2 Methods:

Identifying a Signal: To each time series (linearly detrended and normalized to unit variance), multivariate statistical methods were applied. In particular, we used Multi-channel Singular Spectrum Analysis (M-SSA: Broomhead and King 1986; Elsner and Tsonis 1996; Ghil et al. 2002)) to characterize the dominant modes of variability shared by the network of indices. Multi-channel Singular Spectrum Analysis (M-SSA), based on Empirical Orthogonal Function (EOF; Preisendorfer 1988) analysis, and used in previous work on stadium-wave signal propagation, is a multivariate spatio-temporal technique, that is adept at identifying a signal propagating through a collection of indices (Ghil et al. 2002 and references therein).

M-SSA is, in fact, EOF analysis applied to an extended time series. This time series is generated from the original time series, augmented by M lagged, or shifted, copies thereof. M is also considered to be the filter window. We use M=20. This gives us an extended lagged covariance matrix. Each multivalued time series in this matrix is referred to as a channel. As in EOF analysis, the goal of M-SSA is to identify a common pattern among all the channels. EOF seeks this common pattern at a zero-lag among indices. M-SSA identifies a common pattern at a non-zero lag – thus a propagating signal. The patterns of variability common to all indices are referred to as modes of variability, or simply 'modes'. M-SSA identifies a specified number of

these modes. Each mode is characterized by a function that best reflects fluctuations that all index time series share at a lag. This function, or eigenfunction, is essentially a time series of the mode's variance. We generate an M-SSA spectrum that reflects the mean variances of these modes. These are the mean values of the shared patterns of variability. They are sequentially ordered on the spectrum according to their dominance in characterizing the index-set's shared variability. Mode one is the pattern of variability shared by all indices that explains most of the observed variance. Mode two identifies the second most pervasive pattern of shared variability. In this present study, we identify the first ten modes of co-variability. Seven of these are subsequently plotted. This plot is an M-SSA spectrum. **Figure 4.1**a shows an example of an M-SSA spectrum adapted from Wyatt et al. (2011). This spectrum identifies modes of variability identified in the original stadium-wave data set. Figure 4.1b depicts the cumulative variance accounted for by the first twenty modes identified in the original study.

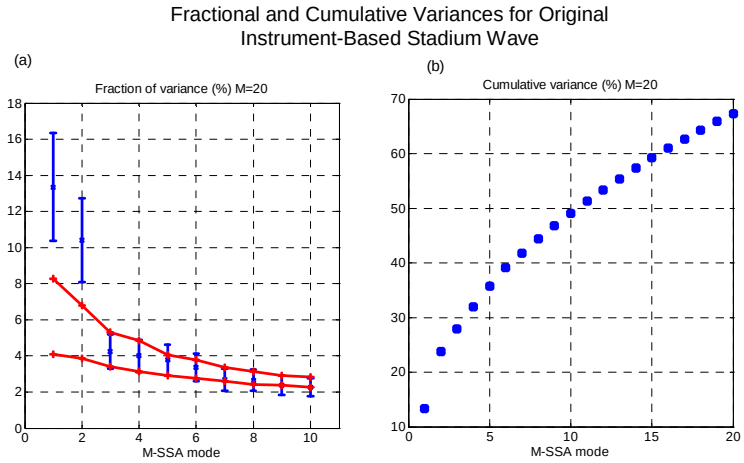

Fig. 4.1: Statistical Results from Original Stadium-Wave analysis, given here for comparison to model results. (a) Shows the fractional and (b) cumulative variances of the modes of variability shared by the collection of eight instrumental climate indices. Note the leading two modes of variability; they are widely separated from the remaining modes; their error bars overlap.

Eigenfunctions provide a temporal filter that captures this identified pattern of variability in each index of the data set. How much of an index's variability is accounted for by this eigenfunction is referred to as an index's channel-fraction variance, or fractional variance. Because the extended matrix consists of a collection of indices representing diverse geographical regions, a spatial dimension is conveyed to this otherwise purely temporal filter. Thus, in our stadium-wave studies, M-SSA provides us with spatio-temporal filters that identify a mode of variability that propagates through each index.

The mode of variability in each index's time series identified by this spatio-temporal filter is represented by a new time series. This new time series is referred to as a reconstructed component (RC). Effectively, each RC is the narrow-band filtered version of an original multivariate time series. The filters are related to coefficients, or EOF weights, related to the eigenfunction that best captures the pattern of variability shared by the index set. **Figure 4.2** illustrates RCs of the indices for each of the first eight modes of variability found in the data set of the original Wyatt et al. (2011) study.

The stadium-wave signal identified in previous studies is characterized by a pair of modes, specifically, leading modes one and two. We summed the RCs of these two modes. This new combination defined the stadium-wave climate signal. Expression of this signal as it propagates through each of the indices in the original study's data set can be visualized through the index normalized RCs (**Fig. 4.3**). It is this signal we seek in the current study.

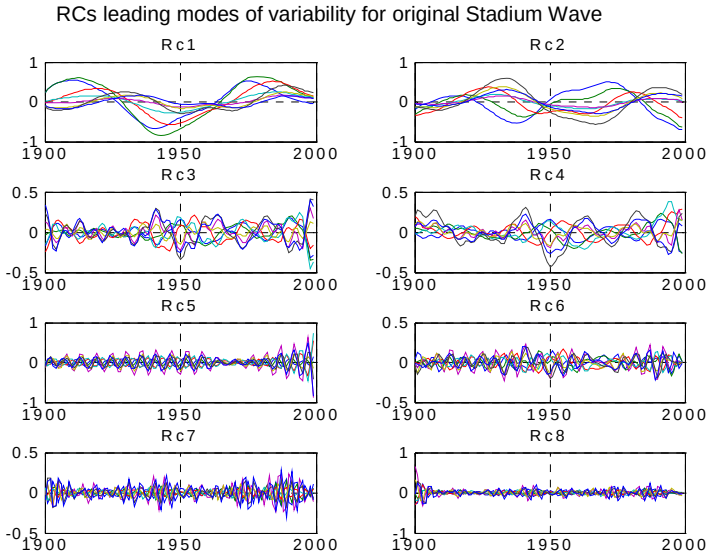

Fig. 4.2: From the original Wyatt et al. (2011) analysis. Shown here are reconstructed components (RCs) for each of the eight modes of variability derived in the original analysis. The leading two modes show similar periodicities and phasings, requirements for an oscillatory signal. Combined, they are the "stadium-wave" signal (see Fig. 4.3).

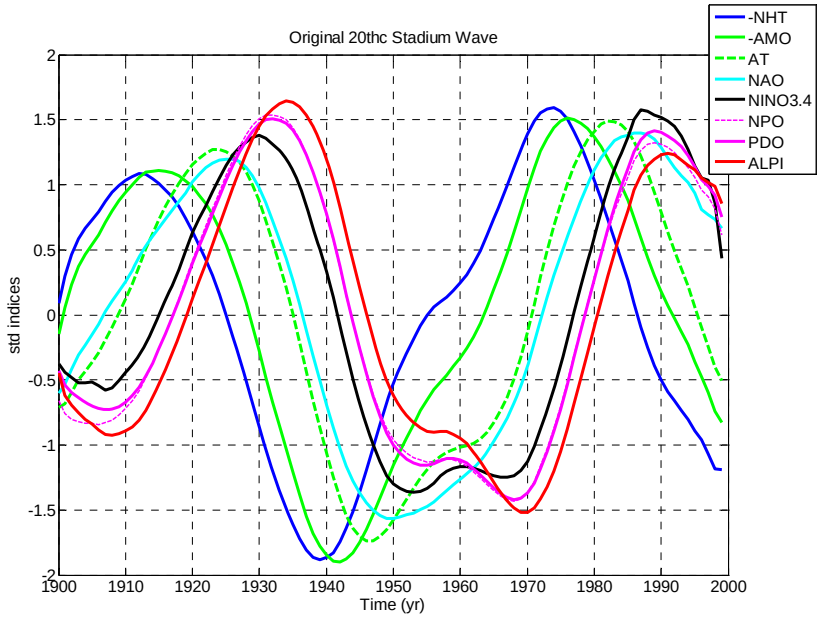

Fig. 4.3: Statistical Results from Original Stadium-Wave analysis, given here for comparison to model results. Normalized reconstructed components (RCs) of M-SSA leading two modes of variability are plotted. Note that each index carries this signal, and that the signal propagates through the network of regionally diverse indices – an occurrence that is quite significant. (Adapted from Wyatt et al. (2011)). RC time series have been normalized to have unit variance. Note: RCs of NHT and AMO are negative.

Assessing Significance of the Identified Signal: To assess the unlikelihood that the signal identified is not a random pattern of a noisy data set, we subject the data to a series of statistical tests. First, we fit red-noise model (1) to the non-filtered time series of each index.

$$x^{n+1} = ax^n + \sigma w, \qquad (1)$$

where x^n is the simulated value of a given index at time n; x^{n+1} is its value at time $n+1$; w is a random number drawn from a normal distribution with zero mean and unit variance; parameters a and σ are computed from such fits by linear regression. The red-noise model generates surrogate time series that are characterized by a lag-one autocorrelation (shifted copies of the time series). This is the same procedure followed with the model data. We applied M-SSA to this surrogate set and identified ten modes of variability. The range of mean variances of modes identified in the surrogate data sets is determined. We use the range of standard uncertainty – the 95% confidence level. This range sets an envelope of uncertainty by which we compare results of M-SSA applied to the model data. For modes of variability identified in the model data to be considered significant to the $p < 5\%$ level, their mean variances plotted on an M-SSA spectrum must fall outside this envelope of uncertainty. If they do fall outside this envelope, as defined by the surrogate data, there is a presumed 5% chance or less that an assumption of non-randomness is false.

Next we calculated error bars variances of the modes identified in the model data. These represent the 95% confidence interval of the mean variances of the modes. Each error bar attached to the mean variance on the M-SSA plot can be considered to be the observed variance of the model-data's mode plus/minus the standard deviation of the variances generated by the red-noise data.

To calculate the error bars, the variance of the mode was multiplied by the square root of $2/N^*$, where N^*= the number of degrees of freedom. N^* was estimated from the formula of Bretherton et al. (1999): $N^* = N(1-r^2)/(1+r^2)$, where N is the length of each time series in the index set, and $r \approx 0.65$ is the maximum lag-1 autocorrelation among the set of indices. Thus, the effective number of degrees of freedom, N^*, in the case of a 100-year time series, is equal to 40. The estimated decorrelation time is $N/N^* = 100/40 = 2.5$. This is considered the amount of time after which each data point can be considered independent from the ones preceding and following it. For the longer time series used in the control runs, where N was not equal to 100, the formula $(2/N^*)^{1/2}$ was adjusted accordingly.

If we could identify variances of modes of variability whose error bars fell outside the red-noise envelope, we then applied another set of criteria to them in search of the stadium-wave signal. First, were could we identify an oscillatory pair? Or even an oscillatory trio? We were seeking two or three consecutive modes, preferably leading modes, whose error bars overlapped. This would indicate that their mean values were not statistically different from one another. If these could be identified, we next had to consider if they were well separated from the remaining modes (according to the North et al. 1982 criterion). This would ensure that their mean values were distinct from other modes of variability. If this test was passed, we then evaluated their periodicities and phasing. Did they exhibit similar periodicities in their variability? Visual examination of the plotted RCs of each mode reflects this. If a similar periodicity was detected, its phasing was considered. To be a propagating oscillatory signal, the phasing of RCs of one mode needed to be in-quadrature with the phasing of RCs in the companion mode. An example of this can be seen in Fig. 4.2. Or, in the case of three modes, phasings of each needed to be offset.

In this analysis, if significance could not be assigned to the first two or three *leading* modes, any statistically significant oscillatory RC-pair or trio was sought. Finally, if a significant oscillatory pair (or collection) of modes was identified, these modes were combined into a "climate signal". This hybrid signature, now constituting the filter applied to each index, allows visualization of a shared quasi-oscillatory signal in each network index (e.g. Fig. 4.3). After completing this analysis for all index sets for all models analyzed, results were compiled.

4.3 Results

In total, 60 model runs were analyzed. Of these, 20 runs showed at least one mode of variability to be significant at the $p < 5\%$ level. Most of these leading modes were single modes. Only five model runs showed evidence of a pair. Three of these five exhibited high frequency variability – bi-annual to sub-decadal, one with non-stationary trends (IAP_fgoals_1_0_g_20csm_run1) – but none were consistent with stadium-wave propagation. Two of the five identified RC-pairs varied at a relatively a low-frequency time scale – 35-year variability. Further testing on this pair showed no signal propagation. Thus, of all runs evaluated from the CMIP data base, none reproduced a quasi-oscillatory, low-frequency propagating signal. We found no stadium wave. **Table 4.2** shows all model results of all 20^{th} century experiments evaluated. Results for the ten runs of pre-industrial (long-control) experiments are outlined in **Table 4.3**.

Table 4.2: 20thc Model results (total of 50 runs of 20th-c simulations): Five of the 50 runs showed significance (95% level) for a pair of leading modes. Despite these 5 analyses passing the red-noise significance test, none met the requirements for an oscillatory pair, which include similar periodicities and phases being in-quadrature, the latter a requirement for signal propagation. GFDL models, in particular the 2_0 version came the closest to the original 'stadium-wave' signal found in instrumental and proxy data; yet the leading modes did not generate a propagating signal; instead, they were in exact phase, the reason for which is unclear.

Model	Run	Sample Interval	Significant RCs	Grouping Character	Frequency/ Propagation Traits
BCCR_bcm2_0	1	Annual	None		
BCCR_bcm2_0	1	5y	None		
CCCMA_cgcm3	1	Annual	RC1	Single	
CCCMA_cgcm3	1	5y	None		
CNRM_cm3	1	Annual	RCs 1,2,3	RCs 1,2 = pair RC3=single	Bi-annual
CNRM_cm3	1	5y	None		
CSIRO_mk3	1	Annual	RCs 3,4,5,6,7	RCs 6,7 pair All others single	Bi-annual Non-stationary
CSIRO_mk3	1	5y	RC1	Single	
CSIRO_mk3	2	Annual	None		
CSIRO_mk3	2	5y	None		
GFDL_2_0	1	Annual	RCs 1,2	Pair	Non-stationary No propagation
GFDL_2_0	1	5y	RCs 1,2	Pair	
GFDL_2_0	2	Annual	RC3	Single	
GFDL_2_0	2	5y	None		
GFDL_2_1	1	Annual	None		
GFDL_2_1	1	5y	None		
GFDL_2_1	3	Annual	None		
GFDL_2_1	3	5y	Rcs 1,2	Pair	No propagation
GISS_aom	1	Annual	None		
GISS_aom	1	5y	None		
GISS_aom	2	Annual	None		
GISS_aom	2	5y	None		
GISS_e_h	1	Annual	None		
GISS_e_h	1	5y	None		
GISS_e_r	1	Annual	None		
GISS_e_r	1	5y	None		
IAP_fgoals1_0_g	1	Annual	RCs 1,2,3	Singles	
IAP_fgoals1_0_g	1	5y	RC1	Single	
INGV_echam4	1	Annual	None		
INGV_echam4	1	5y	None		
INMcm3_0	1	Annual	None		
INMcm3_0	1	5y	None		

IPSL_cm4	1	Annual	None		
IPSL_cm4	1	5y	None		
MIROC3_2_hires	1	Annual	None		
MIROC3_2_hires	1	5y	None		
MIROC3_2_medres	1	Annual	None		
MIROC3_2_medres	1	5y	None		
MIUB_echo_g	2	Annual	RCs 1,2,3 (4,5 marginal)	Singles	
MIUB_echo_g	2	5y	RCs 1,2 marginal	Singles	
MPI_echam	1	Annual	None		
MPI_echam	1	5y	None		
MRI_cgcn_2_3_2	1	Annual	None		
MRI_cgcn_2_3_2	1	5y	None		
NCAR_CCSM3_0	1	Annual	None		
NCAR_CCSM3	1	5y	None		
NCAR_pcm1	1	Annual	RC3		
NCAR_pcm1	1	5y	None		
UKMO_hadcm3	1	Annual	RCs 1,2,3 (all marginal)	Singles	
UKMO_hadcm3	1	5y	None		

Table 4.3: Control Models (total of 10 runs of Pre-industrial simulations). There were no significant pairs ($p < 5\%$ or 95% significance level) identified in any control runs analyzed.

Model	Run	Sampling Interval	Significant Modes	RC Character	Comments
BCCR_bcm2_0	1	5y	none		
CCCMA_cgcm3	1	Annual	none		
CCCMA_cgcm3	1	5y	RC1	single	
CNRM_cm3	1	Annual	none		
CNRM_cm3	1	5y	RC1	single	
CSIRO_mk3	1	Annual	none		
CSIRO_mk3	1	5y	RC2	single	
GFDL_2_0	1	5y	RCs 1,2	singles	
GISS_aom	1	Annual	none		
GISS_aom	1	5y	none		

Table 4.4 on the following page summarizes those models for which at least one mode of statistically significant variability could be identified.

Table 4.4: 20th century and pre-industrial model-results: significant to the 95% significance level. Both 20th century and pre-industrial control model runs are represented. Of these 20 model runs, five had significant pairs; yet only GFDL_2_0 run 1 and GFDL_2_1 run 3 models for the 20th century had a pair whose RCs showed multidecadal behavior, potentially an oscillatory pair. When the leading two modes in each of these runs were combined, no propagating behavior was exhibited. All indices are in exact phase together.

RC Number	Group	Periodicity	Model	Experiment	Run	Significant with Annual Sampling	Significant with Sampling @ 5y Running Mean	Comments Related to Signal Propagation or Other Behavior
1	single	~70y	CCCMA_cgcm3	20c	1	yes	no	
1,2	pair	bi-annual	CNRM_cm3	20c	1	yes	no	
3	single	~25y	CNRM_cm3	20c	1	yes	no	
3	single	subdecadal	CSIRO_mk3	20c	1	yes	no	
5	single	subdecadal	CSIRO_mk3	20c	1	yes	no	
6,7	pair	bi-annual	CSIRO_mk3	20c	1	yes	no	
1	single	~70y	CSIRO_mk3	20c	1	no	yes	
1,2	pair	~35y	*GFDL_2_0	20c	1	marginal	yes	no propagation
1,2	pair	~35	GFDL_2_1	20c	3	no	marginal	no propagation
1	single	100y	IAP_fgoals_1_0_g	20c3m	1	yes	yes	
2,3	pair	biannual	IAP_fgoals_1_0_g	20c3m	1	yes	no	non-stationary behavior
1	single	interannual	MIUB_echo_g	20c	2	yes		
1	single	~60y	MIUB_echo_g	20c	2		yes	
2	single	~60y	MIUB_echo_g	20c	2	yes	no	
3	single	~25y	MIUB_echo_g	20c	2	yes	no	
3	single	~55y	UKMO_hadcm3	20c	1	marginal	no	
1	single	~50y	CNRM_cm3	control	1	no	marginal	
2	single	~25y	CSIRO_mk3	control	1	no	yes	
1	single	~55 to 75y	GFDL_2_0	control	1	n/a	yes	
2	single	~25y	GFDL_2_0	control	1	n/a	yes	

4.3.1 Results of Select Models:

Evaluations of the indices reconstructed from the CMIP3 collection of model-generated data sets showed no evidence of a low-frequency, hemispherically propagating climate signal. No patterns of biases could be discerned in the outcome. In attempt to provide a cross-section of results, an arbitrary selection of model-based analyses is described below.

Model results from run 1 of the 20th-century experiment of GFDL_2_0 appeared promising at first glance. The M-SSA spectrum indicated two leading modes outside the red-noise envelope that were well-separated from the remaining modes. Their error bars overlapped, indicating similar mean variances. This is characteristic of an oscillatory pair (**Fig. 4.4**a). We show plots of reconstructed components (RCs) of the indices for each of seven modes of variability. Those for modes one and two are the ones of interest. They appear to display similar periodicities; yet their phasing is not in-quadrature. Instead, the RCs are in-phase (Fig. 4.4b).

This indicates a non-propagating signal. This is not the signature of a stadium-wave signal. To show what is meant by this, we combined the RCs for modes one and two to obtain the dominant signal characterizing this data set. It can be seen that signal expression in each of the seven indices occurs either in-phase or 180º out-of-phase. There is no signal propagation through the indices (**Fig. 4.5**).

(a)

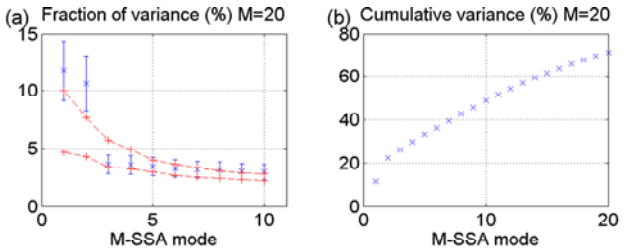

GFDL_2_0_20c run 1
annual sampling
1900-1999

(b)

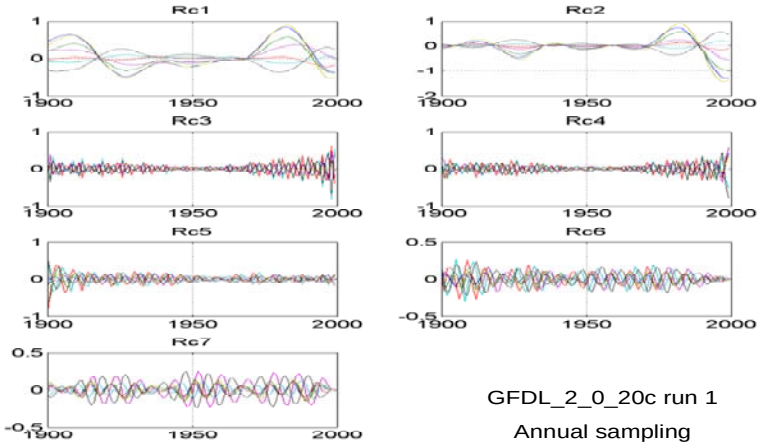

GFDL_2_0_20c run 1
Annual sampling
1900-1999

Fig. 4.4: GFDL_2_0_20c: Output from certain GFDL 20thc models showed promise. While the two M-SSA-identified leading modes showed potential for an oscillatory pair in GFDL_2_0_20thc Run 1, as deduced from the two leading modes (at 95% significance level) being outside the red-noise-established envelope of uncertainty in the M-SSA spectrum (a); and the RCs of leading modes one and two showing similar periodicity (b).

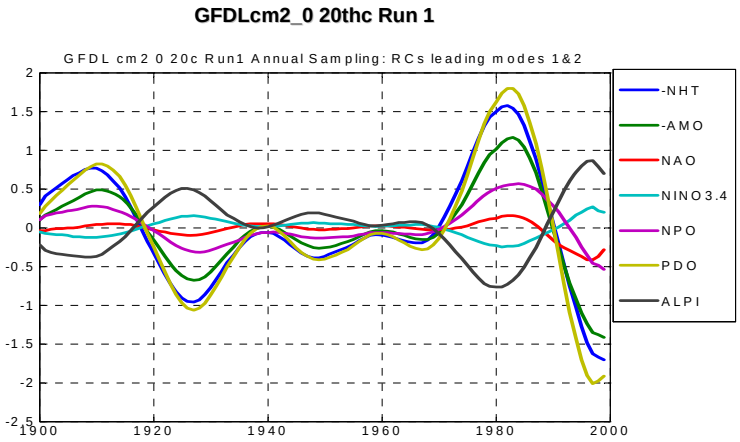

Fig. 4.5: GFDLcm2_0 20thc Run 1 model experiment showed promise, as indicated by its statistics in Fig. 4.4a,b. Despite these promising results, they failed to produce a propagating signal due to the modes being in exact phasing (see Fig. 4.4b), not in quadrature (see text). Thus, this cannot be considered the "stadium wave".

The M-SSA plot for the 20th-century experiment for model CCCMA_cgcm3 run 1 is shown in **Figure 4.6**a. Mode one falls outside the red-noise envelope, indicating its statistical significance. But there is no second mode of a similar mean value. Therefore, no oscillatory signal is identified. This single mode reflected in the companion RC plot (Fig. 4.6b) shows a multidecadal character. It is likely a radiative signal. No stadium-wave signal is indicated.

For the CNRM 20th-century model, run 1 three modes fall outside the red-noise envelope of the M-SSA spectrum and several others are almost outside it (**Fig. 4.7**a). The first two overlap. In fact, they are parallel. Their mean values are essentially identical. A glance at their associated RCs reveals they are high-frequency modes, likely seasonal (Fig. 4.7b). These are not candidates for the signal we seek. Other modes might be considered; yet no pair meets the criterion of being

widely separated from their neighbors. Furthermore, the associated RCs show no signals of similar periodicities. Thus, again, we detect no stadium-wave signal.

(a)

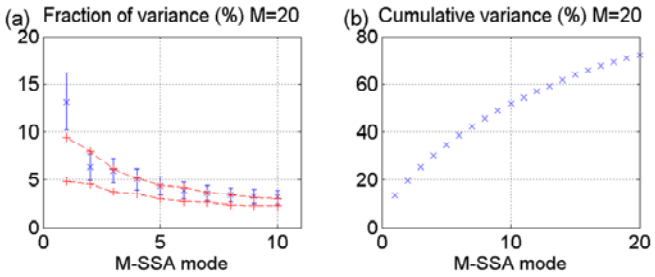

(b)

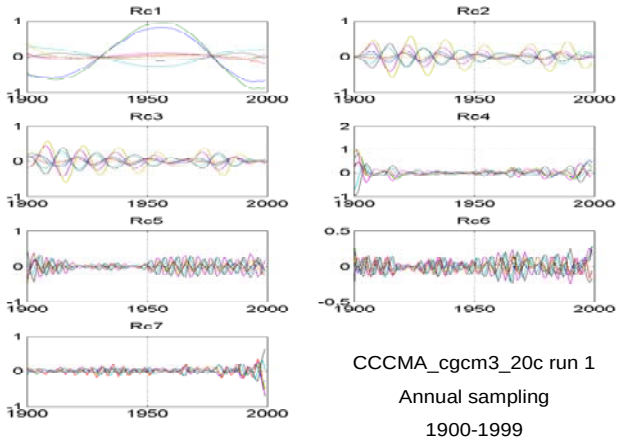

Fig. 4.6: CCCMA 20thc run1: No stadium-wave signature. (**a**) Two plots are given. The first is the M-SSA spectrum for this model. It shows leading mode 1 is significant. There is no indication of an oscillatory pair. The second plot in (a) is the cumulative variance of the first 20 modes identified. (**b**) Shows the RCs for each mode. Mode 1 is likely a forced radiative signal.

(a)

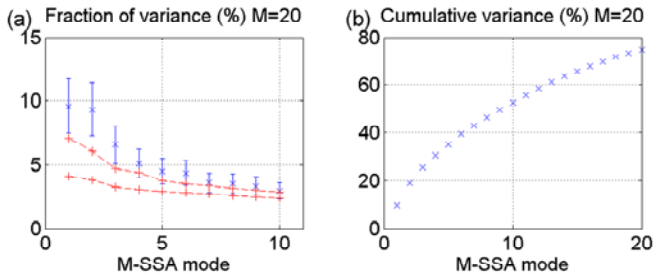

CNRM_cm3_20c run1
Annual sampling
1900-1999

(b)

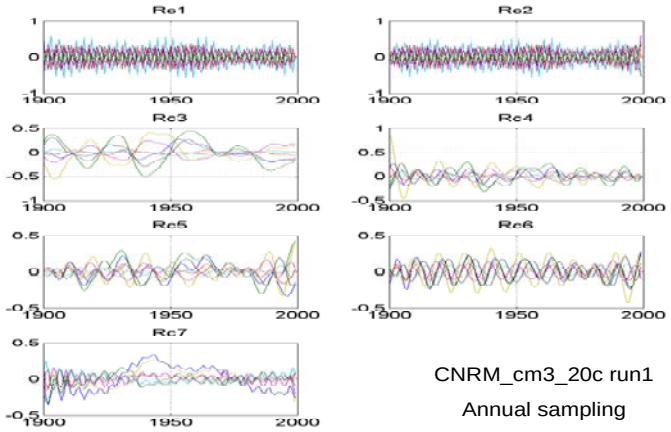

CNRM_cm3_20c run1
Annual sampling
1900-1999

Fig. 4.7: CNRM 20thc run 1: No stadium-wave signature. (**a**) Two plots are given. The first is the M-SSA spectrum for this model. It shows leading modes 1&2 to be outside the red-noise envelope. Their error bars overlap. There is overlapping of error bars for modes 2&3 and there is no separation from the remaining modes. Thus, the leading pair (or trio) does not meet the criteria for a stadium-wave signal. The second plot in (a) shows the cumulative variance accounted for by the first twenty modes. (b) Shows the RCs. They are high-frequency modes.

GISS_aom is the next 20th century model whose results are shown. These results are for run 2. No modes fall outside the red-noise envelope, rendering the results negative (**Fig. 4.8**a). Non-stationarity of data characterizes all associated RCs (Fig. 4.8b). There is no stadium-wave signal found in this data set.

Twentieth-century runs of models MRI_cgcm_2_3_2 (run 1), NCAR_CCSM3_0 (run 3), and NCAR_pcm1 (run 1) show no significant modes in their results (**Figs. 4.9 - 4.11**). No mode falls outside the red-noise envelope. Thus no stadium-wave signal is identified, despite the fact that the first modes of each of the models show a multidecadal character. For both versions of the NCAR models (Figs. 4.10 and 4.11), the first mode is a single one. There is no oscillatory pair. In the MRI model, the first multidecadal mode does form a pair with its neighbor. Were the modes' occurrence deemed non-random, we might consider this pair, based on their periodicities being similar and their phasing being offset.

The UKMO_hadcm3 20th-century model results (run 1) show three leading modes whose error bars overlap, are distinct from the remaining modes, and are almost fully outside the red-noise envelope (**Fig. 4.12**a). Despite these positive results, the first two RCs show decadal variability with non-stationarity in the time series. The third RC is a multidecadal mode; yet it is a single one (Fig. 4.12b). Thus, no stadium wave is found in this data pool.

Results from control experiments CCCMA_cgcm3 (run 1) and CNRM_cm3 (run 1) are shown in **Figures 4.13 and 4.14**. No modes fall outside the red-noise envelope. Centennial-scale variability characterizes mode one of the CCCMA model and a more interdecadal character can be seen in modes 2 and 3. The remaining modes in this model and all the modes of the CNRM model are high-frequency modes. No results for these models suggest a stadium-wave signal.

(a)

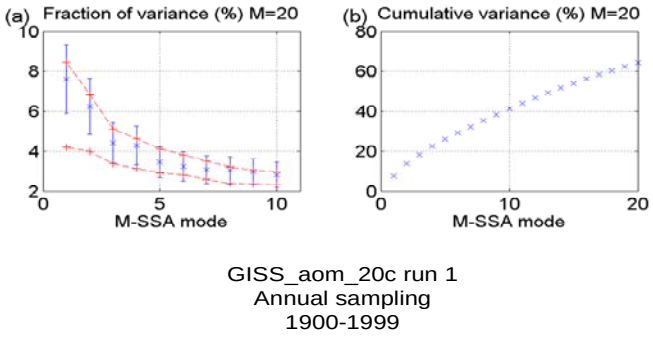

(b)

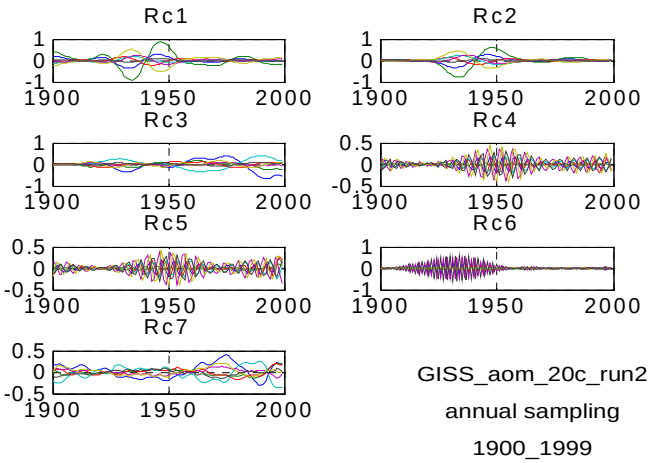

Fig. 4.8: GISS_aom 20thc run 2: No stadium-wave signature. (**a**) Two plots are given. The first is the M-SSA spectrum for this model. No modes fall outside the red-noise envelope; thus no significant mode can be identified. The second plot in (a) shows the cumulative variance accounted for by the first twenty modes. (b) Shows the RCs. The first two are interdecadal; yet their phasing is in-phase. All tests for a stadium-wave signal are failed for this model's data set.

(a)

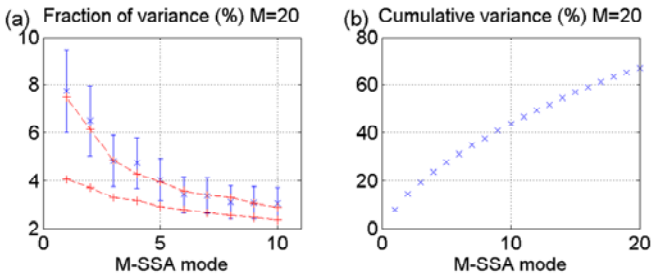

MRI_cgcm_2_3_2_20c run1
Annual sampling
1900-1999

(b)

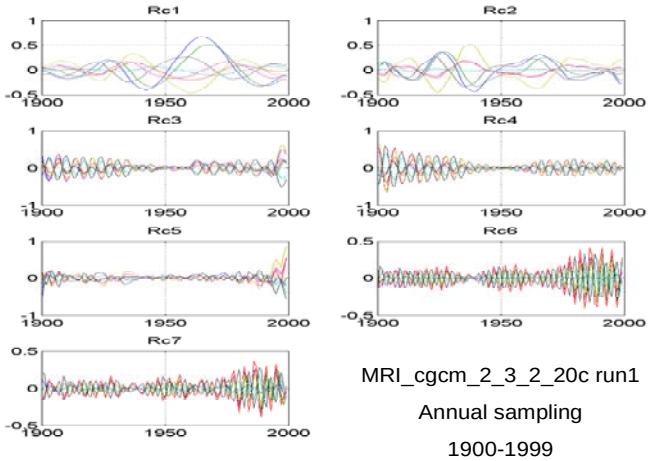

MRI_cgcm_2_3_2_20c run1
Annual sampling
1900-1999

Fig. 4.9: MRI_cgcm_2_3_2 20thc run 1: No stadium-wave signature. (**a**) Two plots are given. The first is the M-SSA spectrum for this model. No modes fall outside the red-noise envelope and no modes are well-separated from others; thus no significant mode can be identified. The second plot in (a) shows the cumulative variance accounted for by the first twenty modes. (b) Shows the RCs reflecting a periodicity of ~35 years.

(a)

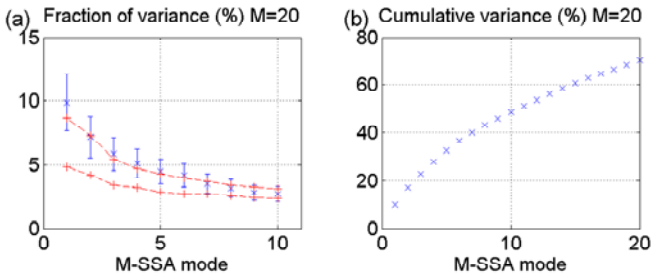

NCAR_CCSM3_0_20c3 run 1
Annual sampling
1900-1999

(b)

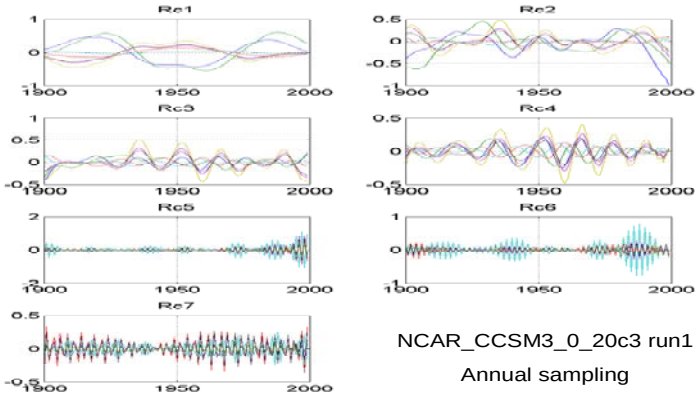

NCAR_CCSM3_0_20c3 run1
Annual sampling
1900-1999

Fig. 4.10: NCAR_CCSM3 20thc run 1: No stadium-wave signature. (**a**) Two plots are given. The first is the M-SSA spectrum for this model. No modes fall outside the red-noise envelope and no modes are well-separated from others; thus no significant mode can be identified. The second plot in (a) shows the cumulative variance accounted for by the first twenty modes. (b) Shows the RCs for this model. RC1 has a periodicity similar to the stadium-wave signal found in previous studies, but it is a single mode and therefore not an oscillatory signal. It is a moot point, as none of the modes fall outside the red-noise envelope.

(a)

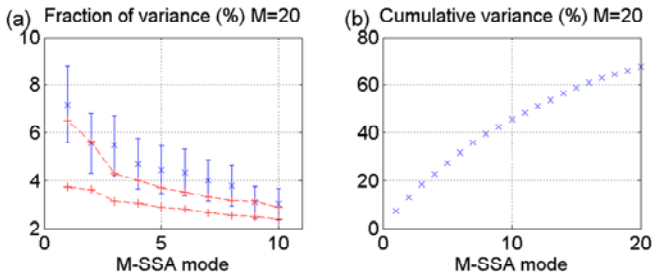

NCAR_pcm1_20c3m_run1
Annual sampling
1900-1999

(b)

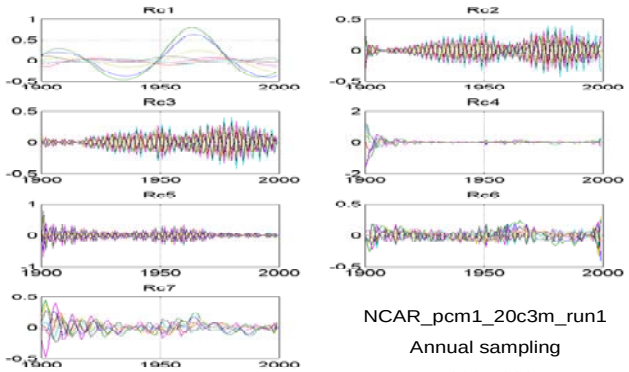

NCAR_pcm1_20c3m_run1
Annual sampling
1900-1999

Fig. 4.11: NCAR pcm1 20thc run 1: No stadium-wave signature. (**a**) Two plots are given. The first is the M-SSA spectrum for this model. No modes fall outside the red-noise envelope and no modes are well-separated from others; thus no significant mode can be identified. The second plot in (a) shows the cumulative variance accounted for by the first twenty modes. (b) Shows the RCs for this model. As in the other NCAR model (fig. 4.10), RC1 has a periodicity similar to the stadium-wave signal found in previous studies, but it is a single mode and therefore not an oscillatory signal. It is a moot point, as none of the modes fall outside the red-noise envelope

(a)

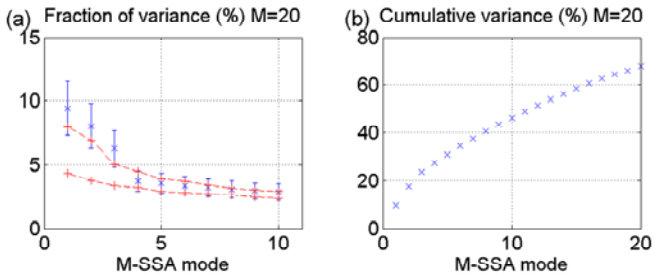

UKMO_hadcm3_20c run1
Annual sampling
1900-1999

(b)

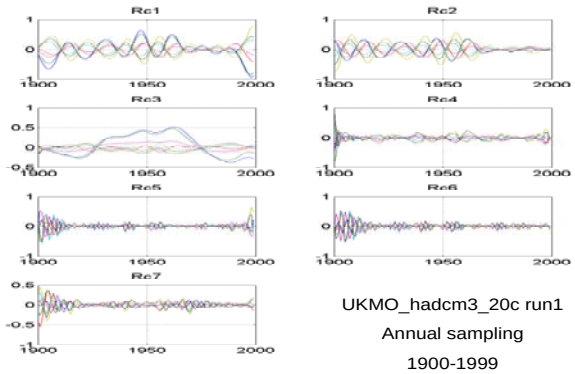

UKMO_hadcm3_20c run1
Annual sampling
1900-1999

Fig. 4.12: UKMO_hadcm3 20thc run 1: No stadium-wave signature. (**a**) Two plots are given. The first is the M-SSA spectrum for this model. The first three modes in UKMO_hadcm3 20thc run 1 overlap and are fairly well separated from the remaining modes; yet error bars for these three are not completely out of the envelope of uncertainty. The second plot in (a) shows the cumulative variance accounted for by the first twenty modes. (b) Shows the RCs for this model. Even if we were to consider the first few modes as being significant, one can see that modes one and two are higher frequency modes (not what we are looking for) and those modes display some non-stationarity in the data (again, not what we are looking for). Mode 3 exhibits the periodicity of the stadium-wave signal; yet this is a single mode, not a pair.

(a)

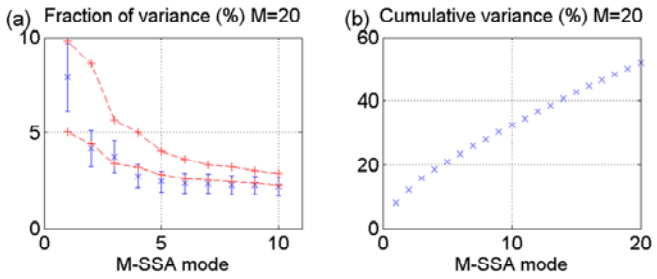

CCCMA_cgcm3_control _ run 1

Annual sampling

1851-2199

(b)

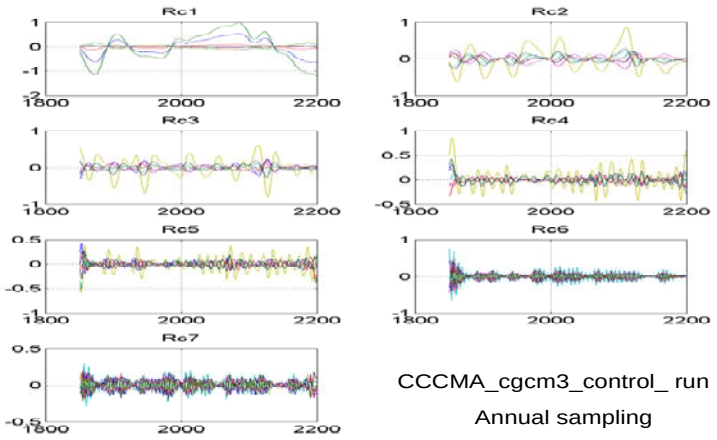

CCCMA_cgcm3_control_ run 1

Annual sampling

1851-2199

Fig. 4.13: CCCMA_cgcm3_control run1: No stadium-wave signature. (**a**) Two plots are given. The first is the M-SSA spectrum for this model. No modes fall outside the red-noise envelope. The second plot in (a) shows the cumulative variance accounted for by the first twenty modes. (**b**) Shows the RCs for this model. Most modes display high frequency variability, with the first mode showing some of the indices displaying a multidecadal timescale; while the amplitude of the other index RCs is minimal to zero.

(a)

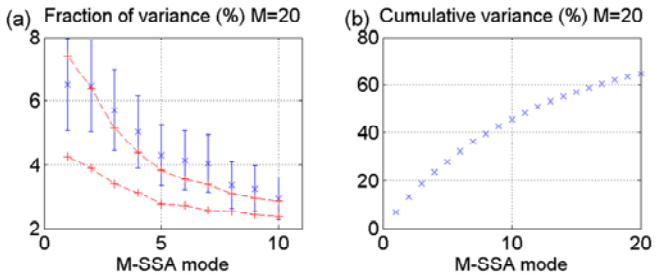

CNRM_cm3_control_run 1

Annual sampling

1930-2329

(b)

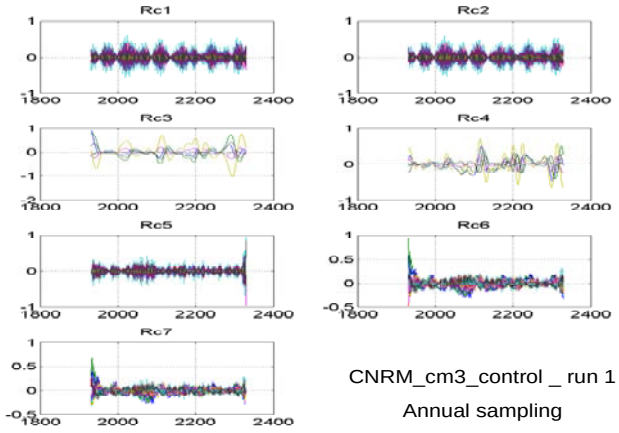

CNRM_cm3_control _ run 1

Annual sampling

1930-2329

Fig. 4.14: CNRM_cm3_control run1: No stadium-wave signature. (**a**) Two plots are given. The first is the M-SSA spectrum for this model. No modes fall outside the red-noise envelope. The second plot in (a) shows the cumulative variance accounted for by the first twenty modes. (**b**) Shows the RCs for this model. Most modes display high frequency variability. No semblance of a stadium-wave signal is seen.

The last model discussed here is the control experiment of GFDL_2_1. The leading two modes of variability fall outside the red-noise envelope, overlap, and are mostly separated from the remaining modes. RCs for mode one indicate a multidecadal tempo; yet RCs for mode two reflect a higher frequency (**Fig. 4.15**a, b). Thus, there exists no oscillatory pair of modes that might reflect the signal we seek. Again, no stadium-wave signal is detected.

4.4 Summary and Discussion

We analyzed reconstructed indices from model-generated data from the third Coupled Model Intercomparison Project (CMIP3) in order to determine if a hemispherically propagating climate signal, previously detected at secularly varying time scales in analogous indices reconstructed from instrumental data, could be identified. Using methods identical to those used in two prior companion studies (Wyatt et al. 2011; Wyatt (*submitted manuscript* 2012)), which documented a multidecadal quasi-oscillatory signature propagating hemispherically through a regionally and physically diverse collection of synchronized geophysical indices. We were unable to discern similar behavior in model-based simulations. Model-to-model differences were apparent; yet model-to-observation differences were stark. The CMIP3 ensemble simulations appear to be dominated by higher-frequency fluctuations, with the most dominant ones at biannual to sub-decadal periodicities, which are often marked by non-stationarity across the time interval evaluated. Radiative-forcing signatures are apparent at the secular-scale (i.e. a long, non-periodic variation; at most only one full cycle per hundred years).

(a)

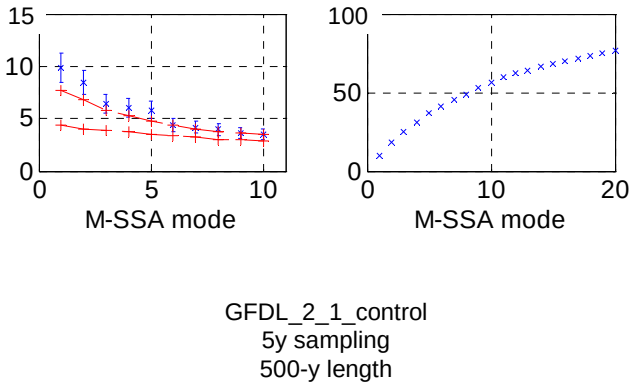

(b)

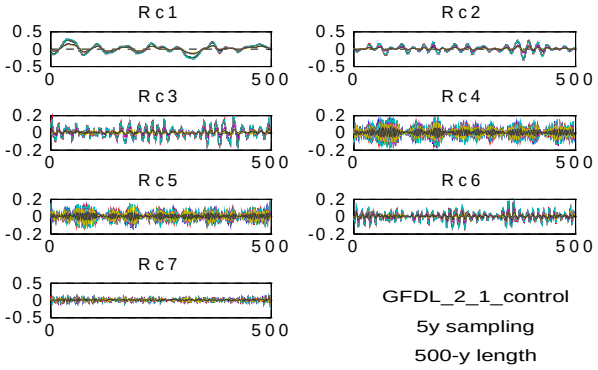

Fig. 4.15: GFDL_2_1 control run1 (smoothed with 5-y running mean): No stadium-wave signature. (**a**) Two plots are given. The first is the M-SSA spectrum for this model. Modes 1&2 fall outside the red-noise envelope. Their error bars overlap and they are somewhat separated from the remaining modes. The second plot in (a) shows the cumulative variance accounted for by the first twenty modes. (**b**) Shows the RCs for this model. Most modes display high frequency variability. Mode one reflects a periodicity similar to that of the stadium-wave, but mode two is of a different, much higher frequency. Thus, no oscillatory pair can be identified.

The CMIP3 collection reflects significant improvements in model design over its predecessors – versions 1 and 2. These versions had no energy balance at the top-of-the-atmosphere; their forcings were held constant in time, requiring addition of numerous flux adjustments. While CMIP3 is markedly improved and has more realistic parameterizations, with refined sub-grid-scale process-parameterizations, and therefore less reliance on flux adjustments, deficiencies remain. Continued testing of models against observed behavior, where possible, is necessary for their furthered improvement (Reichler et al. 2007).

Most such model-validity tests focus on one raw variable – temperature, sea-level-pressure, or the like. A good reproduction of observations can be found in a variety of models but the reason for the good reproduction is not necessarily the same for each model. In short, variability between models and observations may be almost identical from model to model, but the reasons behind the results may differ. In some, clouds provide a greater-than-observed negative feedback; yet within the same model, upper-tropospheric moisture exerts a greater-than-observed positive feedback (Sun et al. 2007). In short, a "good" climate reproduction can be the product of compensating errors (Palmer and Weisheimer 2011), which cancel out.

The mean state of the climate, as simulated by the CMIP3 ensemble, has been evaluated, showing its performance to be enhanced over the previous CMIP versions; yet what has not been evaluated is the modeled temporal variability (Reichler et al. 2007). Our results, here, may contribute to that effort, noting that in our previous studies on the "stadium-wave" hemispheric signal propagation, the significance of our findings was that the same signal was found time-after-time in so many diverse indices, but the temporal expression within each index was not simultaneous. Phase differences exist between pairs of indices, underscoring the foundation of the signal's propagating signature. Testing this behavior is what we have done here.

Most tests of model validity are executed with the assumption of model independence. Independence in this usage is defined in a statistical sense. It implies that model errors are not similar. This implies that the independent models can be averaged together via the multimodel-mean approach, their errors, assumed to vary around a "true" climate mean, cancelling out, yielding better results than those from individual models. Uncertainty of the projection decreases as more models are considered together. Yet if the models are not, indeed, independent, the number of effective degrees-of-freedom diminishes accordingly, with implications for statistical significance (Jun et al. 2008a).

Jun et al. (2008b) challenged this assumption of model independence, finding that the CMIP3 collection cannot be treated as a set of individual models. The effective degrees-of -freedom for the ensemble is far fewer than the number of members of the ensemble. They contend that these biases of a model relative to those biases in other models in the CMIP collection have a different character from the bias of a model relative to that in observations. They state, "…intercomparison of the models can give limited information about the bias with respect to the observations". Spatially, models developed by the same institutions share similar biases. For example, errors related to the sea-ice region north of the Bering Strait were highly correlated among models within a group; examples include GFDL, GISS, NCAR, and UKMO. Furthermore, most models have poor performance in simulating this variable. Kwok (2011) evaluated simulations of Arctic sea-ice motion, thickness, and export in the CMIP3 collection and found their performance poor. The key to the failures lay in geographical positioning of the polar high, which plays a strong role in the Arctic freshwater balance, and therefore in sea-ice-behavior, and, by extension, in climate responses and behavior (Wyatt (2012) *submitted*

manuscript). Placement of large-scale centers-of-action[3], whether atmospheric or oceanic, has been found critical to connectivity among regional circulations, establishing communication links that help make sense of intra-hemispheric signal propagation (Dima and Lohmann 2007, Wang et al. 2007 for examples; refer to Wyatt et al. 2011 for more discussion and references within.).

Climate science is perennially faced with the question; how can a climate hypothesis be tested? We have no controlled experiments. Quality control issues with instrumental data further complicate. In an attempt to address this collective challenge, we have tried to approach our hypothesis with the three available strategies – data from instruments, proxies, and models – yet recognize all means can be argued as being hypotheses, themselves. Thus we are left with a conundrum. Non-linearity of the system exacerbates the challenge.

Van den Berge et al. (2011) have made strides in taming these challenges. They invoke the seminal work done by Pecora and Carroll (1990) on non-linear systems, applying principles of synchronized theory to modeling climate. In essence, they have found that with a limited amount of information exchanged, a system's behavior can be reconstructed. This information exchange is accomplished by connecting each variable of a model to each variable of two other models. By linking chaotic systems, synchronization of the network of systems follows (Pecora and Carroll 1990). In short, chaos "sounds" like white noise. If chaos can be synchronized, the shared signal emerges from the noise.

In similar fashion, previous work done on "the stadium wave" has focused on network behavior rather than on detailed scrutiny of component parts. The results of these studies based on instrumental and proxy data suggest that the stadium-wave network is an intrinsically variable

[3] The term 'centers-of-action' (COA) refers to circulation centers. In the atmosphere, the Aleutian Low and Icelandic Low are examples of COAs. In the ocean, the subpolar and subtropical gyres are COAs.

system, fluctuating at low-frequency timescales, stabilized by negative feedbacks within the system, effectively re-locating heat from where it is in excess to where there is a deficit. In this network approach, individual processes are compressed into nodes of an interconnected, interactive system – not unlike Van den Berge et al's approach in developing the "super-modeling" strategy. Applying this view of synchronized networks to climate models, Van den Berge et al. developed a network in which models actually exchange information during simulation – introducing links between model equations - with results that showed "a very good approximation to the truth" – far better than individual models and better than using the multimodel-ensemble-mean approach.

4.5 Conclusion

Analyses performed on indices reconstructed from data generated by models archived in the CMIP3 database failed to detect a statistically significant stadium-wave climate signal. Results were the same for both 20th-century experiments and long-control runs of pre-industrial experiments. We cannot offer an explanation for this, only speculation.

In previous studies, this signal was identified for the 20th century in a wide variety of geographically diverse instrumental and proxy-reconstructed geophysical indices. Ocean-ice-atmospheric coupling is hypothesized to lie at the heart propagating this signal (Wyatt (*submitted manuscript*) 2012

In light of the nature of the CMIP3 architecture – its interdependence among models, its inability to capture well the sea-ice processes considered critical to the signal's propagation, its focus on component parts of the system versus network behavior – we propose that this failure to

support the stadium-wave signal's existence implies physical mechanisms relevant to signal propagation may be missing from this suite of general circulation models.

Acknowledgements

I thank John M. Peters for his invaluable contributions to the computer coding aspect of this project. I am grateful to him for his tireless efforts toward teaching me the ins and outs of Matlab idiosyncrasies and toward the success of this project, in general. Sergey Kravtsov rescued us both when two heads needed a third, and both Sergey and Anastasios Tsonis guided us through interpretations of our findings and, in cases, suggested further testing of those findings. All this input gave our study a solid base. If this work is converted into a paper, these three colleagues – all from University of Wisconsin, Milwaukee – will be asked to be co-authors on the resulting work. In addition, we thank Peter Molnar for his useful feedback and editorial suggestions.

References:

Broomhead DS, King GP (1986) Extracting qualitative dynamics from experimental data. Physica D 20: 217–236

Dima M, Lohmann G (2007) A Hemispheric Mechanism for the Atlantic Multidecadal Oscillation. J Climate 20: 2706-2719. doi:10.1175/JCL14174.1

Elsner JB, Tsonis AA (1996) Singular Spectrum Analysis: A New Tool in Time Series Analysis. Springer, 177 pp.

Ghil M, Allen MR, Dettinger MD, Ide K, Kondrashov D, Mann ME, Robertson AW, Saunders A, Tian Y, Varadi F, Yiou P (2002) Advanced spectral methods for climatic time series. Rev Geophys **40**(1): 3.1–3.41. doi:10.1029/2000GR000092.

Jun M, Knutti R, Nychka DW (2008a) Spatial analysis to quantify numerical model bias and dependence: how many climate models are there? J Am Stat Assoc 103(483):934-947. DOI: 10.1198/016214507000001265.

Jun M, Knutti R, Nychka DW (2008b) Local eigenvalue analysis of CMIP3 climate model errors. Tellus 60A (5): 992-1000. DOI: 10.1111/j.1600-0870.2008.00356.x

Kwok R (2011) Observational assessment of Arctic Ocean sea ice motion, export, and thickness in CMIP3 climate simulations. J of Geophy Res vol 116 C00D05. doi:10.1029/2011JC))7004

North GR, Bell TL, Cahalan RF, Moeng FJ (1982) Sampling errors in the estimation of empirical orthogonal functions. Mon Wea Rev 110, 669–706

Palmer TN, Weisheimer A (2011) Diagnosing the causes of bias in climate models – why is it so hard? Geophy and Asrophy Fluid Dyn, 105(2-3): 351-365. doi.org/10.1080/03091929.2010.547194

Pecora L, Carroll T (1990) Synchronization in Chaotic Systems. Phys Rev Lett 64: 824-824

Pohlman H, Sienz F, Latif M (2006) Influence of the Multidecadal Atlantic Meridional Overturning Circulation Variability on European Climate. J of C (special section) 19: 6062-6067. doi: 10.1175/JCLI3941.1

Preisendorfer RW (1988) Principal component analysis in Meteorology and Oceanography. Elsevier, Amsterdam, 425pp

Reichler T and Kim J (2007). How Well do Coupled Models Simulate Today's Climate? Bull AMS DOI:10.1175BA<S-89-3-303

Sun D-Z, Zhang T, Covey C, Klein SA, Collins WD, Hack JJ, Kiehl JT, Meehl GA, Held IM, Suarez M (2006). Radiative and Dynamical Feedbacks over the Equatorial Cold Tongue: Results from Nine Atmospheric GCMs. J of C. vol 19: 4059-4074

Trenberth K (1997) The Definition of El Niño. BAMS. Vol 78 (12): 2771-2777.

Van den Berge LA, Selten FM, Wiegerinck W, Duane GS (2011) A multi-model ensemble method that combines imperfect models through learning. Earth Syst Dyn 2: 161-177. doi:10.5194/esd-2-161-2011

Wang L, Chen W, Huang R (2007) Changes in the Variability of North Pacific Oscillation around 1975/1976 and its relationship with East Asian winter climate. J Geophys Res 112: D11110. doi: 10.1029/2006JD008054

Wyatt MG, Kravtsov S, Tsonis AA (2011) Atlantic Multidecadal Oscillation and Northern Hemisphere's climate variability. Clim Dyn DOI: 10.1007/s00382-011-1071-8

Wyatt MG (*submitted manuscript 2012*) Northern Hemisphere Multidecadal Climate Variability: dynamics and history of climate-signal hemispheric propagation: 1700 to 2000

Chapter Five:

Dissertation Summary and Discussion:

The body of research presented in this collection of studies grew out of curiosity regarding a well-documented multidecadal signal found in numerous geophysical indices - from commercial-fish populations to Earth's rotational-rate anomalies, to climate indices defining atmospheric and oceanic circulation patterns. This cadence is evident in a variety of proxy and instrumental records. My interest in this pervasive similarity led to step one of this project: preliminary analysis of raw time series of a variety of climate indices. Results of this initial step suggested not only a shared multidecadal signal, as had been detected in numerous previous studies, but in addition, a propagation of this signal across the Northern Hemisphere.

Was this just an unsystematic low-frequency signal in a noisy data set, no more than a random occurrence? Three separate, yet related studies, each based on a different data set and guided by slightly differing motivations, have been conducted in an attempt to answer this question quantitatively.

The strategy underpinning all studies was to forego detailed examination of individual regional circulation patterns. Instead, I focused on collective behavior. This meant evaluating interactions among individual regional circulation patterns. These regional patterns, or climate indices, can be considered to be nodes of a network.

Network theory lies at the heart of collective behavior, where the collective behavior of "parts" is not merely the sum total of those parts. How nodes of a network are configured and connected determines intra-nodal communication and network stability.

Nodal character can play a role in network function. If the nodes of a network are self-oscillating systems, a component of self-organization is conveyed to the network's collective system. All self-oscillating systems (nodes) can easily synchronize. With certain conditions met, upon coupling, intrinsic frequencies of the systems[1] adjust to a shared frequency – hence, they synchronize. Furthermore, within synchronized systems, if nodes are locally coupled, a signal can be propagated sequentially through them (Pikovsky et al. 2003). This propagating signal – a "stadium-wave[2]" signal- is consistent with the hypothesis proposed here: a low-frequency signal propagating through a network of synchronized climate indices across the Northern Hemisphere.

The original stadium-wave study (chapter two), based on the 20th-century instrumental data, to which multichannel-singular-spectrum analysis (M-SSA) was applied, characterized the dominant modes of climate variability *shared* among all indices considered. Eight indices were first analyzed. Seven additional ones were subsequently evaluated. All 15 possessed the M-SSA-identified shared oscillatory signal with strong statistical significance. While periodicity could not be assigned to this signal's tempo of variability, because defining its time-specific secular-scale[3] variability with statistical significance is not possible within the short time series available to us, a cadence of approximately 64 years was suggested in the 20th century analysis. No shorter-period timescales of variability were found to be shared by the collection of indices representing the Northern Hemisphere; although *regional* subsets of indices do share higher-

[1] In the case of climate indices, they all tend to exhibit quasi-oscillatory patterns of variability at various timescales. This tendency is intrinsic, based on numerous internal factors of the system. Thus, these systems are prone to synchronize with other quasi-oscillatory systems, given the right circumstances of 1.) a not-too-large frequency mismatch between them and 2.) a strong enough, but not too strong, coupling strength uniting the systems.

[2] This is an allusion to the phenomenon sometimes known as the audience wave, where a group of spectators, typically in a stadium, stands, with hands raised, and then sits, with hands down, while succeeding sections of spectators follow suit, one stadium section after the next – akin to the envisioned "stadium-wave" climate signal, manifesting at peak intensity in one regional climate pattern, followed by maximum expression in the next, until the signal has propagated across the hemisphere, back to its point of origin, albeit in reversed polarity.

[3] Secular-scale refers to a cycle that occurs one time or fewer per century.

frequency timescales of variability. More significant than the similar timescale of variability found in numerous indices is the statistically significant *succession* of geographically and dynamically diverse indices carrying this low-frequency signal. This sequential propagation within an index-network is what distinguishes this line of research from those studies that evaluate periodicity of a single index or variable.

Findings from the original study (chapter two) indicate that an Atlantic-born signal manifests as an oppositely signed hemispheric signal about thirty years after initiation. The atmospheric, lagged-oceanic teleconnection sequence, as identified in the original study, is as follows: -AMO → +AT → +NAO → +NINO3.4 → +NPO/+PDO → +ALPI → +NHT → +AMO. Translated, this sequence reflects a cool Atlantic Ocean leading intensified large-scale wind flow over the North Atlantic Ocean and Eurasian continent. Circulation in and over the North Pacific Ocean strengthens, and Northern Hemisphere temperatures rise. Maximum warmth in the North Atlantic ensues, ushering in the reversed-polarity second half-cycle. Lags of two to eight years temporally separate signal expression in these regionally diverse nodes. An extensive literature-base provides support for the numerous identified links within this described stadium-wave teleconnection sequence. Details are provided in the discussion section of the original study (Wyatt et al. 2011 (chapter two)).

For chapter three, I attempted to ascertain historical persistence of the stadium wave and to gain insight into potential dynamics underlying the propagating signal. The approach adopted for this step of research was to expand the index set and extend the time-interval considered. To the original index set I appended two categories of data: 1) a 300-year record of proxy data representing several core indices used in the original stadium-wave study (chapter two), and 2)

20th-century instrumental data representing newly introduced regions to the climate network, the Arctic and the Intertropical Convergence Zone (ITCZ).

With this extended data base, I analyzed a variety of subsets with M-SSA. In all cases for the 20th century, a statistically significant, secularly varying, quasi-oscillatory, shared signal was identified. For the proxy data extending to dates prior to the 20th century, robustness of results depended upon proxy subset used and length of time series evaluated. Stadium-wave-like behavior was found, but statistical significance diminished in all analyses as time series were extended further back in time. In addition, amplitude and frequency of the M-SSA-identified signal changed character in all subsets prior to 1800. The reasons for these observations are not clear. Whether the reasons lie with the signal or with quality issues of proxy data is something I cannot conclude from this analysis.

In attempt to approach the problem of signal longevity from a different angle, with the goal of extracting more information about signal history, I employed alternate strategies to this three-hundred-year data base. The strategy involved use of identified or inferred physical relationships among network members, based on 20th-century observations. With that information, I extrapolated into the past. Using this approach, combined with computing correlations between pairs of indices, evidence mounted in support of the historical persistence of the stadium-wave dynamic, possibly as far back as at least the time interval of this study, to 1700.

Incorporation of indices representing the Arctic, the Intertropical Convergence Zone (ITCZ), and wind patterns of the Pacific-North American region into the original data set built upon work done in the first study (chapter two). These indices provided insights into a few ‘missing links’. Two such examples include: 1) the relationship between Atlantic sea-surface

temperatures and large-scale wind patterns and 2) the transition between Pacific-based circulation patterns and polarity of the Atlantic basin-scale sea-surface-temperature distribution.

In the first example, the relationship between a cool (warm) Atlantic and intensified (weakened) basin-scale winds became clearer. This link is explained through the Arctic sea-ice. Ocean-ice-atmospheric coupling is evident.

In the second example, indications of negative feedback from circulations in and over the Pacific onto the Atlantic emerged, their cumulative impact remotely influencing freshwater export from the Atlantic, ultimately contributing toward the perpetuation of the stadium-wave propagation.

Furthermore, a weak solar signal identified in this study appears to be synchronized to the climate network, being in parallel alignment with negative polarities of Atlantic atmospheric circulations affecting the Atlantic ITCZ, and co-varying with negative inventories of Eurasian Arctic sea-ice. How this might be explained is through entrainment of tempo - solar variability being a *possible* metronome, of sorts, for the stadium-wave signal. Entrainment of a self-sustained oscillatory system by an external oscillatory system is common in synchronized networks (Pikovsky et al. 2001). This may be the case here, with tempo modification by this external force, coupled weakly to atmospheric circulation patterns related to the Atlantic sector. I suggest this possibility with caution, as solar's exact role in the climate system cannot be deduced from the analysis done here.

For the third study, chapter four, I analyzed a large data set comprising model-generated data from the third version of the Coupled Model Intercomparison Project (CMIP3 (Meehl et al. 2007)). A total of sixty data sets from a collection of 22 models were examined – with most analyses being of 20th-century experiments, and several being of long-control (pre-industrial)

experiments. From each model's raw simulated data set, I reconstructed climate indices analogous to those used in the original study (chapter two). From these reconstructions, climate-index networks were assembled and analyzed. Methods used in the original study were applied to these simulated index sets.

No statistically significant stadium-wave signal could be identified in the network of indices reconstructed from this vast model-generated data base. These results do not speak to the ability of CMIP3 models to simulate individual regional patterns, only to the models' ability to reconstruct communication of a low-frequency signal through a sequence of indices, as seen in the propagating 'stadium-wave' signal identified in the proxy and instrumental data. What is the message of these negative model-based results?

An answer may lie in results from the two previous studies presented here (chapters two and three). Nuances related to certain sub-processes appear to be vital to the signal's hemispheric propagation. These sub-processes are not well-represented in the CMIP3 ensemble. Should this matter? Geographically, these features appear minor in scale and amenable to generalization.

Seminal work on network behavior done by sociologist, Mark Granovetter (1973) underscores the crucial role of weak ties in enlarging and stabilizing a network. Could geographically small details of the climate system, ones that are poorly represented in the CMIP3 model ensemble, be analogous to Granovetter's "weak ties"?

I offer some potential support for this reasoning. Arctic sea-ice presents a good case. The role of Arctic sea ice described here is three-fold. First, it influences large-scale wind patterns. Second, it impacts Arctic temperatures. And third, its export from the Arctic Ocean into the Atlantic affects the salinity balance of these interlinked oceans – an important factor in Arctic

sea-ice growth and dynamics of ocean circulation in the North Atlantic sector. How do these features relate to the stadium-wave signal?

In chapter three, Eurasian Arctic sea ice was found to play a key role in the propagation of the stadium wave signal. In essence, increased sea-ice-extent in and to the east of the North Atlantic sector of the Arctic generates an ice-induced basin-scale meridional temperature gradient (Outten and Esau; Petoukhov and Semenov 2010). In response to this temperature gradient is the amplification of basin-scale winds. These winds increase in intensity and become more westerly at the mid-latitudes, enhancing the transfer of heat from tropical latitudes of the Atlantic Ocean to mid-latitudes of the Eurasian continent downwind.

Sea-ice behavior also strongly influences Arctic temperature. Convergence and ridging of sea ice collectively lead to open pockets of water, thereby providing an avenue for heat flux from the ocean to the overlying atmosphere. Open pockets of water also result in diminished albedo (reflectivity). Both of these processes result in increased Arctic temperatures, which ultimately lead to a reduced basin-scale meridional temperature gradient, weakened winds, and cooler temperatures downwind. Sea-ice dynamics and its related consequences are poorly represented in CMIP3 models (Jun et al. 2008; Kwok 2011).

Arctic sea-ice-export is a function of a few features. One is the geographical placement of the Arctic High. In the CMIP3 models, this atmospheric center-of-action is not positioned realistically; it is centered too far within the Arctic (Kwok 2011). One consequence of this mal-placement is the poor model simulation of Arctic wind patterns. These winds govern not only the sea-ice dynamics of convergence and ridging, but also sea-ice export out of the Arctic through the Fram Strait into the North Atlantic.

Dima and Lohmann (2007) found geographical positioning of Atlantic-based centers-of-action, features not well modeled, also to be critical to sea-ice export out of the Arctic through the Fram Strait. This export of sea ice influences Arctic salinity and contributes to modification of the Atlantic's fresh-water balance. Salinity plays a strong role in Arctic sea-ice growth, and by extension, in basin-scale atmospheric response. There is evidence of a sixty-year quasi-periodicity in high-latitude North Atlantic salinity concentrations (Frankcombe and Dijkstra 2011).

Problems exist in model representations of other centers-of-action. For example, multidecadal longitudinal/latitudinal migrations of oceanic centers-of-action may play a strong role in upper-ocean-heat inventory in, and flux from, western-boundary regions and their extensions in the Pacific and Atlantic Oceans (Dong and Kelly 2004; Kelly and Dong 2004; Hasegawa et al. 2007). Concentrated heat flux from this narrow region may, in turn, ultimately affect intra-basin atmospheric communication (Peng et al. 2002; Xie et al. 2004; Minobe et al. 2008; Wyatt et al. 2011 and references within). While these patterns may be incorporated in select regional-scale models, the CMIP3 models show poor skill in their representation (Kwok 2011).

In a stadium-wave-like sequence, certain behaviors of a sub-process depend upon the sub-process it follows. Such non-linearity in responses is a challenge for models to simulate, but is a feature of a communicating network. Van den Berge et al. (2012) may have made strides toward overcoming this obstacle with their design of a network-like "super-model". Their super-model design allows communication among models. The models exchange information during simulations. Results of this rather novel modeling approach are far better than those from individual models and from multimodel-ensembles. Such a modeling strategy may illuminate

more information about what we have attempted to describe here – a hemispheric network of coupled oceanic, ice, and atmospheric circulations.

In closing, it is clear from diverse examples in natural and manmade systems, that collective behaviors emerge in networks that are not easily anticipated solely based on knowledge of the individual components of these networks. What we are able to see tends to be largely a function of how we view it. In this collection of studies, the multidecadal character of climate was viewed as a synchronized, locally coupled network, more specifically, a hemispheric network of coupled oceanic, ice, and atmospheric circulations through which the shared low-frequency climate signal propagated sequentially in stadium-wave-like fashion, paced by the Atlantic "metronome", with Pacific circulations negatively feeding back on the Atlantic, promoting reversed polarity of the signal, thereby perpetuating signal propagation.

References:

Dima M, Lohmann G (2007) A Hemispheric Mechanism for the Atlantic Multidecadal Oscillation. J Climate 20: 2706-2719. doi:10.1175/JCL14174.1

Dong S, Kelly K (2004) Heat Budget in the Gulf Stream Region: The Importance of Heat Storage and Advection. J Phys Ocean 34: 1214-1231

Frankcombe LM and Dijkstra HA (2011) The role of Atlantic-Arctic exchange in North Atlantic multidecadal climate variability. Geophy Res Lett 38: L16603. doi:10.1029/2011GL048158.

Frankignoul C, Sennechael N, Kwon Y, Alexander M (2011) Influence of the Meridional Shifts of the Kuroshio and the Oyashio Extensions on the Atmospheric Circulation. J.Clim 24:762-777, doi 10.1175/2010 JCLI 3731.1

Frolov IE, Gudkovich AM, Karklin BP, Kvalev EG, Smolyanitsky VM (2009) Climate Change in Eurasian Arctic Shelf Seas, Springer-Praxis Books, ISBN 978-3-540-85874-4, 165p.

Giles KA, Laxon SW, Ridout AL, Wingham DJ, Bacon S (2012). Western Arctic Ocean freshwater storage increased by wind-driven spin-up of the Beaufort Gyre. Nature Geosc: 194-197 DOE:10.1038/NGE01379.

Granovetter MS (1973). The Strength of Weak Ties. American Journal Sociology:78(6) 1360-1380.

Grosfeld K, Lohmann G, Rimbu N, Fraedrich K, Lunkeit F (2007) Atmospheric multidecadal variations in the North Atlantic realm: proxy data, observations, and atmospheric circulation model studies. Clim of the Past 3: www.clim-past.net/3/39/2007 :39-50

Hasegawa T, Yasuda T, Hanawa K (2007) Multidecadal Variability of the Upper Ocean Heat Content Anomaly Field in the North Pacific and its Relationship to the Aleutian Low ans the Kuroshio Transport. Papers in Meteorology and Geophysics 58: 155-166: doi: 10.2467/mripapers.58.155

Izrael Yu A, Gruza V, Katsovv VM, and Meleshko VP (2001) Global climate changes: Role of anthropogenic impacts. Meteorology and Hydrology, 2001(5): 5-21 [in Russian]

Jun M, Knutti R, Nychka DW (2008) Local eigenvalue analysis of CMIP3 climate model errors. Tellus 60A (5): 992-1000. DOI: 10.1111/j.1600-0870.2008.00356.x

Kelly K, Dong S (2004) The Relationship of Western Boundary Current Heat Transport and Storage to Midlatitude Ocean-Atmosphere Interaction. Ocean-Atmosphere Interaction and Climate Variability, Edited by Chunzai Wang, Shang-Ping Xie, and James A. Carton, AGU Monograph

Kirov B, Georgieva K (2002) Long-term variations and interrelations of ENSO, NAO, and solar activity. Physics and Chemistry of the Earth 27: 441-448

Kwok R (2011) Observational assessment of Arctic Ocean sea ice motion, export, and thickness in CMIP3 climate simulations. J of Geophy Res vol 116 C00D05. doi:10.1029/2011JC))7004

Meehl GA, Covey C, Delworth T, Latif M, McAveney B, Mitchell JFB, Stouffer RJ, Taylor KE (2007) The WCRP CMIP3 Multimodel Dataset: A new era in climate change research. Bull Amer Meteo Soc 88(9): 1383-1394. doi: 10.1175/BAMS-88-9-1383

Minobe S, Kuwano-Yoshida A, Komori N, Xie S-P, Small RJ (2008) Influence of the Gulf Stream on the troposphere. Nature 452: 206-209. doi: 10.1038/nature06690

Outten SD, Esau I (2011) A link between Arctic sea ice and recent cooling trends over Eurasia. Climate Change. DOI 10.1007/s1058-011-0334-z

Peng S, Robinson WA, Li S (2002) North Atlantic SST forcing of the NAO and relationships with intrinsic hemispheric variability. Geophys Res Lett 29: 1276. doi: 10.1029/2001GL014043

Petoukhov V, Semenov VA (2010) A link between reduced Barents-Kara sea ice and cold winter extremes over northern continents. J Geophy Res 115 (D21111). Doi:1029/2009JD013568.

Pikovsky A, Rosenblum M, Kurths J (2001; reprinted 2003), Synchronization: A universal concept in nonlinear sciences. Cambridge University Press. ISBN 0 521 59285 2, 370p

Polonsky AB, Basharin DV, Voskresenskaya EN, Worley SJ, Yurovsky AV (2004) Relationship between the North Atlantic Oscillation, Euro-Asian climate anomalies and Pacific variability. Marine Meteorology. Pacific Oceanography 2(1-2): 52-66

Schmittner A, Appenzeller C, Stocker TF (2000). Enhanced Atlantic freshwater export during El Nino. Geophy Res Lett 27(8):1163-1166.

Sugimoto S, Hanawa K (2009) Decadal and Interdecadal Variations of the Aleutian Low Activity and Their Relation to Upper Oceanic Variations over the North Pacific. Journal of the Meteorological Society of Japan 87 (4): 601-614. DOI:10.2151/jmsj.87.601

Van den Berge LA, Selten FM, Wiegerinck W, Duane GS (2011) A multi-model ensemble method that combines imperfect models through learning. Earth Syst Dyn 2: 161-177. doi:10.5194/esd-2-161-2011

Wang L, Chen W, Huang R (2007) Changes in the Variability of North Pacific Oscillation around 1975/1976 and its relationship with East Asian winter climate. J Geophys Res 112: D11110. doi: 10.1029/2006JD008054

Wyatt MG, Kravtsov S, Tsonis AA (2011) Atlantic Multidecadal Oscillation and Northern Hemisphere's climate variability. Clim Dyn DOI: 10.1007/s00382-011-1071-8

REFERENCES for DISSERTATION:

Alekseev GV (1995) Interaction of atmosphere and ocean in the polar regions. Problems of the Arctic and the Antarctic 70: 193-200 [in Russian]

Alexander MA, Deser C (1995) A mechanism for the recurrence of wintertime midlatitude SST anomalies. J Phys Oceanogr 25: 122-137.

Beamish RJ, Boullion DR (1993) Pacific salmon production trends in relation to climate. Canadian Jour Fish and Aquat Sci 50:1002-1016.

Beamish RJ, Neville CM, Cass AJ (1997) Production of Fraser River sockeye salmon (*Oncorhynchus nerka*) in relation to decadal-scale changes in the climate and the ocean. Canadian Journ Fish and Aquat Sci 56: 516-526.

Beamish RJ, Noakes D, McFarlane GA, Klyashtorin L, Ivanov VV, Kurashov V (1999) The regime concept and natural trends in the production of Pacific salmon. Canadian Journal of Fisheries and Aquatic Sciences 56: 516-526

Beckers J, Rixen M (2003) EOF calculations and data filling from incomplete oceanographic data sets. J Atmos Ocean Technol 20: 1839–1856. doi: 10.1175/1520-0426(2003)

Bell GD, Halpert MS (1995) Atlas of intraseasonal and interannual variability, 1986-1993. NOAA Atlas No. 12. Climate Prediction Center, NOAA/NWS/NMC, Washington D. C. Request copy via e-mail from Gerald Bell at wd52gb@hp32.wwb.noaa.gov

Beckers J, Rixen M (2003) EOF calculations and data filling from incomplete oceanographic data sets. J Atmos Ocean Technol 20: 1839–1856. doi: 10.1175/1520-0426(2003)

Biasutti MA, Giannini A (2006) Robust Sahel drying in response to late 20th century forcings. Geophys Res Lett 33: L11706. doi:10.1029/2006GL026067

Biondi F, Gershunov A, Cayan DR (2001) North Pacific Decadal Climate Variability since 1661. J. Climate, 14: 5-10

Bjerknes J (1964) Atlantic air-sea interaction. Advances in Geophysics 10. Academic Press: 1–82

Black D, Peterson LC, Overpeck JT, Kaplan A, Evans MN, Kashgarian M (1999) Eight Centuries of North Atlantic Ocean Atmosphere Variability. Science 286: 1709-1713. doi: 10.1126/science.286.5445.1709

Broomhead DS, King GP (1986) Extracting qualitative dynamics from experimental data. Physica D 20: 217–236

Bretherton, C.S, Widmann M, Dymnikov VP, Wallace JM, Blade I (1999) The effective number of spatial degrees of freedom of a time-varying field. J. Climate, 12: 1990–2009

Bryden H, Longworth HR, Cunningham SA (2005): Slowing of the Atlantic meridional overturning circulation at 25°N. Nature 438: 655-657. doi:10.1038/nature04385

Cassou C, Deser C, Terray L, Hurrell JW, Drevillion M (2004): Summer Sea Surface Temperature Conditions in the North Atlantic and Their Impact upon the Atmospheric Circulation in Early Winter. J Climate 17: 3349-3363. doi: 10.1175/1520-0042(2004)

Cayan DR (1992) Latent and Sensible Heat Flux Anomalies over the Northern Oceans, Driving the Sea Surface Temperature. J Phys Ocean 22: 859-881

Ceballos LI, Di Lorenzo E, Hoyos CD, Schneider N, Taguchi B (2009) North Pacific Gyre Oscillation synchronizes climate fluctuations in the eastern and western boundary systems. J Clim 22: 5163-5174.

Chang P, Zhang Li, Saravanan R, Vimont DJ, Chiang JCH, Link Ji, Seidel H, Tippett MK (2007) Pacific meridional mode and El Niño-Southern Oscillation. Geophys Res Lett 34. L16608. doi:10.1029/2007GL030302.

Chavez PF, Ryan J, Lluch-Cota SE, Niquen MC (2003) From Anchovies to Sardines and Back: Multidecadal Change in the Pacific Ocean. Science 299: 217- 221

Chhak K, Di Lorenzo E (2007) Decadal variations in the California Current upwelling cells. Geophys Res Lett 314: L14604. doi10.1029/2007GL030203.

Chiang JCH, Vimont D (2004) Analogous Pacific and Atlantic Meridional Modes of Tropical Atmosphere-Ocean Variability. J. Climate 17: 4143-4158. doi: 10.1175/JCLI4953.1

Cook ER, D'Arrigio RD, Mann ME (2002) A Well-Verified, Multiproxy Reconstruction of the Winter North Atlantic Oscillation Index since A.D. 1400. Jour of Clim 15: 1754-1764

Courtillot V, Gallet Y, Le Mouel JL, Fluteau F, Genevey A (2007) Are there connections between the Earth's magnetic field and climate? Earth and Planetary Science Letters 253: 328-339

Crowley TJ (2000) Causes of Climate Change Over the Past 1000 Years. Science 289: 270-277. doi: 10.1126/science.289.5477.270

Cubasch U, Voss R, Hergerl GC, Waszkewitz J, Crowley TJ (1997) Simulation of the influence of solar radiation variations on the global climate with an ocean-atmosphere general circulation model. Clim Dyn 13: 757-767

Cubasch U, Voss R (2000) The Influence of Total Solar Irradiance on Climate. Space Science Rev 94: 185-198. doi: 10.1023/A:1026719322987

Czaja A, Frankignoul C (2002) Observed Impact of Atlantic SST Anomalies on the North Atlantic Oscillation. J. Climate 15: 606-623

Czaja A, Marshall J (2001) Observations of Atmosphere-Ocean Coupling in the North Atlantic. OJR Met. Soc. 27: 1893-1916. doi:10.1002/qj.49712757603

Danabasoglu G (2008) On Multidecadal Variability of the Atlantic Multidecadal Overturning Circulation in the Community Climate System Model Version 3. J Climate 21: 5524-5544. DOI: 10.1175/2008JCLI2019.1

D'Arrigio R, Wilson R (2006) On the Asian Expression of the PDO. International Jour of Climatology 26: 1607-1617

Delworth TL, Dixon KW (2006) Have anthropogenic aerosols delayed a greenhouse gas-induced weakening of the North Atlantic thermohaline circulation? Geophys Res Lett 33: L02606. doi:10.1029/2005GL024980

Delworth TL, Greatbatch RJ (2000) Multidecadal Thermohaline Circulation Variability Driven by Atmospheric Surface Flux Forcing. J Climate 13: 1481-1495

Delworth TL, Manabe S, Stouffer RJ (1993) Interdecadal Variations of the Thermohaline Circulation in a Coupled Ocean-Atmosphere Model. J Climate 6: 1993-2011

Delworth TL, Manabe S, Stouffer RJ (1997) Multidecadal climate variability in the Greenland Sea and surrounding regions: a coupled mode simulation. Geophys Res Lett 24 (3) 96GL03927: 257-260

Delworth TL, Mann ME (2000) Observed and simulated multidecadal variability in the Northern Hemisphere. Climate Dyn 16: 661–676. doi:10.1007/s003820000075

Delworth TL, Zhang R, Mann ME (2007) Decadal to centennial variability of the Atlantic from observations and models. In: Past and Future Changes of the Oceans Meridional Overturning Circulation: Mechanisms and Impacts, Schmittner A, Chiang JCH, Hemming SR, Eds., Geophysical Monograph Series 173, American Geophysical Union, pp. 131–148

Deser C, Blackmon ML (1995) On the Relationship between Tropical and North Pacific Sea Surface Temperature Variations. J. Climate 8: 1677-1680

Di Lorenzo E, Schneider N, Cobb KM, Franks PJS, Chhak K, Miller AJ, McWilliams JC, Bograd SJ, Arango H, Curchitser E, Powell TM (2008) North Pacific Gyre Oscillation links ocean climate and ecosystem change. Geophys Res Lett 35: L08607. doi:10.1029/2007GL032838

Di Lorenzo E, Fiechter J, Schneider N, Miller AJ, Franks PJS, Bograd SJ, Moore A, Thomas A, Crawford W, Pena A, Herman AJ (2009) Nutrient and salinity decadal variations in the central and eastern North Pacific. Geophys Res Lett 36: L14601. doi:10.1029/2009GL038261.

Di Lorenzo E, Cobb KM, Furtado JC, Schneider N, Anderson BT, Bracco A, Alexander MA, Vimont DJ (2010) Central Pacific El Niño and decadal climate change in the North Pacific Ocean. Nature Geosci 3 (11): 762-765. doi10.1038/NGEO984.

Dima M, Lohmann G (2007) A Hemispheric Mechanism for the Atlantic Multidecadal Oscillation. J Climate 20: 2706-2719. doi:10.1175/JCL14174.1

Dong BW, Sutton RT (2002) Adjustment of the coupled ocean-atmosphere system to a sudden change in the Thermohaline Circulation. Geophys Res Lett 29 (15): doi:10.1029/2002GL015229

Dong BW, Sutton RT (2005) Mechanism of interdecadal thermohaline circulation variability in a coupled ocean-atmosphere GCM. J. Climate 18: 1117–1135. doi: 10.1175/JCLI3328.1

Dong, BW, Sutton RT, Scaife AA (2006) Multidecadal modulation of El Niño Southern Oscillation (ENSO) variance by Atlantic Ocean sea surface temperatures. Geophys Res Lett 3: L08705. doi:10.1029/2006GL025766

Dong BW, Sutton RT (2007) Enhancement of ENSO Variability by a Weakened Atlantic Thermohaline Circulation in a Coupled GCM. J. Clim 20: 4920-4939. doi: 10.1175/JCLI4282.1

Dong BW, Sutton RT, Scaife AA (2006) Multidecadal modulation of El Nino Southern Oscillation (ENSO) variance by Atlantic Ocean sea surface temperatures. Geophys Res Lett 3**:** L08705. doi:10.1029/2006GL025766

Dong S, Kelly K (2004) Heat Budget in the Gulf Stream Region: The Importance of Heat Storage and Advection. J Phys Ocean 34: 1214-1231

Eden C, Jung T (2001) North Atlantic Interdecadal Variability: Oceanic Response to the North Atlantic Oscillation. J Clim 14: 676-691

Elsner JB, Tsonis AA (1996) Singular Spectrum Analysis: A New Tool in Time Series Analysis. Springer, 177 pp.

Enfield DB, Mestas-Nuñez AM (1999) Multiscale Variabilities in Global Sea Surface Temperatures and Their Relationships with Tropospheric Climate Patterns. J. Clim 12: 2719-2733

Enfield DB, Mestas-Nuñez AM, Trimble PJ (2001) The Atlantic Multidecadal oscillation and its relation to rainfall and river flows in the continental U. S. Geophys Res Lett 28: 277-280

Esper J, Cook ER, Schweingruber FH (2002) Low-Frequency Signals in Long Tree-Ring Chronologies for Reconstructing Past Temperature Variability. Science 295 (5563)

Federov A, Philander SG (2000) Is El Niño Changing? Science 288**:** 1997-2002. doi: 10.1126/science.288.5473.1997

Folland CK, Palmer TN, Parker DE (1986) Sahel rainfall and worldwide sea temperature 1901-1985. Nature320: 602-607

Frankcombe LM and Dijkstra HA (2011) The role of Atlantic-Arctic exchange in North Atlantic multidecadal climate variability. Geophy Res Lett 38: L16603. doi:10.1029/2011GL048158.

Frankignoul C, Sennechael N, Kwon Y, Alexander M (2011) Influence of the Meridional Shifts of the Kuroshio and the Oyashio Extensions on the Atmospheric Circulation. J.Clim 24:762-777, doi 10.1175/2010 JCLI 3731.1

Frolov IE, Gudkovich AM, Karklin BP, Kvalev EG, Smolyanitsky VM (2009) Climate Change in Eurasian Arctic Shelf Seas, Springer-Praxis Books, ISBN 978-3-540-85874-4, 165p.

Georgieva K, Kirov B, Tonev P, Guineva V, Atanasov D (2007) Long-term variations in the correlation between NAO and solar activity: the importance of north-south solar activity asymmetry for atmospheric circulation. Adv in Space Res 40: 1152-1166. doi: 10.1016/j.asr.2007.02.091

Getzlaff J, Böning CW, Eden C, Biastock A (2005) Signal propagation related to the North Atlantic overturning. Geophys Res Lett 32: doi:10.1029/2004GL021002

Ghil M, Vautard R (1991) Interdecadal oscillations and the warming trend in global temperature time series. Nature 305: 324–327

Ghil M, Allen MR, Dettinger MD, Ide K, Kondrashov D, Mann ME, Robertson AW, Saunders A, Tian Y, Varadi F, Yiou P (2002) Advanced spectral methods for climatic time series. Rev Geophys **40**(1): 3.1–3.41. doi:10.1029/2000GR000092.

Girs AA (1971) Girs AA (1971) Multiyear oscillations of atmospheric circulation and long-term meteorological forecasts. L. Gidrometeroizdat 480 p. (in Russian)

Girs AA (1974) Macrocirculation method for long-term meteorological prognosis. Hydrometizdat Publ, Leningrad, 480p. (in Russian)

Girs AA, Kondraovich KV (1978) Methods of Long Term Weather Forecasts. Gidrometeroizdat, Leningrad (in Russian).

Granovetter MS (1973). The Strength of Weak Ties. American Journal Sociology:78(6) 1360-1380.

Gray ST, Graumlich LJ, Betancourt JL, Pederson GT (2004) A tree-ring based reconstruction of the Atlantic Multidecadal Oscillation since 1567 A.D. Geophys Res Lett 31. L12205:

doi:10.1029/2004GL019932

Grosfeld K, Lohmann G, Rimbu N, Fraedrich K, Lunkeit F (2007) Atmospheric multidecadal variations in the North Atlantic realm: proxy data, observations, and atmospheric circulation model studies. Clim of the Past 3: www.clim-past.net/3/39/2007 :39-50

Grosfeld K, Lohmann G, Rimbu N (2008) The impact of Atlantic and Pacific Ocean sea surface temperature anomalies on the North Atlantic multidecadal variability. Tellus A: doi: 10.1111/j.1600-0870.2008.00304.x

Gudkovich ZM, Kirillov AA, Kovalev YeG, Smetannikova AV, and Spichkin VA (1972) Long-range Ice Forecasting Mehodology for the Arctic Seas. Leningrad: Gidrometeoizdat.: 348pp [in Russian]

Gudkovich ZM and Kovalev YeG (2002a) On some mechanisms of cyclic climate changes in the Arctic and the Antarctic. Oceanology 42(6): 1-7 [in Russian]

Gudkovich ZM and Kovalev YeG (2002b) Fluctuations of sea-ice extent of the Russian Arctic Seas in the 20th century and assessment of its possible changes in the 21st century. Paper presented at Hydrometeorological Support for Economic Activity in the Arctic and the Ice-covered Seas, St. Petersburg, March 27-29, pp 36-45.

Hakkinen S (1999) A Simulation of Thermohaline Effects of a Great Salinity Anomaly. J Clim12: 1781-1795

Hansen DV, Bedzek HF (1996) On the nature of decadal anomalies in North Atlantic SST. JGR 101: 8749-8758

Hasegawa T, Yasuda T, Hanawa K (2007) Multidecadal Variability of the Upper Ocean Heat Content Anomaly Field in the North Pacific and its Relationship to the Aleutian Low ans the Kuroshio Transport. Papers in Meteorology and Geophysics 58: 155-166: doi: 10.2467/mripapers.58.155

Hasselmann K (1976) Stochastic climate models.Pt.1. Tellus 28:473-485

Hilmer M, Jung T (2000) Evidence for a recent change in the link between the North Atlantic Oscillations and Arctic sea ice export. Geophys Res Lett 27(7): 989-992. doi: 10.1029/1999GL010944

Hurrell JW (1995) Decadal Trends in the North Atlantic Oscillation: Regional Temperatures and Precipitation. Science 269: 676-679

Hurrell JW (2003) The North Atlantic Oscillation: Climatic significance and environmental effect. EOS 84(8): 73

Hurst HE (1951) Long-Term Storage Capacity of Reservoirs. Transactions of the American

Society of Civil Engineers 116: 770-799

Izrael Yu A, Gruza V, Katsovv VM, and Meleshko VP (2001) Global climate changes: Role of anthropogenic impacts. Meteorology and Hydrology, 2001(5): 5-21 [in Russian]

Jones PD, Briffa KR, Barnett TP, Tett SFB (1998) High-resolution Palaeoclimatic Records for the last Millennium: Interpretation, Integration and Comparison with General Circulation Model Control-run Temperatures. The Holocene 8: 455-471

Jones PD, Moberg A (2003) Hemispheric and large-scale surface air temperature variations: an extensive revision and an update to 2001. J Clim 16: 206-223. doi:10.1175/1520-0442(2003)

Jun M, Knutti R, Nychka DW (2008a) Spatial analysis to quantify numerical model bias and dependence: how many climate models are there? J Am Stat Assoc 103(483):934-947. DOI: 10.1198/016214507000001265.

Jun M, Knutti R, Nychka DW (2008b) Local eigenvalue analysis of CMIP3 climate model errors. Tellus 60A (5): 992-1000. DOI: 10.1111/j.1600-0870.2008.00356.x

Jungclaus JH, Haak H, Latif M, Mikolajewicz U (2005) Arctic-North Atlantic Interactions and Multidecadal Variability of the Meridional Overturning Circulation. J Clim 18: 4013-4031. doi: 10.1175/JCLI3462.1

Jun M, Knutti R, Nychka DW (2008a) Spatial analysis to quantify numerical model bias and dependence: how many climate models are there? J Am Stat Assoc 103(483):934-947. DOI: 10.1198/016214507000001265.
Jun M, Knutti R, Nychka DW (2008b) Local eigenvalue analysis of CMIP3 climate model errors. Tellus 60A (5): 992-1000. DOI: 10.1111/j.1600-0870.2008.00356.x

Kaplan A, Cane M, Kushnir Y, Clement A, Blumenthal M, Rajagopalan B (1998) Analyses of global sea surface temperature 1856–1991. J Geophys Res 103: 18, 567–18, 589.

Karklin VP Yulin AV, Karelin ID, and Ivanov VV (2001) Climatic fluctuations of sea-ice extent of the Arctic Seas of the Siberian shelf. AARI Proc. 443: 5-11 [in Russian].

Kawasaki, T (1994) A decade of the regime shift of small pelagics – from the FAO expert Consultation (1983) to the PICES III(1994). Bull. Japanese Soc. Fish. Oceanogr 58: 321-333

Keenlyside N.S., Latif M, Jungclaus J, Kornblueh L, Roeckner E (2008) Advancing decadal-scale climate prediction in the North Atlantic sector. Nature 453: 84-88. doi:10.1038/nature06921.

Kelly K, Dong S (2004) The Relationship of Western Boundary Current Heat Transport and Storage to Midlatitude Ocean-Atmosphere Interaction. Ocean-Atmosphere Interaction and Climate Variability, Edited by Chunzai Wang, Shang-Ping Xie, and James A. Carton, AGU Monograph

Kelly K, Small RJ, Samelson RM, Qiu B, Joyce TM, Kwon Y-O, Cronin MF (2010) Western Boundary Currents and Frontal Air-Sea Interaction: Gulf Stream and Kuroshio Extension. J Climate 23: 5644-5667. DOI: 10.1175/2010JLCI3346.1

Kerr RA (2000) A North Atlantic climate pacemaker for the centuries. Science 288: 1984-1986. doi: 10.1126/science.288.5473.1984

King, JR, Ivanov VV, Kurashov V, Beamish RJ, McFarlane GA (1998) General Circulation of the atmosphere over the North Pacific and its relationship to the Aleutian Low. (NPAFC Doc. No. 318) 18p, Dept. of Fisheries and Oceans, Sciences Branch

Kirov B, Georgieva K (2002) Long-term variations and interrelations of ENSO, NAO, and solar activity. Physics and Chemistry of the Earth 27: 441-448

Klimenko VV (2007) Climatic sensation: What awaits us in the near and distant future? "Polit. Ru" public lectures. Available at www.polit.ru/lectures/2007/02/15/klimenko.html

Klyashtorin LB (1998) Long-term climate change and main commercial fish production in the Atlantic and Pacific. Fisheries Research (37): 115-125

Klyashtorin LB Lyubushin AA (2007) Cyclic Climate Changes and Fish Productivity. Moscow, VNIRO Publishing, Editor for English version: Dr. Gary D. Sharp, Center for Climate/Ocean Resources Study, Salinas, CA. USA: 223pp

Klyashtorin LB, Borisov V, Lyubushin AA (2009) Cyclic changes of climate and major commercial stocks of the Barents Sea. Marine Biology Research 5: 4-17

Knight JR, Allan RJ, Folland CK, Vellinga M, Mann ME (2005) A signature of persistent natural thermohaline circulation cycles in observed climate Geophy Res Lett 32: L20708. doi: 10.1029/2005GRL024233

Knight JR, Folland CK, Scaife AA (2006) Climate impacts of the Atlantic Multidecadal Oscillation. Geophys Res Lett 33: L17706. doi:10.1029/2006GL026242

Kondrashov D, Ghil M (2006) Spatio-temporal filling of missing points in geophysical data sets. Nonl Proc Geophys 13: 151–159

Kravtsov S (2010) An empirical model of decadal ENSO variability. J Climate, submitted

Kravtsov S, Dewar WK, Ghil M, McWilliams JC, Berloff P (2008) A mechanistic model of mid-latitude decadal climate variability. Physica D 237: 584–599. doi:10.1016/j.physd.2007.09.025

Kravtsov S, Kondrashov D, Ghil M (2005) Multi-level regression modeling of nonlinear processes: Derivation and applications to climatic variability. J Climate 18: 4404–4424. doi: 10.1175/JCLI3544.1

Kug J-S, Jin F-F (2009) Left-hand rule for synoptic eddy feedback on low-frequency flow. Geophys Res Lett 36: L05709. doi: 10.1029/2008GL036435

Kushnir Y (1994) Interdecadal Variations in North Atlantic Sea Surface Temperature and Associated Atmospheric Conditions. J Climate 7(1): 141-157

Kushnir Y, Held I (1996) Equilibrium atmospheric response to North Atlantic SST anomalies. J Climate 9: 1208-1220

Kushnir Y, Robinson WA, Blade I, Hall NMJ, Peng S, Sutton R (2002) Atmospheric GCM response to extratropical SST anomalies: Synthesis and evaluation. J. Climate 15: 2233–2256

Kwok R (2011) Observational assessment of Arctic Ocean sea ice motion, export, and thickness in CMIP3 climate simulations. J of Geophy Res vol 116 C00D05. doi:10.1029/2011JC))7004

Kwon Y, Alexander MA, Bond NA, Frankignoul C, Nakamura H, Qiu B, Thompson L (2010) Role of the Gulf Stream and Kuroshio-Oyashio Systems in Large-Scale Atmosphere-Ocean Interaction: A Review. J Climate special collection: DOI: 10.1175/2010JCLI3343.1

Latif M, Barnett TP (1994) Causes of Decadal Climate Variability over the North Pacific and North America. Science 266: 634-637

Latif M, Barnett TP (1996) Decadal Climate Variability over the North Pacific and North America: Dynamics and Predictability. J Climate 9: 2407-2423

Latif M, Arpe K, Roeckner E (2000) Oceanic control of decadal North Atlantic sea level pressure variability in winter. Geophys Res Lett 27: 727-730. doi: 10.1029/1999GL002370

Latif M, Roeckner E, Mikolajewicz U, Voss R (2000) Tropical Stabilization of the Thermohaline Circulation in a Greenhouse Warming Simulation. J of Clim 13: 1809-1813.

Latif M (2001) Tropical Pacific/Atlantic Ocean Interactions at Multi-Decadal Time Scales. Geophy Res Lett 28: 539-542.

Latif M, Roeckner E. , Botzet M, Esch M, Haak H, Hagemann S, Jungclaus J, Legutke S, Marsland S, Mikolajewicz U, Mitchell J (2004) Reconstructing, Monitoring, and Predicting Decadal-Scale Changes in the North Atlantic Thermohaline Circulation with Sea Surface Temperature . J Climate 17: 1605-1614. doi: 10.1175/1520-0442(2004)

Latif M, Böning C, Willebrand J, Biastoch A, Dengg J, Keenlyside N, Schweckendiek U, Madec G (2006) Is the thermohaline circulation changing? J Climate 19 (18): 4631-4637. doi: 10.1175/JCLI3876.1

Lau N-C (1988) Variability of the observed midlatitude storm tracks in relation to low-frequency changes in the circulation pattern. J Atmos Sci 45: 2718-2743

Lau N-C, Nath MJ (1994) A modeling study of the relative roles of tropical and extratropical SST anomalies in the variability of the global atmosphere-ocean system. J Climate 7: 1184-1207

Lean J (2000) Evolution of the Sun's Spectral Irradiance Since the Maunder Minimum. Geophysicsl Res Lett 27 (16): 2425-2428

Lean J (2004) Solar Irradiance Reconstruction. IGBP PAGES/World Data Center fro Paleoclimatology. Data Contribution Series # 2004-035

Loehle C, Scafetta N (2011), Climate Change Attribution Using Empirical Decomposition of Climatic Data. The Open Atm Sc Jour 5: 74-86.

Luterbacker J, Xoplaki E, Dietrich D, Jones PD, Davies TD, Portis D, Gonzalez-Rouco JF, von Storch H, Gyalistras D, Casty C, Wanner H (2002) Extending North Atlantic Oscillation Reconstructions Back to 1500. Atmos Sci Lett. Doi:10.1006/asle.2001.0044

Mann ME, Park J (1994) Global-scale modes of surface temperature variability on interannual to century timescales. J Geophys Res 99: 25819–25833

Mann ME, Park J, Bradley RS (1995) Global interdecadal and century-scale oscillations during the past five centuries. Nature 378: 266-270

Mann ME, Park J (1996) Joint Spatiotemporal Modes of Surface Temperature and Sea Level Pressure Variability in the Northern Hemisphere during the Last Century. J. Climate 9: 2137-2162

Mann ME, Bradley RS, Hughes MK (1998) Global-scale temperature patterns and climate forcing over the past six centuries. Nature 392: 779-787

Mantua NJ, Hare SR, Zhang Y, Wallace JM, Francis RC (1997) A Pacific interdecadal climate oscillation with impacts on salmon production. Bull Amer Meteor Soc 78: 1069-1079

Marshall J, Johnson H, Goodman J (2001a) A study of the interaction of the North Atlantic Oscillation with ocean circulation. J Climate 14: 1399–1421

Marshall J, Kushnir Y, Battisti D, Chang P, Czaja A, Dickson R, Hurrell J, McCartney M, Saravanan R, Visbeck M (2001b) North Atlantic climate variability: phenomena, impacts and mechanisms. Internat J Climatology 21: 1863–1898. doi: 10.1002/joc.693

Mazzarella A, Scafetta N (2011) Evidences for a quasi 60-year North Atlantic Oscillation since 1700 and its meaning for global climate change. Theor Appl Climatol DOI 10 1007/s00704-011-0499-4

McCartney M (1997) Climate change: Is the ocean at the helm? Nature 388: 521-522

Meehl GA, Covey C, Delworth T, Latif M, McAveney B, Mitchell JFB, Stouffer RJ, Taylor KE (2007) The WCRP CMIP3 Multimodel Dataset: A new era in climate change research. Bull Amer Meteo Soc 88(9): 1383-1394. doi: 10.1175/BAMS-88-9-1383

Mehta VM, Suarez MJ, Manganello JV, Delworth TL (2000) Oceanic influence on the North Atlantic oscillation and associated Northern Hemisphere climate variations: 1959-1993. Geophys Res Lett 27(1): 121-124. doi: 10.1029/1999GL002381

Metzger EJ, Hurlburt HE (2001) The importance of high horizontal resolution and accurate coastline geometry in modeling South China Sea Inflow. Geophys Res Lett 28(6): 1059-1062. doi: 10.1029/2000GL012396

Miller AJ, Chai Fei, Chiba S, Moisan JR, Neilson DJ Decadal-Scale Climat and Ecosystem Interactions in the North Pacific Ocean (2004). J of Oceanog (60) 163:188.

Minobe S (1997) A 50-70-year climatic oscillation over the North Pacific and North America. Geophys Res Lett 24: 683-686

Minobe S (1999) Resonance in bidecadal and pentadecadal climate oscillations over the North Pacific: role in climatic regime shifts. Geophys Res Lett 26: 855-858

Minobe S, Kuwano-Yoshida A, Komori N, Xie S-P, Small RJ (2008) Influence of the Gulf Stream on the troposphere. Nature 452: 206-209. doi: 10.1038/nature06690

Moron V, Vautard R, Ghil M (1998) Trends, interdecadal and interannual oscillations in global sea-surface temperatures. Climate Dyn 14: 545–569.

Msadek R, Dixon KW, Delworth TL, Hurlin W (2010a) Assessing the predictability of the Atlantic meridional overturning circulation and associated fingerprints. Geophys Res Lett 37: L19608. doi: 10.1029/2010GL044517

Msadek R, Frankignoul C, Li LZX (2010b) Mechanisms of the atmospheric response to North Atlantic multidecadal variability: a model study. Climate Dyn online: DOI 10.1007/s00382-010-0958-0

Nakamura H, Sampe T, Tanimoto Y, Shimpo A (2004) Observed Associations Among Storm Tracks, Jet Streams, and Midlatitude Ocean Fronts. from AGU Monograph: The Earth's Climate: The Ocean-Atmosphere Interaction Geophysical Monograph 147: 329-346. doi: 10.1029/147GM18

Niebauer H (1998) Variability in Bering Sea ice cover as affected by a regime shift in the North Pacific in the period 1947-1996. J Geophys Res 103 (C12): 27717-27737.

North GR, Bell TL, Cahalan RF, Moeng FJ (1982) Sampling errors in the estimation of empirical orthogonal functions. Mon Wea Rev 110, 669–706

Nowak K, Hoerling M, Rajagopalan B, Zagona E (2011) Colorado River Basin Hydro-Climatic Variability. (in press Journ Climate)

Nurhati IS, Cobb KM, Di Lorenzo E (2010) Decadal-scale SST and Salinity Variations in the Central Tropical Pacific: Signatures of Natural and Anthropogenic Climate Change. Jour of Clim 24 (13): 3294-3308. DOI: 10.1175/2011JCLI3852.1

Ogurtsov MG, Nagovitsyn YA, Kocharov GE, Jungner H (2002) Long-period cycles of the Sun's activity recorded in direct solar data and proxies. Solar Physics 211: 371-394

Outcalt SI, Hinkel KM, Meyer E, Brazel AJ (1997) Application of Hurst Rescaling to Geophysical Serial Data. Geographical Analysis 29 (1): 72-87

Outten SD, Esau I (2011) A link between Arctic sea ice and recent cooling trends over Eurasia. Climate Change. DOI 10.1007/s1058-011-0334-z

Overland JE, Adams JM, Bond NA (1999) Decadal Variability of the Aleutian Low and Its Relation to High-Latitude Circulation. J Climate12: 1542-1548

Palmer TN, Sun Z (1985) A modeling and observational study of the relationship between sea surface temperature in the northwest Atlantic and the atmospheric general circulation. QJR Meteorol Soc 111: 947-975

Palmer TN, Weisheimer A (2011) Diagnosing the causes of bias in climate models – why is it so hard? Geophy and Asrophy Fluid Dyn, 105(2-3): 351-365. doi.org/10.1080/03091929.2010.547194

Pan L-L (2007) Synoptic eddy feedback and air-sea interaction in the North Atlantic region. Clim Dyn 29: 647-659. DOI: 10.1007/s00382-007-0256-7

Patterson RT, Prokoph A, Chang A (2004) Late Holocene sedimentary response to solar and cosmic ray activity influenced climate variability in the NE Pacific. Sedimentary Geology 172: 6784

Pecora L, Carroll T (1990) Synchronization in Chaotic Systems. Phys Rev Lett 64: 824-824

Peng S, Robinson WA, Hoerling MP (1997) The modeled atmospheric response to midlatitude SST anomalies and its dependence on background circulation states. J Climate 10: 971-987

Peng S, Whitaker JS (1999) Mechanisms Determining the Atmospheric Response to Midlatitude SST Anomalies. J Climate 12: 1393-1408

Peng S, Robinson WA (2001) Relationships between atmospheric internal variability and the response to an extratropical SST anomaly. J Climate 14: 2943-2959. doi:10.1175/1520-0442(2001)

Peng S, Robinson WA, Li S (2002) North Atlantic SST forcing of the NAO and relationships with intrinsic hemispheric variability. Geophys Res Lett 29: 1276. doi: 10.1029/2001GL014043

Penland, C (1989) Random forcing and forecasting using principal oscillation pattern analysis. Mon Wea Rev 117: 2165–2185

Penland, C (1996) A stochastic model of Indo-Pacific sea-surface temperature anomalies. Physica D 98: 534–558

Penland C, Ghil M (1993) Forecasting Northern Hemisphere 700-mb geopotential height anomalies using empirical normal modes. Mon Wea Rev 121: 2355–2372

Petoukhov V, Semenov VA (2010) A link between reduced Barents-Kara sea ice and cold winter extremes over northern continents. J Geophy Res 115 (D21111). Doi:1029/2009JD013568.

Philander GS (1990), El Nino, La Nina, and the Southern Oscillation, Academic Press. ISBN 0 12 553235 0, 289p

Pikovsky A, Rosenblum M, Kurths J (2001; reprinted 2003), Synchronization: A universal concept in nonlinear sciences. Cambridge University Press. ISBN 0 521 59285 2, 370p

Pohlmann H, Sienz F, Latif M (2006) Influence of the Multidecadal Atlantic Meridional Overturning Circulation Variability on European Climate. J Climate (special section) 19: 6062-6067. doi: 10.1175/JCLI3941.1

Polonsky AB (1997) Variability in the NW Black Sea associated with the large-scale atmospheric processes. Meteor and Hydrol 3: 59-70 (in Russian)

Polonsky AB (2001) The role of the ocean in the recent climate changes. Marine Hydrophys. Journal 6: 32-58 (in Russian).

Polonsky AB, Basharin DV, Voskresenskaya EN, Worley SJ, Yurovsky AV (2004) Relationship between the North Atlantic Oscillation, Euro-Asian climate anomalies and Pacific variability. Marine Meteorology. Pacific Oceanography 2(1-2): 52-66

Polyakov IV, Alekseev GV, Timokhov LA, Bhatt JS, Colony RL, Simmons HL, Walsh D, Walsh JE, and Zakharov VF (2004) Variability of the intermediate Atlantic water of the Arctic Ocean over the last 100 years. J of Clim 16(12): 2067-2077.

Polyakov IV, Alexeev VA, Bhatt US, Polyakova EI, Zhang X (2009) North Atlantic warming: patterns of long-term trend and multidecadal variability. Clim Dyn (Springerlink.com). DOI: 10.1007/s00382-008-0522-3

Preisendorfer RW (1988) Principal component analysis in Meteorology and Oceanography. Elsevier, Amsterdam, 425pp

Press, WH, Teukolsky SA, Vetterling WT, Flannery, BP (1994) Numerical Recipes. 2nd edition, Cambridge University Press, 994pp

Rayner NA, Brohan P, Parker DE, Folland CK, Kennedy J, Vanicek M, Ansell T, Tett SFB (2006) Improved analyses of changes and uncertainties in sea-surface temperature measured in situ since the mid-nineteenth century. J Climate 19: 446-469. doi: 10.1175/JCLI3637.1

Reichler T and Kim J (2007). How Well do Coupled Models Simulate Today's Climate? Bull AMS DOI:10.1175BA<S-89-3-303

Rigor, IG, Wallace JM, Colony RL (2002) Response of sea ice to the Arctic Oscillation, J of Clim 15: 2648-2663.

Roberts PH, Yu ZJ, Russell CT (2007) On the 60-year signal from the core. Geophysical and Astrophysical Fluid Dynamics 101: 11-35

Robertson AW, Mechoso CR, Kim Y-J (2000) The influence of Atlantic sea surface temperature anomalies on the North Atlantic Oscillation. J Climate 13: 122-138. doi: 10.1175/1520-0442(2000)

Rodwell MJ, Rowell DP, Folland CK (1999) Oceanic forcing of the wintertime North Atlantic Oscillation and European climate. Nature 398: 320-323

Roe G (2009) Feedbacks, Timescales, and Seeing Red. Annu Rev Earth Planet Sci 37: 5.1-5.23. doi: 10.1146/annurev.earth.061008.134734

Rogers JC (1981) The North Pacific Oscillation. Int J Climatol 1: 39-57

Rotstayn L.D, Lohman U (2002) Tropical rainfall trends and the indirect aerosols effect. J Climate 15: 2103-2116

Rudyaev FI, Trofimov VK, Kravchuk YA (1985) Rhythmic changes of the Earth's rotation speed during the period 1664 to 1976. Izvestiya VO 117(3):252-257 [in Russian]

Scafetta N (2011), A shared frequency set between the historical mid-latitude aurora records and the global surface temperature. Jour Atm and Solar-Terrestrial Physics (in press).

Schlesinger ME, Ramankutty N (1994) An oscillation in the global climate system of period 65-70 years. Nature 367: 723-726

Schmittner A, Appenzeller C, Stocker TF (2000). Enhanced Atlantic freshwater export during El Nino. Geophy Res Lett 27(8):1163-1166.

Schneider T (2001) Analysis of incomplete climate data: estimation of mean values and covariance matrices and imputation of missing values. J Climate 14: 853–871. doi:

10.1175/1520-0442(2001)

Schneider N, Miller AJ, Pierce DW (2002) Anatomy of North Pacific decadal variability. J Climate 15: 586–605. doi: 10.1175/1520-0442(2002)

Shabalova MV, Weber SL (1999) Patterns of temperature variability on multidecadal to centennial timescales. J Geophys Res 104: 31,023-31,041

Shaffrey L, Sutton R (2006) Bjerknes Compensation and the Decadal Variability of the Energy Transports in a Coupled Climate Model. J Clim19: 1167-1181. doi: 10.1175/JCLI3652.1

Shen C, Wang WC, Gong W, Hao Z (2006) A Pacific Decadal Oscillation record since 1470 AD reconstructed from proxy data of summer rainfall over eastern China. Geophysical Res Lett 33: L03702. doi:10.1029/2005GL024804

Sidorenkov NS (2005a) Physics of the Earth's rotation instabilities. Astronomical and Astrophysical Transactions 24 (5): 425-439 DOI:10.1080/10556790600593506

Sidorenkov NS, Lutsenko OV, Bryazgin NN (2005b) Variation of the mass of the sheet of Antarctica and instability of the Earth's rotation. Russian Meteorology and Hydrology 8: 5-13

Sidorenkov NS (2009) The interaction between Earth's rotation and geophysical processes. WILEY-VCH Verlag GmbH and Co. KGaA, Weinheim 305pp

Shindell DT, Schmidt GA, Miller RL, Rind D (2001) Northern Hemisphere winter climate response to greenhouse gas, ozone, solar, and volcanic forcing. J. Geophys Res 106: 7193-7210. doi:10.1029/2000JD900547

Stocker TF, Mysak LA (1992) Climatic fluctuations on the century time scale: a review of high-resolution proxy data and possible mechanisms. Clim Change 20: 227-250

Stommel H (1961) Thermohaline convection with two stable regimes of flow. Tellus 13: 224–230

Stott PA, Tett SFB, Jones GS, Allen MR, Mitchell JFB, Jenkins GJ (2000) External Control of 20th Century Temperature by Natural and Anthropogenic Forcings. Science 290: 2133-2137. DOI: 10.1126/science.290.5499.2133

Sugimoto S, Hanawa K (2009) Decadal and Interdecadal Variations of the Aleutian Low Activity and Their Relation to Upper Oceanic Variations over the North Pacific. Journal of the Meteorological Society of Japan 87 (4): 601-614. DOI:10.2151/jmsj.87.601

Sun D-Z, Zhang T, Covey C, Klein SA, Collins WD, Hack JJ, Kiehl JT, Meehl GA, Held IM, Suarez M (2006). Radiative and Dynamical Feedbacks over the Equatorial Cold Tongue: Results from Nine Atmospheric GCMs. J of C. vol 19: 4059-4074

Sutton RT, Allen MR (1997) Decadal predictability of North Atlantic sea surface temperature and climate. Nature 388: 563-567

Sutton RT, Hodson DLR (2003) Influence of the Ocean on North Atlantic Climate Variability 1871-1999. J Climate 16: 3296-3313. doi: 10.1175/1520-0442(2003)

Sutton RT, Hodson DLR, Mathieu P (2003) The Role of the Atlantic Ocean in Climate Forecasting, Proceedings of the ECMWF Workshop on the Role of the Upper Ocean in Medium and Extend Range Forecasting, ECMWF, Reading, UK

Sutton RT, Hodson DLR (2005) Atlantic Ocean forcing of North American and European summer climate. Science 309: 115-118. doi: 10.1126/science.1109496

Sutton RT, Hodson DLR (2007) Climate response to basin-scale warming and cooling of the North Atlantic Ocean. J Climate 20: 891-907. doi: 10.1175/JCLI4038.1

Swanson K, Tsonis AA (2009) Has the climate recently shifted? Geophys Res Lett 36. doi:10.1029/2008GL037022

Taylor KE, Stouffer RJ, Meehl GA (2008) A Summary of the CMIP5 Experiment Design.http://www.pcmdi.llnl.gov/ipcc/model_documentation/ipcc_model_documentation.php

Timlin MS, Alexander MA (2002) On the Reemergence of North Atlantic SST Anomalies. J Climate 15: 2707-2712. doi:10.1175/1520-0442(2002)

Timmermann A, Latif M, Voss R, Grotzner A (1998) Northern Hemispheric interdecadal variability: a coupled air-sea mode. J Climate 11: 1906-1931

Timmermann A, Okumura Y, An SI, Clement A, Dong B, Guilyardi E, Hu A, Jungclaus JH, Renold M, Stocker TF, Stouffer RJ, Sutton R, Xie SP, Yin J (2007) The influence of a weakening of Atlantic meridional overturning circulation on ENSO. J Climate 20: 4899–4919. doi:10.1175/JCLI4283.1

Trenberth K (1997) The Definition of El Niño. BAMS. Vol 78 (12): 2771-2777.

Tsonis AA, Swanson K, Kravtsov S (2007) A new dynamical mechanism for major climate shifts. Geophys Res Lett 34: L13705. doi:10.1029/2007GL030288

Van den Berge LA, Selten FM, Wiegerinck W, Duane GS (2011) A multi-model ensemble method that combines imperfect models through learning. Earth Syst Dyn 2: 161-177. doi:10.5194/esd-2-161-2011

Van der Swaluw E, Drijfhout SS, Hazeleger W (2007) Bjerknes Compensation at High Northern Latitudes: The Ocean Forcing the Atmosphere. J Climate 20: 6023-6032. doi: 10.11752007JCLI1562.1

Vangenheim GYa (1940) The long-term temperature and ice break-up forecasting. Proc State Hydrological Institute Iss. 10: 207-236 (in Russian)

Vautard R, Ghil M (1989) Singular spectrum analysis in nonlinear dynamics, with applications to paleoclimatic time series. Physica D 35: 395–424

Vautard R, Yiou P, Ghil M (1992) Singular Spectrum Analysis: A toolkit for short, noisy and chaotic series. Physica D 58: 95 – 126

Vellinga M, Wood RA (2002) Global climatic impacts of a collapse of the Atlantic thermohaline circulation. Climatic Change 54: 251-267. doi: 10.1023/A:1016168827653.

Vellinga M, Wu P (2004) Low-latitude freshwater influence on centennial variability of the Atlantic thermohaline circulation. J Climate 17: 4498-4511. doi:10.1175/3219.1

Vimont DJ, Battisti DS, Hirst AC (2001) Footprinting: A seasonal connection between the Tropics and mid-latitudes. Geophys Res Lett 28: 3923:3926.

Vimont DJ, Battisti DS, Hirst AC (2003a) The seasonal Footprinting mechanism in the CSIRO general circulation models. J Climate 16: 2653-2667. doi:10.1175/1520-0442(2003)

Vimont DJ, Wallace JM, Battisti DS (2003b) The Seasonal Footprinting Mechanism in the Pacific: Implications for ENSO. J Clim 16: 2668-2675.

Vimont DJ, Kossin JP (2007) The Atlantic Meridional Mode and hurricane activity. Geophy Res Lett 34: L07709. doi:10.1029/2007/GL029683

Walker GT, Bliss EW (1932) World weather. Mem R Met Soc 4: 53-84

Wallace JM, Gutzler DS (1981) Teleconnections in the geopotential height field during the Northern Hemisphere winter. Mon Wea Rev 109: 784-812.

Wallace JM, Zhang Y, and Renwick JA (1995) Dynamic contribution to hemispheric mean temperature trends. Science 270: 780-783.

Wang L, Chen W, Huang R (2007) Changes in the Variability of North Pacific Oscillation around 1975/1976 and its relationship with East Asian winter climate. J Geophys Res 112: D11110. doi: 10.1029/2006JD008054

Willis JK, Roemmich D, Cornuelle B (2004) Interannual variability in upper ocean heat content, temperature, and thermosteric expansion on global scales. J Geophys Res 109: C12036. doi: 10.1029/2003C002260

Wilson IRG, Carter BD, White IA (2008) Does a Spin-Orbit Coupling Between the Sun and the Jovian Planets Govern the Solar Cycle? Publications of the Astronomical Society of Australia 25: 85-93

Wu P, Gordon C (2002) Oceanic Influence on North Atlantic Climate Variability. J Climate 15: 1911-1925. doi: 10.1175/1520-0442(2002)

Wu LP, Rodwell M (2004) Gulf Stream forcing of the winter North Atlantic oscillation. Atm Sc Lett 5: 57-64. doi: 10.1016/j.atmoscilet.2003.12.002

Wyatt MG, Kravtsov S, Tsonis AA (2011) Atlantic Multidecadal Oscillation and Northern Hemisphere's climate variability. Clim Dyn DOI: 10.1007/s00382-011-1071-8

Wyatt MG (*submitted manuscript 2012*) Northern Hemisphere Multidecadal Climate Variability: dynamics and history of climate-signal hemispheric propagation: 1700 to 2000

Xie SP (2004) Satellite observations of cool ocean-atmosphere interaction. Bull Am Meteorol Soc 85: 195-208. doi: 10.1175/BAMS-85-2-195

Xie SP, Carton J (2004) Tropical Atlantic Variability: Patterns, Mechansims, and Impacts. Earth Climate: The Ocean-Atmosphere Interaction. C. Wang, S.P. Xie, and J. A. Carton (eds.), Geophys Monograph. AGU. Washington, D. C., pp 121-142. doi: 10.1029/147GM07

Yualeva EN, Schneider N, Pierce DW, Barnett TP (2001) Modeling of North Pacific climate variability forced by ocean heat flux anomalies. J Climate 14: 4027-4046. doi: 10.1175/1520-0442(2001)

Zhang YJ, Wallace M, Iwasaka N (1996) Is Climate Variability over the North Pacific a Linear Response to ENSO? J Climate 9: 1468-1478

Zhang R, Delworth TL (2005) Simulated tropical response to a substantial weakening of the Atlantic thermohaline circulation. J Climate 18: 1853-1860. doi: 10.1175/JCLI3460.1

Zhang R, Delworth TL (**2007**) Impact of Atlantic multidecadal oscillations on India/Sahel rainfall and Atlantic hurricanes. Geophys Res Lett 33: L17712. doi:10.1029/2006GL026267

Zhang R, Delworth TL, Held IM (2007) Can the Atlantic Ocean drive the observed multidecadal variability in Northern Hemisphere mean temperature? Geophys Res Lett 34: L02709. doi:10.1029/2006GL028683

Zhen-Shan L, Xian S (2007) Multi-scale analysis of global temperature changes and trend of a drop in temperature in the next 20 years. Meteor and Atmos Physics: 95: 115-121